

**CATALYTIC UPGRADATION OF VANILLYL ALCOHOL
AS A LIGNIN MODEL COMPOUND VIA OXIDATION BY
TRANSITIONAL METAL-BASED MIXED OXIDE
CATALYSTS**

SUBRATA SAHA

**INSTITUTE OF GRADUATE STUDIES
UNIVERSITY OF MALAYA
KUALA LUMPUR**

2018

**CATALYTIC UPGRADATION OF VANILLYL
ALCOHOL AS A LIGNIN MODEL COMPOUND VIA
OXIDATION BY TRANSITIONAL METAL-BASED
MIXED OXIDE CATALYSTS**

SUBRATA SAHA

**THESIS SUBMITTED IN FULFILMENT OF THE
REQUIREMENTS FOR THE DEGREE OF DOCTOR OF
PHILOSOPHY**

**INSTITUTE OF GRADUATE STUDIES
UNIVERSITY OF MALAYA
KUALA LUMPUR**

2018

UNIVERSITY OF MALAYA
ORIGINAL LITERARY WORK DECLARATION

Name of Candidate: Subrata Saha

Matric No: HHC130010

Name of Degree: Ph.D

Title of Project Paper/Research Report/Dissertation/Thesis ("this Work"): Catalytic upgradation of vanillyl alcohol as a lignin model compound via oxidation by transitional metal-based mixed oxide catalysts

Field of Study: Chemistry

I do solemnly and sincerely declare that:

- (1) I am the sole author/writer of this Work;
- (2) This Work is original;
- (3) Any use of any work in which copyright exists was done by way of fair dealing and for permitted purposes and any excerpt or extract from, or reference to or reproduction of any copyright work has been disclosed expressly and sufficiently and the title of the Work and its authorship have been acknowledged in this Work;
- (4) I do not have any actual knowledge nor do I ought reasonably to know that the making of this work constitutes an infringement of any copyright work;
- (5) I hereby assign all and every rights in the copyright to this Work to the University of Malaya ("UM"), who henceforth shall be owner of the copyright in this Work and that any reproduction or use in any form or by any means whatsoever is prohibited without the written consent of UM having been first had and obtained;
- (6) I am fully aware that if in the course of making this Work I have infringed any copyright whether intentionally or otherwise, I may be subject to legal action or any other action as may be determined by UM.

Candidate's Signature

Date:

Subscribed and solemnly declared before,

Witness's Signature

Date:

Name:

Designation:

***CATALYTIC UPGRADATION OF VANILLYL ALCOHOL AS A LIGNIN MODEL
COMPOUND VIA OXIDATION BY TRANSITIONAL METAL-BASED MIXED
OXIDE CATALYSTS***

ABSTRACT

In recent days, lignin valorization has attracted a great deal of interests to minimize the dependency on under earthed fossil fuels. Lignin is the third abundant source in the earth which can be the source of potential alternative as renewable energy. However, lignin valorization in industrial scale become a great challenge because of the structural complexity of lignin. Extensive researches has been done in this arena using homogeneous and heterogeneous catalysts. And also, adaptation of other strategies such as unconventional reaction media or activation methods were also explored. But, the low yield of products and less economically valuable products obtained in current valorization techniques drives the thrust of this work to develop heterogeneous catalysts to improve the amount of yield to more valuable products.

To build a sustainable lignin valorization strategy, many issues such as a stable heterogeneous catalyst with simple and cost effective synthesis protocol, economically friendly process conditions, as well as high amount of yield need to be addressed. In this work, a simple, facile and economically effective solvent evaporation method has been developed to synthesize highly crystalline, mesoporous, and stable mixed oxide catalysts. The catalytic activity of prepared mixed oxide catalysts was tested in liquid phase oxidation of vanillyl alcohol which represent as a model compound of lignin monomeric structure. In the synthesis protocol of mixed oxide catalysts, different loading of metals and different valent cations (Cu^{2+} , Mn^{3+} , Fe^{3+} , Ti^{4+} , Ce^{4+}) were experimented to observe the apparent effect of cation charge on the catalytic activity. In order to establish the

correlation of the physico-chemical properties of the mixed oxide catalyst with the catalytic activity, various characterization techniques such as XRD, HRTEM, Raman, XPS, FESEM, SAED, H₂-TPR etc. were applied. In addition, to investigate the best suitable and environmentally benign oxidant for oxidation of vanillyl alcohol in terms of catalytic activity such as H₂O₂ and air was considered in this report. And also, the optimum reaction conditions such as time, pressure, temperature, oxidants concentration were found for liquid phase oxidation of vanillyl alcohol. The highest catalytic activity (94 % conversion with 86 % selectivity to vanillin) was measured for the catalyst in aerobic oxidation prepared by combination of Cu and Ti with ratio Cu/ Ti= 0.5. The other catalysts was in order of Ce-2Ti > Cu-2Zr > Cu-Mn > Fe-2Ti in view of both conversion and selectivity. The catalytic conversion of the catalysts was in order of Cu-2Ti > Cu-2Zr > Ce-2Ti > Fe-2Ti > Cu-Mn using H₂O₂ oxidant. In addition, the catalytic activity of prepared mixed oxide catalysts was found to promote the catalytic conversion to a certain extent to transform vanillyl alcohol into selective vanillin product with the presence of base NaOH using H₂O₂. Moreover, the spent mixed oxide catalysts was examined for stability measurement in there subsequent oxidation reactions of vanillyl alcohol at the obtained suitable reaction parameters for fresh catalysts. It was worth to note that the catalysts was stable with minimum loss of catalytic activity.

Keywords: Vanillyl alcohol, oxidation, air, lignin, catalysts, H₂O₂.

***UPGRADASI PEMANGKIN ALKOHOL VANILLYL SEBAGAI MODEL
KOMPOUND LIGNIN MELALUI PENGOKSIDAAN DENGAN LOGAN
PERALIHAN BERASASKAN PEMANGKIN***

ABSTRAK

Sejak kebelakangan ini, kegunaan lignin telah menarik perhatian pengguna untuk mengurangkan pergantungan kepada bahan api fosil. Lignin adalah sumber ketiga terbanyak di bumi dan boleh menjadi alternatif yang berpotensi sebagai tenaga boleh diperbaharui. Walau bagaimanapun, pemprosesan lignin dalam skala industri telah menjadi satu cabaran yang besar kerana kerumitan struktur lignin. Banyak kajian pemprosesan lignin telah dilakukan dengan menggunakan pemangkin homogen dan heterogen. Selain itu, penyesuaian strategi lain seperti kaedah tidak konvensional juga telah diterokai. Tetapi, hasil produk adalah rendah dan produk yang dihasilkan tidak bermutu dari segi ekonomi. Oleh itu, keadaan ini telah mencetuskan perancangan pemangkin heterogen untuk meningkatkan jumlah hasil produk yang bermutu tinggi.

Untuk membina pemprosesan lignin yang mampan, beberapa kriteria seperti penghasilan pemangkin heterogen yang stabil, kos efektif, keadaan proses mesra dari segi ekonomi, dan juga hasil product yang tinggi adalah diperlukan. Dalam kajian ini, kaedah penyejatan pelarut telah digunakan untuk mensintesis pemangkin campuran oksida yang bersifat kristal, mesoporous, dan stabil. Aktiviti pemangkin campuran oksida tersebut telah diuji dalam tindak balas pengoksidaan dengan menggunakan alkohol vanillyl sebagai sebatian model struktur monomeric lignin. Dalam process sintesis pemangkin campuran oksida, beberapa parameter seperti kandungan logam and kation valen yang berbeza (Cu^{2+} , Mn^{3+} , Fe^{3+} , Ti^{4+} , Ce^{4+}) telah digunakan untuk mengkaji kesan aktiviti pemangkin. Selain itu, hubungan antara sifat-sifat fiziko-kimia pemangkin campuran oksida dengan aktiviti pemangkin telah dikaji dengan menggunakan pelbagai teknik pencirian seperti

XRD, HRTEM, Raman, XPS, FESEM, SAED dan H₂-TPR. Pelbagai jenis oksidan seperti H₂O₂ dan udara telah dikaji terhadap kesan pengoksidaan alkohol vanillyl. Keadaan tindak balas optimum seperti masa, tekanan, suhu, kepekatan oksidan ditemui untuk tindak balas pengoksidaan alkohol vanillyl telah dikaji. Aktiviti pemangkin tertinggi (94% penukaran dengan selektif 86% kepada vanillin) telah didapati dengan pemangkin campuran oksida Cu-Ti dalam nisbah logam Cu/Ti=0.5. Selain itu, pemangkin oksida yang dibelanjakan telah diperiksa untuk pengukuran kestabilan di dalam tindak balas pengoksidaan seterusnya vanillyl alkohol pada parameter reaksi yang sesuai untuk pemangkin segar. Hasil kajian menunjukkan bahawa pemangkin yang dihasilkan adalah stabil dengan kehilangan minimum aktiviti katalitik.

Kata Kunci: Vanillyl alkohol, oksidan, udara, lignin, pemangkin, H₂O₂.

ACKNOWLEDGEMENTS

With the grace of Almighty

I dedicated my thesis to the most important people in my life,

For their unconditional love, wisdom and encouragement.

My parents, particularly my Father Gouranga Chandra Saha, who is the real hero behind all my success from my childhood and whose inspiration, prayer and intensive supports led me to overcome all the hurdles to go through this long journey of my study.

Most of all, I am fully indebted to both of my supervisors for their patience, enthusiasm and guidance, Dr. Lee Hwei Voon and Late Professor Dr. Sharifah bee Abd Hamid who was supporting me till her last breath.

I would like to express my sincere gratitude to Biplob Saha without his kind assistance I would not be able to start this Ph.D journey.

Cordial thanks to my best companion, Dr. Emy Marlina who was there in every circumstances of my journey. And also, heartfelt gratitude to Prof. Dr. Abe kawsar and Prof. Dr Dwaipayana Sikdar who inspired me to pursue Ph.D.

Millions of thanks to the rest of nanotechnology and catalysis research centre (Nanocat) team for their hard work and dedication on behalf of all postgraduate students.

Thank you.

Sincerely

Subrata Saha

TABLE OF CONTENTS

Abstract	iii
Abstrak	v
Acknowledgements.....	1
Table of Contents.....	2
List of Figures.....	9
List of Tables.....	15
List of Symbols and Abbreviations	17
CHAPTER 1: INTRODUCTION	22
1.1 State of art	22
1.2 Catalysis.....	22
1.3 Lignin	25
1.3.1 Structure of lignin	27
1.3.2 Importance of lignin modifications.....	28
1.3.3 Oxidation as the modification approach	31
1.3.4 Problem statement of lignin oxidation	31
1.4 Research Objectives.....	32
1.4.1 Specific research objectives	33
1.5 Thesis organization.....	33
CHAPTER 2: LITERATURE REVIEW.....	35
2.1 Lignin isolation.....	35
2.2 Oxidation.....	36
2.2.1 Oxidizing agents	39
2.2.1.1 Chlorine	40

2.2.1.2	Chlorine dioxide.....	41
2.2.1.3	Oxygen.....	41
2.2.1.4	H ₂ O ₂	42
2.2.1.5	Ozone	44
2.2.1.6	Peroxy acids	45
2.2.1.7	Economics of using oxidizing agents	45
2.2.1.8	Comparison of oxidants used generally for oxidation reactions.....	47
2.2.2	Catalytic system used for lignin oxidation reactions	48
2.2.2.1	Homogeneous catalysts used for oxidation of lignin	48
2.2.2.2	Heterogeneous catalysts used for oxidation of lignin and its model compounds	51
2.2.2.3	Unconventional methods	58
2.3	Vanillyl alcohol as lignin model compound	58
2.4	Why mixed oxides catalysts.....	59
2.5	Some preparation techniques of mixed oxide catalysts	60
2.5.1	Supported mixed oxide catalysts	61
2.6	Why solvent evaporation method.....	62
2.7	Reaction mechanism of metal catalyzed oxidation reactions	63
2.7.1	Homolytic mechanism	64
2.7.1.1	Direct homolytic mechanism of organic substrate.....	65
2.7.2	Heterolytic mechanism.....	65
2.7.2.1	Catalytic oxygen transfer.....	66
CHAPTER 3: METHODOLOGY		68
3.1	Scope of work.....	68
3.1.1	Cu based mixed oxide catalysts.....	68
3.1.2	Replacement of Cu in mixed oxide catalysts	68

3.1.3	Characterizations of Catalysts	69
3.1.4	Catalytic evaluation in oxidation of vanillyl alcohol	69
3.1.5	Plausible reaction mechanism	71
3.2	Research approach (flow chart).....	72
3.3	Equipment and consumables	73
3.4	Catalysts preparation method	73
3.4.1	Materials.....	73
3.4.2	Catalyst synthesis method	74
3.5	Catalysts Characterization tools	75
3.5.1	X-Ray powder diffraction (X-Ray).....	76
3.5.1.1	Background of X-Ray.....	76
3.5.1.2	Sample analysis procedure.....	76
3.5.2	Field emission scanning electron microscopy (FESEM).....	76
3.5.2.1	Background of FESEM.....	76
3.5.2.2	Sample analysis procedure.....	77
3.5.3	Energy dispersive X-Ray (EDX).....	77
3.5.3.1	Background of EDX.....	77
3.5.3.2	Sample analysis procedure.....	77
3.5.4	High resolution transmission electron microscopy (HRTEM).....	78
3.5.4.1	Background of HRTEM	78
3.5.4.2	Sample analysis procedure.....	78
3.5.5	Selection area electron diffraction	78
3.5.5.1	Background of SAED.....	78
3.5.5.2	Sample analysis procedure.....	79
3.5.6	Brunner-Emmet-Teller (BET)	79
3.5.6.1	Background of BET.....	79

3.5.6.2	Sample analysis procedure.....	79
3.5.7	Raman analysis	79
3.5.7.1	Background of Raman	79
3.5.7.2	Sample analysis procedure.....	80
3.5.8	Temperature programmed reduction (H ₂ -TPR).....	80
3.5.8.1	Background of H ₂ -TPR.....	80
3.5.8.2	Sample analysis procedure.....	80
3.5.9	Temperature programmed desorption (O ₂ -TPD).....	81
3.5.9.1	Background of the O ₂ -TPD.....	81
3.5.9.2	Sample analysis procedure.....	81
3.5.10	Thermogravimetric analysis (TGA).....	81
3.5.10.1	Background of TGA.....	81
3.5.10.2	Sample analysis procedure.....	81
3.5.11	X-Ray Photoelectron Spectroscopy	82
3.5.11.1	Background of XPS.....	82
3.5.11.2	Sample analysis procedure.....	82
3.6	Calculations.....	82
3.6.1	Scherrer's equation	82
3.7	Catalytic activity measurement	83
CHAPTER 4: RESULTS AND DISCUSSION		85
4.1	Structural properties of synthesized mixed oxide catalysts	85
4.1.1	Structural properties of synthesized Cu-Ti mixed oxide catalysts	85
4.1.1.1	Thermogravimetric analysis (TGA/DTG).....	85
4.1.1.2	Crystal phase and crystallinity (XRD)	86
4.1.1.3	Raman analysis.....	87
4.1.1.4	Textural properties (BET).....	89

4.1.1.5	Surface composition and oxidation state (XPS).....	90
4.1.1.6	Redox properties (H ₂ -TPR and O ₂ -TPD)	92
4.1.1.7	Morphology.....	94
4.1.2	Structural properties of Cu-Zr mixed oxide catalysts.....	98
4.1.2.1	Thermogravimetric analysis (TGA/DTG)	98
4.1.2.2	Crystal phase and crystallinity (XRD)	99
4.1.2.3	Raman analysis.....	100
4.1.2.4	Textural properties (BET).....	101
4.1.2.5	Morphology analysis	103
4.1.2.6	Surface composition and oxidation state (XPS).....	106
4.1.2.7	Redox properties (H ₂ -TPR and O ₂ -TPD)	108
4.1.3	Structural properties of Cu-Mn mixed oxide catalysts	110
4.1.3.1	Thermogravimetric analysis (TGA/DTG)	110
4.1.3.2	Crystal phase and crystallinity (XRD)	111
4.1.3.3	Surface composition and oxidation state (XPS).....	112
4.1.3.4	Morphology.....	115
4.1.3.5	Redox properties (H ₂ -TPR and O ₂ -TPD)	118
4.1.4	Structural properties of Ce-2Ti mixed oxide catalyst.....	121
4.1.4.1	Crystal phase and crystallinity (XRD)	121
4.1.4.2	Raman analysis.....	123
4.1.4.3	Surface composition and oxidation state (XPS).....	125
4.1.4.4	Morphology.....	127
4.1.4.5	Textural properties (BET).....	129
4.1.4.6	Redox properties (H ₂ -TPR and O ₂ -TPD)	130
4.1.5	Structural properties of Fe-2Ti mixed oxide catalyst	131
4.1.5.1	Crystal phase and crystallinity (XRD)	131

4.1.5.2	Raman analysis.....	132
4.1.5.3	Surface composition and oxidation state (XPS).....	133
4.1.5.4	Redox properties (H ₂ -TPR and O ₂ -TPD)	136
4.1.5.5	Morphology.....	137
4.1.5.6	Textural properties (BET).....	138
4.2	Catalytic activity assessment.....	139
4.2.1	Cu-Ti mixed oxide catalysts.....	139
4.2.1.1	Oxidation under H ₂ O ₂ by Cu-2Ti mixed oxide catalysts	139
4.2.1.2	Oxidation under air by Cu-2Ti mixed oxide catalysts.....	146
4.2.2	Catalytic activity of Cu-Zr mixed oxide catalysts	150
4.2.2.1	Oxidation under H ₂ O ₂ by Cu-Zr mixed oxide catalysts	150
4.2.2.2	Oxidation under air by Cu-2Zr mixed oxide catalysts	156
4.2.3	Catalytic evaluation of Cu-Mn mixed oxide catalyst	160
4.2.3.1	Oxidation under H ₂ O ₂ by Cu-Mn mixed oxide catalysts	160
4.2.3.2	Oxidation under air by Cu-Mn mixed oxide catalysts.....	165
4.2.4	Catalytic performance of Ce-2Ti mixed oxide catalyst	168
4.2.4.1	Oxidation under H ₂ O ₂ by Ce-2Ti mixed oxide catalyst	168
4.2.4.2	Oxidation under air by Ce-2Ti mixed oxide catalyst	173
4.2.5	Catalytic activity measurement of Fe-2Ti mixed oxide catalyst.....	176
4.2.5.1	Oxidation under H ₂ O ₂ by Fe-2Ti mixed oxide catalyst.....	176
4.2.5.2	Oxidation under air by Fe-2Ti mixed oxide catalyst.....	180
4.3	Comparison of overall catalytic activity of synthesized mixed oxides catalysts	183
4.4	Reaction mechanism of vanillyl alcohol oxidation over synthesized mixed oxide catalysts.....	185
4.4.1	Possible reaction mechanism of vanillyl alcohol transformation under H ₂ O ₂	185

4.4.2 Postulated reaction mechanism of vanillyl alcohol conversion using air as oxidant.....	187
--	-----

CHAPTER 5: CONCLUSION AND RECOMMENDATION..... 189

5.1 Conclusion.....	189
---------------------	-----

5.2 Recommendations	190
---------------------------	-----

REFERENCES	192
------------------	-----

List of Publications and Papers Presented	226
---	-----

Appendix.....	229
---------------	-----

University of Malaya

LIST OF FIGURES

Figure 1.1: A schematic diagram showing free energy profile diagram courses of a hypothetical chemical reaction	23
Figure 1.2: Percentage of lignin in different woods.	27
Figure 1.3: Representation of structure of lignin showing monomeric units.....	28
Figure 1.4: Modification approaches of lignin valorization.....	30
Figure 1.5: Applications of lignin.....	31
Figure 2.1: Oxidation of lignin using different techniques (Behling et al., 2016).	35
Figure 2.2: Classification of oxidation process.	36
Figure 2.3: Oxygen activation on the surface of heterogeneous catalysts (a) Through chemisorption (b) By replenishing consumed lattice oxygen (Weckhuysen & Keller, 2003).	38
Figure 2.4: Lignin activation in acidic and alkaline media.	40
Figure 2.5: Oxygen reaction in oxidizing lignin A) stepwise electron adsorption of oxygen to reactive species; B) combined reaction mechanism for all reactive oxidation species during oxygen oxidation of lignin.	42
Figure 2.6: Some examples of selected model compounds of lignin (monomeric units).	59
Figure 2.7: Two conventional methods of vanillin preparation.	59
Figure 2.8: Metal-Oxygen species.	63
Figure 2.9: Metal initiated and mediated oxidation.....	64
Figure 2.10: Direct homolytic oxidation of benzylic compounds.....	65
Figure 2.11: Wacker oxidation of Alkenes.	65
Figure 2.12: Mars-Van Krevelen mechanism.	66
Figure 2.13: Catalytic oxygen transfer process over catalysts.	66
Figure 2.14: Peroxometal versus oxometal pathway.	67
Figure 3.1: Research approach (flow chart).....	72

Figure 3.2: Oxidation of vanillyl alcohol using air and H ₂ O ₂ oxidants over mixed oxide catalyst.	83
Figure 4.1: Synthesized Cu-Ti mixed oxide catalysts illustrating TGA/ DTG spectrum (left); XRD analysis (right).	85
Figure 4.2: Raman analysis of synthesized Cu-Ti mixed oxide catalysts.....	88
Figure 4.3: N ₂ adsorption-desorption curve of synthesized Cu-Ti mixed oxide catalysts (a) Cu: 2Ti; (b) Cu: Ti; (c) 2Cu: Ti.....	89
Figure 4.4: XPS analysis of synthesized Cu-2Ti mixed oxide catalyst. (a) Cu 2p; (b) Ti 2p; (c) O 1s.....	92
Figure 4.5: Synthesized Cu-Ti mixed oxide catalysts illustrating (a) H ₂ -TPR analysis (b) O ₂ -TPD analysis.	93
Figure 4.6: FESEM analysis of synthesized Cu-Ti mixed oxide catalysts (a) Cu: 2Ti; (b) Cu:Ti; (c) 2Cu:Ti; (d) spent catalyst.....	96
Figure 4.7: HRTEM and SAED pattern of synthesized Cu-2Ti mixed oxide catalyst. (a) Overview of the catalyst; (b) rhombohedral shape; (c) lattice fringe; (d) SAED pattern.	97
Figure 4.8 EDX analysis of synthesized Cu-Ti mixed oxide catalysts. (a) Cu: 2Ti; (b) Cu: Ti; (c) 2Cu: Ti (d) spent catalysts.	97
Figure 4.9: Chemical mapping of synthesized Cu-2Ti mixed oxide catalyst (a) elemental distribution; (b) Ti distribution; (c) O distribution (d) Cu distribution.....	98
Figure 4.10: Synthesized Cu-Zr mixed oxide catalysts illustrating TGA/DTG analysis (left); XRD analysis (right).	99
Figure 4.11: Raman analysis of synthesized Cu-Zr mixed oxide catalysts.	101
Figure 4.12: N ₂ adsorption –desorption curve of synthesized Cu-Zr mixed oxide catalysts. (a) Cu: Zr; (b) Cu: 2Zr; (c) 2Cu: Zr; (d) Spent catalyst.	102
Figure 4.13: FESEM analysis of synthesized Cu-Zr mixed oxide catalysts. (a) Cu: Zr; (b) Cu: 2Zr; (c) 2Cu: Zr; (d) Spent catalyst.	103
Figure 4.14: HRTEM and SAED pattern of Cu-Zr (Cu: 2Zr) mixed oxide catalyst. (a) Overview; (b) lattice fringe; (c) lattice size; (e) grain boundary.	105
Figure 4.15: EDX pattern of synthesized Cu-Zr mixed oxide catalysts (a) Cu: Zr; (b) Cu: 2Zr; (c) 2Cu: Zr; (d) Spent catalyst.	106

Figure 4.16: XPS analysis of synthesized Cu-2Zr mixed oxide catalyst. (a) wide scan; (b) Zr 3d; (c) O 1s; (d) Cu 2p.....	108
Figure 4.17: Synthesized Cu-Zr mixed oxide catalysts illustrating H ₂ -TPR (left); O ₂ -TPD analysis (right).	110
Figure 4.18: Synthesized Cu-Mn mixed oxide catalysts illustrating, TGA-DTG curve (left); XRD analysis (right).	111
Figure 4.19: XPS analysis of Cu-Mn (Cu: Mn) mixed oxide catalysts. (a) wide spectra; (b) Cu 2p; (c) O 1s; (d) Mn 3s.....	115
Figure 4.20: FESEM analysis of synthesized Cu-Mn mixed oxide catalysts. (a) Cu: Mn; (b) Cu: 2Mn; (c) 2Cu: Mn; (d) spent catalyst.....	116
Figure 4.21: HRTEM and SAED analysis of synthesized Cu: Mn mixed oxide catalysts. (a) lattice size; (b) lattice parameter; (c) grain boundary; (d) SAED pattern.....	117
Figure 4.22: EDX and chemical mapping of synthesized Cu-Mn mixed oxide catalysts. (a) Cu: Mn; (b) Cu: 2Mn; (c) 2Cu: Mn; (d) elemental mapping; (e) Cu distribution; (f) Mn distribution; (g) O distribution.	118
Figure 4.23: Synthesized Cu-Mn mixed oxide catalysts, H ₂ -TPR analysis (left); O ₂ -TPD analysis (right).	120
Figure 4.24: XRD analysis of Ce-2Ti mixed oxide catalyst.	123
Figure 4.25: Raman analysis of synthesized Ce-2Ti mixed oxide catalyst.	125
Figure 4.26: XPS analysis of synthesized Ce-2Ti mixed oxide catalyst. (a) Wide scan; (b) Ti 2p; (c) Ce 3d; (d) O 1s.	126
Figure 4.27: FESEM and EDX analysis of synthesized Ce-2Ti mixed oxide catalyst. (a) Fresh Ce-2Ti catalyst; (b) spent catalyst; (c) EDX pattern; (d) chemical mapping; (e) Ce distribution (f) Ti distribution.....	128
Figure 4.28: HRTEM and SAED analysis of synthesized Ce-2Ti mixed oxide catalyst. (a) Lattice parameters; (b) SAED pattern.....	129
Figure 4.29: N ₂ adsorption-desorption curve of Ce-2Ti mixed oxide catalyst.	130
Figure 4.30: Synthesized Ce-2Ti mixed oxide catalyst illustrating, H ₂ -TPR analysis (left); O ₂ -TPD analysis.	131
Figure 4.31: XRD analysis of Fe-2Ti mixed oxide catalyst.....	132
Figure 4.32: Raman spectra of synthesized Fe-2Ti mixed oxide catalyst.	133

Figure 4.33: XPS spectra of synthesized Fe-2Ti mixed oxide catalyst. (a) Survey spectra; (b) O 1s spectra; (c) Fe 2p ³ spectra; (d) Ti 2p spectra.	135
Figure 4.34: Synthesized Fe-2Ti mixed oxide catalyst illustrating, (a) H ₂ -TPR analysis; (b) O ₂ -TPD analysis.....	136
Figure 4.35: Morphology of synthesized Fe-2Ti mixed oxide catalyst. (a) FESEM image (b) EDX pattern.	137
Figure 4.36: HRTEM images of Fe-2Ti mixed oxide catalyst. (a) Overview of the catalyst; (b) SAED pattern; (c) lattice pattern.....	138
Figure 4.37: N ₂ - adsorption-desorption isotherm plot of synthesized Fe-2Ti mixed oxide catalyst.	139
Figure 4.38: Effect of reaction parameters in oxidation of vanillyl alcohol by Cu-Ti (Cu: 2Ti) mixed oxide catalyst using H ₂ O ₂ (a) progress of reaction; (b) concentration of H ₂ O ₂ ; (c) catalyst mass (d) temperature.....	140
Figure 4.39: Effect of catalyst composition (left); and influence of nature of solvents (right) in oxidation of vanillyl alcohol by Cu-Ti mixed oxide catalyst using H ₂ O ₂	143
Figure 4.40: Effect of base media (NaOH) in oxidation of vanillyl alcohol by Cu-2Ti mixed oxide catalyst using H ₂ O ₂ in oxidation of vanillyl alcohol.	146
Figure 4.41: Effect of reaction parameters in oxidation of vanillyl alcohol by Cu-Ti mixed oxide catalyst using air (a) progress of reaction; (b) catalyst mass; (c) temperature; (d) air pressure.	147
Figure 4.42: Recyclability study of Cu-Ti (Cu: 2Ti) mixed oxide catalyst in oxidation of vanillyl alcohol by using H ₂ O ₂ as an oxidant.....	149
Figure 4.43: Effect of reaction parameters in oxidation of vanillyl alcohol by Cu-Zr (Cu: 2Zr) mixed oxide catalyst using H ₂ O ₂ (a) progress of reaction; (b) catalyst mass; (c) concentration of H ₂ O ₂ ; (d) temperature.	151
Figure 4.44: Influence of nature of solvents (left); effect of catalyst compositions (right) in oxidation of vanillyl alcohol by Cu-Zr (Cu: 2Zr) mixed oxide catalyst using H ₂ O ₂	154
Figure 4.45: Influence of base reaction media over Cu-Zr (Cu: 2Zr) mixed oxide catalyst in oxidation of vanillyl alcohol.....	155
Figure 4.46: Effect of reaction parameters in oxidation of vanillyl alcohol by Cu-Zr (Cu: 2Zr) mixed oxide catalyst using air (a) progress of reaction; (b) catalyst mass; (c) temperature; (d) air pressure.....	157

Figure 4.47: Recyclability study of Cu-Zr (Cu: 2Zr) mixed oxide catalyst.....	159
Figure 4.48: Effect of reaction parameters in oxidation of vanillyl alcohol by Cu-Mn (Cu: Mn) mixed oxide catalyst using H ₂ O ₂ (a) progress of reaction; (b) catalyst mass; (c) concentration of H ₂ O ₂ ; (d) temperature.	163
Figure 4.49: Influence of nature of solvents (left); and effect of catalyst compositions (right) in oxidation of vanillyl alcohol by Cu-Mn (Cu: Mn) mixed oxide catalyst.....	164
Figure 4.50: Effect of reaction parameters in oxidation of vanillyl alcohol by Cu-Mn (Cu: Mn) mixed oxide catalyst using air (a) progress of reaction; (b) catalyst mass; (c) temperature; (d) air pressure.....	166
Figure 4.51: Recyclability study of Cu-Mn (Cu: Mn) mixed oxide catalyst in oxidation of vanillyl alcohol by using air as oxidant.	168
Figure 4.52: Effect of reaction parameters in oxidation of vanillyl alcohol by Ce-2Ti mixed oxide catalyst using H ₂ O ₂ (a) progress of reaction; (b) catalyst mass; (c) concentration of H ₂ O ₂ ; (d) temperature.	170
Figure 4.53: Influence of nature of solvents (left) and effect of base media (right) in oxidation of vanillyl alcohol by Ce-2Ti mixed oxide catalyst using H ₂ O ₂	172
Figure 4.54: Effect of reaction parameters in oxidation of vanillyl alcohol by Ce-Ti mixed oxide catalyst using air (a) progress of reaction; (b) catalyst mass; (c) temperature; (d) air pressure.	175
Figure 4.55: Stability study of Ce-2Ti mixed oxide catalysts in oxidation of vanillyl alcohol.....	175
Figure 4.56: Effect of reaction parameters in oxidation of vanillyl alcohol by Fe-2Ti mixed oxide catalyst using H ₂ O ₂ (a) progress of reaction; (b) catalyst mass; (c) concentration of H ₂ O ₂ ; (d) temperature.	178
Figure 4.57: Liquid phase oxidation of vanillyl alcohol using H ₂ O ₂ oxidant (a) effect of nature of solvent; (b) influence of base NaOH.....	179
Figure 4.58: Effect of reaction parameters in oxidation of vanillyl alcohol by Fe-2Ti mixed oxide catalyst using air (a) progress of reaction; (b) catalyst mass; (c) temperature; (d) air pressure.....	181
Figure 4.59: Reusability study of Fe-2Ti mixed oxide catalysts in aerobic oxidation of vanillyl alcohol.	183
Figure 4.60: NH ₃ -TPD analysis of synthesized catalysts.	185

Figure 4.61: Production of peroxo intermediates by Cu-2M (M=Ti & Zr) mixed oxide catalyst with H₂O₂..... 186

Figure 4.62: Catalytic transformation of vanillyl alcohol to vanillin over synthesized Cu/Ti mixed oxide catalysts..... 187

Figure 4.63: Possible reaction mechanism of aerobic oxidation of vanillyl alcohol over Cu-M (where M= Ti, Zr and Mn) mixed oxide catalyst..... 188

University of Malaya

LIST OF TABLES

Table 1.1 Comparison between homogeneous and heterogeneous catalysts.	24
Table 1.2: Global comparison of various characteristics of lignin extracted from different processes.(Lange, Decina, & Crestini, 2013).....	26
Table 2.1: Summary of oxidants used for lignin oxidation, reactive species, mechanisms and products.	46
Table 2.2: Economics of general oxidants used for oxidation reactions.	47
Table 2.3: Heterogeneous catalysts used for raw lignin oxidation.....	50
Table 2.4: List of heterogeneous catalysts used for lignin model compound oxidation	52
Table 3.1: Cu based mixed oxide catalysts (Cu: M, M= Ti, Zr, and Mn)	68
Table 3.2: List of Characterization techniques used.....	69
Table 3.3: List of equipments and consumables used in this study.....	73
Table 3.4: The composition of metal precursor's in the synthesis method.....	75
Table 4.1: Textural properties of synthesized Cu-Ti mixed oxide catalysts.....	90
Table 4.2: Textural properties of synthesized Cu-Zr mixed oxide catalysts.....	102
Table 4.3: Surface composition of synthesized Cu-2Zr mixed oxide catalyst from XPS wide scan.....	108
Table 4.4: The surface composition of mixed oxide catalyst Cu: Mn from XPS wide scan.	114
Table 4.5: The area percentage of oxygen species from O 1s spectra.....	114
Table 4.6: The surface composition of Ce-2Ti mixed oxide catalysts from XPS survey spectra.	127
Table 4.7: The area percentage of oxygen species from O 1s XPS spectra.....	127
Table 4.8: The surface elemental ration of Fe-2Ti mixed oxide catalysts in XPS survey spectra.	135
Table 4.9: The area percentage of oxygen (O) species based on O 1s XPS spectra.	135

Table 4.10: Overall comparison of performance by synthesized mixed oxide catalysts.
..... 184

University of Malaya

LIST OF SYMBOLS AND ABBREVIATIONS

VA	:	Vanillyl alcohol
ZrO ₂	:	Zirconium (IV) Oxide
Fe ₂ O ₃	:	Iron (III) oxide
etc	:	And so forth
Å	:	Angstrom
a.u	:	Arbitrary unit
Atm	:	Atmospheric
wt %	:	Weight percent
CeO ₂	:	Cerium (IV) Oxide
Θ	:	Bragg's angle
BET	:	Brunauer-Emmett-Teller
Da	:	Dalton
C	:	Carbon
H ₂ -TPR	:	Hydrogen Temperature Program Reduction
O ₂ -TPD	:	Oxygen Temperature Program Desorption
IUPAC	:	International Unit of Pure and Applied Chemistry
THF	:	Tetrahydrofuran
°C	:	Celsius
Mo	:	Molybdenum
CVD	:	Chemical vapor deposition
Cr	:	Chromium
Co	:	Cobalt
V	:	Vanadium
Cu	:	Copper

Fe	:	Ferrum
Ce	:	Cerium
e ⁻	:	Electron
eV	:	Electron Volt
EDX	:	Energy Dispersive X-Ray
EtOH	:	Ethanol
CAN	:	Acetonitrile
SA _{ext}	:	External Surface Area
FESEM	:	Field Emission Scanning Electron Microscopy
F	:	Fluorine
TFA	:	Trifluoroacetic Acid
DMF	:	Dimethylformamide
γ	:	Gamma
Au	:	Gold (Aurum)
RP	:	Reversed Phase
IPA	:	Isopropyl alcohol
HPLC	:	High Pressure Liquid Chromatograph
HR-TEM	:	High Resolution Transmission Electron Microscope
H	:	Hour
V	:	Volt
H ₂	:	Hydrogen
OH ⁻	:	Hydroxyl ion
·OH	:	Hydroxyl radical
cm ³	:	Centimetre cube
Fe ₂ O ₃	:	Iron (III) oxide
TMP	:	Thermo Mechanical Pulping

JCPDS	:	Joint Committee on Powder Diffraction Standards
DCA	:	Drain Cooler Approach
Mn	:	Manganese
MS	:	Mass Spectroscopy
LMWPC	:	Low Molecular Weight Phenolic Compound
Mn	:	Manganese
MHz	:	Mega Hertz
DMS	:	Dimethyl sulphide
mg/L	:	milligram per Liter
Min	:	Minute
N ₂	:	Nitrogen
e.g.	:	For example
Ph	:	Phenol
nm	:	nanometre
CPBA	:	Chloroperoxybenzoic acid
CBA	:	Chlorobenzoic acid
Pd	:	Palladium
Sr	:	Strontium
O ²⁻	:	Oxide
O ₂	:	Oxygen molecule
MCM	:	Mobil Crystalline Materials
SBA	:	Santa Barbara Amorphous
%	:	Percentage
O ₂ ²⁻	:	Peroxide
P	:	Phosphorus
KIT	:	Korean Institute of Technology

Pt	:	Platinum
pH	:	Potential of Hydrogen
H ⁺	:	Proton
BJH	:	Barret-Joyner-Halende method
TEOS	:	Tetraethylorthosilcate
rpm	:	rotation per minute
FWMH	:	Full Width Half Maxima
SAED	:	Selected Area Electron Diffraction
Ag	:	Silver (Argentum)
GDP	:	Gross Domestic Product.
S	:	Sulphur
O ₂ ⁻	:	Superoxide
·O ₂ ⁻	:	Superoxide anion radical
S.A	:	Surface Area
i.e.	:	That is
TGA	:	Thermogravimetric Analysis
BTX	:	Benzene Toluene Xylene
Ti	:	Titanium
TiO ₂	:	Titanium dioxide
TTIP	:	Titanium isopropoxide
\$:	US Dollar
UV	:	Ultraviolet
Ac	:	Acetone
V	:	Vanadium
WO ₃	:	Tungsten trioxide
H ₂ O	:	Water

W	:	Watt
λ	:	Wavelength
Wt %	:	Weight percent
DMSO	:	Dimethyl sulphoxide
XRD	:	X-Ray Diffraction
XPS	:	X-ray Photoelectron Spectroscopy

University of Malaya

CHAPTER 1: INTRODUCTION

1.1 State of art

The exploitation and advancement of renewable energy sources towards a sustainable energy assurance for the future has drawn a great attention to reduce dependency on under earthed fossil based resources, since the reserve of fossil-based resources is markedly reducing with time. Hence dependency on fossil based resources is no longer reasonable in view of viable, eco-friendly and socio-economic purposes. Many renewable resources such as biomass, geothermal, wind and solar based techniques are under ongoing research. A few protocols were successfully developed and effectively implemented in order to replace fossil-dependent energy production. Biomass is considered as the best suitable and strategic alternative resource to invent technologies for energy production (Holladay, White, Bozell, & Johnson, 2007; Werpy et al., 2004). Biomass is one of the most available and renewable resource, and thus taken into account as a versatile replacement to explore the possibilities to adapt new strategies in versatile applications including energy production. Biomass derived fuels from biomass-refinery processes are already substituting fossil-based fuels in our day-to-day life. And also, the biomass components and derivatives are being used as important platform chemicals and substrates in multipurpose chemical industries that produces higher value-added products, ranging from pharmaceutical applications to polymer industries. However, the gross use is still in fledging stages (Aresta, Dibenedetto, & Dumeignil, 2012).

1.2 Catalysis

During early nineteenth century, a few scientific groups claimed observation regarding particular substances which accelerate chemical reaction without being consumed at the end of the reactions. The conversion of starch into glucose (Kirchhoff, 1811) or decomposition of ammonia on metal surface (Robertson, 1975) are such examples of catalytic chemical reactions. Jons Jacobs Berzelius introduced the term “Catalysis” first

ever in the history and also explained the phenomenon. Berzelius introduced the term “Catalysis” in his scientific report to Swedish Academy of Science in 1835 and proposed as a classification (Berzelius & Wöhler, 1936). After him, throughout the rest nineteenth century, the term remained as a topic of debate. However, W. Ostwald explained the phenomenon in view of chemical kinetics and defined it as “a catalyst is a substance which affects the rate of a chemical reaction without being part of its end products” (Ostwald, 1923). Now, the term catalyst is defined by IUPAC as “a substance that increases the rate of a reaction without modifying the overall standard Gibbs energy change in the reaction” (McNaught & McNaught, 1997). Now-a-days, in industrial prospect, catalysis is an important platform to reduce the reaction time and enrich the productivity with higher selectivity to targeted product. As it remained unchanged after the catalytic reaction, it can be reused several times.

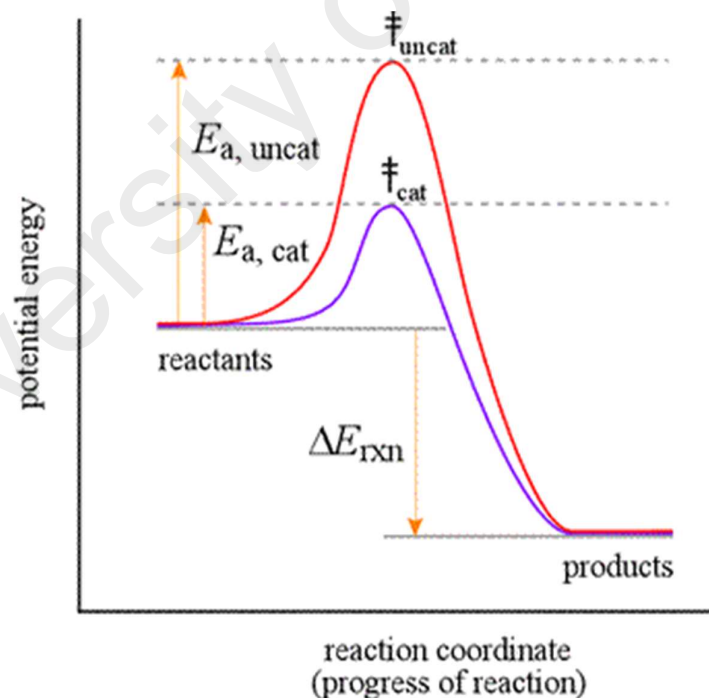


Figure 1.1: A schematic diagram showing free energy profile diagram courses of a hypothetical chemical reaction

Catalysts can be classified into two classes (i) homogeneous catalysts, the catalyst remains in the same phase as the reactant (ii) heterogeneous catalysts, the catalyst which is different from the reactant phase (typically solid/liquid/gas, solid/liquid or solid/gas). The comparison between homogeneous catalysts and heterogeneous catalysts are shown in Table 1.1.

Table 1.1 Comparison between homogeneous and heterogeneous catalysts.

Feature	Homogeneous	Heterogeneous
Form	Metal complex	Solid often metal or metal complex
Activity	high	Variable
Selectivity	high	Variable
Average time life	variable	Long
Reaction conditions	mild	Drastic
Recycling	difficult	Easy
Problems of diffusion	none	Possible
Sensitivity to poison	low	High
Separation from products	difficult	Easy
Intelligibility of the mechanism	possible	Difficult
Variation of steric and electronic feature	possible	Difficult

The key benefit of using homogeneous catalyst in a chemical reaction is that the active sites are well separated likewise enzymes and have similarities to one another which facilitates the interaction between the reactants and active sites.

However, to obey the principles of sustainable and green chemistry, development of heterogeneous catalysts is very crucial as they potentially meet the objectives of sustainable industrial process (Centi & Perathoner, 2003). Recyclability, long life and easy separation techniques are the major advantages of a heterogeneous catalytic system that are potential parameters to cut the cost of an industrial product cost and also causing no harms to the environment. Catalysts are well connected to 90 % chemical

manufacturing process as well as our daily life. Catalysts contribute around 35 % of the world gross domestic product (GDP) (Armor, 2011). The earlier focus of an industrial process was to accelerate the kinetics of a reaction. However, the current goals of a sustainable industrial process is not only to promote high amount yield but also to avoid the side reactions to minimize the production of undesired products which involved costly separation processes (Somorjai & Kliewer, 2009; Zaera, 2002). Many industrial manufacturing processes depend on chemical reactions like Hydroalkylation, Polymerization, Isomerization, Oxidation, Hydrogenation, Etherification, Oligomerization, Esterification, Condensation, and Hydration where catalyst plays a vital role. This aim of this study is to develop potential heterogeneous catalyst in application of oxidation reactions.

1.3 Lignin

Three major constituents such as cellulose, hemicellulose, and lignin form biomass of higher (vascular) plants. The portion of each of these components differs depending on the origin of the biomass (Ek, Gellerstedt, & Henriksson, 2009; Welker et al., 2015). Lignin is a macromolecular component of wood that is composed of phenolic propylbenzene skeletal units. The skeletal units are linked at various sites randomly (McNaught & Wilkinson, 1997). Lignin acts as a glue in between layers of cell, which form an amorphous matrix together with hemicelluloses, and in between cellulose fibrils are embedded. After cellulose, lignin (from Latin *lignum*—wood, timber) is the second most abundant terrestrial organic matter on Earth. Depending on the type of plants and its organ, the abundance of lignin content varies. The broad variations of lignin content in different type of woods is determined e.g., it makes up 9 to 23 weight percent (wt %) in hardwoodⁱⁱⁱ and 25-30 wt % in softwoodⁱⁱ (Sixta et al., 2013). For grasses, the amount is in range of 10 to 30 wt %. The most lignin content is located at the protective tissues of plants, like nut shells, which contain from 30 to 40 wt % (Sun & Cheng, 2002). Vice

versa, the presence of lignin content is almost zero in soft tissues such as cotton seed hairs and leaves. The lignin content was determined by wood structural arrangement at a cellular level. It was found that the highest lignin concentration is in the middle lamella and the cell wall (about 25 wt %). Different types of lignin and their characteristics processed via various are illustrated in Table 1.2.

Table 1.2: Global comparison of various characteristics of lignin extracted from different processes.(Lange, Decina, & Crestini, 2013)

Type of lignin	Number-average Molecular weight [Da]	Polydispersity	Properties compared to native form
Kraft lignin	1000-3000	2-4	Soluble in alkali solution and highly in polar organic solvents. Increase of 5-5 inter subunit linkages, new functional group and linkages, low sulfur content, 70-75 % of the hydroxyl groups could be sulfonated.
Lignosulfonate lignin	36000-61000 (softwood) 5700-12000 (hardwood)	4-9	Soluble in acidic and basic aqueous solutions, highly in polar organic solvents and amines. High molecular weight. Incorporation of sulfonate groups on the arenas.
Organosolv lignin	> 1000	2.4-6.4	Soluble in organic solvents. Increased amount of phenolic hydroxyl groups. Very low Sulfur content. High purity.
Pyrolytic lignin	300-600	2.0-2.2	Soluble in organic solvents, but poorly soluble in water. C8 basic unit skeleton (rather than C9 derived oligomers), lower average molecular weight, very frequent C-C inter subunit linkages.
Steam-explosion lignin	1100-2300	1.5-2.8	High content of phenolic hydroxyl groups. Lower content of methoxy groups. Frequent C-C inter-subunit linkages.
Acidolysis lignin	About 2000	3	Few carbohydrate impurities. Low molecular weight. Increased amount of hydroxyl groups. Lower content of ether and ester linkages.

However, besides plants species, many other parameters such as climate, stresses caused by the weather and pests, soil characteristics and age of tress also governs the lignin concentration in a plant (Moura, Bonine, De Oliveira Fernandes Viana, Dornelas, & Mazzafera, 2010; Rencoret et al., 2010). The percentage of lignin amount in different woods are summarized in Fig. 1.2.

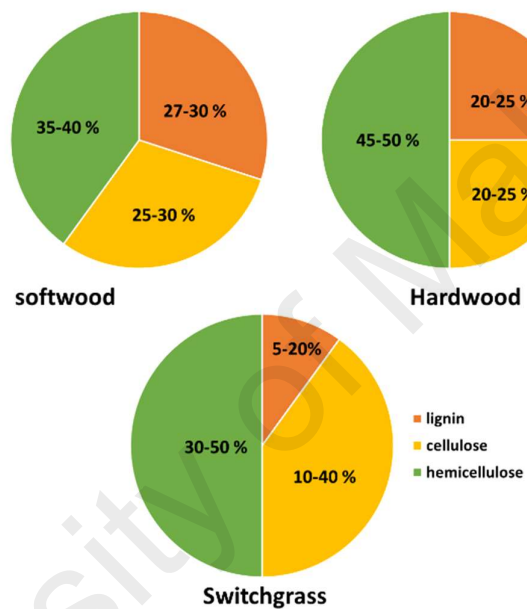


Figure 1.2: Percentage of lignin in different woods.

1.3.1 Structure of lignin

Lignin structure is a complex compound and mainly contains three simple molecular units sinapyl alcohol, coniferyl alcohol, *p*-coumaryl alcohol (Chatel & Rogers, 2013). The structure of lignin with the simple molecular fragments is shown in Fig. 1.3. Also, a detailed reviewd was made on structure of lignin in previous literatures which summarized the lignin and its monomeric units (Joseph et al., 2015).

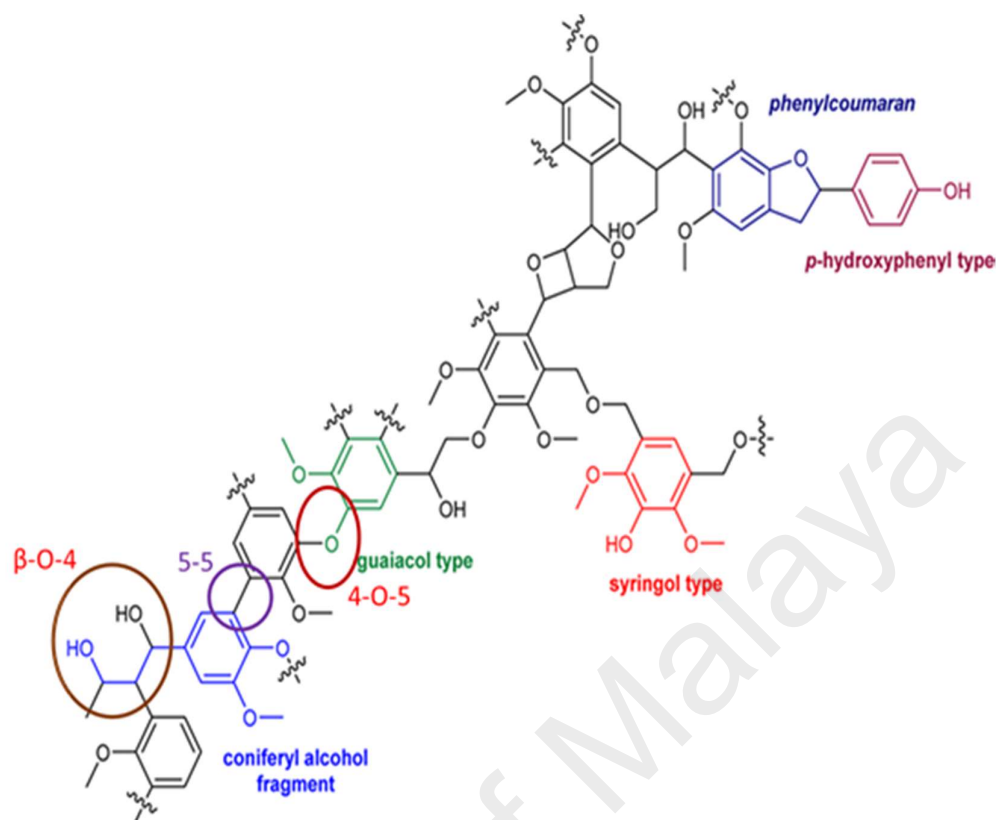


Figure 1.3: Representation of structure of lignin showing monomeric units.

1.3.2 Importance of lignin modifications

Lignocellulosic biorefinery receives a large quantity of lignin for conversion into value added products. Thus, development of a sustainable, efficient and cost friendly protocol to upgrade lignin as a potential source for production of energy as well as platform chemicals in multi purpose chemical industries. Noteworthy, lignin is the only reliable renewable source for synthesis of aromatic fine chemicals (Bozell, Hames, & Dimmel, 1995; Bozell, Hoberg, & Dimmel, 2000; Dimmel, Bozell, Von Oepen, & Savidakis, 2002). And also, lignin can be converted to discrete molecules with low molecular weight by adapting direct and efficient strategic conversion technique. These molecular units from lignin can be potentially used as monomeric building blocks in polymer industries which is a very promising future scope of lignin valorization. . The selective and controlled breaking of carbon–oxygen and carbon–carbon bond cleavage in lignin via

depolymerisation can produce a whole variety of monomeric, aromatic species with different functionalities (Bozell et al., 1995). Moreover, new types of building blocks for polymer industries can be yield from selective bond cleavage in lignin relying on technologies (De Menezes, Pasquini, Curvelo, & Gandini, 2007; Sannigrahi, Pu, & Ragauskas, 2010). In addition, selective upgradation of lignin polymer itself is a suitable pathway to transform it into a structural base for complex co-polymers with various potential applications (Bozell, Hoberg, & Dimmel, 1998). Lignin-derived chemicals has also potential applications to be used as building blocks for the fabrication of microcapsules, or another scope is investigation on the antioxidant features of the polyphenolic structural unit of lignin (Salanti, Zoia, Orlandi, Zanini, & Elegir, 2010). The currently available potential applications of lignin are summarized in Fig. 1.5. Several group of researchers focused on covering present research on lignin, its future aspects, and on technologies developed to valorize lignin. Various methods were adapted till date to valorize lignin ranging from classical chemical approaches such as pyrolysis (thermolysis) (Acharya, Sule, & Dutta, 2012; Brebu & Vasile, 2010; Mohan, Pittman, & Steele, 2006; Pandey & Kim, 2011), hydrolysis (Sun & Cheng, 2002; Van Dyk & Pletschke, 2012), reduction(hydrogenolysis) (Eachus & Dence, 1975; Lange et al., 2013; Son & Toste, 2010), oxidation using catalysts (Argyropoulos, 2001; Crestini, Crucianelli, Orlandi, & Saladino, 2010), to newer biotechnological approaches such as usage of enzymatic catalytic process (Van Dyk & Pletschke, 2012). Currently available modification approaches of lignin and their outcome studied in previous literatures are summarized in Fig. 1.4.

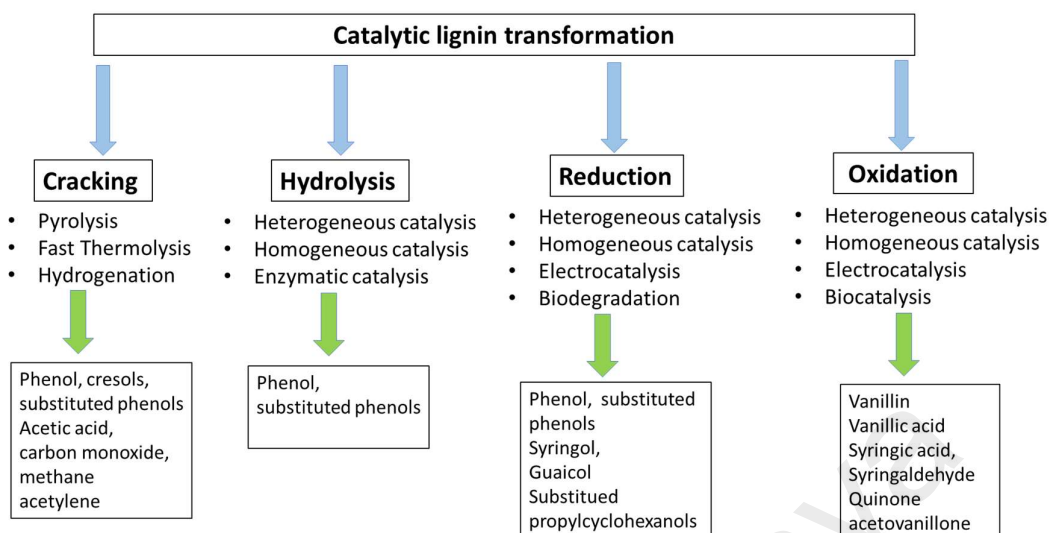


Figure 1.4: Modification approaches of lignin valorization.

However pulp and paper industries obtain Kraft and lignosulfonates burning almost 98% of lignin as a source of energy (Lora & Glasser, 2002; Thielemans, Can, Morye, & Wool, 2002). Nowadays, the global markets for lignin products emphasis mainly on low value products (Stewart, 2008) such as dispersing, binding, or emulsifying agents (Xu, Yang, Mao, & Yun, 2011), low-grade fuel (Piskorz, Majerski, Radlein, & Scott, 1989; Thring, Katikaneni, & Bakhshi, 2000), phenolic resins (Cetin & Özmen, 2002), carbon fibers (Braun, Holtman, & Kadla, 2005; Kadla et al., 2002), wood panel products (Vazquez, Rodríguez-Bona, Freire, Gonzalez-Alvarez, & Antorrena, 1999), automotive brakes, epoxy resins for printed circuit boards (Lora & Glasser, 2002), polyurethane foams (Hatakeyama, Kosugi, & Hatakeyama, 2008) and thus remain limited use. Hence, extensive researches are required for exploitation of new technologies and strategies to extend the lignin valorization to high value added applications. Application scopes of lignin valorization are shown in Fig 1.5.

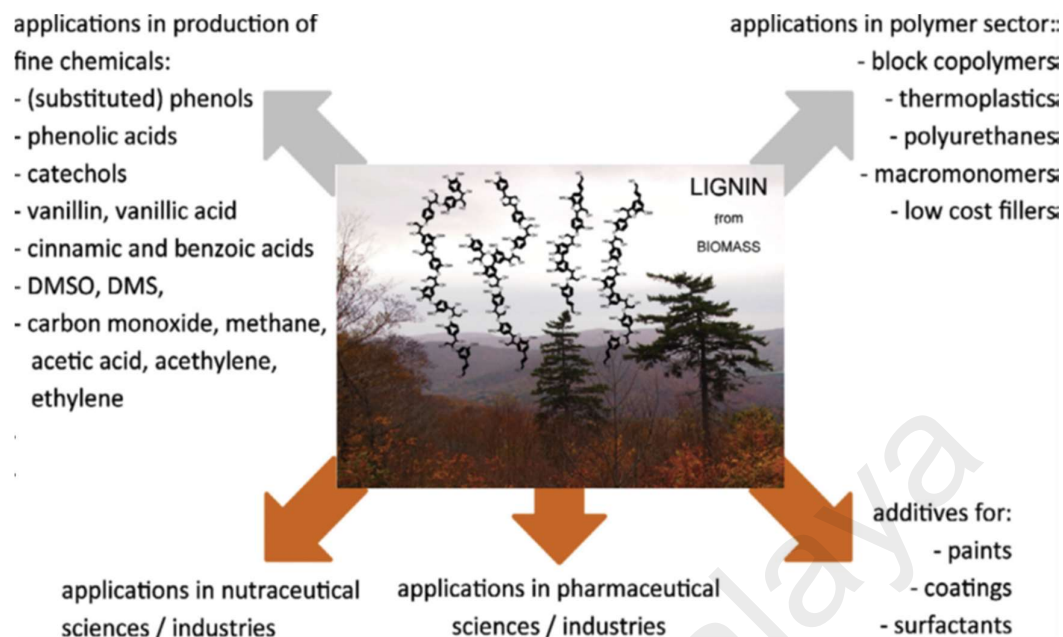


Figure 1.5: Applications of lignin.

1.3.3 Oxidation as the modification approach

Among the available modification techniques of lignin valorization, oxidation is one of the viable as well as cost effective route. Hydrolysis and reduction of lignin causes disruption to the lignin structure or removal of chemical functionalities. As a result, it is not viable to use as platform chemicals or starting materials in Bio-refinery, or petrochemicals, pharmaceutical industries. On contrary, oxidative route of lignin modifications tend to form more complicated platform chemicals with additional functionalities (Behling, Valange, & Chatel, 2016). And also, oxidation process offers direct conversion of lignin into target products with easy separation technique like filtration (Collinson & Thielemans, 2010).

1.3.4 Problem statement of lignin oxidation

Lignin valorization is considered a vital challenge in the biorefinery area due to complexity associated with its transformation (Fellows, Brown, & Doherty, 2011; Klein-Marcuschamer, Oleskowicz-Popiel, Simmons, & Blanch, 2010). The major

challenges of valorizing lignin included, (1) lignin has very much complex polymeric structure with its structure and composition vary depend on the properties of the wood species and several other parameters such as season, weather (Cherubini & Strømman, 2011); (2) the complex structure is chemically stable and its propensity to transform required harsh reaction conditions to modify or break down the polymers; (3) lower cost processes are available for petroleum derived raw materials in stead of lignin for production of plastics or polymers. Therefore, designing lignin valorization technique to high volume aromatic via a cost effective process can potentially reduce the dependency on petroleum derivatives.

1.4 Research Objectives

The main research focus of this study is to synthesis mixed oxide catalysts via newly developed one pot solvent evaporation technique for liquid phase oxidation of vanillyl alcohol (a lignin model compound) by using different environmentally benign oxidants such as air and H₂O₂. The general objectives are:

1. Design and synthesis of transitional metal based mixed oxide catalysts via developed one pot solvent evaporation method.
2. Catalytic evaluation of synthesized mixed oxide catalysts in liquid phase oxidation of vanillyl alcohol (a lignin model compound) using two different oxidants (air and H₂O₂) and investigation of suitable reaction conditions.

Research novelty of this study is to prepare mixed oxide catalysts via newly developed one pot solvent evaporation technique. And also, pioneering investigation of synthesized mixed oxides in application of liquid phase oxidation of vanillyl alcohol (a lignin model compound).

1.4.1 Specific research objectives

- I. To develop an effective method to synthesize mixed oxide catalysts.
- II. To evaluate the catalytic activity of prepared mixed oxide catalysts in liquid phase oxidation of vanillyl alcohol (a lignin model compound)
- III. To make a comparison study of two different oxidants such as air and H₂O₂ in liquid phase oxidation of vanillyl alcohol as a lignin model compound.
- IV. To investigate the optimum reaction parameters for liquid phase oxidation of vanillyl alcohol (a lignin model compound) under mediation of both oxidants air and H₂O₂.
- V. To propose a reaction mechanism for transformation of vanillyl alcohol over the catalyst surface of synthesized mixed oxide catalysts.

1.5 Thesis organization

The thesis consisted five (5) chapters namely, (1) Introduction; (2) Literature review; (3) Methodology; (4) Results and discussion; and (5) Conclusion.

Chapter 1 covers the basic concept describing the importance of renewable feedstocks for the sustainable future, lignin as a renewable feedstock, its structure, application of lignin oxidative products, and available modification approaches of lignin and oxidation as the sustainable modification approach. Also, it clearly stated the current problems associated with lignin oxidation in bio-refineries. The research objectives are also stated in this part.

Chapter 2 consisted a brief description on previously studied technologies in literatures for oxidation of lignin and associated problems. The common oxidants practiced in oxidation reaction and also in lignin transformation were listed with their details. And also, it summarizes a wide variety of catalysts previously investigated for lignin oxidation.

Chapter 3 embodied the methodology adapted to complete the scope of work and research goals. The preparation method of mixed oxide catalysts with different metals loading and their compositions was discussed in details. In addition, the characterization techniques, background of the analytical tools, and sample preparation procedures were described. Moreover, the reaction set up and the product analysis procedure were also stated clearly.

Chapter 4 contained results and discussions on the physiochemical properties of synthesized mixed oxide catalysts examined by using various spectroscopic analytical tool. The physiochemical properties of mixed oxide catalysts were presented in this thesis under section 4.1 for Cu-Ti mixed oxide catalysts, section 4.2 for Cu-Zr mixed oxide catalysts, section 4.3 for Cu-Mn mixed oxide catalysts, 4.4 for Ce-2Ti mixed oxide catalyst, and section 4.5 for Fe-2Ti mixed oxide catalyst. The catalytic activity measurement of synthesized catalysts were described in thesis section 4.6.

Chapter 5 summarized the research findings and addressed the research goals. From the comparison of catalytic activity of all synthesized mixed oxide catalysts, the best performed mixed oxide catalyst was concluded. Also, the future scopes of this research study was included in this section.

CHAPTER 2: LITERATURE REVIEW

Oxidation of lignin was performed in adopting many innovative strategies displayed in Fig. 2.1 (Behling et al., 2016). They can be classified in two categories. One is classified as conventional methods and the second one is unconventional methods. The conventional methods involved usage of catalytic systems in conventional solvents with the presence of eco- friendly oxidants. The unconventional methods are usage of different source of mechanistic energy or unconventional solvents media such as using of ionic liquids. Therefore, both conventional and unconventional methods were discussed in this study.

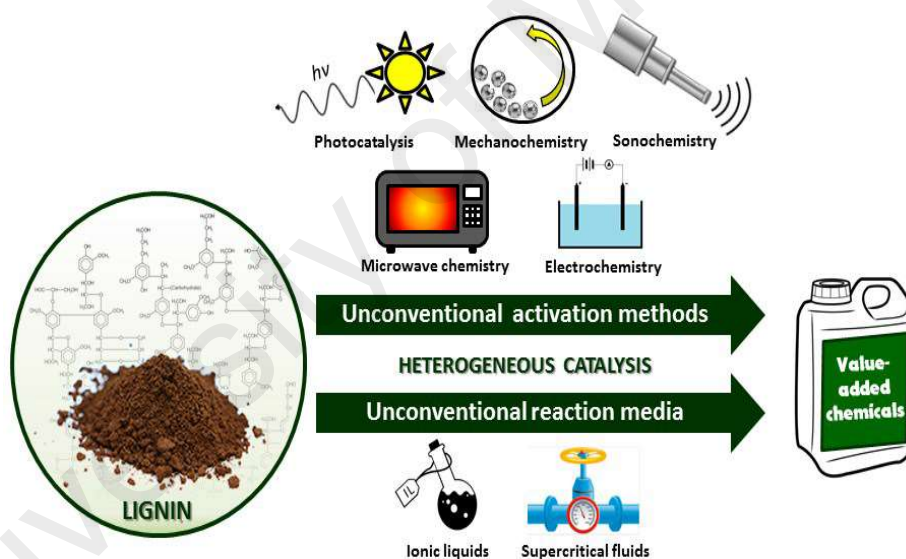


Figure 2.1: Oxidation of lignin using different techniques (Behling et al., 2016).

2.1 Lignin isolation

Biomass fractionation is the first and vital step for lignin isolation from the rest of lignocellulosic biomass. This isolation process from the lignocellulosic biomass strongly control the properties and structure of the lignin (Bouxin et al., 2015). Mainly four isolation methods are available such as Kraft, Soda, the Sulphite and Organosolv.

Worldwide gross production of lignin via Organosolve lignin isolation process is 40-50 million tons annually (Strassberger, Tanase, & Rothenberg; Zoia, Salanti, Frigerio, & Orlandi, 2014). The aim of isolation was to separate the lignin matrix from the cellulosic part via breaking the bonds between lignin and polysaccharides. And also, this process facilitates to increase the solubility of lignin (Crocker, 2010). Two type of reactions generally occurs during lignin fraction process. One is electrophilic reaction (delignifying reagents accepts one pair electron) and another one is nucleophilic reaction (delignifying reagents donates one pair of electron). Nucleophilic reaction governs the pulping process whereas the bleaching process is governed by electrophilic reaction and followed by both (Gierer, 1985).

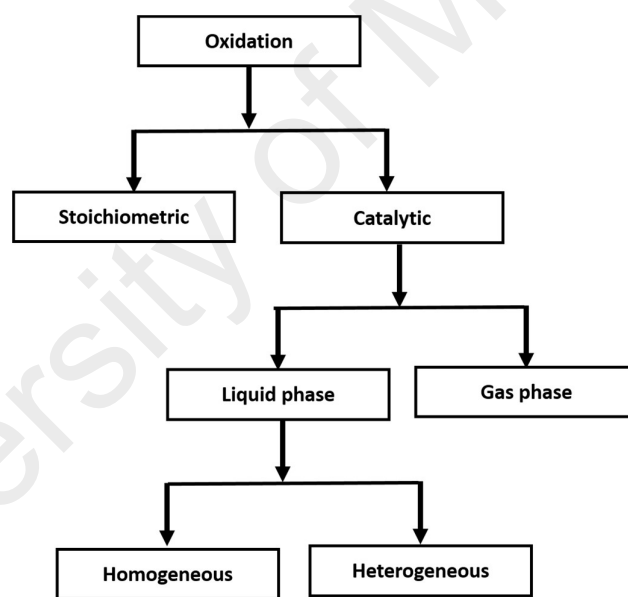


Figure 2.2: Classification of oxidation process.

2.2 Oxidation

The chemical term “Oxidation” is defined as consumption of oxygen by any organic or inorganic substances or removal of hydrogen atoms from any substrate (Sheldon, 1993a). Oxidation is half part of a redox reaction. In a redox reaction, a substrate is

reduced by accepting one electron from any other substance and the electron donating substrate is consequently oxidized. Hence, redox reaction undergoes by electron transfer from one substrate to another. Oxidation reaction is very useful and commonly practiced reaction in the industries as they produce valuable products from petroleum as well as biomass feedstocks (Punniyamurthy, Velusamy, & Iqbal, 2005). Generally, oxidation reactions are performed many following ways displayed in Fig 2.2.

Liquid phase oxidation involved usage of stoichiometric amounts of various inorganic salts such as chromium reagents, manganese dioxide and permanganate salts etc. Usage of such salts for oxidation process in the industries caused production of huge amounts of inorganic wastes which is environmentally harmful. Hence, the environmental pressure on the industries to make the process green, ecofriendly is growing which needs more attention to develop a effective protocol without causing damages to the environment (Sheldon & Van Santen, 1995; Sheldon, Wallau, Arends, & Schuchardt, 1998). One of the attempt to attain a green process is using molecular oxygen which is a challenging task. Liquid phase oxidation of thermally stable molecules in fine chemical synthesis is not viable due to problems with vaporization and conversion into gas phase. Hence, the reaction consumed high amounts of solvents which makes the process not environmental and economic friendly. Therefore, reducing the activation energy of the reactant at lower reaction conditions is only viable by using a catalytic system. Also, other serious issues such as low cost, green process, easy separation protocol, recyclability has to be focused in case of designing the effective catalytic system for lignin valorization.

The oxidation can be performed in two phase such as liquid and gas depending on the reactant phase. In case of gas phase oxidation reaction, reactants concentration are much lower and radical chain reactions are less favored. Oxidation reaction under mediation of molecular oxygen occurs by adsorption of an oxygen molecule on the surface of

heterogeneous catalysts which lead to the formation of surface oxo species (Fig. 2.3). The species are more reactive when it is adsorbed on the defective sites of the catalysts. This chemisorbed oxygen species were claimed to promote oxidation applications such as CO to CO₂ (Clerici & Kholdeeva, 2013), ethylene oxidation (Omae, 2007) and catalytic combustion (Dalla Betta, 1997; Kummer, 1975).

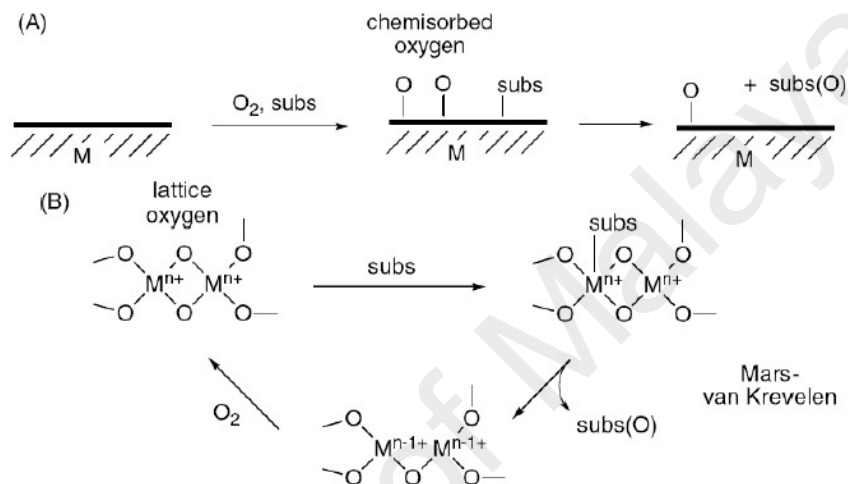


Figure 2.3: Oxygen activation on the surface of heterogeneous catalysts (a) Through chemisorption (b) By replenishing consumed lattice oxygen (Weckhuysen & Keller, 2003).

The benefits of using metal oxides or mixed oxide as catalysts are that they employ their existing surface oxo species in the oxidation reaction of hydrocarbons. Typically, the lower oxidation state of n type's semiconductor type oxides (Ti, V, and Mo) are easily accessible to the central metal atoms. And, oxygen vacancies are again fulfilled by the chemisorbed molecular oxygen. This phenomenon is known as Mars-Van Krevelen reaction mechanism. Lattice oxygen is strongly bonded relative to chemisorbed species, this is why they partake in the selective oxidation reactions in more controlled way such as synthesis of acrolein from acetonitrile (Burrington, Kartisek, & Grasselli, 1984). Liquid phase oxidation reactions are also performed industrially at mild reaction

conditions over supported metals catalysts and considered as a potential candidate due to their high selectivity under clean process. Many applications such as cyclohexane to cyclohexanol/ cyclohexanone, oxidation of isobutene, *p*-cresol to *p*-hydroxybenzaldehyde, *n*-butane to acetic acid, *p*-xylene to terephthalic acid, diisopropyl benzene to hydroquinone, epoxidation of propylene to propylene oxide, oxidation of alcohols to aldehydes, *p*-cresol to *p*-hydroxybenzaldehyde, vanillyl alcohol to vanillin, *o*-hydroxybenzylalcohol to salicylaldehyde are performed under liquid phase oxidation reactions over supported metal catalysts.

2.2.1 Oxidizing agents

Oxidation of lignin is generally performed in both alkaline and acidic media. Guaiacyl that is present in all types of lignin, was considered to illustrate the activation mechanism of lignin in Fig. 1.4. The side chain, hydroxyl or methoxyl groups on the aromatic rings contains lone pairs of electrons on the oxygen atom. Due to the overlapping of lone pair electrons with the unsaturated electrons inside the aromatic ring, it create electron rich centers in ortho- and para- positions. Therefore, these positions were easily susceptible to be attacked by electrophiles (Fleming, 1976). In lignin structures with an aliphatic double bond conjugated to the aromatic ring, partial negative centers (δ^-) are also extended to the β carbon atom. And lignin structure containing a aliphatic double bond with a α -carbonyl group, the equivalent resonance structure with partial negative centers (δ^-) were only observed in the O-C $_{\alpha}$ -C $_{\beta}$ region as shown in the Fig. 1.4. Formation of negative centers in the structure could promote oxidation by the presence of cations Cl $^+$, OH $^+$ formed during oxidation. Conversely, the elimination of an α -substituent (γ -substituent in ring-conjugated structures) could result in the formation of enone intermediates of the quinone methide type, and the formation of centers with relatively low electron density (δ^+) at both the carbonyl carbon and at carbon atoms in vinylogous position to the carbonyl carbon (Patai & Rappoport, 1988). These δ^+ sites could be actively attacked by

nucleophiles. In acidic media, both phenolic and non-phenolic units can react with electrophilic and nucleophilic agents (Nimz, 1966). In alkaline media however, a similar distribution of electron sites for electrophilic and nucleophilic reactions was encountered in phenolic units (Gierer, 1985). Several oxidative agents are commonly used for lignin oxidation or have been reported is listed in the following Table 2.1.

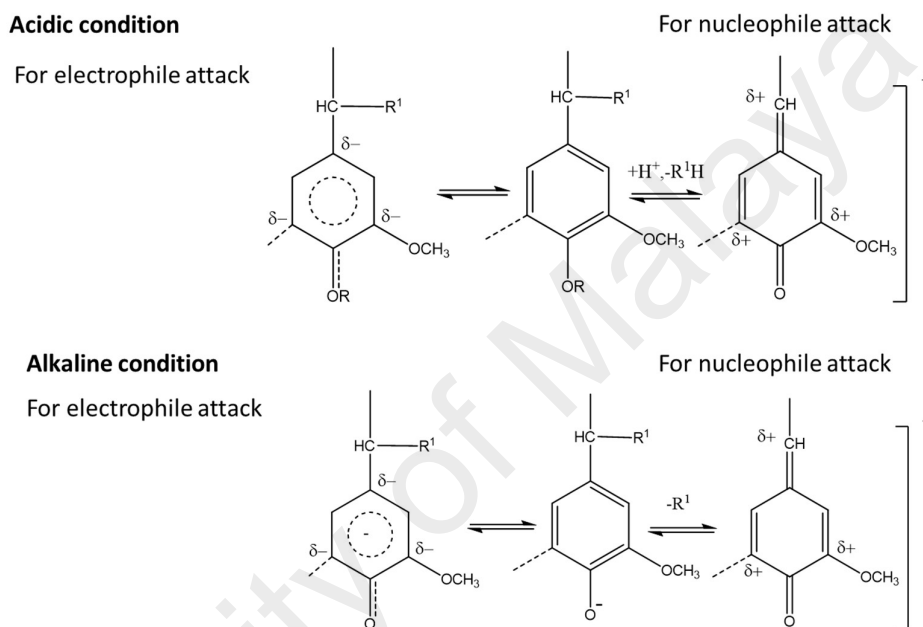


Figure 2.4: Lignin activation in acidic and alkaline media.

2.2.1.1 Chlorine

Chlorine was widely used and highly efficient oxidation agent in lignin oxidation chemistry. Chloronium ions preferentially attack the partial negative sites in lignin units at the ortho- and para- positions, which lead to the formation of cyclohexadienyl cation intermediates (Dence, 1996). For non-phenolic units without an α -hydroxy group, chlorine substitution on the methoxy group was the predominant reaction pathway (Dence & Sarkanen, 1960). Mechanistically, chlorine could completely depolymerize lignin to mono- and multi-chlorinated phenolic monomers. Despite its high activity and selectivity towards lignin, the formation of chlorinated phenolics which is referred as

organohalogens (AOX)—as end products generated significant environmental concerns in the 1960s, which led to the elimination of elemental-chlorine-based chemicals in paper based industries (Dence & Reeve, 1996). The use of Chlorine in lignin conversion also encountered the same fate due to environmental regulations.

2.2.1.2 Chlorine dioxide

Chlorine dioxide was the second generation oxidant used in application of lignin oxidation after prohibition of Chlorine as a oxidant. Since organohalogens product formation in this process was much lower, it stood as the potential candidate for replacement of Chlorine (Ni, Shen, & Van Heiningen, 1994; Svenson, Jameel, Chang, & Kadla, 2006). About 95 % of all bleached kraft pulp was prepared via Chlorine dioxide bleaching sequence (Svenson et al., 2006). Chlorine dioxide is 2.38 times more reactive than an equivalent mass of Chlorine theoretically. Chlorine dioxide oxidation in lignin structure proceeded via radical reaction mechanism (Gierer, 1985). The preferable attacks of chlorine dioxide was on the phenolic lignin units or olefinic side chains (Brogdon, Mancosky, & Lucia, 2005; Ni et al., 1994). Aromatic ring opening was also another favored pathway during lignin oxidation by Chlorine dioxide (Kolar, Lindgren, & Pettersson, 1983). This pathway led to the formation of dicarboxylic acids and their derivatives as oxidative products.

2.2.1.3 Oxygen

Oxygen attracted enormous attraction as an oxidant in lignin valorization via catalytic transformation in recent years. It offered many suitable advantages in oxidation reaction of lignin such as, (i) not require the usage of additional stoichiometric reagents hence no inorganic waste materials; (ii) produced environmentally friendly by-products; (iii) highly abundance; and (iv) green and cost effective. The reaction pathway of lignin oxidation by oxygen was previously discussed in detailed (Bessone et al., 2001; Gratzl,

1987; McDonough, 1989; Pan, Zhang, Gregg, & Saddler, 2004). The Fig. 2.5 illustrated the stepwise formation of different oxidative species in oxygen based lignin catalytic transformation of lignin.

However, present studies reported that oxygen-based catalytic oxidation of lignin tends to stop at the depolymerization step and form aldehyde/ benzoic acid derivatives under alkaline conditions. Identifying more effective catalysts to improve oxygen efficiency and selectivity towards targeted products is an area of interests which requires extensive exploration.

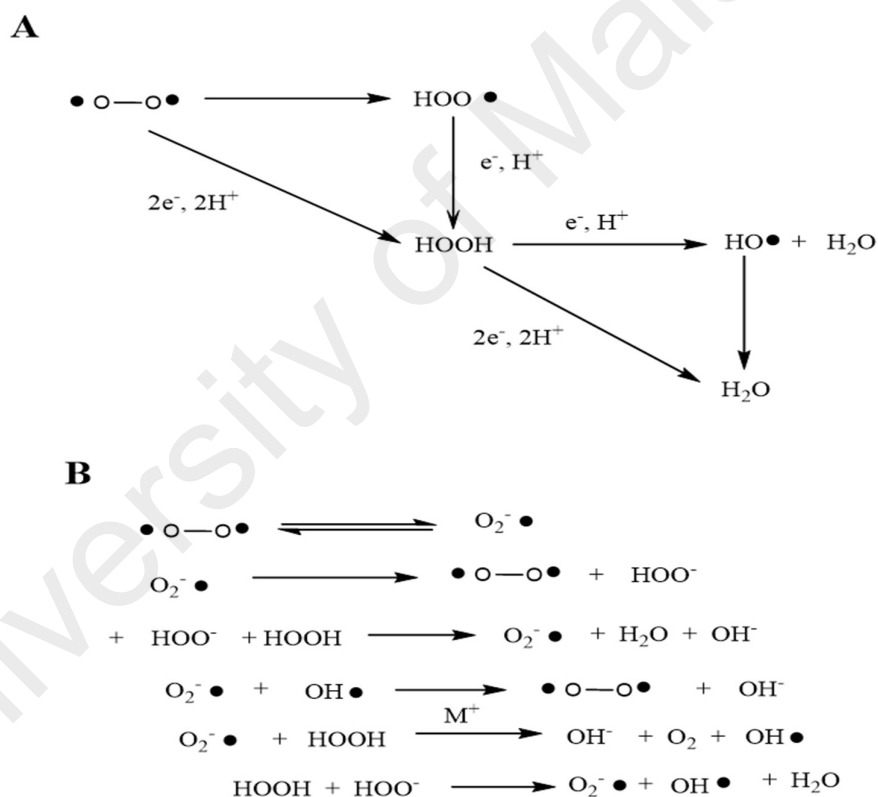


Figure 2.5: Oxygen reaction in oxidizing lignin A) stepwise electron adsorption of oxygen to reactive species; B) combined reaction mechanism for all reactive oxidation species during oxygen oxidation of lignin.

2.2.1.4 H₂O₂

Hydrogen peroxide was well considered as an environmentally benign chemical, which made it an ideal candidate and common oxidant for pulp bleaching (Beeman, 1953;

Beeman & Reichert, 1951; Rapson, 1963; Singh, 1979). Hydrogen peroxide is a more reactive oxidant than oxygen. In acidic medium, the reduction potential of the $\text{H}_2\text{O}_2/\text{H}_2\text{O}$ pair is +1.763 V, compared to only +1.229 V of the $\text{O}_2/\text{H}_2\text{O}$ pair. In alkaline medium, the reduction potential of the $\text{H}_2\text{O}_2/\text{H}_2\text{O}$ pair is +0.994 V, whereas it is only +0.401 V for the $\text{O}_2/\text{H}_2\text{O}$ pair. The peroxide and oxygen bleaching processes were mediated under alkaline conditions to conserve the content of cellulose fibers while maximizing the lignin removal. Most hydrogen peroxide bleaching processes aimed at damaging chromophore structures in lignin rather than removing them (Gierer & Imsgard, 1977). For example, *p*-hydroxybenzoic acid and *p*-hydroxylguaiacol are produced as the result of 3-(4-hydroxy-3-methoxyphenyl)-2-acrolein oxidation.

Noteworthy, these fragmented products could also be further oxidized to quinones by hydrogen peroxide treatment through Dakin-like oxidation of lignin phenolic units which eventually produce back new chromophore structures (Crestini et al., 2010; Hall, 1984). *p*-Hydroquinone, *p*-quinone, and *o*-quinone were detected in considerable amount in the waste produced by peroxide bleaching of mechanical pulp TMP (Nonni, Falk, & Dence, 1982). Hydrogen peroxide is also known as an efficient oxidant for aromatic ring cleavage reactions. Hydrogen peroxide was reported to generate reactive free-radical species over transitional metal surface to promote the degradation of lignin into *o*- and *p*-quinone structures. However, the reaction pathway was also governed to produce smaller molecules resulting decrease in product selectivity (Egami & Katsuki, 2007; W. Zhang, Wang, Tanev, & Pinnavaia, 1996). In lignin valorization strategies via oxidation process, hydrogen peroxide treated with heterogenic catalytic system exhibited high efficiency without causing any means of harm to the environment for aromatic ring cleavage (Crestini, Caponi, Argyropoulos, & Saladino, 2006; Crestini, Pro, Neri, & Saladino, 2005; Lange et al., 2013). Most previous literatures reported lignin delignification under treatment of alkaline conditions to activate the lignin as well as to

preserve the cellulose fibers. Although lignin conversion under mediation of acidic or neutral conditions was not studied in detailed. Also, a few studies were reported on aromatic ring opening reactions favored under mild acidic buffers (Crestini et al., 2006; Ma, Guo, & Zhang, 2014). Usage of mild acid along with hydrogen peroxide to transform biorefinery lignin into selective dicarboxylic acids is a promising and effective pathway to convert lignin to high value-added products. The key factor to increase the reaction efficiency is the lifetime of hydrogen peroxide. A wide number of previous literatures reported on decomposition of hydrogen peroxide into molecular oxygen accelerated by the presence of transitional metals such as Fe, Cu, and Mn (Brown & Abbot, 1995; Gellerstedt & Pettersson, 1982; Pu, Lucia, & Ragauskas, 2002; Salem, El - Maazawi, & Zaki, 2000). Also, compounds containing earth metals (e.g., Mg salts, Na silicate) was studied as function of stabilizers to reduce the decomposition rate of hydrogen peroxide even in the presence of transition metals (Christiansen, 1986; Z. Li et al., 2004). Although an ideal metal profile is not yet known for such application, the addition of chelating agents such as ethylenediaminetetraacetic acid (EDTA) prior to reaction was found to promote the performance of hydrogen peroxide for delignification. Besides inorganic salts, some organic compound such as organophosphonates (Ma, Xu, & Zhang, 2015) and polylactones (Ma et al., 2015) were investigated as stabilizers to retard the fast degradation of hydrogen peroxide and improve reaction efficiency.

2.2.1.5 Ozone

Ozone was also known as the highly efficient oxidant, capable of oxidizing almost all types of lignin. It could be used at low temperatures (20° C - 40° C) owing to its reactivity towards all unsaturated lignin structures (Lenoir, 2006; Subramaniam, 2010). The high reactivity towards both phenolic and non-phenolic nuclei was the distinguishable benefit of using ozone as an oxidant over molecular oxygen. In summary, the high reduction potential of ozone could completely destroy lignin aromatic nuclei to produce simple

organic compounds (e.g., acetic acid, formic acid, methanol) as the main products along with carbon dioxide (Ma et al., 2015). This nonselective nature of ozone limited its application in lignin valorization industries to produce the targeted product in high yield.

2.2.1.6 Peroxy acids

A peroxy acid is defined as the acid containing perhydroxyl group (-OOH) instead of (-OH) group in its parent acid. Peroxyacetic acid is produced from sulphuric acid or organic acid such as acetic acid or formic acid. Both type of peroxy acids shown effectiveness as oxidants in lignin valorization. The heterolytic cleavage of peroxy acids generates hydroxonium ion (HO^+) which is a strong electrophilic specie that readily attack on the electron- rich sites in lignin, including both aromatic ring and olefinic side chain structures. Oxygen transfer from peroxy acids to lignin was also a favored characteristic reaction (Argyropoulos et al., 2002; Young & Akhtar, 1998). The application of peroxy acids for wood pulping and bleaching attracted a considerable amount of interests in the past and at present. However, the mechanism and kinetics is yet unambiguous. Hence, it requires further study to establish the potential of peroxyacetic acids as an oxidant for lignin valorization.

2.2.1.7 Economics of using oxidizing agents

The above discussed oxidants such as chlorine dioxide, oxygen, ozone, and peroxide were generally practiced in the paper industry to bleach pulp to increase the brightness. A substantial amount of these chemicals were consumed in the bleaching process. For example, a chlorine dosage of around 2–4% based on dry weight of pulp was generally employed for commercial chemical bleaching processes whereas the dosage of peroxide for mechanical pulp bleaching was between 4–8%. Hence, a huge amount of carbon based wastage was produced as the chemical loading on lignin is approximately 100–200% on a weight basis. The cost of bleaching for white paper production is between \$30–50 per

metric ton of paper. It could be concluded that oxidative transformation of lignin to value added chemicals such as LMWPC, DCAs, and quinones compared to commodity paper is a significant development. And also, these products could be further used as a versatile platform chemicals for other value added industries. In addition, lignin valorization via oxidation technique was evidently proven to build a sustainable future with assurance of a healthy environment. Therefore, there is a crucial need of an effective catalytic system to overcome the drawbacks such as minimize the use of stoichiometric use of oxidants and high selectivity to the targeted products in order to sustain the economic potential in lignin valorization industries.

Table 2.1: Summary of oxidants used for lignin oxidation, reactive species, mechanisms and products.

Oxidizing agent	Reactive species	Mechanisms	Main products	Potential products
Chlorine	Cl^+	Electrophilic	chlorinated phenol	o-quinone
Chlorine dioxide	ClO_2 , HClO , Cl_2	Electrophilic, radical	dicarboxylic acids, simple acids	
Oxygen	$\text{O}_2^{\cdot-}$, $\text{OOH}^{\cdot-}$, OOH^{\cdot} , HO^{\cdot}	Electrophilic, radical	vanillaldehyde/acid syringaldehyde/acid, p-hydrobenzaldehyde/acid	low molecular weight aromatic aldehyde/acid, dicarboxylic acids, simple acids
Hydrogen peroxide	$\text{OOH}^{\cdot-}$, HOO^{\cdot} , HO^{\cdot} , $\text{O}_2^{\cdot-}$	Nucleophilic, radical	Vanillaldehyde syringaldehyde p-hydrobenzaldehyde vanillic acid p-hydrobenzoic acid	low molecular weight aromatic aldehyde/acid, dicarboxylic acids, simple acids
ozone	-O-O-O-	electrophilic	acetic acid/methanol simple acids	
peroxyacids	HO^+	electrophilic	p-hydroquinone methoxyhydroquinone vanillaldehyde syringaldehyde acid	low molecular weight phenolics, dicarboxylic acids, simple acids

2.2.1.8 Comparison of oxidants used generally for oxidation reactions

Many oxidants were reported for the oxidation purpose. As, the current industrial focus is towards green technology, the choice of a oxidant needs to meet many criteria (Trost, 1995). Under careful evaluation of the properties and economics of the generally practiced oxidants (Table 2.2), molecular oxygen and H₂O₂ possessed the maximum potential characteristics as they both produce water as side product and no other environmentally harmful byproducts (Sheldon, 2007, 2008). And also, in terms of other parameters such as economics and E-factor of O₂ and H₂O₂ assisted to draw the similar conclusion.

Table 2.2: Economics of general oxidants used for oxidation reactions.

Oxidants	Byproduct ^a	Atom efficiency ^a (%)	E-factor ^b	Cost (\$/Kg) Or (\$/l) ^c
O ₂	H ₂ O	50	0	57.5
H ₂ O ₂	H ₂ O	47	0	103.5
CH ₃ C(O)OOH	CH ₃ C(O)OH	27	1.03	640.8
t-BuOOH	t-BuOH	22	1.27	246.4
NaClO	NaCl	21	101	26.3
Pyridine-N-oxide	Pyridine	17	1.36	739.4
CumOOH	CumOH	12	2.34	180.7
KMnO ₄	MnO ₂ +H ₂ O	10	1.50	146.2
2KHSO ₅ + KHSO ₄ + K ₂ SO ₄ (oxone)	2KHSO ₄ + K ₂ SO ₄	10d	10.03	119.9
m-CPBA	m-CBA	9	2.70	755.8
PhIO	PhI	7	3.52	E

^aAtom efficiency

^bE-factor

Barry Trost first introduced the term “Atom efficiency” in 1991 (Sheldon, 2008). It is defined as the following equation

$$\text{Atom efficiency (\%)} = \frac{\text{Molecular mass of desired product}}{\text{molecular mass of all reactants}} \times 100 \%$$

Roger Sheldon first introduced the term E-factor. It is to determine the impact of waste on the environment from a chemical process. The ratio of waste per unit of product is defined as E-factor (Sheldon & Van Santen, 1995). It is written as

$$\text{E-factor} = \frac{\text{Total waste (kg)}}{\text{product (kg)}}$$

2.2.2 Catalytic system used for lignin oxidation reactions

Two types of catalyst were widely studied for lignin oxidation. Only a few catalytic systems were reported for direct lignin oxidation displayed in Table 2.3. As lignin contains many functional units, and complexity associated with the analysis, model compounds representing the structural units of lignin were frequently studied. Many former studies reported on oxidation of a wide variety of lignin model compounds representing various structural units or different linkages present on the lignin structure listed in Table 2.4.

2.2.2.1 Homogeneous catalysts used for oxidation of lignin

Many metal salts and other homogeneous catalytic system such as Polyoxometalates, Organometallics, and Organocatalysts were used in oxidation of lignin. Different types of Polyoxometalates catalyst were used in lignin oxidation (Kholdeeva et al., 2005; Sonnen, Reiner, Atalla, & Weinstock, 1997; Weinstock et al., 2001; Yokoyama et al., 2004). Different types of organometallic catalysts such as metallosalen complexes (Badamali, Luque, Clark, & Breeden, 2009; Canevali et al., 2002; Drago, Corden, & Barnes, 1986; Sippola & Krause, 2005), metallopolyporphyrins complexes (Cui &

Dolphin, 1995; Robinson, Wright, & Suckling, 2000; Zhu & Ford, 1993), organorheniums (Ayres & Loike, 1990; Granata & Argyropoulos, 1995; Jiang, Argyropoulos, & Granata, 1995), vanadium complexes (Hanson, Baker, Gordon, Scott, & Thorn, 2010; He, Sun, & Han, 2013) were employed in previous reports. A few former reports also mentioned usage of organocatalysts for such transformation of lignin (R. Liu, Liang, Dong, & Hu, 2004; Rahimi, Azarpira, Kim, Ralph, & Stahl, 2013). Although, homogeneous catalytic systems offer the advantage of high yield, it comes with many disadvantages as well such as (i) product contamination during the product separation protocol due to the homogeneous phase of both reactants and products (ii) low selectivity due to over oxidation of targeted products.

Table 2.3: Heterogeneous catalysts used for raw lignin oxidation

Entry	catalyst	Solvent	Oxidants	Experimental conditions	substrate	Products	Conve (%)	Yield (%)	Ref
1	Pd/Al ₂ O ₃	H ₂ O	O ₂	373-413K, 0.2-1 Mpa, 0-2 h	Alkaline lignin from sugarcane bagasse	Vanillin Syringaldehyde p-Hydroxybenzaldehyde	0-80%	0-4.4 0-6.7 0-7.3	(Sales, Maranhão, Lima Filho, & Abreu, 2007)
2	LaFe _{1-x} Cu _x O ₃	NaOH/H ₂ O	O ₂	393K, 2 MPa, 0-3 h	Lignin from enzymatic hydrolysis of steam explosion cornstalks	Vanillin Syringaldehyde p-Hydroxybenzaldehyde	0-70	2.4-4.6 0-12 0.4-2.5	(J. Zhang, Deng, & Lin, 2009)
3	LaMnO ₃	NaOH/H ₂ O	O ₂	393K, 2 MPa, 0-3 h	Lignin from enzymatic hydrolysis of steam explosion cornstalks	Vanillin Syringaldehyde p-Hydroxybenzaldehyde	4-57	3.7-4.32 3.6-9.33 0.8-2.2	(H. Deng et al., 2008b)
4	LaCo _{1-x} Cu _x O ₃	NaOH/H ₂ O	O ₂	393K, 2 MPa, 0-3 h	Lignin from enzymatic hydrolysis of steam explosion cornstalks	Vanillin Syringaldehyde p-Hydroxybenzaldehyde	9-65	2.4-5.3 0-12.8 0.9-2.88	(H. Deng, Lin, & Liu, 2010)
5	LaCoO ₃	NaOH/H ₂ O	O ₂	393K, 2 MPa, 0-3 h	Lignin from enzymatic hydrolysis of steam explosion cornstalks	Vanillin Syringaldehyde p-Hydroxybenzaldehyde	8-61	3.9-4.55 2.1-9.99 0.9-2.23	(H. Deng et al., 2008a)
6	Pd/CeO ₂	MeOH	O ₂	458 K, 0.1 MPa 0-3 h	Organosolv Lignin	Vanillin Guaicol p-Hydroxybenzaldehyde	Not provided	5.2 0.87 2.4	(W. Deng et al., 2015)
7	La/SBA-15	NaOH/H ₂ O	H ₂ O ₂		Organosolv beech wood lignin	Vanillin Syringaldehyde Vanillic acid	Not provided	0.38 0.52 0.58	(Gu, Kanghua, Ming, Shi, & Li, 2012)

2.2.2.2 Heterogeneous catalysts used for oxidation of lignin and its model compounds

A heterogeneous catalyst is considered the best potential replacement over its counterpart as it offers many advantages such as mild reaction conditions, easy separation and recyclability and also excellent selectivity. A list of heterogeneous catalytic system was successfully employed for direct oxidation of raw lignin in Table 2.3. Most of the literatures explored oxidation of lignin using model compounds as complexity associated with structure of lignin. The Table 2.4 shows the model substrates used, experimental conditions, oxidants and catalytic systems used for lignin transformation till date. However, the yield obtained using those heterogeneous catalysts in oxidation purpose of lignin model compounds indicated very low conversion with moderate selectivity to target products. In addition, requirement of harsh reaction conditions with the examined catalysts causes economic unfriendliness process for production in industrial scale. Hence, other potential heterogeneous catalysts need to be designed to enrich the yield to target products at lower reaction parameters.

Table 2.4: List of heterogeneous catalysts used for lignin model compound oxidation

Entry	Catalyst	Solvent	Experimental conditions	Substrate	Products	Conv (%)	Yield (%)	Ref
1	Co ₃ O ₄	H ₂ O	413K, 0.5-4 MPa, 7 h	Veratryl alcohol	Veratraldehyde Veratric Acid	40—85	39.2-81.6 0.8-3.4	(Mate, Shirai, & Rode, 2013)
2	Co ₃ O ₄	H ₂ O	413K, 0.689-4 MPa, 7 h	Vanillyl alcohol	Vanillic Acid Vanillin Other	86	69.66 9.46 6.88	(Mate et al., 2014)
3	Co ₃ O ₄	H ₂ O	413K, 0.689-4 MPa, 7 h	Veratryl alcohol	Veratric Acid Veratraldehyde	85	81.6 3.4	(Mate et al., 2014)
4	Co ₃ O ₄	H ₂ O	413K, 0.689-4 MPa, 7 h	p-Sinapyl alcohol	Acid Aldehyde Others	77	60 7.7 9.24	(Mate et al., 2014)
5	Co ₃ O ₄	H ₂ O	413K, 0.689-4 MPa, 7 h	3,4,5- trimethoxy benzyl alcohol	Acid Aldehyde	76.8	60.7 16.13	(Mate et al., 2014)
6	Co ₃ O ₄	H ₂ O	413K, 0.689-4 MPa, 7 h	p-Anisic alcohol	Acid Aldehyde	55	54.95 0.006	(Mate et al., 2014)
7	Co ₃ O ₄	H ₂ O	413K, 0.689-4 MPa, 7 h	Coniferyl alcohol	Acid Aldehyde	61	50 11	(Mate et al., 2014)
8	Co ₃ O ₄	H ₂ O	413K, 0.689-4 MPa, 7 h	p-Hydroxy benzyl alcohol	Acid Aldehyde	51.8	43.5 8.3	(Mate et al., 2014)
9	Co ₃ O ₄	H ₂ O	413K, 0.689-4 MPa, 7 h	p-Coumaryl alcohol	Acid Aldehyde	28	28 0.03	(Mate et al., 2014)

Table 2.4, continued

Entry	Catalyst	Solvent	Experimental conditions	Substrate	Products	Conv (%)	Yield (%)	Ref
10	Co ₃ O ₄	H ₂ O	413K, 0.689-4 MPa, 7 h	4-hydroxy-3-methoxy- α -methylbenzyl alcohol	1-(4-hydroxy-3-methoxyphenyl)ethanone	90	81	(Mate et al., 2014)
11	Co ₃ O ₄	H ₂ O	413K, 0.689-4 MPa, 7 h	Benzyl alcohol	Acid Aldehyde	17.4	13.6 3.83	(Mate et al., 2014)
12	Co ₃ O ₄	CH ₃ CN	433 k, 2.1 MPa, 2 h	Vanillyl alcohol	Vanillin Vanillic acid	48	42.2 2.4	(Jha, Patil, & Rode, 2013)
13	Mn-Co Mixed oxide	H ₂ O	433 k, 2.1 MPa, 2 h	Vanillyl alcohol	Vanillin Vanillic acid others	52	22.9 4.2 25	(Jha et al., 2013)
14	Mn-Co Mixed oxide	CH ₃ CN	373-433k, 0.7-2.8 MPa, 1-4 h	Vanillyl alcohol	Vanillin Vanillic acid others	43-80	23-60 4-7 4-16	(Jha et al., 2013)
15	Mn-Co Mixed oxide	Toluene	433k, 0.7-2.8 MPa, 1-4 h	Vanillyl alcohol	Vanillin Vanillic acid	35	22 >1	(Jha et al., 2013)
16	Mn-Co Mixed oxide	Isopropyl alcohol	433k, 0.7-2.8 MPa, 1-4 h	Vanillyl alcohol	Vanillin Vanillic acid others	70	43.4 15.4 11.9	(Jha et al., 2013)
17	Mn ₂ O ₃ -Co ₃ O ₄ Mixture	CH ₃ CN	433k, 0.7-2.8 MPa, 1-4 h	Vanillyl alcohol	Vanillin Vanillic acid others	45	33.3 6.75 4.5	(Jha et al., 2013)

Table 2.4, continued

Entry	Catalyst	Solvent	Experimental conditions	Substrate	Products	Conv (%)	Yield (%)	Ref
18	Mn ₂ O ₃	CH ₃ CN	433k, 0.7-2.8 MPa, 1-4 h	Vanillyl alcohol	Vanillin Vanillic acid others	73	54 11 7.3	(Jha et al., 2013)
19	Co-ZIF-9	NaOH/ Toluene	423 K, 0.5 MPa, 0-4 h	Veratryl alcohol	Veratradehyde	0-45	46	(Zakzeski, Dębczak, Bruijninx, & Weckhuysen, 2011)
20	Co-ZIF-9	NaOH/ Toluene	423 K, 0.5 MPa, 0-4 h	Vanillyl alcohol	Vanillin	0-90	Not provided	(Zakzeski et al., 2011)
21	Co-ZIF-9	NaOH/ Toluene	423 K, 0.5 MPa, 0-4 h	Cinnamyl alcohol	Cinnamaldehyde Epoxide	0-34	0-30 0-3	(Zakzeski et al., 2011)
22	Al ₂ O ₃	MeOH	458 K, 1 MPa, 24 h	2-phenoxy-1-phynylethanol	Benzoic acid Methyl benzoate Acetophenone phenol	9.4	0.24 3.6 0 2.4	(W. Deng et al., 2015)
23	SiO ₂	MeOH	458 K, 1 MPa, 24 h	2-phenoxy-1-phynylethanol	Benzoic acid Methyl benzoate Acetophenone	2.1	0 0 0	(W. Deng et al., 2015)

Table 2.4, continued

Entry	Catalyst	Solvent	Experimental conditions	Substrate	Products	Conv (%)	Yield (%)	Ref
24	CeO ₂	MeOH	458 K, 1 MPa, 24 h	2-phenoxy-1-phynylethanol	Benzoic acid Methyl benzoate Acetophenone phenol	9.1	0.26 3.2 0 0	(W. Deng et al., 2015)
25	MgO	MeOH	458 K, 1 MPa, 24 h	2-phenoxy-1-phynylethanol	Benzoic acid Methyl benzoate Acetophenone phenol	5.1	0.18 3.4 0 0.96	(W. Deng et al., 2015)
26	Pd/Al ₂ O ₃	MeOH	458 K, 0.1 MPa, 24 h	2-phenoxy-1-phynylethanol	2-phenoxy-1-phynylethanone Benzoic acid Methyl benzoate Acetophenone phenol	34	30 0 0 3.9 3.0	(W. Deng et al., 2015)
27	Pd/SiO ₂	MeOH	458 K, 0.1 MPa, 24 h	2-phenoxy-1-phynylethanol	2-phenoxy-1-phynylethanone Benzoic acid Methyl benzoate	10	6.0 0 0.34 3.8	(W. Deng et al., 2015)

Table 2.4, continued

Entry	Catalyst	Solvent	Experimental conditions	Substrate	Products	Conv (%)	Yield (%)	Ref
28	Pd/MgO	MeOH	458 K, 0.1 MPa, 24 h	2-phenoxy-1-phynylethanol	2-phenoxy-1-phynylethanone Benzoic acid Methyl benzoate Acetophenone phenol	22	12 0 0 6 4	(W. Deng et al., 2015)
29	Pd/Al ₂ O ₃ + CeO ₂	MeOH	458 K, 0.1 MPa, 24 h	2-phenoxy-1-phynylethanol	2-phenoxy-1-phynylethanone Benzoic acid Methyl benzoate Acetophenone phenol	25	2.0 0 18 5 20	(W. Deng et al., 2015)
30	Pd/CeO ₂	MeOH	458 K, 0.1 MPa, 24 h	2-phenoxy-1-phynylethanol	2-phenoxy-1-phynylethanone Benzoic acid Methyl benzoate Acetophenone phenol	64-70	12-15 0.03-0.1 14-27 27-38 38-48	(W. Deng et al., 2015)
31	Pd/CeO ₂	MeOH	458 K, 0.1 MPa, 24 h	2-phenoxy-1-phynylethanol	Methyl benzoate Acetophenone Substituted phenol Substituted ketone	86-90	25-40 34-38 64-82 0-13	(W. Deng et al., 2015)

Table 2.4, continued

Entry	Catalyst	Solvent	Experimental conditions	Substrate	Products	Conv (%)	Yield (%)	Ref
32	5 % Pt/MOF-5	NaOH/H ₂ O	353 K, 1 h	Vanillyl alcohol	vanillin	24.5	24.3	(Tarasov et al., 2011)
33	1 % Pd/sibunit	NaOH/H ₂ O	353 K, 1 h	Vanillyl alcohol	vanillin	47.8	34.8	(Tarasov, Kustov, Bogolyubov, Kiselyov, & Semenov, 2009)
34	1 % Pd/ TiO ₂	NaOH/H ₂ O	353 K, 1 h	Vanillyl alcohol	vanillin	32.8	14.8	(Tarasov et al., 2009)
35	4 % Pd/ SiO ₂	NaOH/H ₂ O	353 K, 1 h	Vanillyl alcohol	vanillin	62.9	43.6	(Tarasov et al., 2009)
36	9 % Pt/ SKT-4	NaOH/H ₂ O	353 K, 1 h	Vanillyl alcohol	vanillin	94.8	90	(Tarasov et al., 2009; Tarasov et al., 2011)
37	2.3%Pd/sibunit	NaOH/H ₂ O	353 K, 1 h	Vanillyl alcohol	vanillin	46.8	38.5	(Tarasov et al., 2009)
38	2.3 % Pt/SKT6	NaOH/H ₂ O	353 K, 1 h	Vanillyl alcohol	vanillin	45.5	34.8	(Tarasov et al., 2009)
39	2.3 % Pt/ MgO	NaOH/H ₂ O	353 K, 1 h	Vanillyl alcohol	vanillin	71.5	48.5	(Tarasov et al., 2009)
40	Pd/ C	EtOAc/H ₂ O	353 K, 12 h	2-aryloxy-1-arylethnols	Aryl ketones	50-100	18-93	(Dawange, Galkin, & Samec, 2015)

2.2.2.3 Unconventional methods

Some unconventional methods were also reported for lignin valorization. Behelig et al (Behling et al., 2016) reviewed some unconventional reaction media such as using an ionic liquid, or a supercritical fluid as a solvent system, and using microwave energy, or sonochemistry as the activation method of lignin. Chatel et al summarized the ionic liquids used for lignin valorization (Chatel & Rogers, 2013).

2.3 Vanillyl alcohol as a lignin model compound

The frequently used lignin model compounds are listed in Fig. 2.6. Here, in this study we used vanillyl alcohol as phenolic model compound which represents the β -O-4 linkage of lignin structure. Vanillyl alcohol is not directly available as a structural unit in the lignin structure. As it mimicked the one of the linkages in the lignin structure, it was thoroughly studied in previous literature as a model compound representing one of the simplest molecular units of the structure. Oxidative products obtained from oxidation of vanillyl alcohol have great industrial value. As they have flavor properties, food industries use it as a flavor. Also, perfume industries are benefitted from the flavor feature. The direct synthesis of vanillin from vanillyl alcohol has a great industrial potential as the global demand for vanillin is very high. Also, *p*-vanillin and its derivatives are generally used in various consumer products. Owing to the costly production process of vanillin from natural resources, it is produced by a synthetic process. The cost of vanillin extracted from vanilla pods is very high (\$1200 per kilo) compared to synthetic vanillin (\$15 per kilo). Global demand of vanillin is 16000 tons per annum. The production of vanillin from natural resources is only 0.2 % and 15 % from delignification process against the high demand of vanillin. The major production 85 % is obtained from synthetic process. Industrially, vanillin is synthesized by guaiacol hydroxyalkylation reactions catalyzed by Lewis acids such as AlCl_3 , bases and mineral Brønsted acids. Some recent literatures reported usage of zeolite as a catalyst for such reactions. The industrial synthetic process

of vanillin production is displayed in Fig. 2.7. Moreover, oxidative products of vanillyl alcohol are used as a platform chemical in many pharmaceutical industries.

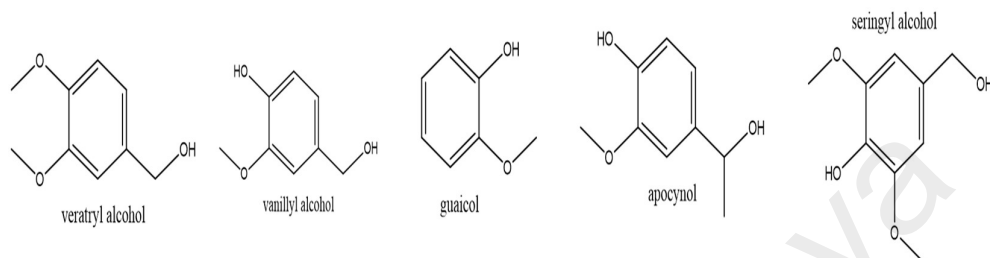


Figure 2.6: Some examples of selected model compounds of lignin (monomeric units).

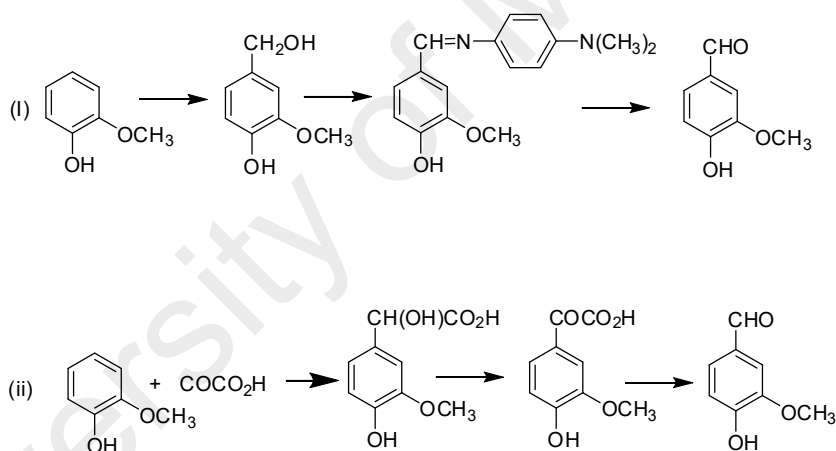


Figure 2.7: Two conventional methods of vanillin preparation.

2.4 Why mixed oxides catalysts

Recently, mixed oxide catalyst is a potential candidate in versatile applications such as oxidation, reduction of complex substrates as they showed promising catalytic activity in aspect of high yield to selective products than their counterpart, isolated oxide form. The synergy of metal oxides significantly alter the electronic configuration and geometry of the catalyst (McFarland & Metiu, 2013). Moreover, the acid-base and redox properties of mixed oxide catalysts play a vital role in the oxidation chemistry (Gawande, Pandey,

& Jayaram, 2012). In addition, co-operative effect of mixed oxide catalysts promotes the characteristics such as stabilizing the active sites, increment of oxygen mobility on the catalyst surface and favor the redox cycle for reactivation of the catalyst (Aguilera, Perez, Molina, & Moreno, 2011). MnOx doped on Co₃O₄ was used for the oxidation of CO in H₂ stream. From this application, a postulation was made that incorporation of the MnOx in the Co₃O₄ framework enhanced the reactive oxygen species on the surface resulting the reactivation of the reduced catalyst by O₂ (Q. Zhang, Liu, Fan, & Wang, 2011). Furthermore, other bimetallic oxides such as CuCo bimetallic combination for transformation of o-cresol to salisaldehyde (Feng, Xu, & Liao, 2002), Cupper-Manganese oxide for liquid phase aerobic oxidation of p-cresol to p-Hydroxybenzaldehyde (Feng, Yang, Zhang, Wu, & Xu, 2004) with excellent catalytic activity were reported.

2.5 Some preparation techniques of mixed oxide catalysts

Catalyst preparation is the vital step to alter the morphology, geometry, and textural properties of inorganic materials. It is due to the fact that the performance of a catalyst strongly depends on the shape and crystallite size as well as exposure of specific crystal plane. For preparation of mixed oxide catalysts, some general synthesis methods were used such as sol-gel, solvothermal, hydrothermal, slurry method, and co-precipitation methods. These methods offers some advantages as well as some disadvantages. Many former reports such as yttrium- aluminum based mixed oxide (H. Wang, Gao, & Niihara, 2000), Mn doped ZnO nanoparticles (Jayakumar et al., 2006), Strontium hexaferrite (SrFe₁₂O₁₉) (Hessien, Rashad, & El-Barawy, 2008), ZnO-SnO₂ mixed oxide (M. Zhang et al., 2005), and Co_{1-x}Zn_xFe₂O₄ non-stoichiometric oxide (Gul, Abbasi, Amin, Anis-ur-Rehman, & Maqsood, 2007) synthesized using co-precipitation method. This method employed usage of base NaOH, KOH which caused residual of metal impurities in the prepared catalyst. Sol-gel synthesis method was also widely deployed to prepare mixed oxide catalysts such as CeO₂-TiO₂ (Shi, Yang, Tao, & Zhou, 2016), MnO_x-CeO₂ (Xingfu

Tang et al., 2006), CeO₂-ZrO₂ (Alifanti et al., 2003). However, sol-gel process is very much complicated and time consuming as it has few steps. Moreover, hydrolysis and polymerization of transitional metal ions are difficult to control. In addition, solvothermal method is also used to synthesize CuCeO_x (Mrabet, Abassi, Cherizol, & Do, 2012), CeO₂-ZrO₂ (Devaraju, Liu, Yusuke, Yin, & Sato, 2009), and rare earth-iron mixed oxides (Hosokawa, Jeon, Iwamoto, & Inoue, 2009). Hydrothermal synthesis was also reported for preparation of mixed oxide catalysts using supercritical conditions (Adschiri, Hakuta, & Arai, 2000). However, solvothermal and hydrothermal methods requires harsh conditions such as high temperature and pressure for crystallization of the materials. Furthermore, slurry method was also used for preparation of mixed oxides which is also performed at harsh conditions (Xie, Chen, Weng, & Wan, 2005).

2.5.1 Supported mixed oxide catalysts

For modification approaches, soft templating and hard templating techniques were employed to synthesize ordered mesoporous metal oxides. Soft templating involves usage of cationic or anionic surfactants. Two pathways were described for soft templating. One was the direct co-condensation with opposite charged species mediated by the intercalation of counter ions Na⁺, or K⁺. Another was the indirect co-condensation of similar charged species. Hard templating synthesis technique involved usage of some hard templates such as MCM-41, MCM-48, SBA-15, SBA-16, KIT-6, FDU-12 and also mesoporous carbon (Ren, Ma, & Bruce, 2012). However, in a hard templating process, it was not easy to fill the mesoporous silica template completely because there were complex interactions between the silica and filtrated metal ion precursor such as hydrogen bonding, Coulombic interactions, coordinating interaction, and van der Waals interaction (H. Yang & Zhao, 2005). Therefore, different methods were developed to improve the impregnation of the metals in the pore and minimize the loading outside the pores. Metal ion precursors interact with the fresh silica template through weak Coulombic interactions

with Si–OH. In order to achieve better replication, one possible way is to create silanols as many as possible (B. Tian et al., 2004; B. Tian et al., 2003). The functionalization (post synthesis grafting or one-pot preparation) of the mesoporous silica templates by certain organic groups (for instance, –NH₂, –COOH) was also studied for a strong interaction between the organic group and metal ion precursor, thus improving the loading of metal ion precursor (Yangang Wang, Wang, et al., 2008; Yanqin Wang et al., 2005; Yangang Wang, Yuan, et al., 2008). However, both soft and hard templating methods possess advantages and disadvantages. Materials prepared via soft templating methods had low thermal stability and amorphous or semi crystalline walls. And also, the preparation technique is comparatively complicated likewise sol-gel method. On the other side, presence of amine or acid groups in the functionalized material synthesized via hard templating method lead to poisoning of the catalyst.

2.6 Why solvent evaporation method

The synthesis technique is very much crucial to control the physico-chemical characteristics of the synthesized mixed oxides. One step synthesis method is beneficial over multi-step synthesis protocol as it reduces few steps such as filtration, washing etc. Simple and facile one pot solvent evaporation method was developed in this study to synthesis mixed oxides via a simplified protocol. And also, for better synergistic combination of the metals to great extent, one pot method is preferred as bimetallic complex of the metal precursors is precipitated as the residual after the solvent removal. It is a reproducible technique which could be potentially involved to prepare the material in large scale. In general synthesis protocols, metal salts such metal chlorides or nitrates are used which required filtration, washing and harsh heat treatments for removal of the anionic part of the precursor. On contrary, in this technique, metal organic precursors were used as they are easily eliminated at low calcination temperature. And also, this process minimizes usage of solvents in large scale.

2.7 Reaction mechanism of metal catalyzed oxidation reactions

Molecular oxygen contains two unpaired electrons in the triplet state with parallel spins. Hence, the direct reaction of $^3\text{O}_2$ with a singlet organic molecule is a spin forbidden process and also the rate of kinetics was low. To overcome the activation energy barrier, there are two possible reaction pathways. The first one involves a free radical pathway in which $^3\text{O}_2$ reacts with singlet molecule to form two doublets (free radicals) which are allowed spin orientation process. This mechanism is only possible in case of very reactive substrate which can produce spin resonance free radicals (Eq. 1).



Another possible way is to reaction between $^3\text{O}_2$ and paramagnetic transitional metals which form superoxometal complex shown in Eq. 2.



A wide variety of reactive species are formed subsequently via inter- or intramolecular electron transfer which also play vital roles in oxidation reactions of organic molecules (Fig. 2.8).

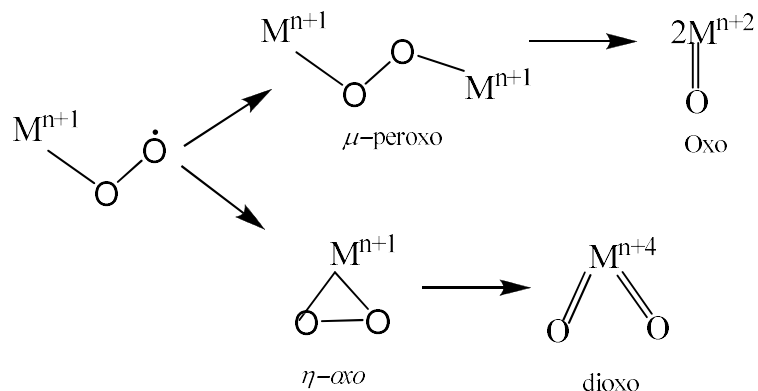


Figure 2.8: Metal-Oxygen species.

Previously, metal catalyzed oxidation reactions by molecular oxygen was rationalized in two classes i.e. homolytic and heterolytic by Sheldon and Kochi (Sheldon, 2012). These are described in details below.

2.7.1 Homolytic mechanism

Homolytic mechanism undergoes free radical species catalyzed by first row transition metals via one step electron transfer ($\text{Cu}^{\text{I}}/\text{Cu}^{\text{II}}$, $\text{Mn}^{\text{II}}/\text{Mn}^{\text{III}}$ and $\text{Co}^{\text{II}}/\text{Co}^{\text{III}}$) (Fig. 2.9). In a homolytic reaction, the oxidation of organic substrate takes place outside the coordination sphere of the metals via radical chain formation. The key role of a metal in the homolytic reaction mechanism is to disintegrate the organic hydroperoxide formed in the solution. This process is spontaneous or initiated by a metal. This phenomenon is known as the Haber-Weiss mechanism displayed in scheme (Fig 2.9).

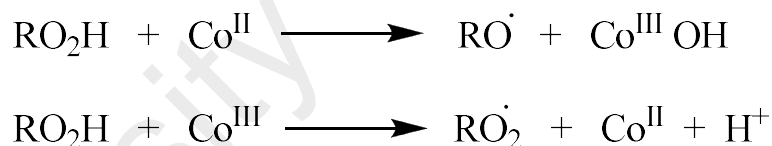


Figure 2.9: Metal initiated and mediated oxidation.

Many industrial application such as synthesis of adipic acids (Musser, 2005) and terephthalic acids (Sheehan, 2000) are based on such radical processes. However, the problems associated with this process was production of few side products as the results of series of consecutive reactions. And also, it is hard to control the pathway of radical chain reactions as the intermediate products of the process are more prone to oxidize than the reactants.

2.7.1.1 Direct homolytic mechanism of organic substrate

This phenomenon is applied in case of one-electron autoxidation of the organic substrate by the oxidized metal framework e.g. Co^{II} is used as catalyst with reactive substrate which leads to formation of large concentration of Co^{III} as the initiator of the reactions (Fig. 2.10).

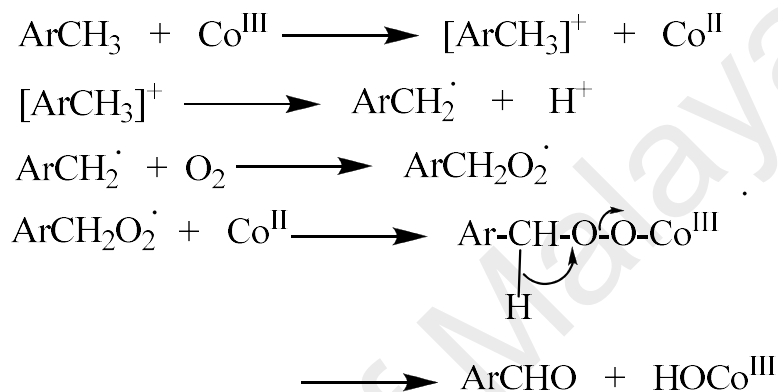


Figure 2.10: Direct homolytic oxidation of benzylic compounds.

2.7.2 Heterolytic mechanism

This metal catalyzed heterolytic reaction mechanism proceed by two electron transfers from the metal ion to the organic substrate. The reduced metal part reacts with molecular oxygen and regenerate oxidized metal ion e.g. Oxidation of alkene by Pd catalyst (Wacker process) (Fig. 2.11).

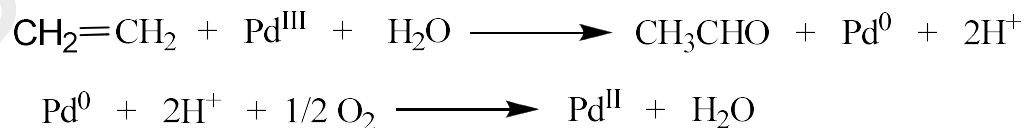


Figure 2.11: Wacker oxidation of Alkenes.

But, in case of gas phase reaction, an oxometal species oxidize the substrate and be reduced which is re-oxidized by molecular oxygen (Fig. 2.12).

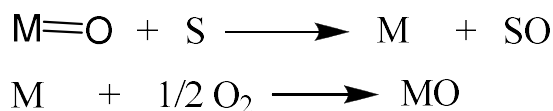


Figure 2.12: Mars-Van Krevelen mechanism.

2.7.2.1 Catalytic oxygen transfer

Reduced species of dioxygen such as RO₂H or H₂O₂ are often called as single oxygen atom donor (Fig. 2.13). The reactions proceed with this oxygen source are referred as catalytic oxygen transfer (Sheldon, 1993b). This technique is widely employed to synthesis organic chemicals in industrial scale.



S = Substrate; SO = Oxidized substrate

XOY = H₂O₂, RO₂H, R₃NO, NaClO, KHSO₅, etc.

Figure 2.13: Catalytic oxygen transfer process over catalysts.

Based on the nature of the active oxidants, heterolytic oxygen transfer process are classified into two categories. One is peroxometal species which is formed by early transitional metals such as Mo, W, Re, V, Ti, Zr. And, oxometal species is generated by later transitional metals such as Os or Ru particularly Fe, Mn (Fig. 2.14).

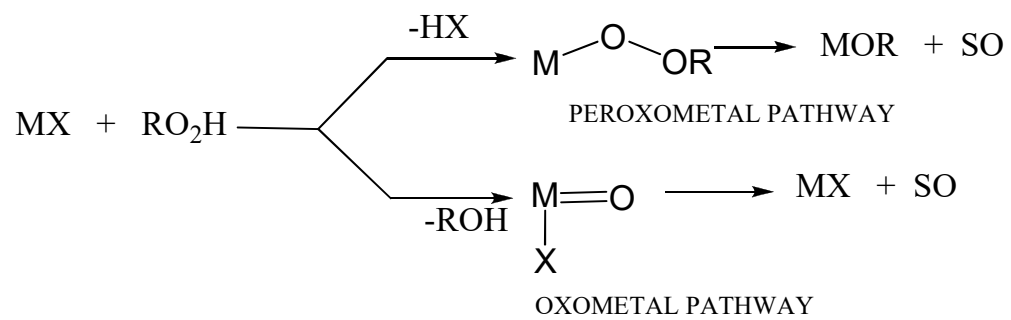


Figure 2.14: Peroxometal versus oxometal pathway.

University of Malaya

CHAPTER 3: METHODOLOGY

3.1 Scope of work

3.1.1 Cu based mixed oxide catalysts (Cu: M, M= Ti, Zr and Mn)

As in previous literatures it is found that Cu based catalysts shown promising performances in lignin oxidation, the focus of this study is to synthesize Cu based mixed oxide catalysts in a effective and simplified method. Therefore, design the of copper based (Cu: M) mixed oxide catalysts where M refers to Ti, Zr and Mn were prepared via one pot solvent evaporation method. And also, the composition of the metal loading in the bulk phase of the catalysts was optimized in order to maximize the catalytic activity. The list of Cu based mixed oxide catalysts prepared in this study are listed in Table 3.1.

Table 3.1: Cu based mixed oxide catalysts (Cu: M, M= Ti, Zr, and Mn)

Catalysts Cu:M Ratio	Cu: Ti	Cu: Zr	Cu: Mn
Cu : M	Cu: Ti	Cu: Zr	Cu: Mn
Cu : 2M	Cu : 2Ti	Cu: 2Zr	Cu: 2Mn
2Cu : M	2Cu: Ti	2 Cu: Zr	2Cu: Mn

3.1.2 Replacement of Cu in (Cu: M) mixed oxide catalysts

After investigation of synthesized catalysts from section 3.1.1 in application of liquid phase oxidation of vanillyl alcohol as a lignin model compound, a comparison was made in view of their catalytic activity. The distinguished catalyst was modified by replacement of Cu by different valent Fe^{3+} and Ce^{4+} metals in optimum Cu based mixed oxide catalyst (Cu: M) after catalytic evaluation using the catalysts obtained from section 3.1.1.

- Fe: 2Ti
- Ce: 2Ti

3.1.3 Characterizations of Catalysts

Table 3.2: List of Characterization techniques used.

No	Characterization/ Instrument	Objective
1	Thermogravimetric Analysis (TGA)	Analyze for thermal stability by weight loss (%)
2	Field Emission Scanning Electron Microscope (FESEM)	Analyze for surface morphology, size and particles distribution
3	Electron Diffractive X-Ray (EDX)	Analyze for elemental composition (surface depth of < 500 nm)
4	Brunner-Emmet-Teller (BET)	Analyze for textural properties (surface area, pore size, pore shape, pore volume)
5	High Resolution-Transmission Electron Microscope (HR-TEM) and Selected Area Electron Diffraction (SAED)	Analyze for crystallinity, crystal size, crystal structure, distribution and lattice spacing
6	X-Ray powder diffractogram (XRD)	Analyze for crystallinity, crystal phase, crystal ratio, crystal planes and lattice spacing
7	Raman spectroscopy	Analyze for catalyst composition based on scattering of light by the vibrating molecules.
8	X-Ray Photoelectron Spectroscopy (XPS)	Analyze for chemical state and binding energy (surface depth ~1-12 nm)
9	H ₂ -TPR and O ₂ -TPD	Analyze the reducing ability and study the oxygen species

3.1.4 Catalytic evaluation in oxidation of vanillyl alcohol

Catalytic activity test of prepared mixed oxide catalysts via developed one pot solvent evaporation technique was performed in liquid phase oxidation of vanillyl alcohol (a lignin model compound) using two different oxidants H₂O₂ and air. And also, a suitable reaction condition was investigated for liquid phase oxidation of vanillyl alcohol via optimization of reaction variables such as time, catalyst mass, temperature, pressure, concentration of H₂O₂ and nature of solvent.

The reaction set up of the vanillyl oxidation in liquid phase by H_2O_2 was done in a typical fumehood. The reaction was carried out in a 100 ml three neck round bottom flask connected with a reflux condenser. The flask was dipped more than half of its volume into a oil bath placed into a magnetic hotplate. Firstly, vanillyl alcohol was weighted with predetermined loading and added to 20 ml solvent on the flask with a magnetic stirrer inside it. After complete dissolve of vanillyl alcohol, predetermined load of mixed oxide catalyst was added to the reaction mixture and followed by well-stirring. After attaining homogeneous mixture of the catalyst and reactant, fixed concentration of H_2O_2 was injected slowly through one neck which was closed by a stopper and also periodically used for sampling. Prior to the addition of oxidant, the reaction mixture temperature was maintained at expected temperature which was measured by a thermometer emerged into the reaction mixture through the other neck of the round bottom flask. The reaction progress with time was investigated as the first reaction parameter in a reaction condition followed in previous literatures of alcohol oxidation (reaction condition: 1 mmol vanillyl alcohol (0.15 g) with 3 mmol H_2O_2 (0.3 ml) and 0.0037 g/cm^3 catalyst in 20 ml acetonitrile, $85 \text{ }^\circ\text{C}$). Other parameters such as concentration of H_2O_2 , catalyst mass, temperature, and nature of solvent were optimized respectively. The similar procedure was followed in all the reactions performed in this study for VA oxidation by H_2O_2 .

The liquid phase aerobic oxidation was performed in a high pressure 200 ml autoclave reactor supplied by Parr Co. In a typical experiment of liquid phase aerobic oxidation, 3 mmol vanillyl alcohol (0.45 g) was taken in 60 ml acetonitrile which was found as the best suitable solvent for VA oxidation under H_2O_2 . The determined loading of catalysts mass was also added to the mixture. The reaction temperature was elevated to $120 \text{ }^\circ\text{C}$ and maintained. The air pressure was initially taken to 21 bar. The stirring speed was set up continuously and to speed rate of 800 rpm. The sample was collected through opening a vent in the reactor after certain interval. Time, followed by catalyst mass, temperature

and air pressure were investigated to find the suitable condition for maximum catalytic activity. All the aerobic oxidation reactions performed in this study was done following the similar procedure. The products from the oxidation reactions were collected after every 30 mins time interval.

3.1.5 Plausible reaction mechanism

The plausible reaction mechanisms of liquid phase oxidation of vanillyl alcohol as a lignin model compound over synthesized mixed oxide catalysts were proposed .

University of Malaysia

3.2 Research approach (flow chart)

This study was carried out according to the illustrated fig 3.1. The catalysts were synthesized via developed one pot solvent evaporation method. And similar catalyst preparation protocol described in details in section 3.4 was followed to synthesized all the catalysts. Also, all the catalysts were thoroughly analyzed by necessary spectroscopic analytical tools (illustrated in section 3.5) to confirm the formation of mixed oxide catalysts. Oxidation of VA was performed using different oxidants with their suitable reaction parameters described in section 3.1.4. Also, the catalytic activity measurement was carried out following the procedure described in section 3.7.

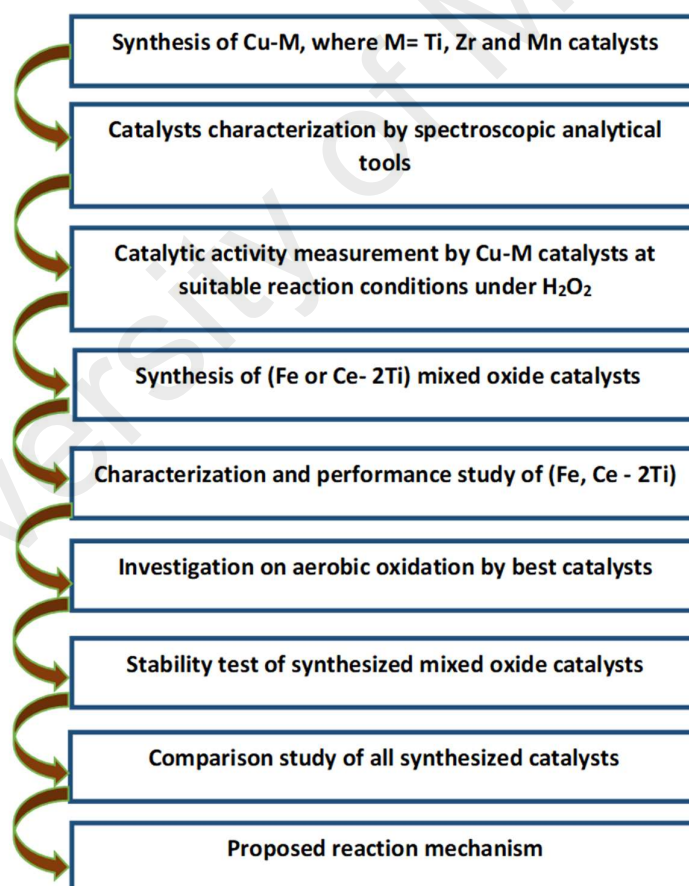


Figure 3.1: Research approach (flow chart).

3.3 Equipments and consumables

Table 3.3: List of equipments and consumables used in this study.

No	Equipment and Apparatus	Chemical and Consumables
1	Beaker	Titanium tetra-isopropoxide (97-98%)
2	Measuring cylinders	Methanol, C ₂ H ₅ O (95% and 99%)
3	Mass balance	Tetrahydrofuran
4	Disposable pipette	Zirconium butoxide, (80 % solution in 1-butanol)
5	Magnetic stirrer	Manganese acetate hydrate (99%)
6	Hot plate	Trifluoroacetic acid, CF ₃ COOH (98%)
7	Vacuum line	Copper acetate hydrate, (98%)
8	Schenk flask	Cerium acetylacetonate
9	Syringe	Sodium hydroxide, NaOH
10	Millipore syringe filter	Vanillyl alcohol (98%)
11	Glass crucible	Acetonitrile (HPLC grade)
12	Spatula	Acetic acid (99%)
13	Drying oven	Dimethyl formamide, (99%)
14	Universal Temperature Programmed (UTP) oven	Ethanol, C ₂ H ₅ OH (99%)
15	Grinder	Deionized water
16	Vials	Compressed air cylinder
17	200 ml Hastelloy Autoclave reactor	Isopropanol
18	Chemical and heat resistant gloves	Nitrogen gas cylinder
19	HPLC-UV (Agilent)	Column C-18 (Zorbax)
20	Three neck round bottom flask	Hydrogen peroxide, H ₂ O ₂ (30% in H ₂ O)
21	Reflux condenser	Iron acetate hydrate (99 %)

3.4 Catalysts preparation method

3.4.1 Materials

All the chemicals used in this study were purchased from various commercial sources and used without further purifications. Copper acetate (Sigma Aldrich 98%), Zirconium butoxide (80 % solution in butanol) (Sigma Aldrich), Iron acetate hydrated (Sigma Aldrich 95%), Cerium acetylacetonate hydrate (Sigma Aldrich), Manganese acetate hydrated (Sigma-Aldrich 98%), Titanium isopropoxide (Sigma Aldrich 97%), Methanol (Sigma Aldrich 99.8%), Tetrahydrofuran (Sigma Aldrich 99.9%).

3.4.2 Catalyst synthesis method

Five different type of catalysts with different metal combinations and their loading were prepared according to the composition illustrated in Table 3.4 via developed one pot solvent evaporation method. In a typical synthesis method, 4 mmol of first metal precursors were completely dissolved in 30 ml methanol inside a 100 ml schlenk flask connected with a vacuum line adaptor. After complete dissolve of the taken metal precursor in the solution, second metal precursors with predetermined metal loading were added to the solution. After complete mixture of both the metal precursors in the solution, a few drops of Trifluoroacetic acid was added dropwise and carefully to attain a slight acidic pH (pH= 4). Afterthat, the mixture was placed for 4 h under vacuum to obtain a homogeneous mixture of the metal precursors into the solution. Then the solvent was extracted slowly under vaccum until dry powder was obtained. The dry powder recovered as residual of bimettalic complex. The powder was grinded finely prior to calcination. The calcination was done in a blast furnace under air at 500 °C using heating rate of 2 °C/min. The material was again grinded finely . The obtained fine powders are the synthesized mixed oxide catalysts.

Table 3.4: The composition of metal precursor's in the synthesis method.

Chemicals	Catalysts	Cu-Ti	Cu-Zr	Cu-Mn	Fe-2Ti	Ce-2Ti
Copper acetate	Cu: Ti	4 mmol 0.79g	4 mmol 0.79 g	4 mmol 0.79 g		
	Cu: 2Ti	4 mmol 0.79 g	4 mmol 0.79 g	4 mmol 0.79 g		
	2Cu: Ti	8 mmol 1.58 g	8 mmol 1.58 g	8 mmol 1.58 g		
Titanium isopropoxide		4 mmol 1.2 ml			8 mmol 2.4 ml	8 mmol 2.4 ml
		8 mmol 2.4 ml				
		4 mmol 1.2 ml				
Zirconium butoxide	Cu: Zr		4 mmol 1.6 ml			
	Cu: 2Zr		8 mmol 3.2 ml			
	2Cu: Zr		4 mmol 1.6 ml			
Manganese acetate	Cu: Mn			4 mmol 0.98g		
	Cu: 2Mn			8 mmol 1.96 g		
	2Cu: Mn			4 mmol 0.98 g		
Iron acetate	Fe: 2Ti				4 mmol 0.76 g	
Cerium acetyl acetate	Ce: 2Ti					4 mmol 1.79 g
Methanol		30 ml		30 ml	30 ml	30 ml
Tetrahydrofuran			30 ml			

3.5 Catalysts Characterization tools

To correlate the physiochemical properties with the catalytic activity, various spectroscopic analytic tools were employed. The principles of such analytical tools, analysis procedure and sample preparation techniques were described in the section 3.5.1 to 3.5.11 in details.

3.5.1 X-Ray powder diffraction (X-Ray)

3.5.1.1 Background of X-Ray

The structural information such as crystal phase, crystallinity, crystal planes, crystal ratio and lattice spacing of any crystalline substance is determined by X-Ray diffraction analysis. It is a non-destructive test based on scattered waves mutually reinforcing one another. When an X-Ray beam hits a crystalline atom, the electrons around the atom oscillate with similar frequency as the incoming beam. After scattering, the X-Ray beams form a constructive interference as the atoms in a crystal are well arranged in a periodic pattern, the combining waves formed constructive interference. Thus well-defined diffracted X-Ray beams are formed when leaving the sample at various directions.

3.5.1.2 Sample analysis procedure

XRD analysis was conducted using Bruker AXS D8 advanced diffractometer at constant voltage 40 kV and 40 mA intensity. Cu K α radiation ($\lambda = 1.5406\text{\AA}$) was used as a source of X-Ray beam. The Bragg angle was analyzed from 10° to 80° and the step size was 2°/ min. Prior to the analysis, the sample was grinded into fine powder and was closely packed in a sample holder. And also, for smooth surface, a non-leaching glass slide was used to smooth. High Score-Plus software was used to analyze the obtained XRD pattern and the observed diffraction peaks were matched against the JCPDS standard reference patterns. The crystal size was calculated using the Scherrer's equations.

3.5.2 Field Emission Scanning Electron Microscopy (FESEM)

3.5.2.1 Background of FESEM

The topography of the sample was analyzed by Field Emission Scanning Electron Microscope (FESEM) with unlimited depths by using high-energy beam of electrons emitted from field emission gun. The exited electrons from the field emission gun are

confined into focused monochromatic beam using metal orifice and magnetic lenses. The detectors of electrons which are placed in the microscope are used to collect signals to generate the sample's image. Different from conventional scanning electron microscope (SEM), FESEM generates vivid images with spatial resolution 3 to 6 times greater

3.5.2.2 Sample analysis procedure

FESEM Quanta FEI 200F was used to analyze the surface morphology, size and particles distribution. The sample was dispersed in ethanol and sonicated in an ultrasonic bath at room temperature for 2 min to obtain a clear cloudy suspension. One drop was carefully fixed on a carbon tape and was left to dry overnight in a desiccator prior to analysis. Both low (5 kV) and high (10 kV) were employed to give the best resolution. Magnification from 50 k to 200 k was used.

3.5.3 Energy Dispersive X-Ray (EDX)

3.5.3.1 Background of EDX

Energy dispersive X-Ray (EDX) that is incorporated with FESEM instrument is used to determine the elemental composition on the material surface within 500 nm in thickness. EDX is able to distinguish all elements in the order of 0.1 percent and is limited to elements having an atomic number greater than boron. X-rays are generated from the atoms when an electron beams from the FESEM scans across the sample surface. The energy of the individual X-Rays is the characteristics of the elements that generate it.

3.5.3.2 Sample analysis procedure

The elemental composition was determined using INCA software. The analysis was conducted per area basis. For EDX, similar sample preparation as FESEM was employed.

3.5.4 High Resolution Transmission Electron Microscopy (HRTEM)

3.5.4.1 Background of HRTEM

High Resolution Transmission Electron Microscopy (HR-TEM) is widely used to evaluate the sample crystallinity, crystal size, crystal structure, surface defects and lattice spacing at atomic scale. This instrument utilized both the transmitted and scattered beams to generate an interference image, and can be as small as the unit cell of crystals. This instrument generally consists of more than one condenser lenses to focus the electron beams on the sample, objective lens to form diffraction patterns and intermediates lenses for image magnification on the screen. Different from conventional TEM, HR-TEM has higher power of lattice resolution

3.5.4.2 Sample analysis procedure

HR-TEM analysis was conducted using JEM-2100F at an accelerating voltage of 200 keV. A small amount of fine powder sample was dispersed in ethanol and sonicated for 0.5 min in an ultrasonic bath at room temperature. Using a disposable pipette, one drop of the suspension was carefully dropped on a 400 square mesh copper grid (3.05 mm) and dried at 40 °C in an oven for 3 days prior to analysis

3.5.5 Selection Area Electron Diffraction

3.5.5.1 Background of SAED

Selection Area Electron Diffraction is widely used to measure crystal structure and lattice parameters. SAED analysis is done inside a TEM instrument. This instrument works on similar as X-Ray diffraction analysis but in several thousand times smaller area than X-Ray diffraction. It can detect the lattice spacing, angle, the type of materials. In SAED, a user can wish to focus on a single crystal and capture a diffractogram of the crystals where a series of bright spots will represent a crystal plane.

3.5.5.2 Sample analysis procedure

The sample preparation was followed as the similar as HRTEM analysis.

3.5.6 Brunner-Emmet-Teller (BET)

3.5.6.1 Background of BET

BET is used to analyze the textural properties such as surface area, pore size, pore shape and pore volume of the sample. BET is a multilayer absorption process whereby non-corrosive gases (such as nitrogen, carbon dioxide, argon, etc.) are used to evaluate the adsorption of gas molecules on the solid surface. The degree of adsorption depends on several factors such as pressure, temperature and solid-gas interactions. After reaching the saturation pressure, the sample is removed from the gas environment and is heated to release adsorbed gas from the material and quantified. The collected data is displayed as BET isotherm which plots the amount of gas adsorbed with the relative partial pressure. There are 5 types of adsorption isotherms which are Type I, II, III, IV and V.

3.5.6.2 Sample analysis procedure

The textural properties of the samples were analyzed using nitrogen adsorption-desorption analyzer TriStar II 3020 series, Microactive 2.0. Prior to BET analysis, 1 g of the solid sample was dried in an oven at 60 °C for 2 h to remove any trapped moistures. The sample was then placed in a 6 mm glass cell and degassed in a vacuum chamber, operating at 350 °C for 6 h to remove remaining moisture and possible contaminants. The sample was measured using relative pressure range of 0.01-0.90 P/P_o.

3.5.7 Raman analysis

3.5.7.1 Background of Raman

Raman spectroscopy is generally employed to analyze the chemical structure of inorganic materials. Raman spectroscopy is based on scattering of light by the vibrating molecules as a result of interaction between the monochromatic laser beam and molecules

of the sample. The Raman spectrum is constructed using the scattered light which has a different frequency from the incident light. This is also referred as inelastic scattering. Thus, Raman spectra are formed due to the inelastic collision between the incident monochromatic beam and molecules of the sample.

3.5.7.2 Sample analysis procedure

An in-built PL-Raman spectroscopy (Renishaw LabRam confocal Raman microscope with 325 nm line of a continuous He–Cd laser at room temperature) was used to analyze chemical structure of the sample. The sample was grinded into fine powder before analysis.

3.5.8 Temperature Programmed Reduction (H₂-TPR)

3.5.8.1 Background of H₂-TPR

H₂-TPR is a very useful tool in heterogeneous catalysis to determine the efficient temperature conditions of reducing the catalyst. An oxidized sample is placed in a sample holder in the instrument and a mixture of 10 % H₂/He gas flowed over the sample. The detector in the instrument determine the temperature and amount of gas which was consumed by the sample.

3.5.8.2 Sample analysis procedure

Temperature Programmed Reduction were performed on a Micrometrics Chemisorb 1100 series instrument. Before the analysis, removal of the surface moisture of 0.2 g catalyst was done via pretreatment at 180 °C for 1 h by N₂ gas (20ml/min). Then, the analysis was carried out in process condition till 900 °C under gas flow 5% H₂ with 95% N₂ mixtures at heating rate of 10 °C/min and was held for 10 mins.

3.5.9 Temperature Programmed Desorption (O₂-TPD)

3.5.9.1 Background of the O₂-TPD

The re-oxidisability of the catalyst was determined using O₂-TPD. A mixture of 10 % O₂/ N₂ gas was passed through the reduced sample after H₂-TPR and the oxygen consumption in different temperature was detected by the detector inside the instrument.

3.5.9.2 Sample analysis procedure

The similar procedure as H₂-TPR was followed during O₂-TPD analysis.

3.5.10 Thermogravimetric Analysis (TGA)

3.5.10.1 Background of TGA

Thermogravimetric Analysis (TGA) is used to determine the change in the material physical and chemical properties as a function of increasing temperature or time. It is generally employed for materials that exhibit either mass loss or gain as a result of decomposition or oxidation process. The instrument continuously measure the weight of the sample as it is gradually heated up to a maximum temperature of 2000 °C. TGA can also be coupled with FTIR and mass spectroscopy gas analysis

3.5.10.2 Sample analysis procedure

The thermal stability of the sample was determined using Mettler-Toledo TGA/SDTA851e instrument. Approximately 50 mg of the sample was placed in an alumina crucible and heated from room temperature up to 700 °C using heating rate of 5 °C/min and constant air flow of 50 ml/min. The change in mass over temperature was plotted and the point of thermal stability of the sample was identified.

3.5.11 X-Ray Photoelectron Spectroscopy

3.5.11.1 Background of XPS

X-ray Photoelectron Spectroscopy (XPS) is used to characterize the surface chemical state of a material from 1 to 12 nm in depth. The chemical element and nature of the chemical bond between these elements can be detected except for hydrogen and helium. In XPS, the material is irradiated with sufficient energy of X-rays to excite the electrons away from the nuclear attraction force of an element into the vacuum state. In the vacuum state, the electron analyzer measures the kinetic energy and produces an energy spectrum of intensity versus binding energy. Each of the energy peaks on the spectrum represents a specific element

3.5.11.2 Sample analysis procedure

The binding energy of different elements in the sample was determined using Thermo Scientific K-alpha instrument. The sample was pressed into tablets before analysis. The analysis was carried out using a non-monochromatized Mg K α (photon energy of 1253.6 eV). A flat gold (Si/10nm Ti/200nm Au) was used as the substrate and reference. The XPS core levels were aligned to the C1s binding energy (BE) of 285 eV.

3.6 Calculations

3.6.1 Scherrer's equation

Scherrer's equation was used to determine the crystallite sizes of nano TiO₂ crystals and is not applicable for grains larger than 0.01 to 0.02 μm .

$$\tau = K \lambda / \beta \cos \theta \quad \text{Eq. 3.1}$$

Where τ is the mean size of the ordered (crystalline) domains, K is a dimensionless shape factor, λ is the X-ray wavelength, β is the line broadening at half the maximum intensity (FWHM) and θ is the Bragg angle. The dimensionless shape factor has a typical

value of 0.9, but varies with the actual shape of the crystallites. The value of 0.9 generally represents spheres particles, but is also valid for cubes, tetrahedral and octahedral particles.

3.7 Catalytic activity measurement

The performance test of the synthesized mixed oxide catalysts using both the oxidants was examined and measured for comparison study. The fig 3.2 illustrates the two possible reaction pathways followed for two different oxidants with the formed products.

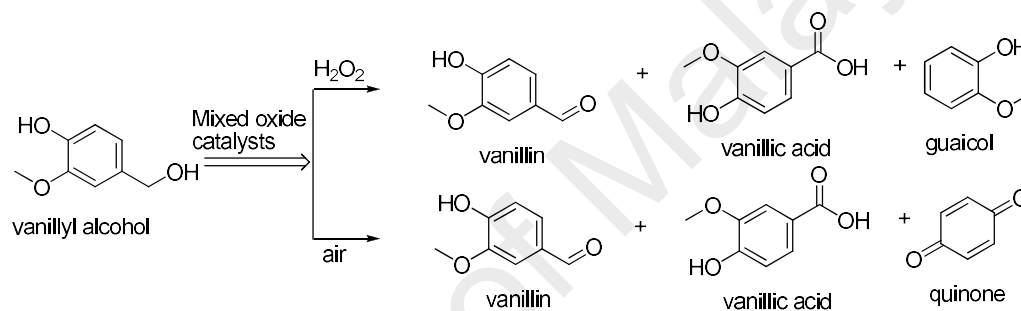


Figure 3.2: Oxidation of vanillyl alcohol using air and H₂O₂ oxidants over mixed oxide catalyst.

Reaction mixture collected in every 30 mins were analyzed using Agilent Technology HPLC Chromatography 1100 series connected with a UV detector and computer interface. A mixture of solvent (85 % water + 15 % acetonitrile) along with 1 % acetic acid was used as the mobile phase and RP-C18 column (4.6×150 mm, 3.5 μm, pore size 80-120 Å) by Zorbax was used. The products and substrates were successfully detected by a UV detector at $\lambda_{\text{max}} = 270$ nm. The column temperature was stable at 28 °C with flow rate 1 ml/min. The conversion, selectivity and yield were measured as follows:

$$\text{conversion (\%)} = \frac{\text{final conc of VA} - \text{intial conc of VA}}{\text{initial conc of VA}} \times 100$$

$$\text{selectivity (\%)} = \frac{\text{no of moles a product formed}}{\text{total no of moles products formed}} \times 100$$

$$\text{Yield} = \frac{\text{number of moles of product}}{\text{initial number of moles of VA}} \times 100$$

University of Malaya

CHAPTER 4: RESULTS AND DISCUSSION

4.1 Structural properties of synthesized mixed oxide catalysts

The structural and chemical properties was investigated using various spectroscopic tools ranging XRD, Raman, XPS, BET, HRTEM, FESEM, EDX, SAED, H₂-TPR and O₂-TPD etc. The results revealed through these techniques indicated the properties of synthesized mixed oxide catalysts to establish an intimate relation with the catalytic activity.

4.1.1 Structural properties of synthesized Cu-Ti mixed oxide catalysts

4.1.1.1 Thermogravimetric Analysis (TGA/DTG)

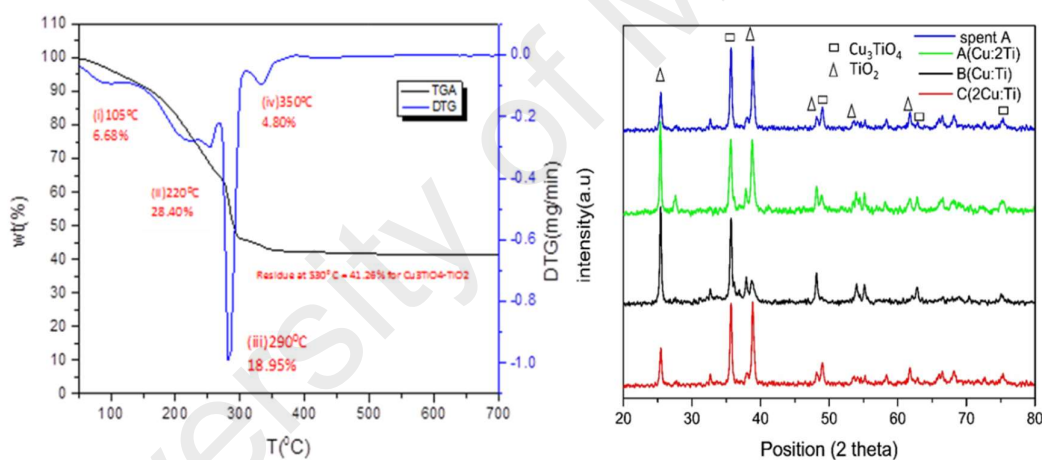


Figure 4.1: Synthesized Cu-Ti mixed oxide catalysts illustrating TGA/DTG spectrum (left); XRD analysis (right).

The thermogravimetric analysis was carried out to examine the thermal stability of the catalyst (Cu: 2Ti) in the temperature range from 50 °C to 700 °C (Fig. 4.1). The Cu: 2Ti mixed oxide catalyst was chosen to analyse by TGA/DTG after primary screening of the catalyst in the oxidation reaction. The TGA/DTG curve shown four distinct weight loss by 6.67 %, 28.40 %, 18.90 %, and 4.80 % at temperature of 105 °C, 220 °C, 290 °C and 350 °C respectively. The weight loss of 6.67 % attributed to the removal of absorbed

moisture from the catalyst. The weight loss by 28.40 % correspond to the removal of crystallite water molecules that was present on the precursors. The removal of organic groups was related to the weight loss by 18.90 %. Further weight loss by 4.80 % could be due to removal of remaining organic residue and any impurities. There was no further weight loss observed till 700 °C which suggested that the catalyst reached it's thermal stability till 700 °C. Therefore, in this work, Cu_3TiO_4 was found to be stable at low temperature relative to the previously reported literature (Hennings, 1980).

4.1.1.2 Crystal phase and crystallinity (XRD)

XRD pattern for all synthesized samples are displayed in Fig. 4.1. In the recorded XRD patterns, two phases TiO_2 and Cu_3TiO_4 were identified from PANalytical X'Pert Highscore Plus software based on Bragg angle (2 theta) and d spacing. The XRD peaks at 2 theta = 25.40°, 38.78°, 48.16°, 54.12°, 61.70° with d spacing (Å) 3.50, 2.32, 1.88, 1.69, 1.50 exactly matched Miller indices of (101), (112), (200), (105), (204) plane of anatase tetragonal TiO_2 in accordance with JCPDS no (ICSD= 01-073-1764). The XRD peaks at 2 theta = 35.65°, 55.13°, 62.84°, 75.24° with d spacing (Å) 2.51, 1.66, 1.47, 1.26 were ascribed to Miller indices of (012), (018), (113), (024) plane of rhombohedral shaped spinel Cu_3TiO_4 phases in accordance with JCPDS no (ICSD= 00-041-0254). However, the peak intensity at 38.78° was more pronounced with the increase of Cu loading as both TiO_2 and CuO phases overlapped at this position. Hence, the prepared catalysts represented mixed phase $\text{Cu}_3\text{TiO}_4\text{-TiO}_2$ with high crystallinity and no other impurities. Moreover, the observed rhombohedral shape of Cu_3TiO_4 phase (space group R-3m) having cell parameters $a= 3.04$, $c= 17.19$ vary from the cell parameters of tetragonal TiO_2 ($a= 3.78$, $c= 9.40$) implied on considerable defect chemistry in form of distortion in the lattice owing to insertion of Cu in the TiO_2 framework. Defect chemistry is a highly desirable characteristic to enhance the catalytic activity of mixed oxide catalysts.

Furthermore, in order to detect any change in the catalyst phases and chemical composition, the spent catalyst was analyzed by XRD after the catalytic reaction. It was worth to mention that the XRD finger print of the used catalyst exactly matched with fresh Cu-2Ti mixed oxide catalyst in terms of peak position at 2 theta. However, the crystallinity of the recycled catalyst was negligibly affected after the catalytic reaction. In addition, the crystallite size of catalyst (Cu: 2Ti) was measured by 36 nm using Scherrer equation while catalysts (Cu: Ti) and (2Cu: Ti) were 41 nm and 43 nm, respectively..

4.1.1.3 Raman analysis

The Raman spectra of synthesized catalysts are reported in Fig. 4.2. The Raman spectra could be related to the typical pattern of Raman active vibrational modes of bulk anatase Titania crystalline phase with apparent of shifting (Samsudin, Hamid, Juan, Basirun, Kandjani, et al., 2015). It was noticeable in the Raman spectra that two Raman modes at E(g) and Eg₍₂₎ shows slight shifting towards higher wavenumber whereas Raman modes at B(g), Bg₍₂₎ in opposite trend. The observed Raman band shift at 146 cm⁻¹, 147 cm⁻¹ and 151 cm⁻¹ for Cu₃TiO₄-TiO₂ catalysts was attributed to the bending vibration Eg₍₁₎ of Ti-O-Cu coordination in contrast to bulk O-Ti-O bending vibration which occur at 144 cm⁻¹. Similarly, the peaks located at Raman shift 202 cm⁻¹, 394 cm⁻¹, 507 cm⁻¹, 628 cm⁻¹ for the catalyst Cu₃TiO₄ could correspond to the Raman active Eg₍₂₎, B(g), Bg₍₂₎, Eg₍₃₎ modes of TiO₂. However, no Raman shift for CuO was visible in the Raman spectra suggested absence of isolated CuO phase in the synthesized catalyst structure. The blue and red shift of these Raman modes revealed that the Raman active modes of O-Ti-O system was affected by the insertion of Cu²⁺ (0.77 Å) ion in the Ti-O lattice and significantly rearrange of the cations in the octahedral and tetrahedral site of the Cu₃TiO₄ lattice. This indicated an expansion of the anatase unit cell as reported in XRD database (from 135x10⁻⁶ m³ to 137.60 x10⁻⁶ m³) (Sathasivam et al., 2015). And

also, the fact of distortion in the lattice was evidenced by the shifting of the Raman modes as E_g band is strongly sensitive to the change in the lattice parameter and attached ligands (Carlucci et al., 2014). Furthermore, the noticeable trend of shifting of the Raman active vibrational modes seemed to depend on the stoichiometry of Cu to Ti in the bulk catalyst.

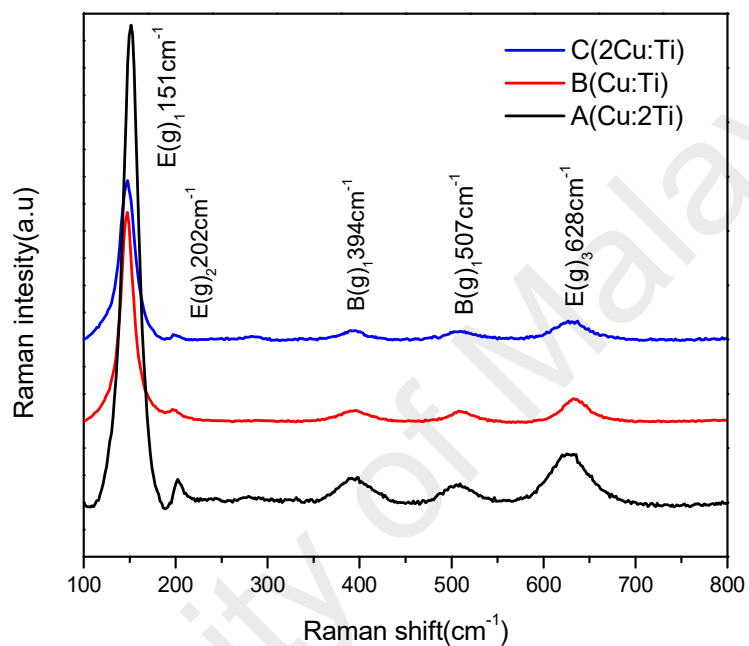


Figure 4.2: Raman analysis of synthesized Cu-Ti mixed oxide catalysts.

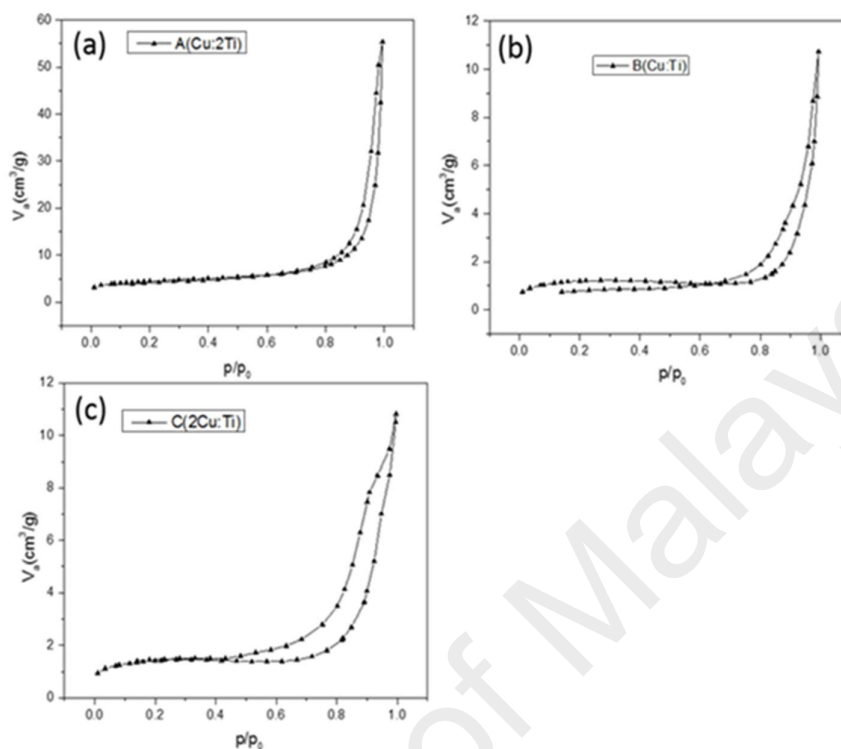


Figure 4.3: N₂ adsorption-desorption curve of synthesized Cu-Ti mixed oxide catalysts (a) Cu: 2Ti; (b) Cu: Ti; (c) 2Cu: Ti.

4.1.1.4 Textural properties (BET)

The N₂ adsorption/desorption isotherm curve for synthesized Cu-Ti composite oxide catalysts (Fig. 4.3) shown type IV isotherm which indicated the mesoporous structure. The measured BET surface area, pore diameter, pore volume for catalyst (Cu: 2Ti), catalyst (Cu: Ti) and catalyst (2Cu: Ti) are displayed in Table 4.1. As the surface area of synthesized catalysts was found low surface are, the catalytic activity of synthesized Cu-Ti composite oxide catalyst was not largely affected by surface area of the catalyst. However, the BET surface area for catalyst (Cu: 2Ti) ($15 \text{ m}^2\text{g}^{-1}$) was slightly higher than catalyst (Cu: Ti) and catalyst (2Cu: Ti). Thr reason of low surface area might be due to treatment at thr high temperature during calcination process. And also, a careful

observation on the pore distribution of catalyst Cu: 2Ti indicated that the pores were uniform.

Table 4.1: Textural properties of synthesized Cu-Ti mixed oxide catalysts.

catalyst	S_{BET} (m²/g)^a	V_t (cm³/g)^b	D_{BJH} (nm)^c
(Cu: 2Ti)	15.67	0.084	21.5
(Cu: Ti)	5.02	0.016	15.3
(2Cu: Ti)	4.11	0.015	13.3

^aBET surface area

^bThe total pore volume

^cBJH average pore diameter.

4.1.1.5 Surface composition and oxidation state (XPS)

It was evident that from the XPS spectra of catalyst (Cu: 2Ti) (Fig. 4.4), there was no other elements detected on the sample surface as impurities except for expected Cu, O, and Ti. The catalyst Cu:2Ti was chosen to analyse under XPS as it shown promising catalytic activity than other two catalysts in primary catalytic evaluation. In Fig. 4.4(a), the photoelectrons splitted from spin orbital of Cu 2p_{1/2} and Cu 2p_{3/2} at binding energy 933.8 eV and 953.88 eV respectively which was evidently ascribed to Cu²⁺ ion (Tseng, Wu, & Chou, 2004). The shaken up peak from 940-955 eV in Cu 2p spectra further confirmed the presence of Cu²⁺ ion (Mathew, Shiju, Sreekumar, Rao, & Gopinath, 2002). Fig. 4.4(b) represented photoelectron from the spin orbital splitting of Ti 2p and Ti 2p binding energy location at 458.66 eV and 464.36 eV which corresponded to the presence of Ti⁴⁺ on the sample (Chu, Younis, & Li, 2012). The slight positive shift in the binding energy of Ti 2p peak position by 0.2 eV might be due to the decrease of the electron cloud density on the outer most shell of Ti (F. Liu et al., 2012). This observation was further supported by the formation Cu-O-Ti bond. The O 1s spectra were deconvoluted following the nonlinear de Gaussian displayed in Fig. 4.4(c). There were two distinguished peaks

identified where the peak located at 529.91.3 eV binding energy could be either Cu-O or Ti-O linkage present on the Cu-Ti mixed oxide catalysts. Robert et al. reported that the XPS binding energy between 531-532 eV could be attributed to weakly held (O^-) species at the surface (i.e. compared to lattice oxygen)(Roberts, 1989) which could be referred as surface defect oxygen or oxygen vacancy in the framework of oxide structure guided by one previous report (O'Connell, Norman, Hüttermann, & Morris, 1999). Similar observation was also made in this work for the peak located at 531.2 eV in O 1s spectra. It was presumed that this surface defect oxygen was originated by the nonstoichiometry of cations and frequent rearrangements of the cations in the distorted lattice of the Cu-Ti composite oxide catalyst. Similar observation was on the formation of oxygen vacancies on stoichiometry of the cations in the mixed oxide was reported (D. Chen, Chen, Baiyee, Shao, & Ciucci, 2015; Liotta et al., 2008). Hence it was predicted that these weakly held oxygen species impacted on enhancement of the catalytic activity for liquid phase oxidation of vanillyl alcohol towards vanillin. Moreover, additional oxygen vacancies were created on the catalyst surface due to the usage of Trifluoroacetic acid (TFA) during the one pot synthesis method. The oxygen vacancies formation were triggered via (i) charge imbalance between the two anions (F^- , O^{2-}) and also (ii) the removal of physisorbed F^- on the catalyst surface during heat treatment (Samsudin et al., 2016).

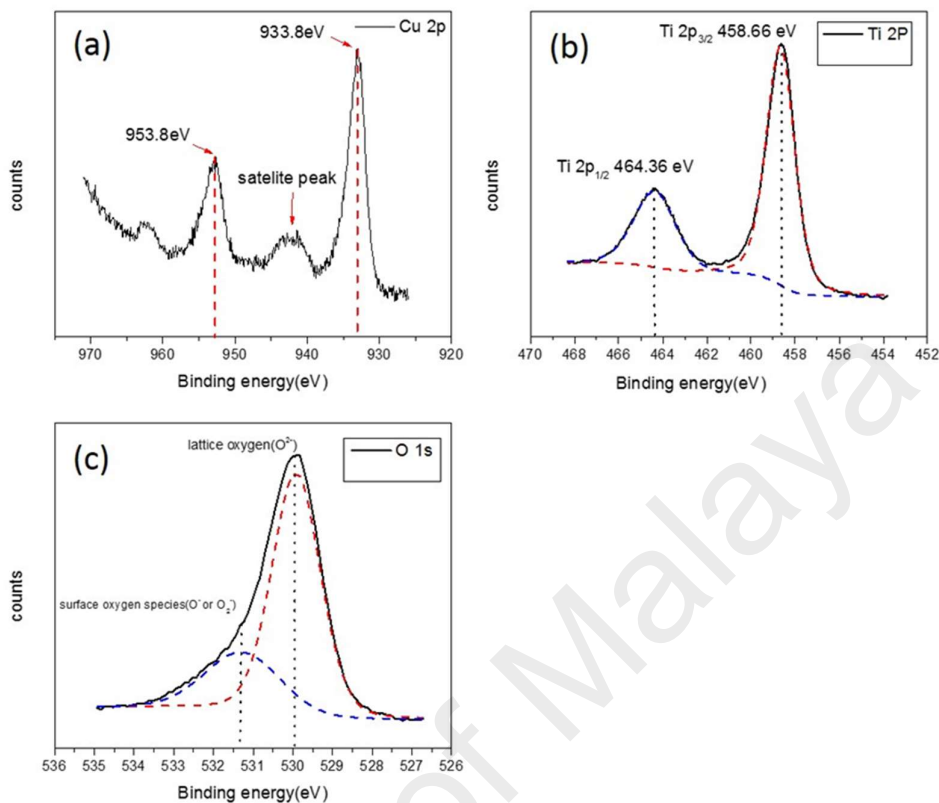


Figure 4.4: XPS analysis of synthesized Cu-2Ti mixed oxide catalyst. (a) Cu 2p; (b) Ti 2p; (c) O 1s.

4.1.1.6 Redox properties (H₂-TPR and O₂-TPD)

To investigate the reducibility ability of the catalysts, TPR profile (Fig. 4.5a) was analyzed for synthesized Cu-Ti mixed oxide catalysts. TiO₂ is difficult to reduce and thus does not show any peak in the H₂-TPR profile in the temperature range of 750 °C to 60 °C (Watanabe, Ma, & Song, 2009). The pure bulk CuO started reduction at 330 °C (Mai, Zhang, Shi, Yan, & Li, 2011). Here, all three catalysts reduction started at 160 °C which indicated that the synergy of Cu and Ti in synthesized mixed oxides greatly improved the reduction capability at low temperature. Therefore, the only detected peaks with peak maxima at 301 °C, 341 °C and 377 °C for catalyst (Cu: 2Ti), while catalyst (Cu: Ti) and catalyst (2Cu:Ti) indicated presence of only one step reduction of Cu²⁺ species on the

catalyst domain, which in agreement with the XPS analysis. Moreover, in case of catalyst (Cu: 2Ti), the markedly shifted peak towards low reduction temperature implies on the highest interaction between Cu and Ti (H. Tian, Zhang, Scott, Ng, & Amal, 2014; Zou, Meng, Guo, & Zha, 2009) (Xiaolan Tang et al., 2005), and also very high dispersion of Cu on the Cu_3TiO_4 framework (L.-F. Chen et al., 2008). Thus, it enhanced the reducibility of catalyst (Cu: 2Ti) and consequently benefitted the catalytic conversion of vanillyl alcohol towards vanillin at low temperature.

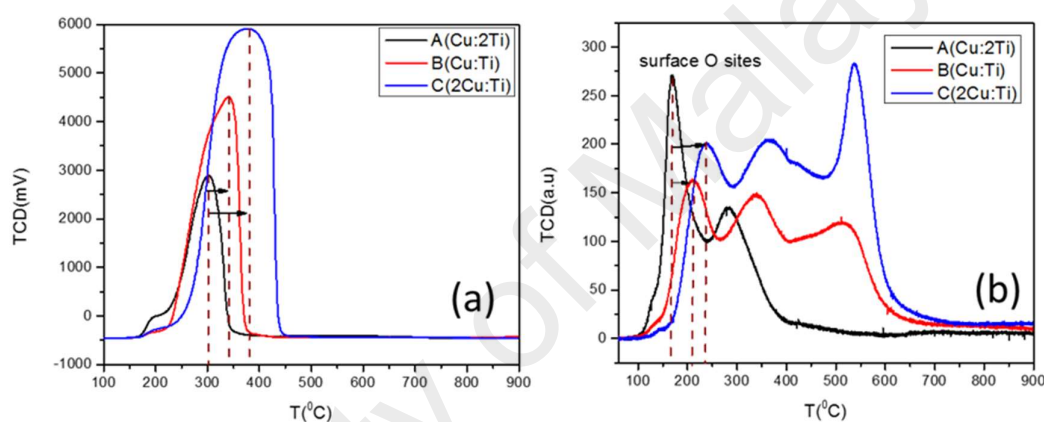


Figure 4.5: Synthesized Cu-Ti mixed oxide catalysts illustrating (a) H₂-TPR analysis (b) O₂-TPD analysis.

To investigate the re-oxidisability of the catalysts, O₂-TPD profile (Fig. 4.5b) was studied on the same sample after H₂-TPR analysis. Much interestingly, there were two distinctive peaks observed in catalyst (Cu: 2Ti) whereas three distinguished peaks for catalyst (Cu: Ti) and catalyst (2Cu: Ti). However, in O₂-TPD profile of catalyst (Cu: 2Ti), the oxidation peak located at higher temperature was missing. Three detected peaks were attributed to three step reoxidation of the catalysts in following steps (Pintar, Batista, & Hočevár, 2005). (i) the peak at the lowest temperature with peak maxima at 167 °C, 209 °C, 239 °C for catalyst (Cu: 2Ti), catalyst (Cu: Ti) and catalyst (2Cu:Ti) respectively, corresponded to desorption of oxygen in the oxygen deficiency present on the highly

dispersed coordinated Cu species on the surface or the oxygen vacancy sites as a form of defects created in the mixed oxide (ii) the peaks positioned at 285 °C, 340 °C, and 362 °C for catalyst (Cu: 2Ti), catalyst (Cu: Ti) and catalyst (2Cu: Ti) respectively attributed to re-oxidation of bulk Cu species to Cu²⁺ ion. Besides these two peaks, the peak located at higher temperature 511 °C, 562 °C was due to oxygen desorption on the consumed H₂ storage on the interface of the phases in the catalyst structure. In O₂ -TPD profile, the most intense oxygen desorption peak at low temperature for catalyst (Cu: 2Ti) was indicative of the presence of larger concentration of oxygen vacancies as a form of surface defects in the mixed oxide than other two catalysts. It was worth to note that catalytic activity can be improved by creating excess amount of oxygen vacancies which could act as possible active sites on the catalyst surface. After removal of Trifluoroacetic acid during calcination process many oxygen vacancies were created by the phenomenon charge compensation on the removal site of Fluorine from the lattice. In addition, the observed apparent shifting of the peak positions towards higher temperature gradually with change of atomic ratio of Cu to Ti indicated the poor accessibility of oxygen on the coordinated tetrahedral and octahedral site Cu²⁺ present on the lattice, and thus required high temperature to be re-oxidized. Nevertheless, a careful observation on the lowest temperature O₂ desorption peak of catalyst contained high amount of Ti was indicative of enrichment of oxygen mobility on the surface of the catalyst at low temperature. This was the vital fact that resulting of improvement of catalytic activity for catalyst (Cu: 2Ti).

4.1.1.7 Morphology

The morphology of fresh and spent Cu-Ti mixed oxide catalyst was characterized by FESEM analysis (Fig. 4.6). FESEM images (Fig. 4.6a, 4.6b, 4.6c) for fresh catalyst (Cu: 2Ti), catalyst (Cu: Ti) and catalyst (2Cu: Ti) respectively revealed an irregular surface of the catalysts and aggregated particles. The uneven surface of the catalysts is predicted to render better catalytic activity due to the exposure of high surface area. However, the

decrement of the catalytic activity for spent catalyst (Cu:2Ti) could be related to the smooth and plane surface of the catalyst (Fig. 4.6d). Moreover, High-resolution Transmission Emission Microscopy (HR-TEM) analysis was performed for the catalyst (Cu: 2Ti) which shown the best catalytic activity. The HRTEM image shows high and regular dispersion of Cu on the TiO₂ surface (Fig. 4.7a). In addition, observation for the lattice fringe of the catalyst (Fig. 4.7c) revealed the presence of grain boundaries and surface disorder between (111) plane for TiO₂ and (012) plane for Cu₃TiO₄ which indicated a form of surface defects that in agreement with previous study (Halilu et al., 2016). Moreover, the formation of rhombohedral shape of Cu₃TiO₄ phase of the catalyst was also confirmed in the high resolution image (marked arrow in the picture). Besides, in order to further ensure the formation of Cu₃TiO₄ phase, selective area electron diffraction (SAED) was studied (Fig. 4.7d). The diffused ring observed in the SAED pattern confirm that the synthesized catalyst was a poly-crystalline. The bright spots visible in the SAED pattern evidently confirm the lattice plane 012, 018, 113 of Cu₃TiO₄ by the measurement of d spacing (Å) 2.51, 1.66, 1.47 respectively.

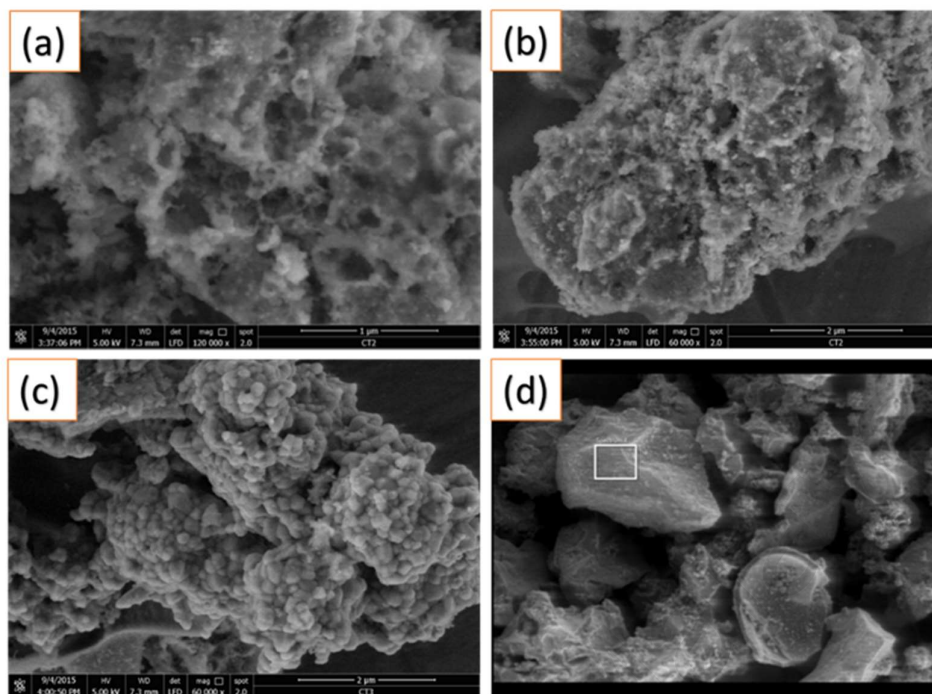


Figure 4.6: FESEM analysis of synthesized Cu-Ti mixed oxide catalysts (a) Cu:2Ti; (b) Cu:Ti; (c) 2Cu:Ti; (d) spent catalyst.

The elemental composition of the synthesized catalysts was also studied by energy dispersive X-ray microscopy (EDX) (Fig. 4.8). The measured stoichiometric ratio of Cu and Ti based on peak area ratio in EDX spectra for catalysts (Cu: 2Ti) (Fig. 4.8a), catalyst B (Cu: Ti) (Fig. 4.8b) and catalyst (2Cu: Ti) (Fig. 4.8c) tentatively matched with the intended molar ratio of Cu and Ti. Moreover, the molar ratio of Cu: Ti before and after (Fig. 4.8d) the catalytic reaction was almost similar which suggested no change in the leaching of active metals occurred during the reaction. In Fig. 4.9, the evenly distributed elements (Cu, Ti, and O) confirmed vivid homogeneity of the oxide composite. This observation thus eliminated the probability of physical mixture of two different oxides.

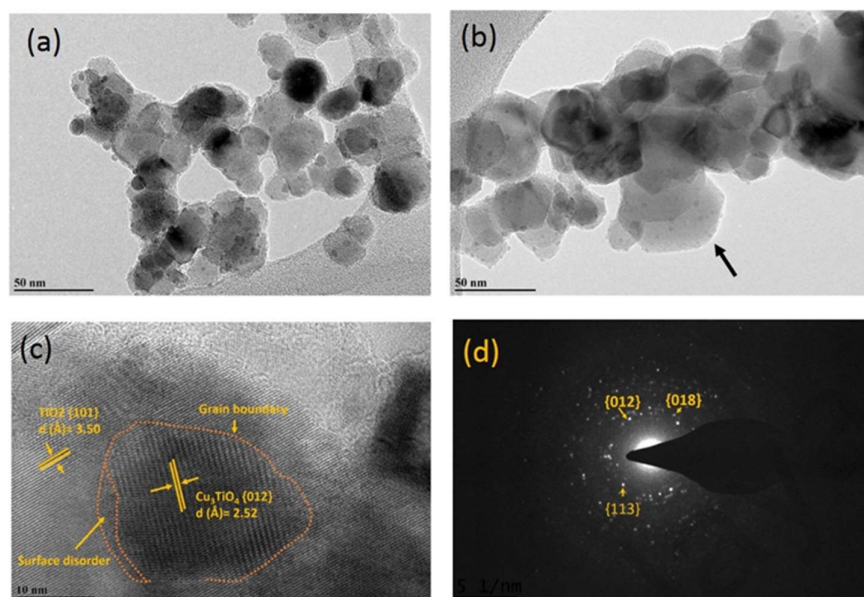


Figure 4.7: HRTEM and SAED pattern of synthesized Cu-2Ti mixed oxide catalyst. (a) Overview of the catalyst; (b) rhombohedral shape; (c) lattice fringe; (d) SAED pattern.

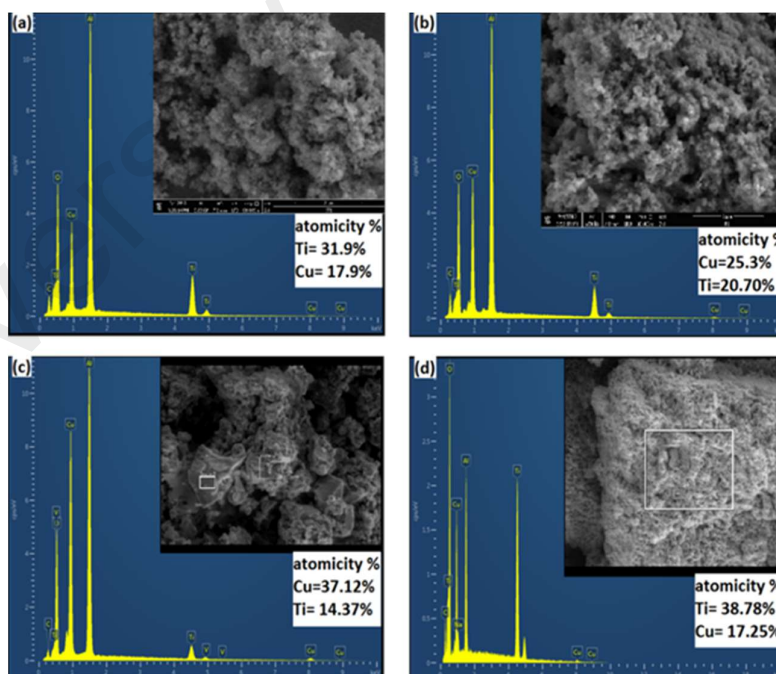


Figure 4.8 EDX analysis of synthesized Cu-Ti mixed oxide catalysts. (a) Cu: 2Ti; (b) Cu: Ti; (c) 2Cu: Ti (d) spent catalysts.

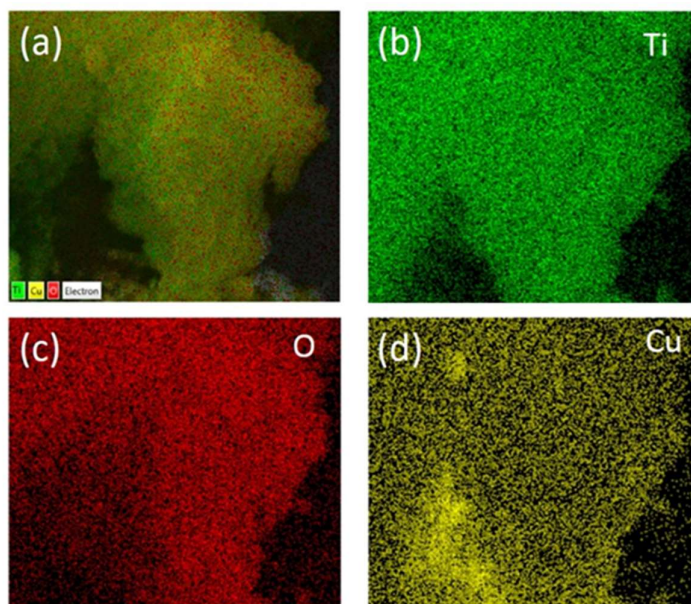


Figure 4.9: Chemical mapping of synthesized Cu-2Ti mixed oxide catalyst (a) elemental distribution; (b) Ti distribution; (c) O distribution (d) Cu distribution.

4.1.2 Structural properties of Cu-Zr mixed oxide catalysts

4.1.2.1 Thermogravimetric Analysis (TGA/DTG)

There were two distinctive weight loss detected on the TGA/DTG analysis of the synthesized CuZrO_3 catalyst (Cu: 2Zr) before calcination (Fig. 4.10). The Cu: 2Zr ration was considered as it shown promising catalytic activity in the primary catalytic evaluation. The continuous weight loss by 13.43 % with a peak maxima at 280 °C could be ascribed to the loss of surface moisture and crystallite water from bulk Cu-2Zr mixed oxide catalyst. The maximum weight loss by 46.30 % with peak maxima at temperature 330 °C possibly corresponded to removal of acetate organic group present in the metal precursors as CO_2 and water. The minor two weight loss by 1.13 % and 0.56 % at 440 °C and 550 °C might be owing to elimination of further impurities from the catalyst. The amount of residue by 38.52 % was constant till 700 °C indicating the thermal stability of the catalyst at higher temperature.

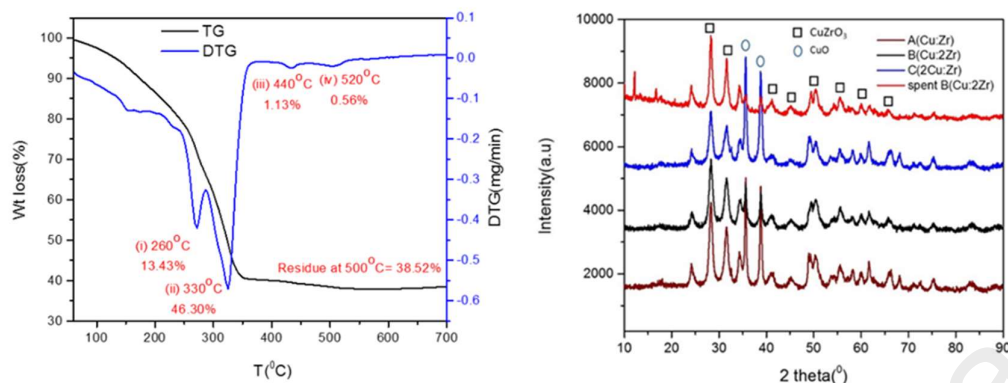


Figure 4.10: Synthesized Cu-Zr mixed oxide catalysts illustrating TGA/DTG analysis (left); XRD analysis (right).

4.1.2.2 Crystal phase and crystallinity (XRD)

The chemical formula and the phases of Cu-Zr catalysts were detected by XRD diffractogram analysis based on Xpert High score plus Analysis database (Fig. 4.10). Careful observation on XRD pattern suggested that the synthesized crystal was identified as CuZrO₃ phase in accordance with JCPDS no (ICSD 00-043-0953). However, presence of a minor phase CuO also was detected which match with the database Terorite (ICSD 98-002-6715). The peak positioned at 2 theta = 24.33°, 28.29°, 31.58°, 34.34°, 41.01°, 49.47°, 50.41°, 54.41°, 55.56°, 58.23°, 60.01°, 61.72° respectively with d spacing(Å) 3.67, 3.15, 2.83, 2.61, 2.20, 1.84, 1.81, 1.69, 1.65, 1.58, 1.54, 1.50 respectively exactly corresponded to miller indices (012) (112) (211) (013) (023) (040) (321) (322) (313) (401) (134),(402) plane of CuZrO₃ respectively. And also, the peaks positioned at 2 theta = 35.61, 38.81 respectively were ascribed to the plane of (11-1), (111) of CuO. Hence the catalyst was synthesized as highly crystalline perovskite shaped CuZrO₃ catalyst with a minor phase CuO and no other impurities. In addition, the orthorhombic shape having the cell parameters (a=6.4465 Å, b= 7.4008 Å, c= 8.3128 Å) was varied from the typical cubic shape perovskite structure (a = 3.905 Å). This fact indicated displacement of B cation (Zr) introducing distortions in the domain of the perovskite crystal (Reller &

Williams, 1989). This phenomenon would imply on appreciable surface defects in the material which was one of the clue to the significant catalytic activity of perovskite type mixed CuZrO_3 catalyst.

The reused catalyst (Cu: 2Zr) was also characterized by XRD to detect any change in the phases, chemical composition and crystallinity. There was no change observed in the phase and chemical composition as the recorded XRD fingerprint for spent catalyst shown same pattern as the fresh catalyst based on peak location at Bragg angle. However, the crystallinity was slightly reduced relative to the fresh catalyst after performing the catalytic reaction.

4.1.2.3 Raman analysis

The Raman spectrum observed in Fig. 4.11 shown two distinctive patterns of Zr-O bonds and Cu-O bonds. Raman shift of Zr-O bonds was present at 146 cm^{-1} , 181 cm^{-1} and 472 cm^{-1} respectively (M. Li, Feng, Ying, Xin, & Li, 2003). The presence of Raman active modes of Cu-O bond were observed at 297 cm^{-1} (Ag), 344 cm^{-1} (Bg) and 629 cm^{-1} (Bg) respectively (Hagemann, Bill, Walker, & François, 1990). In the enlarged Raman spectrum at 616 to 635 cm^{-1} , peak shifting was observed. In bulk (Cu: 2Zr) catalyst, the Raman peak was noticeably shifted to the left relative to bulk (Cu: Zr) catalyst and was attributed to the larger concentration of Zr-O bonds in CuZrO_3 catalyst structure. Contrary, the Raman peak of bulk (2Cu: Zr) catalyst with higher loading of Cu slightly shifted to the right and attributed to the larger concentration of Cu-O bonds. It was worth to mention that shorter bond lengths of Cu-O facilitates a blue Raman shift as a result of stress and strain phenomenon (Samsudin et al., 2016). Furthermore, it was noticed that, larger stoichiometric ratio of Cu in the CuZrO_3 catalyst induces structure defects and thus results to blue Raman shifting as well. In addition, the broadening of the peak illustrates

the structural distortion associated with the formation of perovskite structure CuZrO_3 (Perry, LIU, & INGEL, 1985).

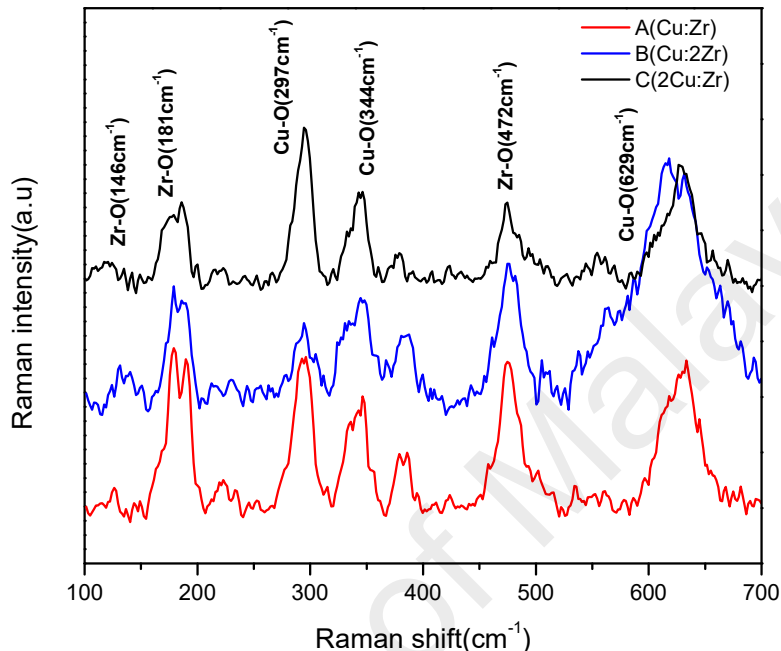


Figure 4.11: Raman analysis of synthesized Cu-Zr mixed oxide catalysts.

4.1.2.4 Textural properties (BET)

In order to correlate effect of textural properties of the catalysts towards the catalytic activity, BET N_2 adsorption-desorption isotherm was employed (Fig. 4.12). Results shown the presence of type (III) isotherm and slit shaped pore distribution for Cu-Zr catalysts. One of the key barrier to obtain high catalytic activity of a perovskite type oxide is low surface area (Tanaka & Misono, 2001). The textural properties such as pore size, pore diameter, and BET surface area (Table 4.2) of synthesized CuZrO_3 catalysts clearly suggested that the catalyst via this facile solution method had moderate surface area with meso-porosity in the structure. In addition, it was worth to note that higher loading of ZrO_2 contributed in the enrichment of the surface area ($40.83\text{ m}^2/\text{g}$) whereas decrement in case of low Zr loading ($20\text{ m}^2/\text{g}$) in the bulk phase of the CuZrO_3 catalyst. The

enrichment by 2 magnitude fold in the BET surface area of catalyst (Cu: 2Zr) was reasonably the key parameter to obtain superior catalytic. Moreover, it was found that the textural properties of spent catalyst remains almost unchanged after the oxidation reaction.

Table 4.2: Textural properties of synthesized Cu-Zr mixed oxide catalysts.

catalyst	S_{BET} (m^2/g) ^a	V_t (cm^3/g) ^b	D_{BJH} (nm) ^c
A (Cu: Zr)	31.52	0.1578	20.02
B (Cu:2Zr)	40.83	0.1387	13.59
C (2Cu:Zr)	20.00	0.1325	26.49

^aBET surface area

^bThe total pore volume

^cBJH average pore diameter.

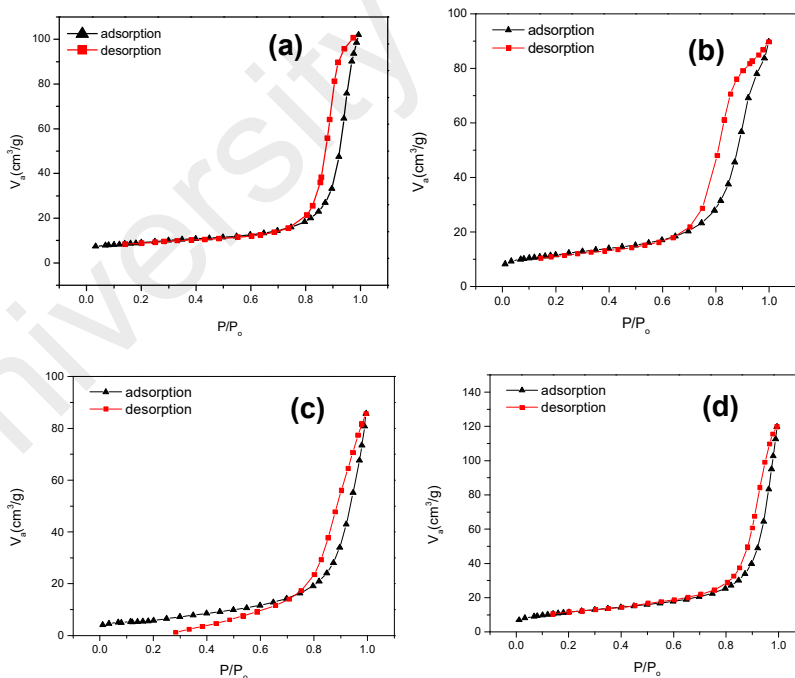


Figure 4.12: N₂ adsorption –desorption curve of synthesized Cu-Zr mixed oxide catalysts. (a) Cu: Zr; (b) Cu: 2Zr; (c) 2Cu: Zr; (d) Spent catalyst.

4.1.2.5 Morphology analysis

The morphology of the fresh and spent catalyst was studied by FESEM analysis under various resolutions shown in Fig. 4.13. The images revealed that the catalyst was agglomerated flakes-type and having rough surface. The uneven surface is believed to perform superior catalytic activity as it facilitates the chemisorption of the reactants to take part in the selective oxidation reaction of vanillyl alcohol to vanillin. However, the FESEM micrographs of the used catalyst demonstrated plane surface which possibly indicated lower adsorption of the reactants to the surface (Fig. 4.13d).

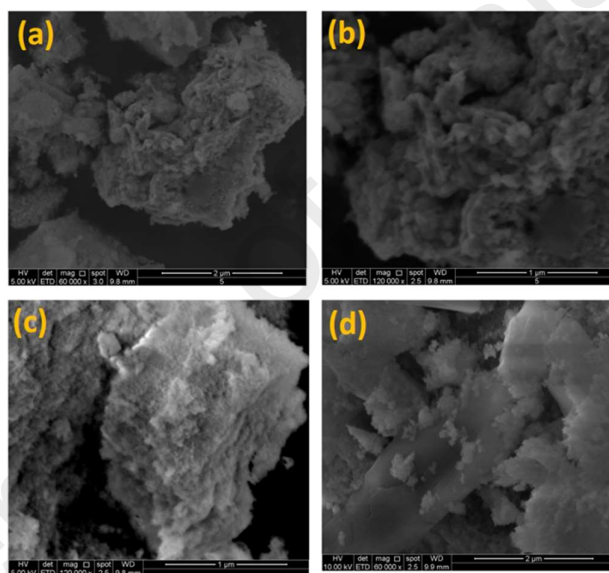


Figure 4.13: FESEM analysis of synthesized Cu-Zr mixed oxide catalysts. (a) Cu: Zr; (b) Cu: 2Zr; (c) 2Cu: Zr; (d) Spent catalyst.

Furthermore, High Resolution TEM equipped with SAED was used on catalyst (Cu: 2Zr) to observe the presence of CuZrO_3 crystal phase in terms of d spacing (\AA) (Fig. 4.14). The only catalyst Cu: 2Zr was considered due to its better catalytic activity in primary catalytic evaluation. The image (Fig. 4.14) of the catalyst (Cu: 2Zr) confirmed the miller plane of (112) and (211) of CuZrO_3 nanocrystalline domain with d spacing of 2.83 \AA and 3.15 \AA respectively. In addition, the images shown presence of numerous

grain boundaries between the lattice planes accommodated by the lattice dislocations (Fig. 4.14b). The grain boundaries dislocations observed in CuZrO_3 catalyst consisted of two types such as full dislocation (labelled as F) and partial dislocation (labelled as T) which led to stacking faults (Fig. 4.14e) (L. Wang et al., 2014). It was postulated that the grain boundaries in the form of surface defects could increase the catalytic activity substantially as it act as trapping sites in the catalyst (Choi et al., 1992; Choo & Lee, 1982; Royer, Duprez, & Kaliaguine, 2005; Vidruk et al., 2009). Moreover, the average crystallite size of CuZrO_3 catalyst were measured in the range of 7 to 10 nm from the observed images (Fig. 4.14c). The Selective Area Electron Diffraction pattern (SAED) was applied to further support the formation of lattice parameters (d spacing) in the CuZrO_3 catalyst (Fig. 4.14d). The diffused rings with the bright spots in the SAED pattern revealed that the catalyst was polycrystallin. In addition, the bright spots observed in the SAED pattern corresponded to the plane index of (112), (211) and (013) of CuZrO_3 nanocrystalline catalyst.

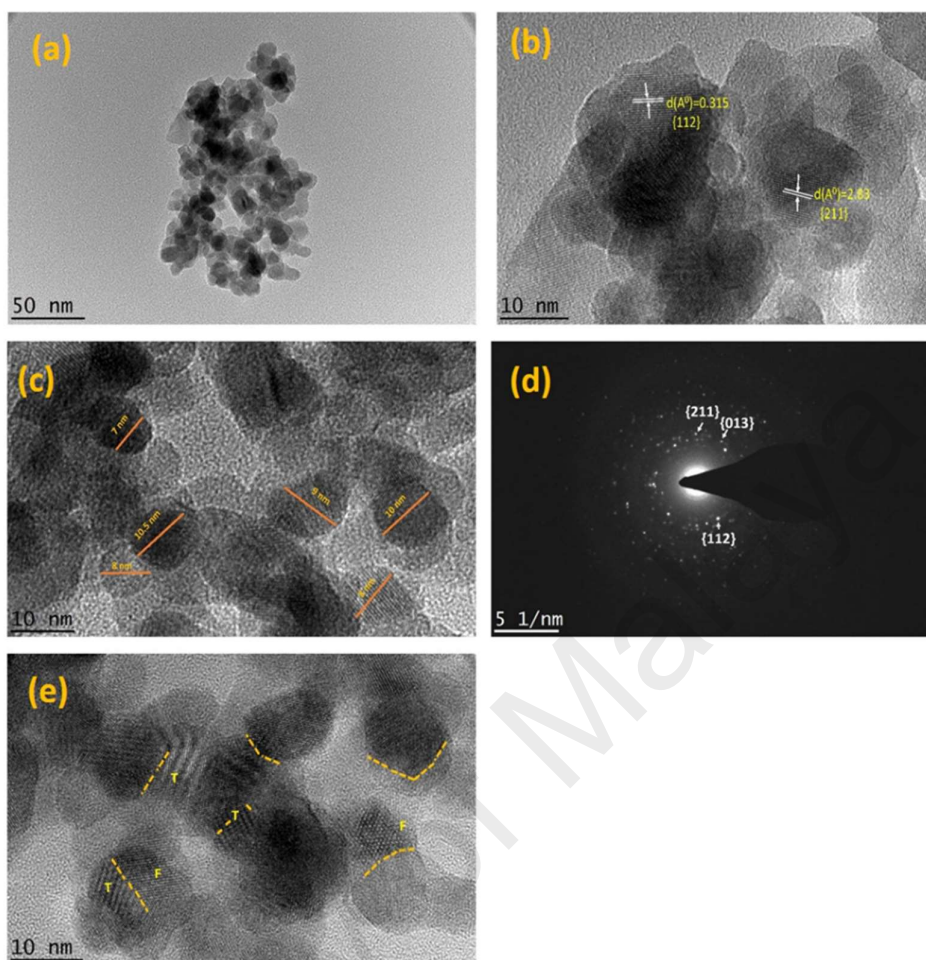


Figure 4.14: HRTEM and SAED pattern of Cu-Zr (Cu: 2Zr) mixed oxide catalyst. (a) Overview; (b) lattice fringe; (c) lattice size; (e) grain boundary.

Additionally, EDX spectrum of synthesized Cu-Zr mixed oxide catalysts were acquired to confirm the elemental composition (Fig. 4.15). The observed percentage of atomicity confirmed tentatively the elemental ratio of Cu and Zr loaded in the catalyst synthesis protocol.

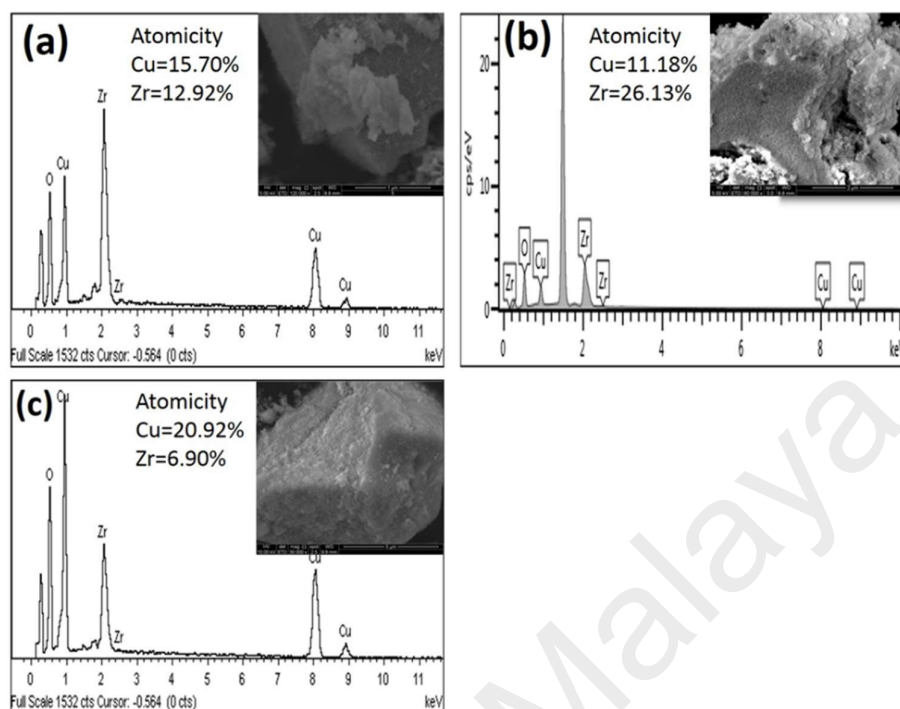


Figure 4.15: EDX pattern of synthesized Cu-Zr mixed oxide catalysts (a) Cu: Zr; (b) Cu: 2Zr; (c) 2Cu: Zr; (d) Spent catalyst.

4.1.2.6 Surface composition and oxidation state (XPS)

The surface elemental composition and the oxidation state of synthesized (Cu: 2Zr) catalyst were investigated using X-Ray Photoelectron Spectrum analytical tool (Fig. 4.16). The XPS wide spectrum of the catalyst further confirmed presence of Cu, Zr and O with no other impurities with binding energy 933.2 eV, 181.9 eV and 529.2 eV for Cu 3d, Zr 3d and O 1s spin orbitals respectively (Fig. 4.16a). And also, the surface elemental composition of CuZrO_3 catalyst was displayed in Table 4.3. In order to obtain further information on the chemical state of the components in the catalyst, high resolution spectra of the particular interested area was examined and shown in Fig. 4.16. There were two distinguishable peaks positioned at 181.81 eV and 184.18 eV which attributed by doublet terms of Zr $3d_{3/2}$ and Zr $3d_{5/2}$ in Zr 3d spectra due to spin orbital coupling (Fig. 4.16b). Moreover, the energy difference between the two spin orbital by 2.4 eV was

further confirmed with the presence of Zr^{4+} oxidation state which was in well agreement with previously reported values of ZrO_2 (J. Wang, Shi, & Jiang, 2009). The photoelectrons splitted from spin orbital of Cu $3d_{3/2}$ and Cu $3d_{5/2}$ at 933.8eV and 953.88 eV respectively was evidently corresponded to the Cu^{2+} oxidation state (Fig. 4.16d) (Tseng et al., 2004). Furthermore, the presence of satellite peak in between 940-950 eV in Cu 2p spin spectra ascertained the Cu^{2+} chemical state (Mathew et al., 2002). There were observed two peaks at binding energy 529.67 eV and 531 eV in O 1s spin orbital using nonlinear de Gaussian (Fig. 4.16c). The peak at low binding energy 529.67 eV corresponded to the O^{2-} chemical state which represented Cu-O and Zr-O linkage present in the catalyst framework. The higher binding energy peaks at 531 eV could be attributed to weakly held oxygen species (O^- , O_2^-) at the surface compared to lattice oxygen species (O^{2-}) which was in good agreement with previously reported by Robert et al (Roberts, 1989). Deng et also reported presence of oxygen vacancy on the surface of perovskite type Cu doped Co based oxide catalyst based on the higher binding energy peak of O 1s spectra in between 531 to 532 eV (H. Deng et al., 2010). Similar observation was also previously reported for La based transitional perovskite catalyst (O'Connell et al., 1999). Thus, standing on similar observation in this work, the presence of oxygen vacancy in the synthesized perovskite type $CuZrO_3$ catalyst was supported. Furthermore, formation of oxygen vacancy on the catalyst surface was further triggered via charge compensation phenomenon and also during calcination process as a result of Trifluoroacetic acid addition during the synthesis step for TiO_2 (Samsudin et al., 2016). Similar demonstration was observed in this $CuZrO_3$ catalyst.

Table 4.3: Surface composition of synthesized Cu-2Zr mixed oxide catalyst from XPS wide scan.

Cu (%)	Zr (%)	O (%)
8.06	25.41	66.39

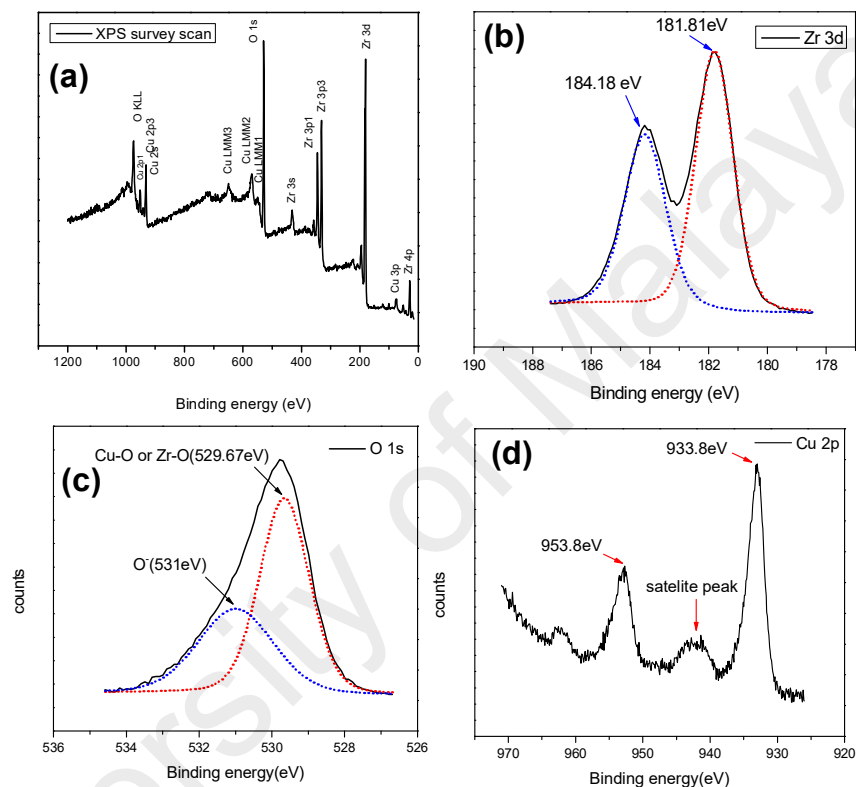


Figure 4.16: XPS analysis of synthesized Cu-2Zr mixed oxide catalyst. (a) wide scan; (b) Zr 3d; (c) O 1s; (d) Cu 2p.

4.1.2.7 Redox properties (H₂-TPR and O₂-TPD)

The H₂-TPR spectrum clearly revealed the reduction potential of the synthesized Cu-Zr mixed oxide catalysts (Fig. 4.17). A careful observation on the spectra in the range of 180 °C to 400 °C indicated a broad reduction peak with a shoulder peak towards lower reduction temperature. The shoulder peak with a maxima at 200 °C could be attributed to desorption of oxygen (O⁻, O₂⁻) from oxygen vacancy sites on the catalyst surface. This

oxidation step required low temperature to be reduced as they were weakly held at the active sites. Moreover, the most intensified shoulder peak of catalyst (Cu: 2Zr) implied on large concentration of desorbed surface oxygen species occurring at low temperature and thus enhanced the catalytic activity. Moreover, the broad peak at higher temperature corresponded to reduction of lattice oxygen (O^{2-}). The catalyst with higher loading of Cu in the preparation protocol required large consumption of H_2 reflected by peak broadening. In addition, the consistent shifting of the broad peaks towards high reduction temperature in the order of catalyst (Cu: 2Zr) < (Cu: Zr) < (2Cu: Zr), indicated magnitude of the interaction between Cu and ZrO_2 in the catalyst framework. Hence, it was worth to mention that high content of Zr in catalyst (Cu:2Zr) favored formation of highest degree of Cu-O-Zr phase. Consequently, this electronic interaction in the Cu-O-Zr phase induced the improvement of the reducing capabilities of the catalyst at low reduction temperature.

In order to further evaluate the catalyst activation and O_2 desorption behavior, O_2 -TPD was investigated (Fig. 4.17). It was speculated that oxidation of the catalyst took place in four distinctive steps denoted by α , β , γ and δ . The oxidation peak at lower temperature around 180 °C-210 °C was possibly owing to the desorption of physisorbed (O^{2-}) species at the present surface oxygen vacant sites suggested by O 1s in XPS spectra. Hence, α peak in Fig. 4.17 at the TPD profile was attributed to O^{2-} . Oxygen desorption at (O^-) species occurred at comparatively higher temperature (>400 °C) than O^{2-} species (< 300 °C). So, it was reasonable to assign β and γ peaks to O^- species. The δ desorption peak could attributed to lattice oxygen species as it required high temperature (>800 °C). It was worth to mention that the oxygen desorption peak at low temperature for catalyst (Cu: 2Zr) with high content of Zr was greatly shifted towards low temperature. It was indicative of enhancement of the oxygen mobility on the surface of the catalyst which facilitated the redox ability. This phenomenon could considerably enhance the catalytic activity observed for catalyst (Cu: 2Zr). In addition, the oxygen uptake at lower

temperature for catalyst (Cu: 2Zr) was greater (566 $\mu\text{mol/g}$) than catalyst (522 $\mu\text{mol/g}$ for Cu: Zr) and catalyst (285 $\mu\text{mol/g}$ for 2Cu: Zr). Based on the amount of oxygen desorption, it could conclude that catalyst B (Cu: 2Zr) contained the highest degree of physisorbed (O^{2-}) species associated with surface defects at low temperature which improved the catalytic activity

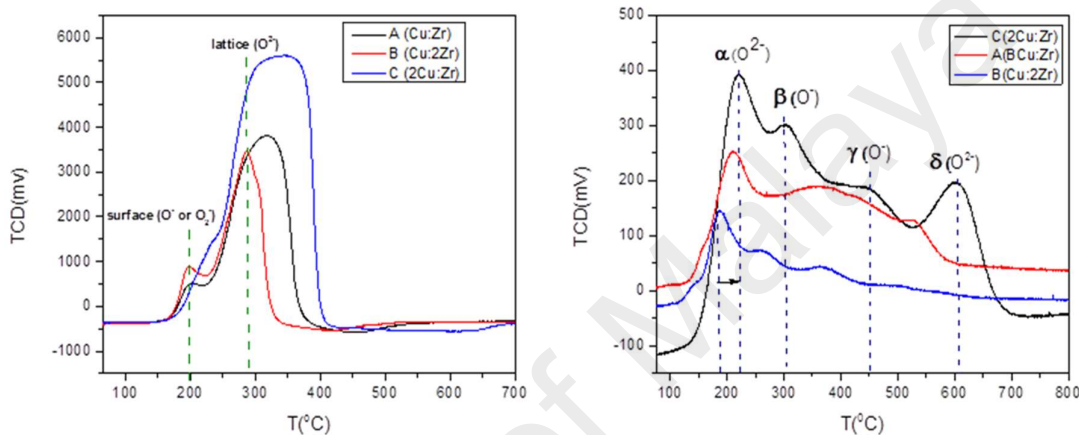


Figure 4.17: Synthesized Cu-Zr mixed oxide catalysts illustrating H₂-TPR (left); O₂-TPD analysis (right).

4.1.3 Structural properties of Cu-Mn mixed oxide catalysts

4.1.3.1 Thermogravimetric analysis (TGA/DTG)

Thermogravimetric analysis was carried out for the uncalcined catalyst (Cu: Mn) in order to determine the stability of the catalyst in temperature range of 60 to 700 °C (Fig. 4.18.) Four distinguished weight loss of 3.18 %, 3.49 %, 29.83 % and 24.44 % were detected at temperature maxima 110 °C, 190 °C, 245 °C and 310 °C respectively. The first and second weight loss by 3.18 % and 3.49 % corresponds to the removal of adsorbed moisture from the surface and bulk catalyst. Furthermore, the elimination of crystallite water present on the precursors [$\text{Cu}(\text{CH}_3\text{COO})_2 \cdot x\text{H}_2\text{O}$ and $\text{Mn}(\text{CH}_3\text{COO})_3 \cdot 2\text{H}_2\text{O}$] could be ascribed to the third weight loss by 29.83 % at 245 °C. Moreover, the final weight loss

by 24.44 % at 310 °C was attributed to the elimination of organic groups from the metal salt precursors. The catalyst was observed to reach its thermal stability at 450 °C.

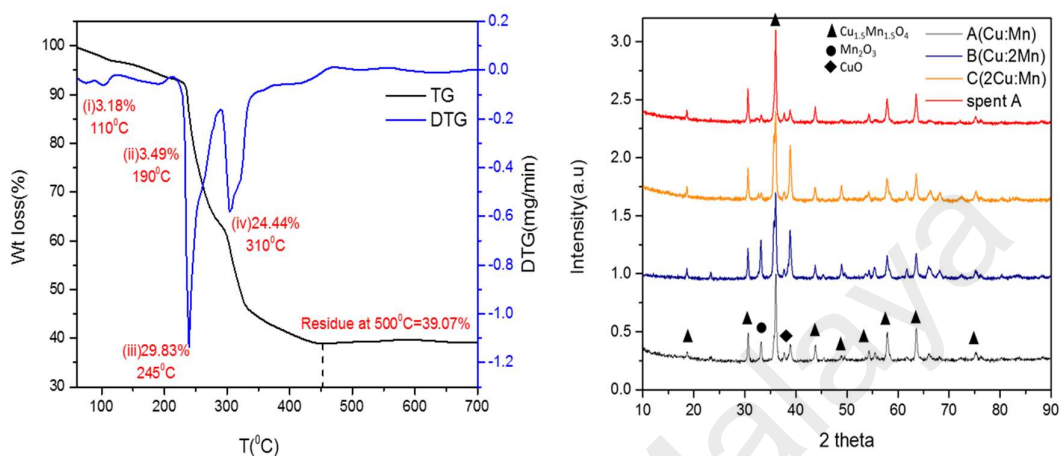


Figure 4.18: Synthesized Cu-Mn mixed oxide catalysts illustrating, TGA-DTG curve (left); XRD analysis (right).

4.1.3.2 Crystal phase and crystallinity (XRD)

The XRD data of synthesized catalysts were evaluated using High score plus Panalytical software in terms of peak position at Bragg angle and lattice spacing (d) (Fig. 4.18). The XRD pattern displayed in Fig. 4.18 shows peaks at Bragg angle 2 Theta = 18.70°, 30.62°, 36.06°, 37.17°, 43.79°, 49.15°, 54.33°, 55.45°, 57.89°, 63.56°, 66.13°, 68.08°, 75.26° with d spacing (Å) 4.74, 2.91, 2.49, 2.38, 2.06, 1.85, 1.68, 1.65, 1.59, 1.46, 1.441, 1.37, 1.26 which corresponds to Miller indices (111), (220), (311), (222), (400), (420), (422), (430), (511), (440), (530), (442), (533) of cubic spinel Cu_{1.5}Mn_{1.5}O₄ phase according to JCPDS No (ICSD-01-070-0260). Also, the peak positioned at Bragg angle 2theta= 33.21 and 38.87 were detected as minor phase (222) and (111) plane of Mn₂O₃ and CuO respectively, in accordance with JCPDS No (ICSD-00-041-1442 and ICSD-00-041-0254). No other impurities or phases were observed in the recorded XRD pattern. Cu_{1.5}Mn_{1.5}O₄ phase was referred as nonstoichiometric form of cubic spinel Cu_xMn_{3-x}O₄ structure.

The $\text{Cu}_{1.5}\text{Mn}_{1.5}\text{O}_4$ phase after calcination at 500 °C observed in the XRD pattern is comply with the previous literature reported on the phase diagram of Cu-Mn-O (Wei, Bieringer, Cranswick, & Petric, 2010). The cubic spinel shaped $\text{Cu}_{1.5}\text{Mn}_{1.5}\text{O}_4$ phase detected in this synthesis protocol was reported stable in low temperature in the phase diagram. It was worth to mention that this simple and facile synthesis protocol and calcined at 500 °C was very effective and successful to synthesis spinel structured, highly crystalline and stable mixed oxide catalyst. Moreover, the spent catalyst was also analyzed by XRD to detect any change in the phase and crystallinity. As expected, there was no change in the XRD pattern as it showed similar pattern at the same Bragg angle as the fresh catalyst. It suggested that the crystallinity and $\text{Cu}_{1.5}\text{Mn}_{1.5}\text{O}_4$ phase of the catalyst are well preserved. Also, the similar reaction conditions was observed not to affect the crystal phase in previously reported literature for CoTiO_3 catalyst in vanillyl alcohol oxidation (Shilpy, Ehsan, Ali, Hamid, & Ali, 2015). However, the intensity of Mn_3O_4 phase was slightly reduced after the catalytic reaction probably due to amorphization and re-distribution of corresponding species (Samsudin, Hamid, Juan, Basirun, & Centi, 2015).

4.1.3.3 Surface composition and oxidation state (XPS)

XPS analysis was conducted to obtain the surface chemistry information along with the chemical bonding state of the elements for catalyst (Cu: Mn) (Fig. 4.19). The wide XPS spectra revealed that there were no trace of other metals as impurities but presence of Cu, Mn and O (Fig. 4.19a). The surface elemental composition was shown in Table 4.4. The surface elemental composition acquired from XPS analysis shown that the surface of the catalysts is highly decorated with Mn co-ordinated species. Cu spin-orbit splitting indicated presence of two Cu species in the oxide cage (Fig. 4.19b). The major peak at binding energy for $2p_{3/2}$ at 933.1 eV and $2p_{1/2}$ at 953.1 eV corresponds to Cu^{2+} species (Hernandez, Fernández - Bertrán, Farias, & Diaz, 2007). And also, the peak at

relatively lower binding energy at 931.07 eV along with a weak satellite peak at 945 eV was attributed to Cu^+ species on the catalyst framework (Angelov, Zhecheva, Petrov, & Menandjiev, 1982; B. Yang, Chan, Chang, & Chen, 1991). It could be mentioned that Cu^{2+} was predominantly present in the catalyst with respect to the peak intensity and FWHM of Cu^{2+} and Cu^+ . Presence of Cu^+ was originated from expected redox resonance of $\text{Cu}^{2+} + \text{Mn}^{3+} \rightarrow \text{Cu}^{1+} + \text{Mn}^{4+}$ which occurs on the catalyst surface. The identification of Mn oxidation state was disputable based on Mn 2p XPS spectra due to high fraction of Mn_2O_3 . Different valences of Mn showed peaks at the same region of 2p. Therefore, the comprehensive approach to identify the oxidation state of Mn in the prepared catalyst was to analyze the Mn 3s spectra. The spin-orbit splitting of Mn 3s shown 5.5 eV binding energy difference between the main peak and satellite peaks in the XPS spectra (Fig. 4.19d). It confirmed the presence of Mn^{3+} species discarding existence of Mn^{2+} and Mn^{4+} in the surface of the catalyst which well agreed with the former result reported in the literature (Wertheim, Hüfner, & Guggenheim, 1973). These observations suggested that the synthesized $\text{Cu}_{1.5}\text{Mn}_{1.5}\text{O}_4$ catalyst contains only Mn^{3+} species with co-existence of Cu^+ as well as Cu^{2+} species. Previously, it was reported in literature that ideal structure of cubic spinel $(\text{Cu}_2)[\text{Mn}_3\text{Cu}]\text{O}_8$ contains two types of Cu species which was supported the current work (Vandenberghe, Legrand, Scheerlinck, & Brabers, 1976).

However, some shake up peaks due to charge transfer was also observed at binding energy 942 eV and 962 eV. It further confirmed the presence of Cu^{2+} species in the Cu-Mn crystal cage (Mathew et al., 2002) In addition, O 1s XPS spectra is displayed in Fig. 4.19c. The asymmetric peak of O 1s spectra was further resolved into three components by Gaussian Fitting. The peak at lowest binding energy by 529 eV corresponds to lattice oxygen species (O_L) (O^{2-}) of Cu-O and Mn-O. The peak at binding energy 531.2 eV could be attributed by surface oxygen vacancy as per previously reported literature (O'Connell et al., 1999; Roberts, 1989). Surface oxygen vacancies (O_V) as surface defects can be

caused by the non-stoichiometry of the metal ions in the nanocrystalline domain. And also, the peak at higher binding energy in range of 531.8 to 532.9 eV was reported as chemisorbed (O_C) or dissociative species (O_2^- , O_2^- or O^-) and OH^- (Yiting Wang et al., 2015). The atomic percentage of the three types oxygen species were calculated from XPS data and shown in Table 4.5.

Table 4.4: The surface composition of mixed oxide catalyst Cu: Mn from XPS wide scan.

Cu (%)	Mn (%)	O (%)
5.82	20.57	73.65

Table 4.5: The area percentage of oxygen species from O 1s spectra.

Lattice oxygen (O_L)	Surface oxygen Vacancy (O_V)	Defective oxygen (O_D)
46.23 %	38.36 %	15.40 %

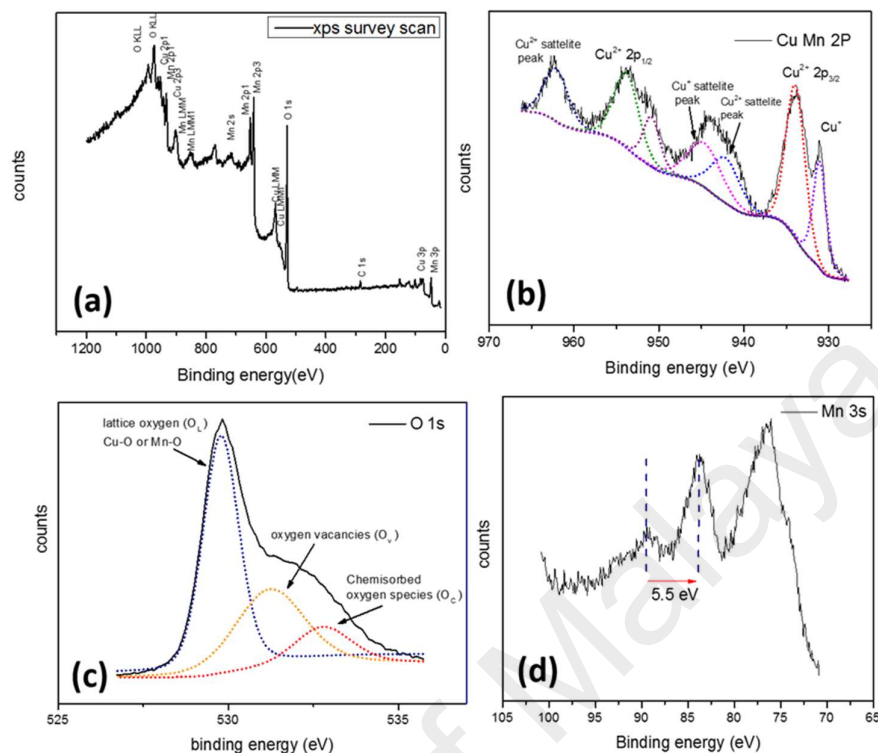


Figure 4.19: XPS analysis of Cu-Mn (Cu: Mn) mixed oxide catalysts. (a) wide spectra; (b) Cu 2p; (c) O 1s; (d) Mn 3s.

4.1.3.4 Morphology

FESEM images for synthesized Cu-Mn catalysts after calcination were shown in Fig. 4.20. It clearly indicates that the nanoparticles grew in agglomerated state in a 3D frame network to form an interconnected clusters. And also, it was visible that the catalyst possessed uneven and jagged pores. The randomly distributed pores were originated from the liberation of any organic residue during the heat treatment process. Furthermore, the rough and stony surface of the catalyst was believed to facilitate to the adsorption between catalyst and substrate and hence the enrichment of the catalytic activity in oxidation reactions. The higher resolution pictures of the well dispersed catalyst shown defined-edges type particle shapes. The spent catalyst was also observed under microscopic analysis to study the probable change on the morphology and the surface of the catalyst

(Fig. 4.20d). There were indication that the particles was segregated after the reaction. The FESEM image of the used catalyst shown that surface roughness was reduced by some degree expectedly.

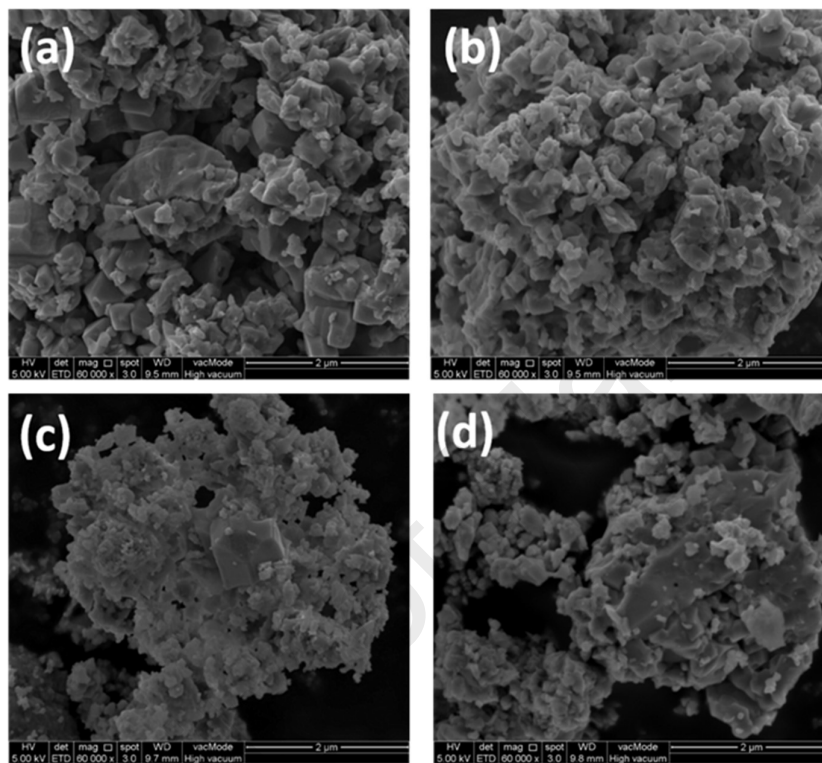


Figure 4.20: FESEM analysis of synthesized Cu-Mn mixed oxide catalysts. (a) Cu: Mn; (b) Cu: 2Mn; (c) 2Cu: Mn; (d) spent catalyst.

HRTEM images was performed for catalyst (Cu: Mn) to further confirm the particle sizes and formation of $\text{Cu}_{1.5}\text{Mn}_{1.5}\text{O}_4$ phase in terms of d spacing of the phase (Fig. 4.21). The d spacing was measured by 4.74 \AA which confirmed (111) plane of $\text{Cu}_{1.5}\text{Mn}_{1.5}\text{O}_4$ (Fig. 4.21b). And also, the crystallite size was measured in range of 8-13 nm. A high resolution insight into the interface of the plane revealed presence of numerous grain boundaries associated by partial dislocations as a form of surface defects. In Fig. 4.21c partial dislocation occurred at the interface of two (111) plane of $\text{Cu}_{1.5}\text{Mn}_{1.5}\text{O}_4$ and was labeled as T. The observed grain boundaries notably contribute to achieve high catalytic

activity by $\text{Cu}_{1.5}\text{Mn}_{1.5}\text{O}_4$ catalyst. Furthermore, selective area electron diffractogram (SAED) was also obtained to confirm the crystallinity and the formation of $\text{Cu}_{1.5}\text{Mn}_{1.5}\text{O}_4$ phase in synthesized catalyst (Fig. 4.21d). The diffuse ring observed at the SAED pattern confirmed that the material was polycrystalline. The presence of bright spots from SAED pattern confirms each plane of the $\text{Cu}_{1.5}\text{Mn}_{1.5}\text{O}_4$. Fig. 4.21d shown formation of (111) of $\text{Cu}_{1.5}\text{Mn}_{1.5}\text{O}_4$ phase in terms of measured d spacing by 4.74 Å and 2.91 Å.

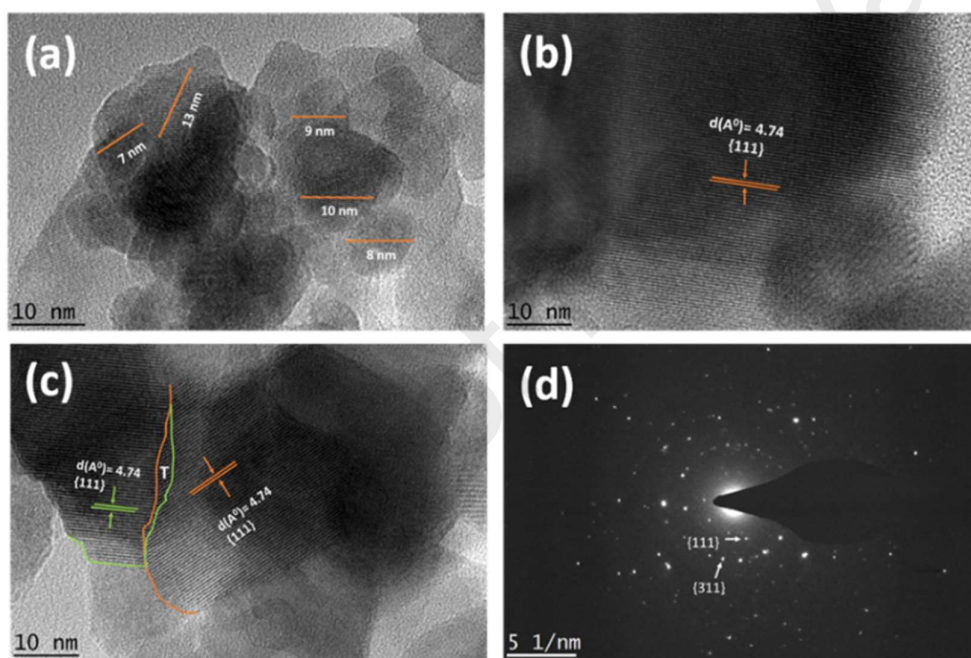


Figure 4.21: HRTEM and SAED analysis of synthesized Cu: Mn mixed oxide catalysts. (a) lattice size; (b) lattice parameter; (c) grain boundary; (d) SAED pattern.

Moreover, the elemental composition of prepared material was determined by EDX analysis (Fig. 4.22). The atomic ratio observed in the EDX spectrum of three catalysts tentatively matched with the primary ratio of metal loading in the synthesis protocol. In addition, the area mapping clearly shown high degree of homogeneity of both metals in the catalyst. (Fig. 4.22d)

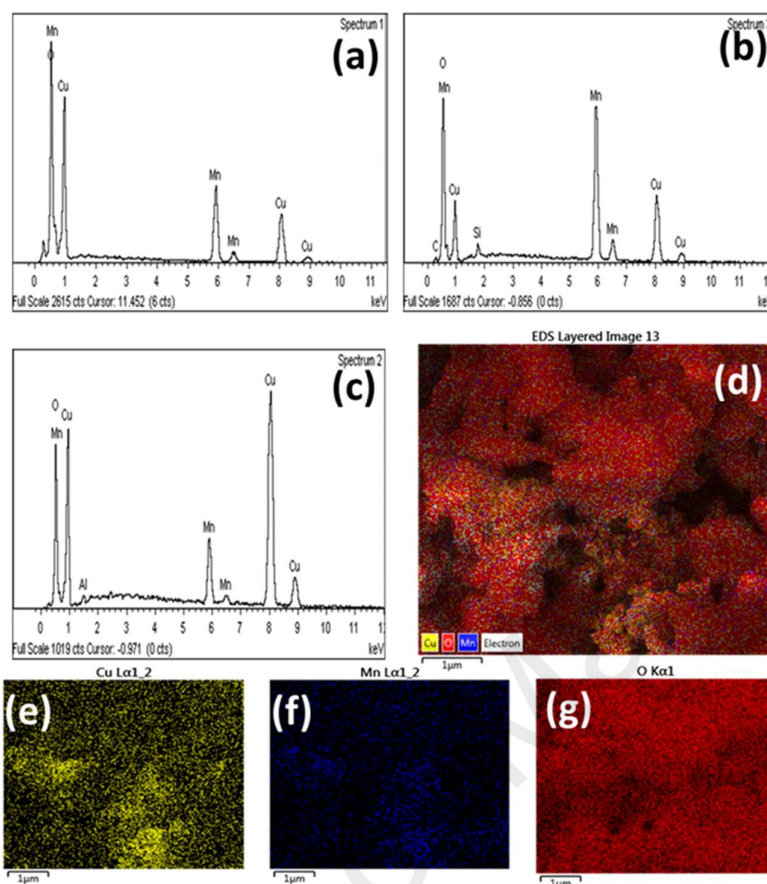


Figure 4.22: EDX and chemical mapping of synthesized Cu-Mn mixed oxide catalysts. (a) Cu: Mn; (b) Cu: 2Mn; (c) 2Cu: Mn; (d) elemental mapping; (e) Cu distribution; (f) Mn distribution; (g) O distribution.

4.1.3.5 Redox properties (H₂-TPR and O₂-TPD)

The quantitative elucidation of reduction profile of Cu-Mn catalysts could not be determined precisely owing to existence of multiple valences for both element Cu and Mn (Fig. 4.23). However, the correlation of reduction temperature with the catalytic activity was established as oxidation reaction involves redox coupling (Kondrat et al., 2011; Morgan et al., 2010). The profile of synthesized catalysts shown that H₂ consumption starts at 220 °C with two distinguishable peak maxima at 340 °C and 430 °C for all three catalysts. Isolated oxide phases shown reduction at higher temperature as per literature (Einaga, Kiya, Yoshioka, & Teraoka, 2014; Morales, Barbero, & Cadús,

2006). Reduction of CuO at around 300 °C whereas Mn³⁺ was slightly higher at range of 350 °C -400 °C. But, reduction profile of synthesized catalysts in this solution method appeared at low reduction temperature. It indicated that the redox ability of the catalyst prepared in solution route was strongly improved by the synergy of Cu and Mn. It was postulated that the initial H₂ consumption occurred at the surface oxygen sites. The continuous reduction was observed for the catalyst till temperature at 480 °C. The large reduction was mainly due to few possible steps of reduction. The lattice oxygen (Cu-O and Mn-O) was reduced at the high reduction temperature relation to surface oxygen sites. In XPS spectra it was confirmed that Mn was present in the catalyst in oxidation state of Mn³⁺. Therefore, the reduction of Mn might be occurred as following steps Mn₂O₃-Mn₃O₄-MnO. Complete reduction of MnO to metallic Mn was not expected even up to 950 °C due to the larger negative value of reduction potential (Carnö, Ferrandon, Björnbom, & Järås, 1997; Kapteijn, Singoredjo, Andreini, & Moulijn, 1994). Moreover, it was formerly reported that firstly reduced Cu⁰ could act as H₂ activation site to decrease the reduction temperature of Mn species (Einaga et al., 2014). This fact could be contribution of reducing spill over species introduced by Ferradon et al (Ferrandon, Carnö, Järås, & Björnbom, 1999).

Moreover, the comprehensive study of TPR profile of synthesized catalysts revealed that the catalyst contains equimolar ratio Cu and Mn had the first peak maxima at the lowest reduction temperature. The catalyst (Cu: Mn) reduction started at 275 °C where other two catalysts at 350 °C and 360 °C respectively. An approach to explain the low reduction temperature of catalyst (Cu: Mn) was due to presence of large concentration of structural defects associated with defective oxygen species which was also suggested at the O 1s XPS spectra as well as the smaller particle sizes. Another possible reason was attributed to the formation of high degree of Cu-O-Mn species which causes electronic interaction between Cu and Mn.

In order to study the oxygen vacancies in the catalysts, temperature programme oxygen desorption was used (Fig. 4.23). In the TPD profile, four distinctive oxygen desorption peaks were noted at temperature maxima around 230 °C, 340 °C, 540 °C and 680 °C respectively. The first oxygen desorption peak at low temperature was attributed by surface oxygen vacancies. Desorption of oxygen at the lattice oxygen vacant sites of Cu occurred at temperature which was indicated by the prominent peak of catalyst (2Cu: Mn) with high loading of Cu. Similar trend was observed in case of catalyst (Cu: 2Mn) with high content of Mn at temperature of 540 °C. So, the third oxygen desorption peak correspond to oxidation of Mn^{2+} to Mn^{3+} . A previous literature stated presence of defective oxygen species in the lattice at high temperature 523 °C to 590 °C for supported MnO_x species (Trawczyński, Bielak, & Mišta, 2005). Similar observation was made by another group of researchers for Al_2O_3 , SiO_2 promoted MnO_x species (Radhakrishnan, Oyama, Chen, & Asakura, 2001). Therefore, in our work, the oxygen desorption peak at high temperature around 680 °C was originated from structural defects associated with defective oxygen species. The most intensive peak at high temperature for catalyst (Cu: Mn) indicated that presence of high degree of defective oxygen species among all three catalysts. Thus, this fact notably lower the reduction temperature of catalyst (Cu: Mn) observed in TPR profile.

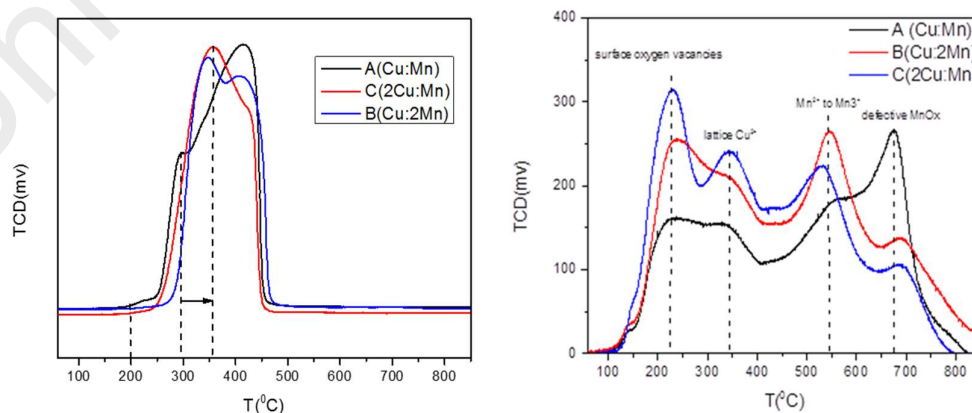


Figure 4.23: Synthesized Cu-Mn mixed oxide catalysts, H₂-TPR analysis (left); O₂-TPD analysis (right).

4.1.4 Structural properties of synthesized Ce-2Ti mixed oxide catalyst

The synthesized catalytic systems Cu-Ti, Cu-Zr, Cu-Mn were investigated in catalytic liquid phase oxidation of vanillyl alcohol using H₂O₂ oxidants. The results indicated that Cu: 2Ti catalysts shown the best catalytic activity in terms of conversion (66 %). Also, from the aerobic oxidation of vanillyl alcohol by synthesized catalysts, it can be concluded that Cu-2Ti was the best performed catalysts in terms of both catalysts conversion (94 %) with selectivity (86 %). Thus, with constant ration of M: 2Ti, other two catalysts were prepared where M corresponds to different valent Ce⁴⁺ and Fe³⁺ metal ions replacing the Cu in Cu: 2Ti catalysts. This is to investigate the effect of different valent cations and their synergy in the mixed oxide in view of catalytic activity. Therefore, for further study two mixed oxide catalysts such as Ce-2Ti and Fe-2Ti were prepared.

4.1.4.1 Crystal phase and crystallinity (XRD)

The XRD diffractogram of synthesized catalyst displayed in Fig. 4.24 was analyzed by a Panalytical Xpert High Score Plus software in terms of Bragg angle (2 theta) and d spacing (Å). The peaks positioned at 2 theta 25.44°, 37.99°, 54.09°, 55.24°, 62.83° with d spacing (Å) 3.50, 2.36, 1.69, 1.66, and 1.47 respectively corresponds to crystal plane 101, 004, 105, 211, and 204 respectively of tetragonal anatase phase of TiO₂ (JCPDS No 01-073-1764). Moreover, the peak located at 2theta 28.71°, 33.25°, 47.66°, 56.51°, 59.29°, 69.60°, 76.89°, and 88.61° with d spacing 3.10, 2.69, 1.90, 1.62, 1.55, 1.35, 1.23, 1.64 and 1.10 respectively ascribed to the crystal plane (111), (200), (220), (311), (222), (400), (331), (420) and (422) respectively of cubic fluorite CeO₂ (JCPDS No 01-075-0076). The XRD pattern of synthesized catalyst indicated that catalyst is highly crystalline mixed phase of CeO₂ -TiO₂ which well agreement with previous reports (Gao et al., 2010; Reddy et al., 2005). Preuss and Gruenn reported existence of different phases such as Ce₂TiO₅, Ce₂Ti₂O₇, and Ce₄Ti₉O₂₄, by heating the appropriate ratio of precursors containing Ce

and Ti at 1250 °C (Preuss & Gruehn, 1994) However, previous literatures did not observe Ce-Ti-O system in the XRD pattern (Reddy et al., 2005; Shi et al., 2016). Similar findings were also observed in this work. This could be due to the low calcination temperature applied during the catalyst preparation. In addition, CeO₂-TiO₂ mixed oxide structure can be different owing to different ratio of Ce/Ti according to previous report. They stated that Ce-Ti-O solid solution can be formed by substitution of Ce⁴⁺ by Ti⁴⁺ which only showed cubic phase CeO₂ when the x value decrease from 1 to 0.6 in Ce_xTi_{1-x}O₂ and mixed phase oxide for x > 0.4 (Luo et al., 2001). Therefore, XRD analysis revealed that mixed phase CeO₂-TiO₂ catalyst with Ce-Ti-O solid solution possibly is formed as the ratio of Ce/Ti = 0.5 was used in the synthesis protocol. Worth mentioning that, in this present synthesis method, no other crystal phase of TiO₂ but anatase was appeared. It was due to inhibition in the phase transformation as a result of Ce incorporation into TiO₂ lattice. The phenomenon explained by Lin and Yu could appeared in current study owing to stabilization of anatase through the formation of Ce-O-Ti bonds (J. Lin & Jimmy, 1998). This was resulting of substitution of cerium in the lattice of the cerium oxide by Ti atom at the interface to form octahedral Ti sites. The interaction between the tetrahedral Ti and octahedral Ti inhibits the phase transformation to rutile. Another group of researchers also observed similar inhibition in phase transformation for TiO₂-SiO₂ (Panayotov & Yates, 2003). The usage of fluorine source during the synthesis of catalyst also favors the formation of anatase crystal phase, as opposed to rutile or brookite. Fluorine acts as a surface stabilizer by controlling the high surface energy of anatase and thus promotes its growth (Samsudin et al., 2016). From the shift of CeO₂ (111) crystal plane of to the low Bragg angle (2 theta = 28.75° to 28.71°) suggests that modification of cell parameters owing to large difference of ionic dimensions between Ce³⁺ (1.03 Å) and Ce⁴⁺ (0.94 Å). This results in the generation of sub stoichiometric fluorite CeO_{2-x} species during the heat treatment by the presence of Ce³⁺ species. It was formerly reported that

the presence of oxygen vacancies in CeO₂ associated with Ce³⁺ species in CeO₂-TiO₂ system (Dauscher et al., 1990).

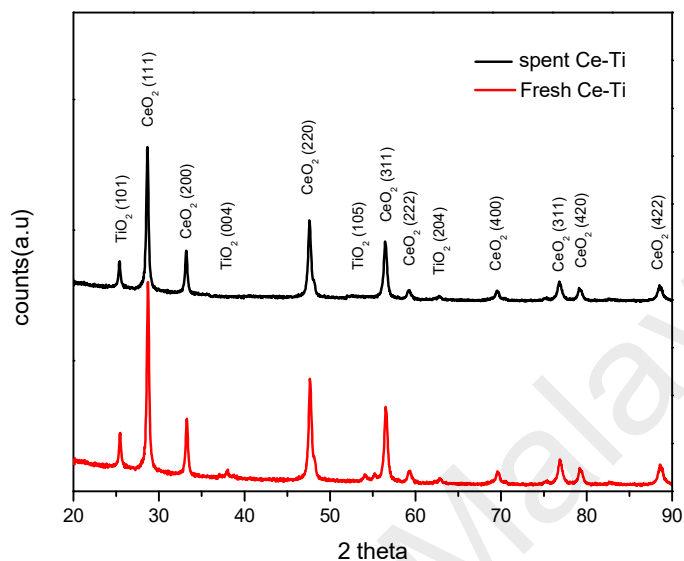


Figure 4.24: XRD analysis of Ce-2Ti mixed oxide catalyst.

In addition, the crystallite size of TiO₂ and CeO₂ was measured based on the most intense peak of corresponding phase by 35.6 nm, and 53.1 nm respectively by Scherer equation. The phase of the catalyst was well conserved as no change was visible in the XRD pattern in terms of Bragg angle and d spacing.

4.1.4.2 Raman analysis

As displayed in Fig. 4.25, Raman analysis of Ce-2Ti mixed oxide catalyst was conducted to further confirm the lattice structure exactly in combination with the XRD data. The distinguished peak at Raman peak 141, 394, 515, 637 cm⁻¹ are in well agreement with previously reported study for typical spectra of anatase TiO₂ (Hadjiivanov & Klissurski, 1996) while CeO₂ exhibited only prominent peak at Raman peak 463 cm⁻¹. CeO₂ is ideally characterized by the strong triply degenerated Raman active mode F_{2g} at 464 cm⁻¹ for Fluorite type structure (X.-M. Lin, Li, Li, & Su, 2001). The clearly observed

symmetric and sharp peak of F_{2g} mode suggests that the CeO_2 in synthesized material was well crystalline.

In addition, previous literatures ascribed a weak band at 260 cm^{-1} with a shoulder peak around 600 cm^{-1} for normal Raman inactive transverse and longitudinal optical phonon modes at the Brillouin zone center for CeO_2 (Shyu, Weber, & Gandhi, 1988). McBride et al studied Raman spectra for solid solutions of $Ce_{1-x}Re_xO_{2-y}$ (Re is rare earth element) for large x values. He found asymmetry of the Raman active mode F_{2g} and also a shoulder peak evolved at 570 cm^{-1} which was attributed to defect spaces by selection relaxation rule (McBride, Hass, Poindexter, & Weber, 1994). Following the similar trend, a very weak and ambiguous peak at 585 cm^{-1} was noted by Shi et al for CeO_2 - TiO_2 binary oxide adopting different preparation method and postulated as oxygen vacancies (Shi et al., 2016). And also, Benjaram et al reported a very least prominent peak around 570 cm^{-1} (Reddy et al., 2003). In contradictory, Nakajima did not observed such peak around 580 cm^{-1} for Zr^{4+} doping in CeO_2 (Nakajima, Yoshihara, & Ishigame, 1994). They explained it as cation doping without oxygen vacancies as no charge neutrality was involved. However, in this study, no peak was observed in that particular region of interest possibly due to three hypothesis (i) adaptation of different synthesis technique; (ii) inappropriate ratio of Ce/Ti (small x value) unlike wise previous reports and; (iii) no charge neutrality due to equivalency of Ti^{4+} and Ce^{4+} cations. Moreover, the weak Raman band near 600 cm^{-1} could correspond to a non-degenerate longitudinal optical (LO) mode of CeO_2 (X.-M. Lin et al., 2001). Normally, this mode should not be observed by Raman spectra. Furthermore, the observed apparent shifting of Raman active mode E_g of TiO_2 towards low wavenumber (141 cm^{-1}) further indicated formation of Ce-Ti-O system as a result of long bond length generation by substitution of Ti^{4+} (0.64 \AA) into the Ce^{4+} (0.97 \AA) lattice. Therefore, the Raman analysis further indicated formation of the Ce-Ti-O solid solution in mixed phase CeO_2 - $2TiO_2$ catalyst.

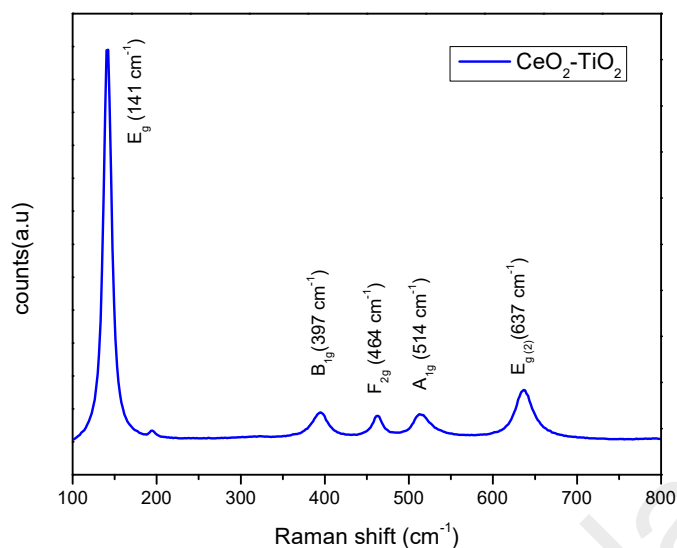


Figure 4.25: Raman analysis of synthesized Ce-2Ti mixed oxide catalyst.

4.1.4.3 Surface composition and oxidation state (XPS)

Oxidation state and surface composition of the catalyst was determined through XPS analysis (Fig. 4.26). The surface composition of synthesized materials revealed that the catalyst's surface contains Ce, Ti and O elements with traces amount of residual. The F might be present as physisorbed in the surface owing to its binding energy (Samsudin et al., 2016) The elemental composition displayed in Table 4.6 indicates that the surface is enriched with Ti atoms. The Fig. 4.26c shows the spin orbit splitting of Ce with three pairs of doublet. The peak positioned at binding energy 900.6 eV, 907.5 eV and 916.6 eV can be ascribed to Ce 3d_{5/2}. And, the peaks at binding energy 882.2 eV, 889.9 eV and 898.2 eV corresponds to Ce 3d_{3/2} (Fan et al., 2008). However, Ce³⁺ species was not detected at by XPS due to the instability of the valence state. As shown in Fig. 4.26b, the peaks located at 458.6 eV and 464.6 eV are successfully attributed to the 3d_{3/2} and 3d_{5/2} state of Ti⁴⁺ (Samsudin, Hamid, Juan, Basirun, & Centi, 2015).

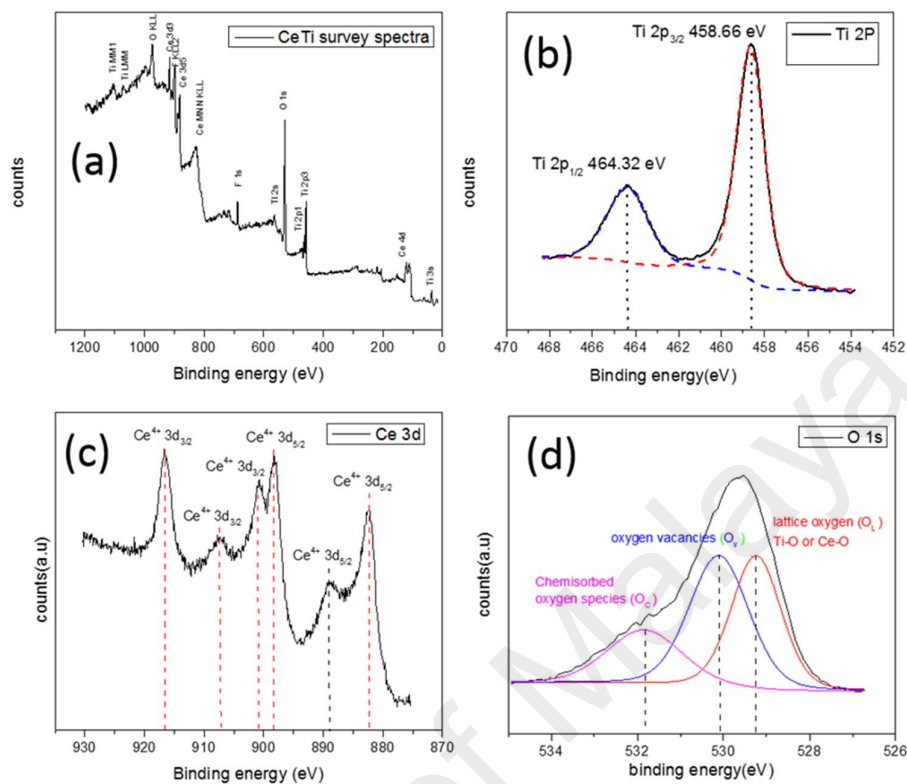


Figure 4.26: XPS analysis of synthesized Ce-2Ti mixed oxide catalyst. (a) Wide scan; (b) Ti 2p; (c) Ce 3d; (d) O 1s.

In Fig. 4.26d, O 1s spectra was displayed. The asymmetric peak of oxygen was deconvulated into three components peaks by Gaussian Fitting. The peak at low binding energy at 529.6 represents lattice oxygen. The peak at relatively high binding energy at 531.2 eV can be successfully attributed to surface oxygen vacancy as a form of surface defects (Roberts, 1989). And also, the peak at higher binding energy between 531.8 eV and 532.9 eV is ascribed to dissociated or chemisorbed oxygen species (O_2^- or O^-) and OH^- (Yiting Wang et al., 2015). The percentage of oxygen species in the catalyst based on peak area were calculated and displayed in Table 4.6. As no Ce^{3+} ions is detected in XPS spectra, it could be conclusive that oxygen vacancies on the surface were created dominantly by the addition of Trifluoroacetic acid during catalyst synthesis step. It was

previously reported that the degree of surface oxygen vacancies can be enriched by the presence of Trifluoroacetic acid (Samsudin et al., 2016). Trifluoroacetic acid can trigger oxygen vacancies via charge compensation and during the calcination process as well.

Table 4.6: The surface composition of Ce-2Ti mixed oxide catalysts from XPS survey spectra.

Ce (%)	Ti (%)	O (%)	F (%)
7.67	15.67	72.69	3.96

Table 4.7: The area percentage of oxygen species from O 1s XPS spectra.

Lattice oxygen (O _L)	Surface oxygen Vacancy (O _v)	Defective oxygen (O _D)
35.90 %	42.24 %	21.85 %

4.1.4.4 Morphology

Morphology of the catalyst was revealed by FESEM analysis under high resolution images. As shown in the Fig. 4.27, the particles were agglomerated and non-uniform. As no structure directing agent was added in the synthesis protocol, the heat treatment resulted to agglomeration. Also, it was clearly shown that the interconnected cluster framework of the synthesized materials possessed unevenly distributed jagged pores. The pores were created via removal of the organic groups during the calcination procedure. Mesoporous structure of the catalyst is believed to enrich the catalytic activity via more access to the active sites. Moreover, it is presumed that the observed rough surface with sharp defined edges of the catalyst facilitate the adsorption between reactants and catalyst which improved the performance of the catalyst. Furthermore, careful observation on the high resolution images revealed that various crystal shapes like truncated, by-

pyramidal, and cuboid exposed (101) plane of TiO₂ which is necessary to obtain good catalytic activity in oxidation reactions.

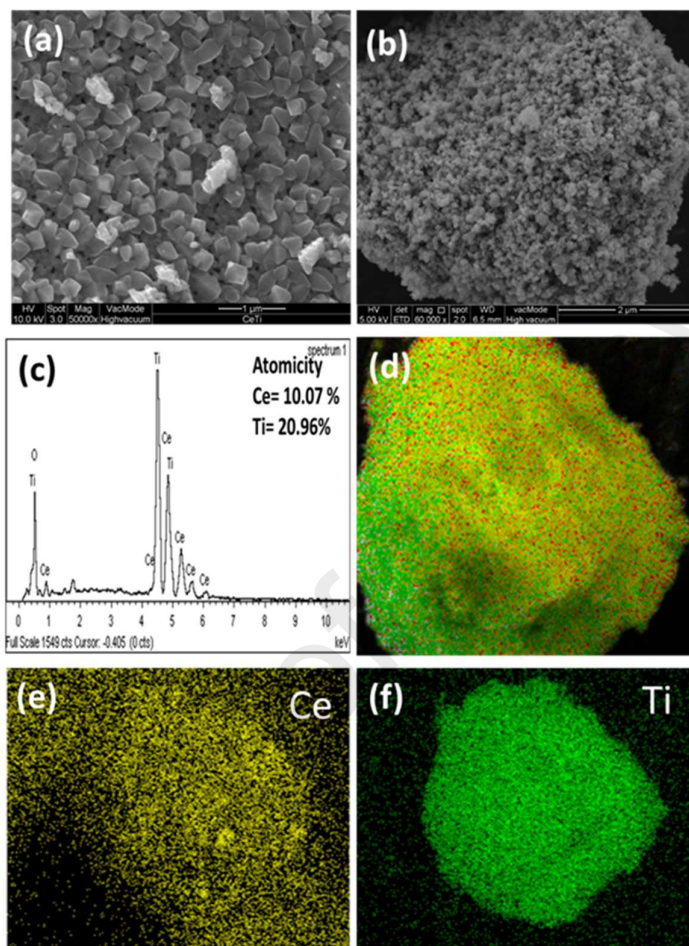


Figure 4.27: FESEM and EDX analysis of synthesized Ce-2Ti mixed oxide catalyst. (a) Fresh Ce-2Ti catalyst; (b) spent catalyst; (c) EDX pattern; (d) chemical mapping; (e) Ce distribution (f) Ti distribution.

Furthermore, HRTEM images of synthesized catalyst were obtained to further confirm the formation of crystal phases in terms of lattice parameters. In Fig. 4.28a shown the measured d spacing 3.5 Å by which undoubtedly confirm the formation of TiO₂ (101) phase of the catalyst. In addition, for further confirmation of the crystallinity and lattice fringes, selective area electron diffraction pattern were employed (Fig. 4.28b). The SAED pattern showed the synthesized materials was polycrystalline. The bright spots observed

in the image represents individual plane of crystals. The crystal plane of (111), (200) of CeO_2 as well as (101) of TiO_2 were confirmed by the measured d spacing 3.10, 2.61, and 3.50 Å respectively from SAED pattern.

The EDX pattern was also collected to ensure the elemental composition of Ce, Ti in the catalyst (Fig. 4.29c). The observed ratio of the Ce and Ti from the EDX spectra tentatively matched with primary metal loading $\text{Ti/Ce} = 2$ in loaded in bulk phase of the catalyst. Moreover, the chemical mapping of the synthesized material were acquired and displayed in Fig. 4.29d. The chemical mapping of the catalyst clearly showed high elemental dispersion which suggests highest interaction between Ce and Ti. This result indicated the possibility of mechanical mixture between CeO_2 and TiO_2 in the prepared catalyst.

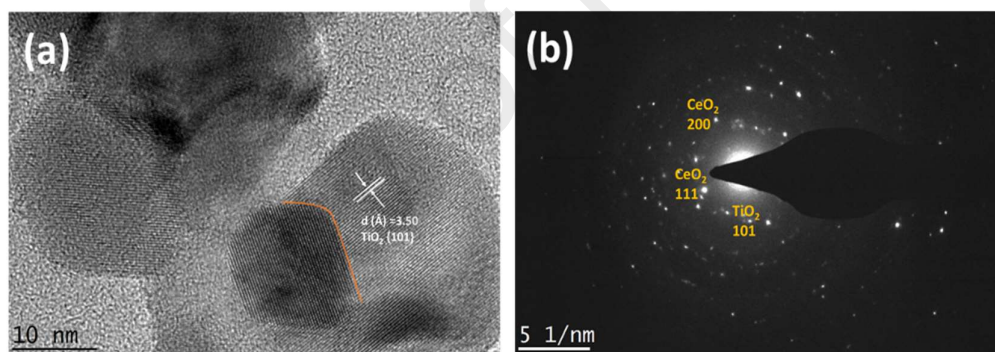


Figure 4.28: HRTEM and SAED analysis of synthesized Ce-2Ti mixed oxide catalyst. (a) Lattice parameters; (b) SAED pattern.

4.1.4.5 Textural properties (BET)

The N_2 adsorption-desorption curve of synthesized catalyst is shown in Fig. 4.29. The observed isotherm match with Type III. The BET surface area of the catalyst was measured low at $12 \text{ m}^2/\text{g}$ due to formation of large agglomerated particles which suggested that the effect of surface area on catalytic activity is less significant. In addition, the measured pore size 32 nm and pore volume $0.096389 \text{ cm}^3/\text{g}$ for Ce-2Ti mixed oxide catalyst is indicated mesoporous structure.

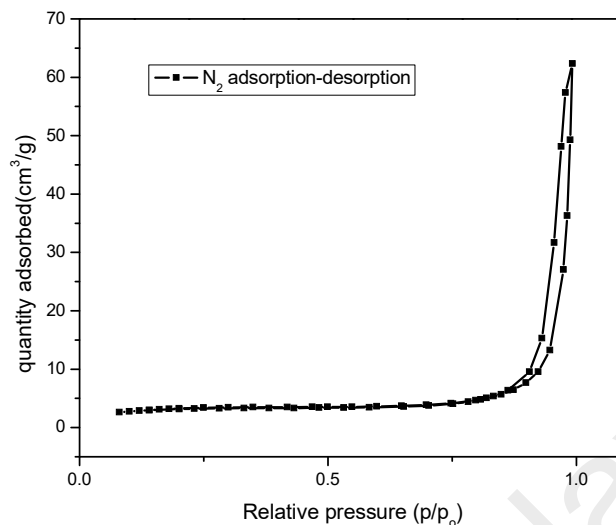


Figure 4.29: N₂ adsorption-desorption curve of Ce-2Ti mixed oxide catalyst.

4.1.4.6 Redox properties (H₂-TPR and O₂-TPD)

The reducing capability was evaluated by H₂-TPR as shown in Fig. 4.30. In general, CeO₂ showed reduction of its surface and bulk oxygen at around 530 °C and 650 °C respectively while TiO₂ shows weak reduction at comparatively high temperature due to difficulties associated with reduction in former reports. The TPR profile observed for Ce-2Ti mixed oxide prepared via solvent evaporation method showed two broad peaks at 430 °C and 490 °C. The observed shifting of reduction temperature towards low region suggests that the reducing ability had been significantly enhanced. As, XRD and Raman data are likely indicative of Ce-O-Ti solid solution generation in the prepared catalyst, therefore the synergy could promoted the reducing ability. And also, Ti might cause weakening of the bond strength between Ce-O which could be a determinant to improve the catalyst reducibility. Besides, the reduction of Ti⁴⁺ might be accelerated at low temperature owing to the synergistic interaction between Ce and Ti.

Furthermore, O₂-TPD study was also investigated to study the oxygen species of reduced CeO₂-2TiO₂ mixed oxide catalyst (Fig. 4.30). The O₂-TPD study revealed three

distinctive peaks at 290 °C, 500 °C and 770 °C for oxygen desorption in the catalyst denoted as α , β and γ . It suggests that three types of oxygen species with different energy are present in the catalyst which supported by XPS data. For the first broad oxygen desorption peak, α corresponds to oxygen vacant sites at the surface which required relative low energy. These surface oxygen vacancies are responsible to favor the enhancement of catalytic performance. The oxygen desorption peak, β is ascribed to the oxygen desorption of lattice oxygens. Hereafter, the peak at higher temperature was possibly due to the presence of defective oxygen species.

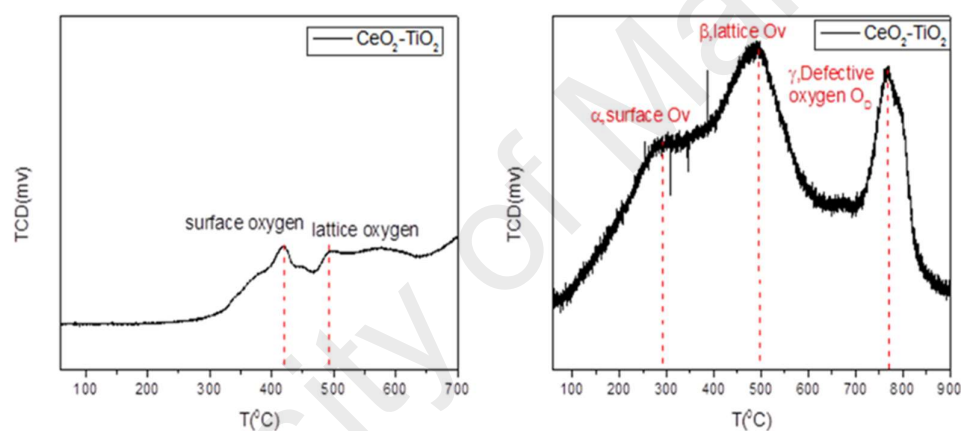


Figure 4.30: Synthesized Ce-2Ti mixed oxide catalyst illustrating, H₂-TPR analysis (left); O₂-TPD analysis.

4.1.5 Structural properties of synthesized Fe-2Ti mixed oxide catalyst

4.1.5.1 Crystal phase and crystallinity (XRD)

The crystal phase of Fe-2Ti mixed oxide catalyst was analyzed by Panlytical Xpert High score plus in Fig. 4.31 in terms of Bragg angle and d spacing (Å). The peak positioned at 2 theta 18.24°, 25.61°, 32.70°, 36.74°, 37.48°, 41.28°, 46.14°, 48.88°, 52.42°, 56.33°, 60.01°, 65.71°, 69.52° with d spacing 4.86, 3.47, 2.73, 2.44, 2.39, 2.18, 1.96, 1.86, 1.74, 1.63, 1.54, 1.42, and 1.35 Å respectively is ascribed to (020), (110), (023), (040),

(113), (042), (043), (200), (220), (152), (062), (142), (243) of orthorhombic diiron titanium oxide (Fe_2TiO_5) crystal phase according to JCPDS no (ICSD 96-200-2303). Worth to mention that no other crystal phase was detected as impurity.

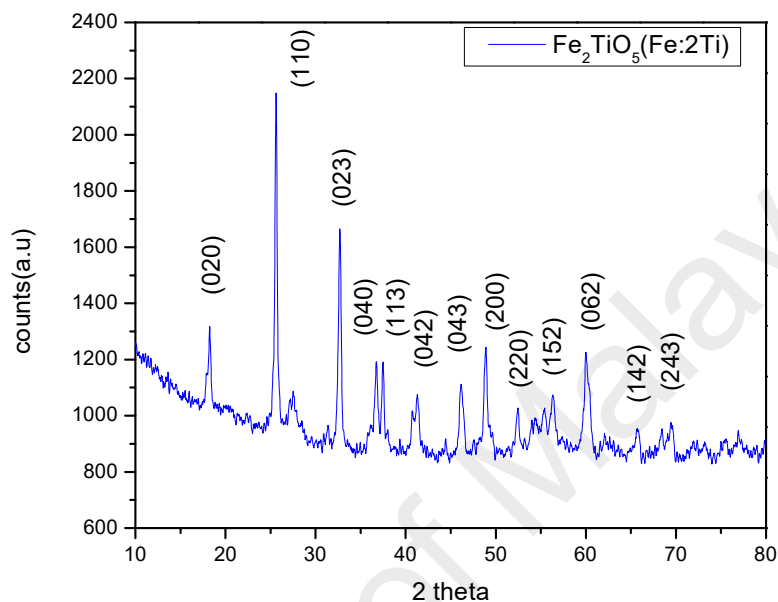


Figure 4.31: XRD analysis of Fe-2Ti mixed oxide catalyst.

4.1.5.2 Raman analysis

Raman analysis of Fe-2Ti mixed oxide catalyst was done to further investigate the qualitative properties of crystalline product. The Raman spectra of Fe-Ti mixed oxide catalyst was displayed in Fig. 4.32. The Raman spectra revealed that the synthesized catalyst contains pure phase of anatase TiO_2 and hematite in terms of the present Raman peaks. The Raman peaks located at 144 cm^{-1} , 199 cm^{-1} , and 659 cm^{-1} ascribed to Raman peaks of anatase TiO_2 in accordance with previously reported literature (Samsudin, Hamid, Juan, Basirun, & Centi, 2015). In addition, the Raman peaks positioned at 225 cm^{-1} , 247 cm^{-1} , 299 cm^{-1} , 412 cm^{-1} , 497 cm^{-1} , and 613 cm^{-1} corresponds to hematite with

absence of impurities like pure Fe_2O_3 and $\gamma\text{-Fe}_2\text{O}_3$ (De Faria, Venâncio Silva, & De Oliveira, 1997; Szatkowski et al., 2015).

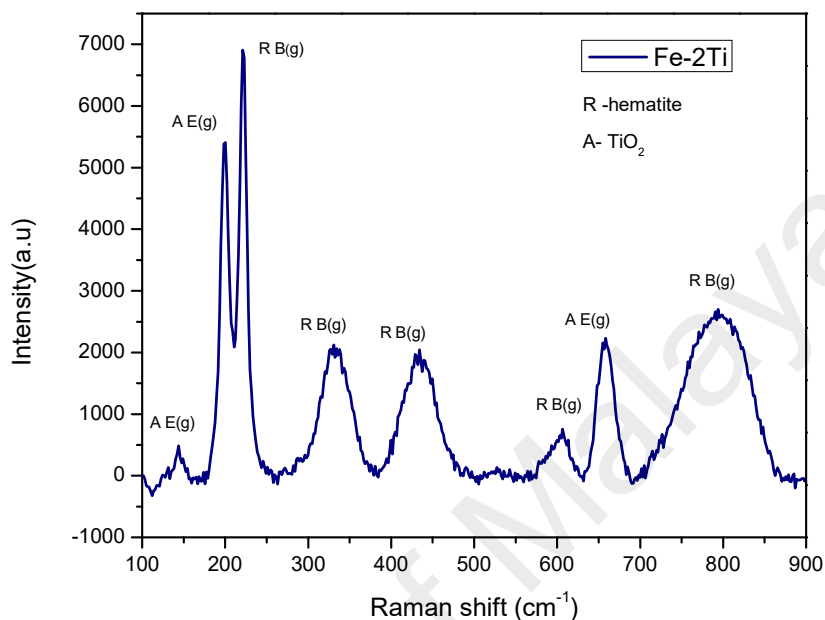


Figure 4.32: Raman spectra of synthesized Fe-2Ti mixed oxide catalyst.

4.1.5.3 Surface composition and oxidation state (XPS)

XPS analytical tool was used to determine the surface composition (Table 4.8) and chemical state of the metals in the synthesized Fe-Ti mixed oxide catalyst and displayed in Fig. 4.33. The peak at binding energy (BE) 458.0 eV in Ti 2p spectrum evidently confirmed that the synthesized crystalline material contain Ti^{4+} chemical state which is consistent with previous literature (Samsudin, Hamid, Juan, Basirun, & Centi, 2015). Moreover, the Fe 2p spectra was fitted with Gaussian-Lorentzian function shown Fe 2p_{1/2} and Fe 2p_{3/2} with multiple splitting with satellite featured peaks (Fig. 4.33c). The dominant peaks located including Fe 2p_{3/2} at binding energy 712.28 eV and Fe 2p_{1/2} at binding energy 725.87 eV with a satellite peak at 719.07 eV which was a characteristics of presence of $\alpha\text{-Fe}_2\text{O}_3$ (Yamashita & Hayes, 2008). And also, fitted Fe 2p_{2/3} peak shows an additional spitted peak at binding energy 710.3 eV which was ascribed to as a resultant

of Fe-O-Ti solid solution presence in the prepared materials as per previous literature (Pham, Dinh, Vuong, Ta, & Do, 2014). And also, absence of peak at binding energy 709.3 eV indicated that Fe^{2+} chemical state was absent in the material. Furthermore, O 1s spectrum was also fitted with Gaussian-Lorentzian and three distinguished peaks were detected (Fig. 4.33b). The peak at binding energy (BE) 529.80 eV was attributed to lattice oxygen (Fe-O or Ti-O). The peak at slightly higher binding energy 530.46 eV was ascribed to surface oxygen vacancies as a form of surface defects (Roberts, 1989). And also, the peak at binding energy (BE) 532.19 eV corresponds to defective oxygen species or chemisorbed oxygen species (O_2^- or O^-) or OH^- (Yiting Wang et al., 2015). The percentage amount of oxygen species (Table 4.9) was determined based on the area of each peaks in O 1s spectrum.

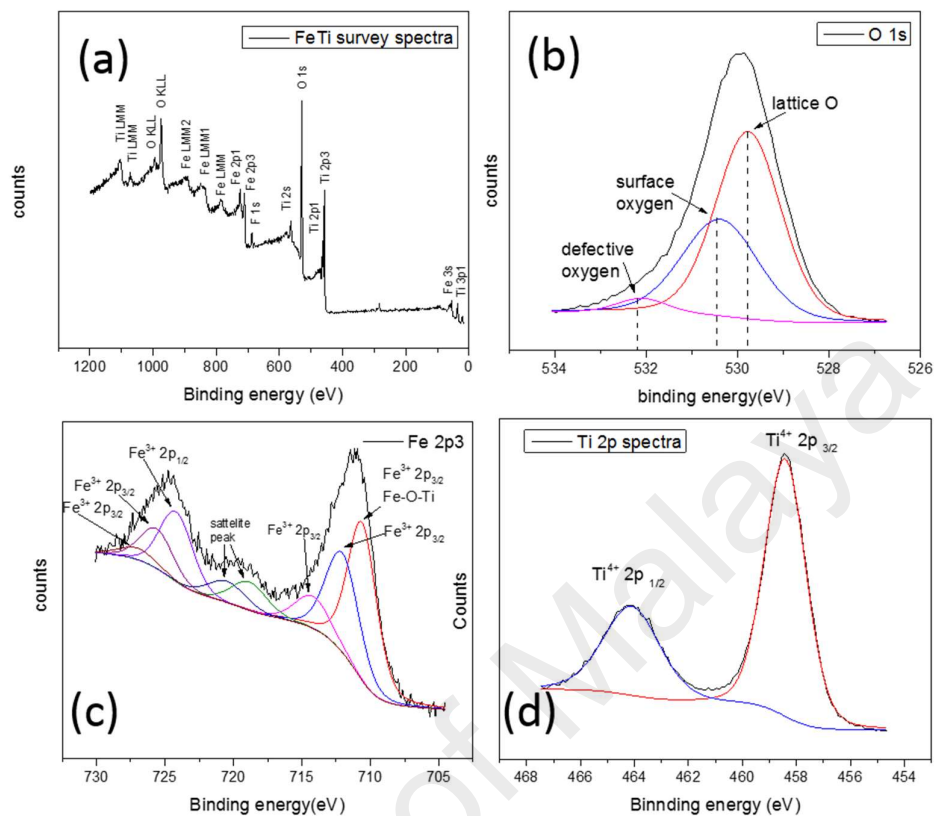


Figure 4.33: XPS spectra of synthesized Fe-2Ti mixed oxide catalyst. (a) Survey spectra; (b) O 1s spectra; (c) Fe 2p³ spectra; (d) Ti 2p spectra.

Table 4.8: The surface elemental ration of Fe-2Ti mixed oxide catalysts in XPS survey spectra.

Fe (%)	Ti (%)	O (%)	F (%)
8.64	18.9	68.48	3.98

Table 4.9: The area percentage of oxygen (O) species based on O 1s XPS spectra.

Lattice oxygen (O _L)	Surface oxygen Vacancy (O _v)	Defective oxygen (O _D)
60.19 %	36.26 %	3.53 %

4.1.5.4 Redox properties (H₂-TPR and O₂-TPD)

In order to investigate the reduction characteristics of the synthesized catalyst, H₂-TPR was done in temperature range of 60 °C to 900 °C (Fig. 4.34). The H₂-TPR spectrum revealed that the prepared materials were reduced in two step indicated by one dominant peak at 595 °C and a shoulder peak at 535 °C. The shoulder peak at low reduction temperature suggested reduction of surface oxygen present on the catalyst. And also, the peak at relatively high reduction temperature might be associated with reduction of lattice oxygen.

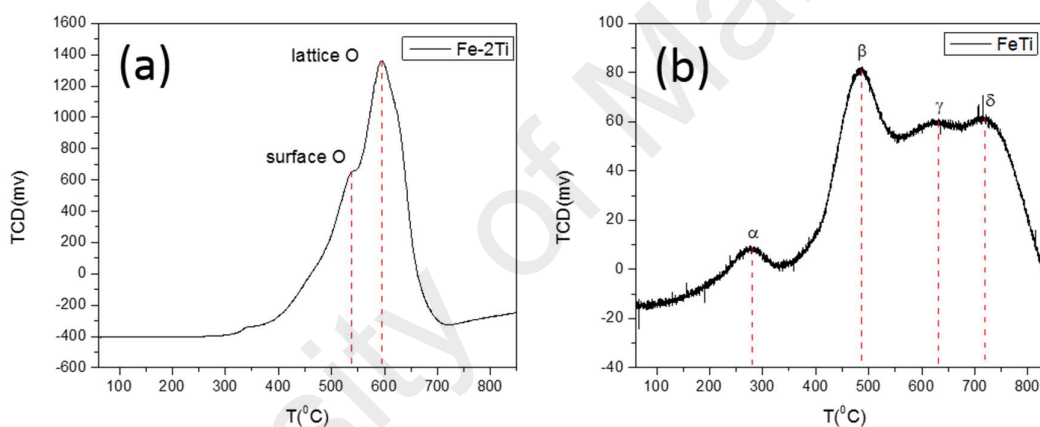


Figure 4.34: Synthesized Fe-2Ti mixed oxide catalyst illustrating, (a) H₂-TPR analysis; (b) O₂-TPD analysis.

O₂-TPD was done towards the reduced catalyst in order to determine the re-oxidation process of the Fe-2Ti mixed oxide catalyst (Fig. 4.34b). O₂-TPD profile of the catalyst indicated that O₂ desorption occurred in four steps on the reduced catalyst suggested by the four distinctive peaks at 281 °C, 483 °C, 629 °C, and 720 °C. The peak towards low temperature corresponds to desorption of oxygen from the vacant surface oxygen sites. The peak at 483 °C was probably associated with desorption of oxygen from the lattice oxygen sites. And also, the peak at higher temperatures might be attributed to desorption of oxygen from the defective oxygen species.

4.1.5.5 Morphology

Morphology of the synthesized materials was analyzed by FESEM analysis under high resolution (Fig. 4.35). The FESEM images of the Fe-2Ti mixed oxide catalyst shown rough and stony surface. And also, the material was agglomerated in 3-dimensional interconnected cluster network as it was calcined under high temperature. Moreover, the surface composition of the metals were determined by EDX (Fig. 4.35b). The observed composition of Fe to Ti in EDX pattern was consistent with the initial ratio during the synthesis in bulk phase (Fe: 2Ti).

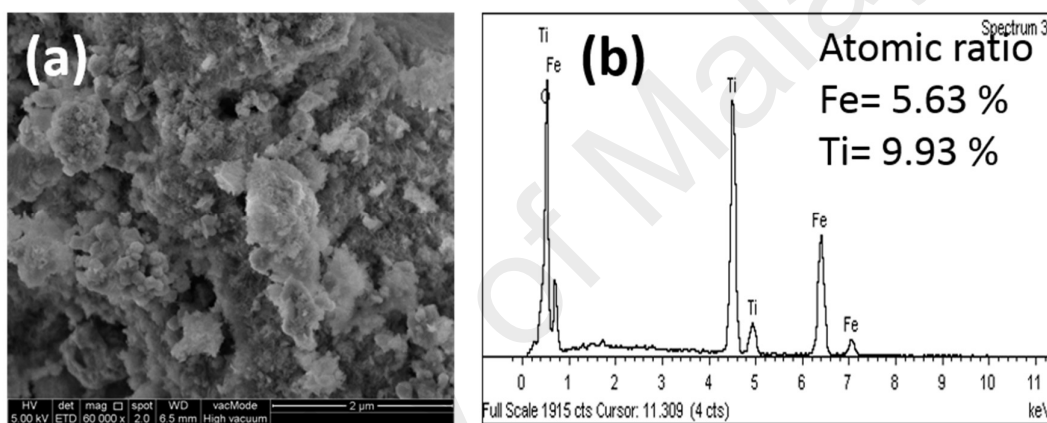


Figure 4.35: Morphology of synthesized Fe-2Ti mixed oxide catalyst. (a) FESEM image (b) EDX pattern.

Furthermore, HRTEM images of the prepared catalyst was captured to confirm the formation of crystals in terms of lattice fringe (Fig. 4.36). The lattice spacing was measured 3.47 Å, 2.73 Å and 2.44 Å which indicated crystal plane of (110) of Fe₂TiO₅ solid solution (Fig. 4.36c). Also, the SAED pattern of the synthesized materials suggested that it was a polycrystalline materials indicated by diffused rings. And the lattice spacing was also measured 3.47 Å and 2.73 Å of crystal plane (110) and (023) of Fe₂TiO₅ from the bright spots in the SAED pattern (Fig. 4.36b). Therefore, the crystal formation of Fe₂TiO₅ solid solution was confirmed by lattice spacing from HRTEM and SAED pattern.

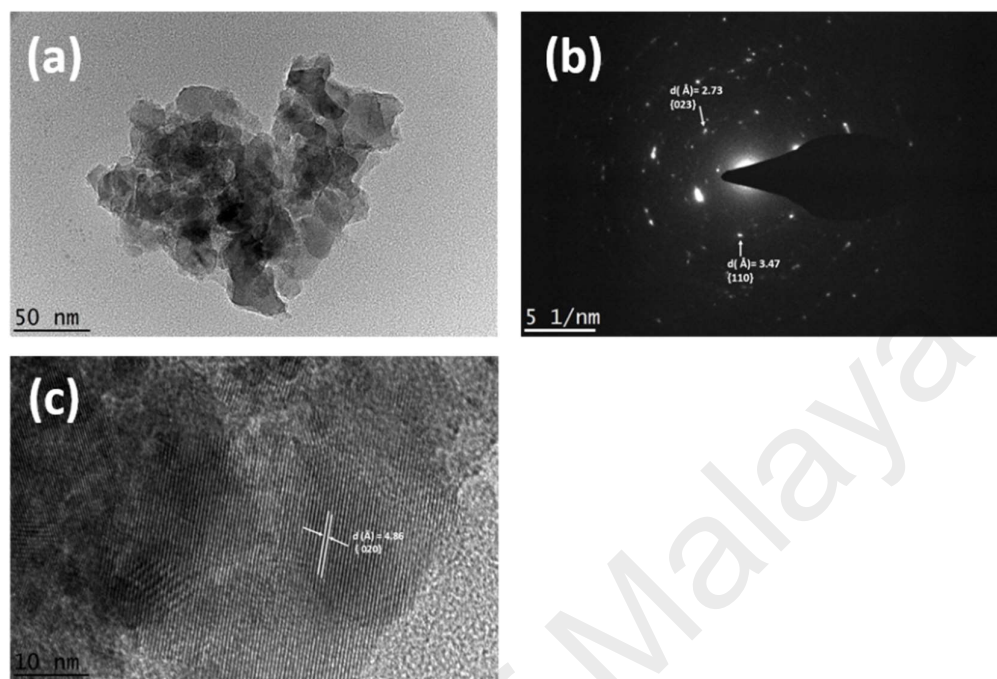


Figure 4.36: HRTEM images of Fe-2Ti mixed oxide catalyst. (a) Overview of the catalyst; (b) SAED pattern; (c) lattice pattern.

4.1.5.6 Textural properties (BET)

The N_2 adsorption-desorption curve for synthesized material is displayed in Fig. 4.37. The isotherm curve observed for the Fe-2Ti mixed oxide catalyst is type III. The surface area of the catalyst was also measured at $43.52 \text{ m}^2/\text{g}$. The surface area seemed moderate to perform better catalytic activity. Moreover, the pore size was calculated with 9.7 nm and pore volume was determined at $0.1057 \text{ cm}^3/\text{g}$.

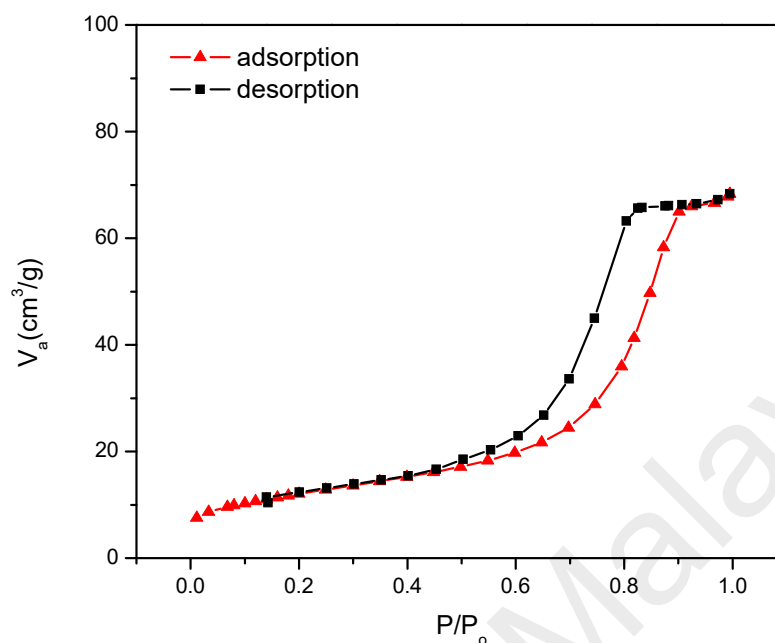


Figure 4.37: N₂- adsorption-desorption isotherm plot of synthesized Fe-2Ti mixed oxide catalyst.

4.2 Catalytic activity assessment

4.2.1 Cu-Ti mixed oxide catalysts

4.2.1.1 Oxidation under H₂O₂ by Cu-2Ti mixed oxide catalysts

These above discussed results suggested that synthesized Cu-Ti mixed oxide catalysts show unique defect properties and chemical activity to enrich the catalytic activity. The catalytic activity of synthesized Cu-Ti composite oxide catalysts with different composition of Cu and Ti were compared for liquid phase oxidation of vanillyl alcohol. The catalyst system (Cu: 2Ti) was taken into account to acquire the suitable reaction parameters such as solvent, temperature, time, catalyst mass, amount of oxidant, catalyst composition as well as presence of base. The other two catalysts (Cu: Ti) and catalyst (2Cu: Ti) were also performed at the same optimum condition of catalyst (Cu: 2Ti) for the oxidation of vanillyl alcohol. In addition, a reaction was carried out in absence of the catalyst, however no conversion of vanillyl alcohol was observed.

It was noted that the conversion significantly increased from 15 % to 61 % whereby the selectivity reduced from 83.0% to 60 % towards vanillin product with an increasing reaction time from 20 mins to 60 mins (reaction conditions: 1 mmol vanillyl alcohol, 3 mmol H₂O₂, catalyst (Cu: 2Ti) mass 0.0025 g/cm³, 20 ml acetonitrile) (Fig. 4.38a). After 60 mins, the constant conversion till 120 mins suggested that the reaction reached the equilibrium maxima. The selectivity decrement was associated with further oxidation of vanillin to vanillic acid in the presence of excess H₂O₂ in the reaction. Furthermore, guaiacol was also produced as one of the side product.

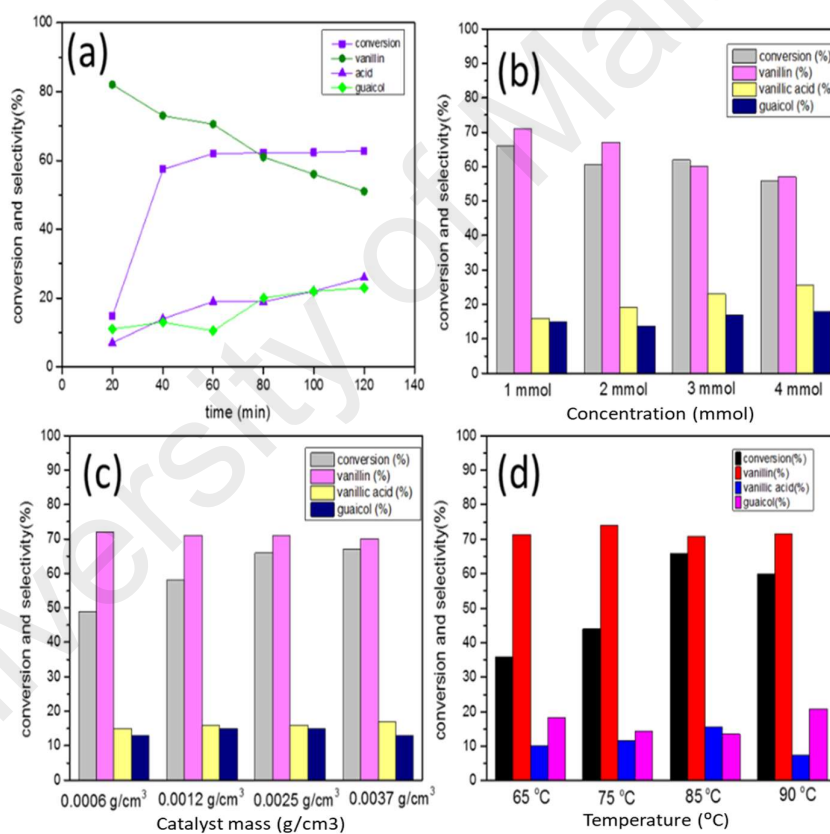


Figure 4.38: Effect of reaction parameters in oxidation of vanillyl alcohol by Cu-Ti (Cu: 2Ti) mixed oxide catalyst using H₂O₂ (a) progress of reaction; (b) concentration of H₂O₂; (c) catalyst mass (d) temperature.

Four different catalyst (Cu: 2Ti) loadings were studied for vanillyl alcohol oxidation reaction (reaction condition: 1 mmol vanillyl alcohol, 3 mmol H₂O₂, 20 ml acetonitrile 85 °C, 1 h) and the results are displayed in Fig. 4.38c. The conversion of vanillyl alcohol

augmented with the loading of the catalyst due to greater concentration of active sites present on the catalyst surface to perform in the reaction. Thus, it was not surprising that the lowest catalysts mass loading 0.0006 g/cm^3 (12 mg) shown the minimum catalytic conversion of 49 %.

The comparative higher loading of catalyst at 0.0012 g/cm^3 (25 mg) shown a slight increase of conversion (58 %). Further increased of catalyst loading from 0.0012 g/cm^3 to 0.0025 g/cm^3 rendered significant increase in the conversion by 66 %. Further increment of catalyst mass to 0.0037 g/cm^3 (75 mg) exhibited marginal improvement in the conversion by 67 % with 70 % selectivity. This was possibly due to mass transfer resistance (Klaewkla, Arend, & Hoelderich, 2011b). Noteworthy, the selectivity was almost constant at 71 % for all catalyst loading. Thus, the optimum catalyst loading was found at 0.0025 g/cm^3 (50 mg) based on the above experimental results. From this observation, it was evident that the catalyst loading play a vital role towards conversion.

In this experiment, various concentrations of oxidant H_2O_2 were used to determine any effect towards the catalytic reactivity (Fig. 4.38b). Four different molar ratios 1 mmol, 2 mmol, 3 mmol and 4 mmol equivalent to substrate of H_2O_2 were taken at the reaction conditions (1 mmol vanillyl alcohol, catalyst (Cu: 2Ti) mass 0.0025 g/cm^3 , 20 ml acetonitrile 85°C , 1 h). It was clearly observed that the concentration of oxidant had a significant impact towards conversion and selectivity. Both conversion and selectivity worsened gradually with an increase in the concentration of H_2O_2 . In the presence of excess H_2O_2 , fast formation of by-product (water) might lead towards fast catalyst deactivation by poisoning the surface active group of the catalyst (Forzatti & Lietti, 1999). And, the selectivity loss was possibly as a result of over oxidation of vanillin to corresponding carboxylic acid under longer reaction time. Moreover, we presumed that the formation of carboxylic acid in organic solvent in absence of base could cause strong

catalyst deactivation as well (Abad, Corma, & García, 2008). The amount of 1 mmol of H₂O₂ showed maximum conversion (66 %) and selectivity (71 %) to vanillin. However, the amount of 2 mmol, 3 mmol and 4 mmol displayed conversion by 63 %, 61 %, and 56 % respectively with selectivity to vanillin by 67 %, 60 %, and 57 % respectively. From the above discussed experimental results, 1 mmol concentration of H₂O₂ was found to be the optimum condition of oxidizing agent in the vanillyl alcohol oxidation process.

Effect of temperature was also examined in liquid phase oxidation of vanillyl alcohol over Cu-2Ti mixed oxide catalyst in a temperature range of 65 °C to 90 °C (reaction conditions: 1 mmol vanillyl alcohol, 1 mmol H₂O₂, catalyst (Cu: 2Ti) mass 0.0025 g/cm³, 20 ml acetonitrile, 1 h) (Fig. 4.38d). With the increase of temperature from 65 °C to 85 °C, there was a sharp enrichment expectedly in the conversion from 36 % to 66 % and no change in the selectivity was observed. The plausible reason is due to fast activation of substrate and oxygen source. However, at 90 °C, the conversion significantly decreased to 60 % possibly owing to fast degradation of H₂O₂ at elevated temperature, thereby minimizing the efficiency of oxidation reaction of the substrate (De, Chaudhuri, & Bhattacharjee, 1999). Moreover, many previous study has demonstrated decomposition of H₂O₂ into O₂ in presence of metals such as Cu (Gellerstedt & Pettersson, 1982; Salem, El - Maazawi, et al., 2000). It was presumed that H₂O₂ stability was affected in oxidation reaction at the high temperature. Thus, the suitable temperature for oxidation of vanillyl alcohol was found to be at 85 °C.

In this investigation, five different nature of organic solvents such as acetonitrile (MeCN), dimethylformide (DMF), Isopropanol, acetic acid (ACH), Tetrahydrofuran (THF) were studied in the liquid phase oxidation of vanillyl alcohol (reaction conditions: 1 mmol vanillyl alcohol, 1 mmol H₂O₂, catalyst (Cu: 2Ti) mass 0.0025 g/cm³, 85 °C, 1 h) (Fig. 4.39). There was a considerable impact on both conversion and selectivity to vanillin

due to the nature of the solvent. In acetonitrile, moderate amount of conversion (66 %) and selectivity (71 %) were obtained. When, isopropanol was used as a solvent, 24 % conversion with 75 % selectivity were measured. In case of dimethylformide, Cu-Ti composite oxide catalyst shown conversion by 29 % with 76 % selectivity towards vanillin. The lowest conversion (21 %) with 74 % selectivity towards vanillin was attained in nonpolar solvent tetrahydrofuran. The other solvents but acetonitrile might not function well due to unfavorable polarity or dielectric constant to the reaction intermediates (Andrade, Carlos, & Alves, 2005). Interestingly, acetic acid media shows the highest conversion (91 %) but moderate selectivity (46 %) towards vanillin. The enhanced catalytic activity in acetic acid media might cause by in situ formation of peroxyacetic acid due to reaction of acetic acid with H_2O_2 (Zhao, Zhang, Zhou, & Liu, 2008). Peroxyacetic acid is stronger oxidant than H_2O_2 . From this observation, acetonitrile was found to be the suitable solvent for vanillyl alcohol oxidation to selective vanillin in base free condition.

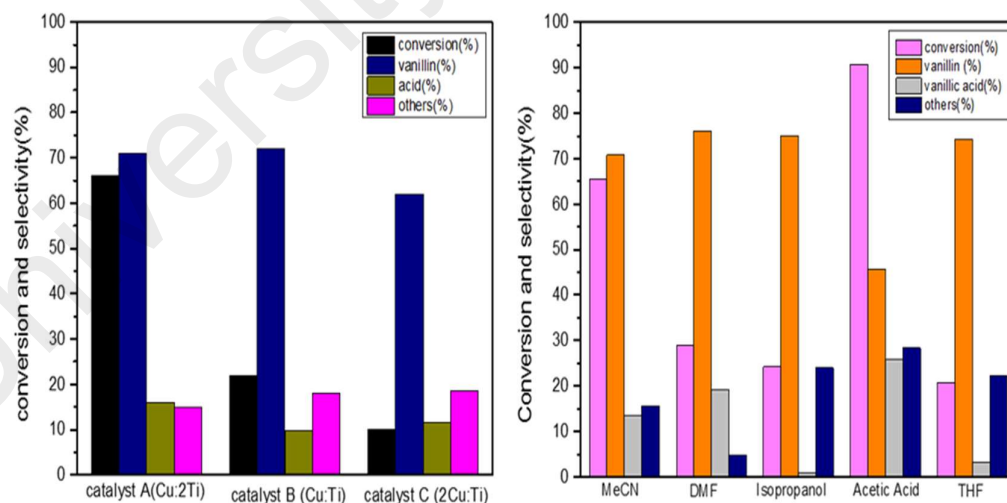


Figure 4.39: Effect of catalyst composition (left); and influence of nature of solvents (right) in oxidation of vanillyl alcohol by Cu-Ti mixed oxide catalyst using H_2O_2 .

As synthesized catalysts were studied for vanillyl alcohol oxidation at observed suitable reaction conditions (catalyst mass 0.0025 g/cm³, vanillyl alcohol 1 mmol, H₂O₂ 1 mmol, time 1 h, 20 ml acetonitrile, 1 h) (Fig. 4.39). For comparison, bulk CuO and TiO₂ (Degussa) catalysts were also studied at same condition as mixed oxides. TiO₂ shows conversion by 3 % with 58 % selectivity and 2 % conversion with 52 % selectivity for CuO in vanillyl alcohol oxidation. Based on the results, it was clearly evidenced that the prepared Cu-Ti mixed oxide catalyst highly promoted the catalytic conversion as well as the selectivity relative to their counterpart individual oxide phase. The catalyst (Cu: 2Ti) containing high loading of Ti in bulk phase which yields the best catalytic activity of substrate conversion by 66 % with significant selectivity of 71 % to vanillin using H₂O₂ whereas the other two synthesized catalysts (Cu: Ti) and catalyst (2Cu: Ti) exhibited poorer catalytic activity. The catalyst (Cu: Ti) shown substrate conversion of 22 % with 72 % selectivity to vanillin while 10 % substrate conversion with 62 % selectivity for catalyst 2Cu:Ti. It was clearly observed in the H₂-TPR and O₂-TPD profile that redox potential of the catalyst Cu: 2Ti was greatly enriched than other two catalysts which strongly supported the maximum conversion achieved. It was believed that Cu-O-Ti was the active phase in the oxidation reaction of vanillyl alcohol. The formation of Cu-O-Ti active phase was larger in concentration for catalyst (Cu: 2Ti) due to high dispersion of Cu into the TiO₂ lattice thus the synergistic combination could significantly improve the reducing ability of the catalyst. And also, the crystallite size observed in XRD analysis for catalyst (Cu: 2Ti) was 36 nm whereas other two catalysts crystallite size was larger by 41 nm. Hence, more surface area was accessible to take part in the catalytic reaction which was further proved by result of BET surface area. Furthermore, the catalytic properties such as grain boundaries and surface oxygen vacancies as surface defects present in catalyst (Cu: 2Ti) played vital role to enrich the degree of active sites. In addition, it was presumed that TiO₂ was strongly modified and reactive than pure TiO₂

under influence of Cu_3TiO_4 phase in the mixed oxide system. Furthermore, metal oxide phases co-operation is an important phenomenon to improve the catalytic activity of a mixed oxide catalyst (Grasselli, 2001). Thus, it was postulated that the composition of Cu_3TiO_4 phase and modified TiO_2 possibly favored the phenomenon of phase co-operation and was active in catalyst (Cu: 2Ti).

An immense number of literature reported the vital role of base in metal oxide catalyzed reaction for alcohol as the formed alkoxide ion (R-O^-) is not stable and thus required a strong base to form the alkoxide (R-O^-) ion (Jha & Rode, 2013; Shilpy et al., 2015; Tarabanko, Petukhov, & Selyutin, 2004; Tomlinson 2nd & Hibbert, 1936). In this experiment, we also focus on the impact of base in the oxidation reaction vanillyl alcohol. Among all of the above mentioned solvents, acetic acid and isopropanol were tested under treatment of base due to their ability towards solubility of the base NaOH (Fig. 4.40). Before proceeding for the oxidation reaction, equimolar (1:1) amount of NaOH (0.15g) was added to the solvents. In the presence of alkaline OH^- , the conversion (91%) remains constant, but there was a modest increase in the selectivity (59%) towards vanillin in acetic acid. In case of isopropanol, the conversion (86%) and selectivity (99%) towards vanillin are significantly improved. The base could play two major roles to enrich the catalytic activity and selectivity. Firstly, NaOH reacts vigorously with H_2O_2 to produce perhydroxy anion (OOH^-) which is a strong oxidizing agent and also can play a role as oxygen source. Secondly, the OH^- anion could deprotonate on the -OH group present on the benzylic carbon which dominates the reaction pathway to only corresponding aldehyde product to form other oxidative products. These results are in harmony with previously reported study, Shilpy et al for vanillyl alcohol oxidation in presence of base over CoTiO_3 catalyst (Shilpy et al., 2015). This evidences that addition of base enhance the oxidation reaction of vanillyl alcohol towards vanillin over Cu-Ti mixed oxide catalyst.

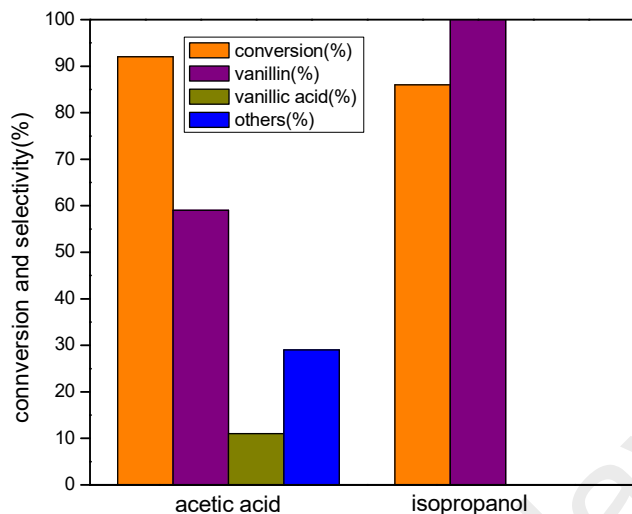


Figure 4.40: Effect of base media (NaOH) in oxidation of vanillyl alcohol by Cu-2Ti mixed oxide catalyst using H₂O₂ in oxidation of vanillyl alcohol.

4.2.1.2 Oxidation under air by Cu-2Ti mixed oxide catalysts

To make the rational study, liquid phase aerobic oxidation of vanillyl alcohol was carried out by using air. The reaction parameters were optimized under air. The above discussed results revealed that catalyst (Cu: 2Ti) shown promising catalytic activity in solvent acetonitrile in base free condition. Therefore, catalyst (Cu: 2Ti) was chosen in solvent acetonitrile to compare the catalytic activity at the optimized process conditions by using air as oxidant. A blank reaction in the absence of catalyst under air condition resulted in no conversion occurred. The progress of the reaction was monitored after every 20 mins time interval (reaction condition: 3 mmol vanillyl alcohol, 0.0025 g/cm³ catalyst, 120 °C and 21 bar air pressure, 60 ml acetonitrile) displayed in Fig. 4.41a. It was found that conversion steeply increased by 94% from 48% while reaction time was 2 hours from 30 mins with almost constant selectivity at 86 %. Hereafter, there was no noticeable change for further increment of conversion. It was worth to mention that vanillic acid and quinone were found as the by-products.

Catalyst loading was also further optimized in range of catalyst loading 0.0012 g/cm^3 to 0.0037 g/cm^3 in liquid phase aerobic oxidation of vanillyl alcohol (reaction condition: 3 mmol vanillyl alcohol, 60 ml acetonitrile, 2 h , $120 \text{ }^\circ\text{C}$, 21 bar) (Fig. 4.41b). In case of 0.0012 g/cm^3 catalyst mass, the least catalytic activity was observed by 62% . Further increment of catalyst loading by 0.0025 g/cm^3 showed excellent catalytic conversion by 94% was obtained. For 0.0037 g/cm^3 , no significant change in the conversion was noticed due to insignificant mass transfer effect (Klaewkla et al., 2011b). Noteworthy, the selectivity was almost constant at 86% .

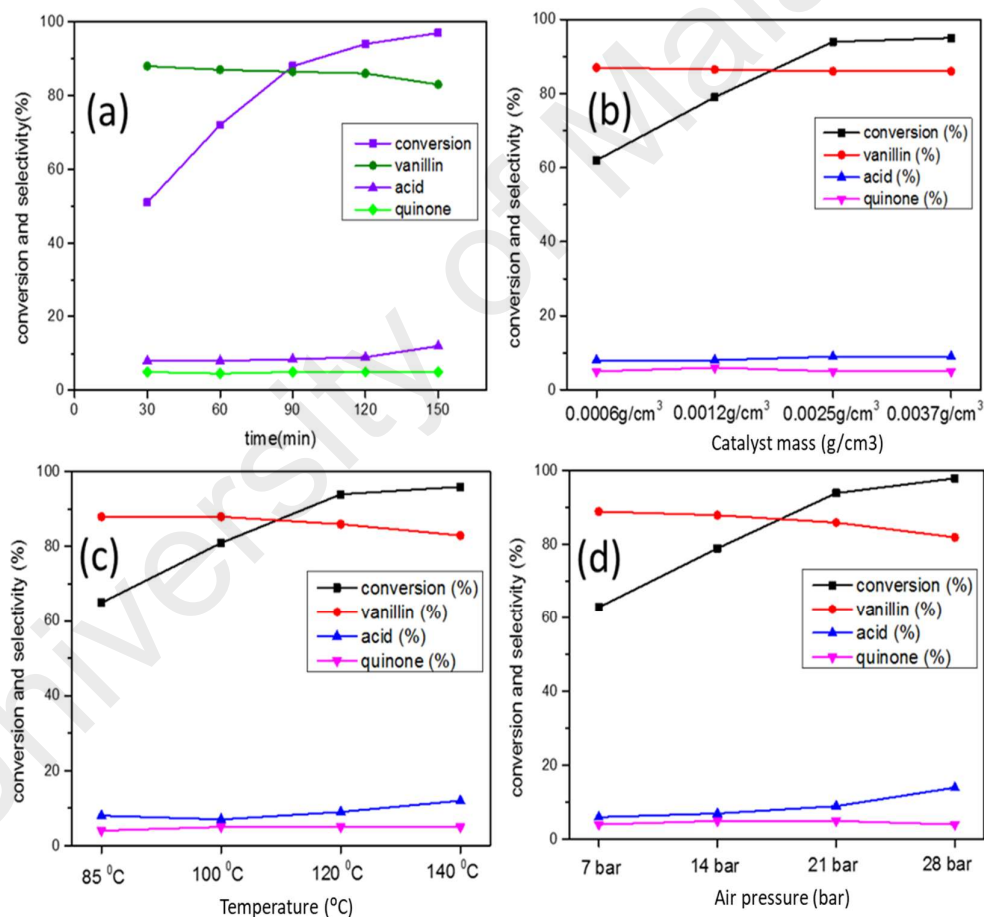


Figure 4.41: Effect of reaction parameters in oxidation of vanillyl alcohol by Cu-Ti mixed oxide catalyst using air (a) progress of reaction; (b) catalyst mass; (c) temperature; (d) air pressure.

Temperature in range of 85 °C to 140 °C was investigated to study the profound effect on the catalytic activity in liquid phase aerobic oxidation of vanillyl alcohol (reaction condition: 3 mmol vanillyl alcohol, 0.0025 cm³/g catalyst mass, 21 bar air pressure, 2 h, 60 ml acetonitrile) (Fig. 4.41c). There was an ascending trend in the catalytic conversion with the increase of temperature. The conversion reached at maximum by 96 % when the reaction was at 140 °C. However, for 120 °C, there was a negligible decrease in the catalytic conversion of 94 %. At reaction temperature of 140 °C, char formation was found. In addition, the selectivity was slightly reduced to 86 % from 89 % within the considered temperature range owing to over oxidation of vanillin to vanillic acid at high temperature. Based on this observation, 120 °C was the optimum temperature found for aerobic oxidation of vanillyl alcohol.

Four different air pressure such as 7 bar, 14 bar, 21 bar, and 28 bar was monitored to study the apparent influence (Fig. 4.41d). Compressed natural air pressure was found to have impact on both conversion and selectivity in liquid phase aerobic oxidation of vanillyl alcohol (reaction condition: 3 mmol vanillyl alcohol, 0.0025 cm³/g catalyst mass, T= 120 °C, 2 h, 60 ml acetonitrile). Improvement of the catalytic conversion by 94 % from 52 % was visible with increase of air pressure from 7 bar to 28 bar. Contradictorily, an inverse effect on the selectivity to vanillin was noticed with increase of pressure. The selectivity was readily dropped from 86 % to 78 %. It was possibly due to next step oxidation of vanillin to corresponding acid in presence of excess desorbed oxygen in the reaction. Thus, 21 bar air pressure was the best process condition to achieve outstanding catalytic activity of 94 % conversion with 86 % selectivity to vanillin. The catalytic conversion by Cu-2Ti mixed oxide was improved substantially in liquid phase aerobic oxidation of vanillyl alcohol. The reaction conditions was comparatively higher than using H₂O₂, as O₂ atom is quite kinetically stable owing to its triplet ground state and strong O-O bond.

In order to investigate the stability of the catalyst, vanillyl alcohol oxidation was carried out using the spent catalyst at the optimum reaction conditions for fresh catalyst using H_2O_2 (Fig. 4.42). After the first run of the freshly prepared catalyst, it was filtered and washed properly with acetonitrile several times to remove desorbed oxygenated products over the catalyst surface and dried under vacuum at $80\text{ }^\circ\text{C}$ for 4 h. Then the spent catalyst was investigated for vanillyl alcohol oxidation. The following procedure was carried out for three subsequent oxidation experiments. The conversion slightly decreased from 66 % to 58 % after the first use. However, the conversion sharply reduced to 38 % after the third run of the catalyst. This decrement might occurred due to reduction in roughness of the catalyst surface as negligible crystallinity change was demonstrated. Surprisingly, the selectivity remains almost constant at 71% in every recycling experiment. It implies that the reaction pathway was constant.

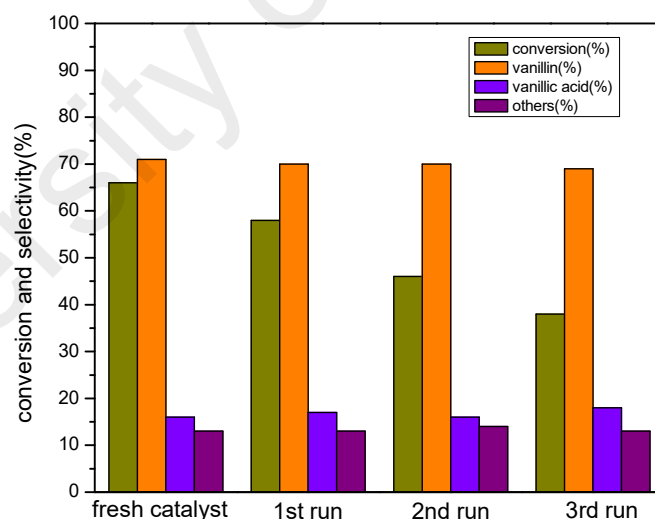


Figure 4.42: Recyclability study of Cu-Ti (Cu: 2Ti) mixed oxide catalyst in oxidation of vanillyl alcohol by using H_2O_2 as an oxidant.

4.2.2 Catalytic activity of Cu-Zr mixed oxide catalysts

4.2.2.1 Oxidation under H₂O₂ by Cu-Zr mixed oxide catalysts

The catalyst CuZrO₃ (Cu: 2Zr) was used to optimize the reaction parameters such as catalyst loading, time, temperature and solvent, concentration of oxidant H₂O₂ in vanillyl alcohol oxidation. Another two catalysts labeled as catalyst (Cu: Zr) and catalyst (2Cu: Zr) was experimented at the determined suitable reaction conditions. A blank reaction was also carried out without the presence of catalyst and results show the poor conversion (>2%). It implies on that the oxidation reaction did not proceed in absence of the catalyst.

In order to monitor the progress of the conversion and selectivity by CuZrO₃ catalyst (Cu: 2Zr) in vanillyl alcohol oxidation, the first parameter taken into account was reaction time (Fig. 4.43a) (reaction condition : 1 mmol vanillyl alcohol, 3 mmol H₂O₂, 0.0037 g/cm³ catalyst , 85 °C, 20 ml acetonitrile). It was clearly observed from the concentration of vanillyl alcohol that there was a gradual progress in the amount of substrate conversion. The conversion reached from 14 % to 62 % by four hours reaction time. However, the selectivity towards vanillin slightly dropped from the initial amount 80 % to 72 % with forwarding of the reaction time. It was associated with the further oxidation of vanillin to corresponding vanillic acid. It was evidenced from the increment of vanillic acid from 6 % to 12 %. Additionally, formation of by-product guaiacol was also observed at 18 %. From the experimental data, four hours was chosen as the optimum reaction time for vanillyl alcohol oxidation as the highest conversion was achieved by such period.

Various amounts of catalyst loading was experimented in the vanillyl oxidation reaction (Fig. 4.41b) to determine the apparent impact of catalyst mass into the oxidation reaction (reaction condition: 1 mmol vanillyl alcohol, 3 mmol H₂O₂, 85 °C, 4 h, 20 ml acetonitrile). From the observed data, it was evidenced that catalyst loading had a remarkable effect on the amount of substrate conversion with constant selectivity. The

conversion reached sharply to 47 % from 37 % while the loading was changed from 0.0012 g/cm³ to 0.0025 g/cm³. Further increment on the catalyst mass 0.0037 g/cm³ into the reaction contributes in enrichment of conversion of 62%. However, the selectivity toward vanillin stood almost unchanged at 72%. It provided the information that mass transfer was significant with 0.0037 g/cm³ of catalyst. In case of catalyst loading 0.050 g/cm³, the conversion remained almost similar 61% as the 75 mg loading owing to insignificant mass transfer effect (Klaewkla et al., 2011b). Based on the above discussion, 0.0037 g/cm³ catalyst mass was the optimum catalyst loading for vanillyl oxidation over CuZrO₃ (Cu: 2Zr) catalyst.

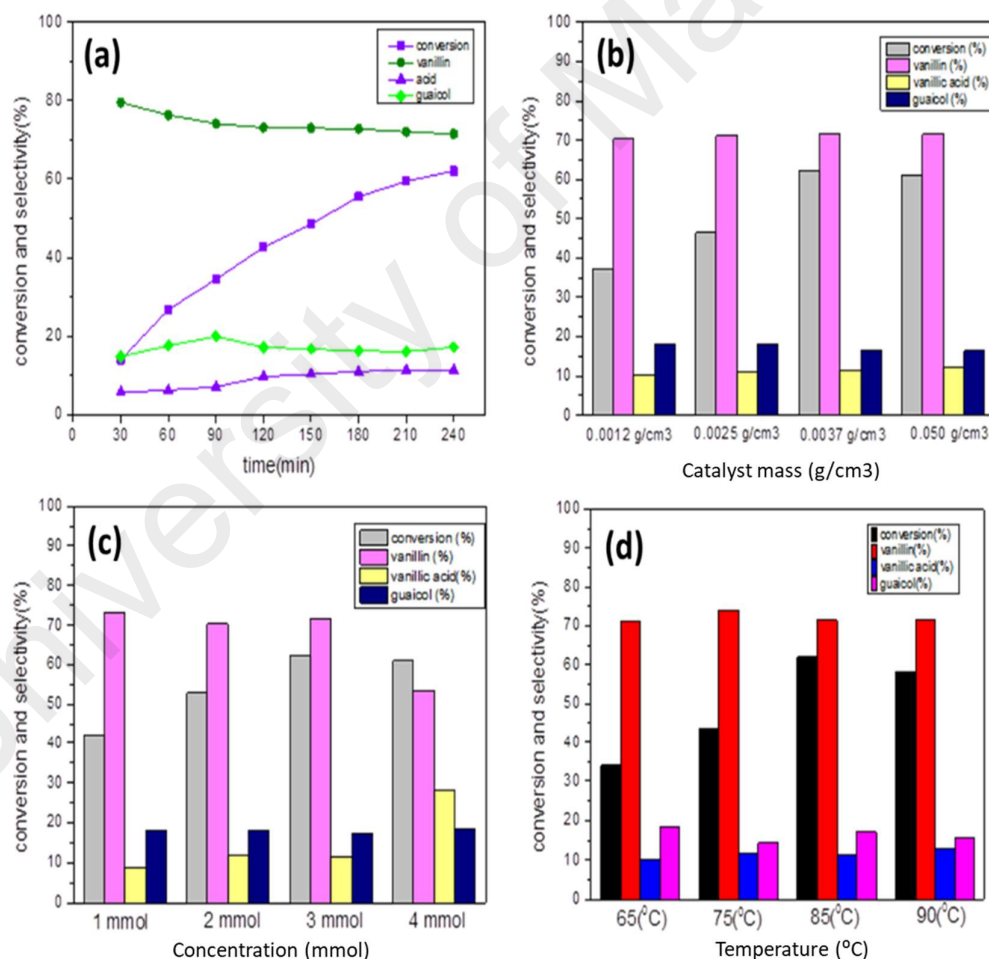


Figure 4.43: Effect of reaction parameters in oxidation of vanillyl alcohol by Cu-Zr (Cu: 2Zr) mixed oxide catalyst using H₂O₂ (a) progress of reaction; (b) catalyst mass; (c) concentration of H₂O₂; (d) temperature.

To investigate the possible consequence of H₂O₂ concentration change, four different molar ratios: 1 mmol, 2 mmol, 3 mmol and 4 mmol to the substrate was injected in the oxidation reaction of vanillyl alcohol (Fig. 4.43c) (reaction condition : 1 mmol vanillyl alcohol, 0.0037 g/cm³ catalyst , 85 °C, 4 h, 20 ml acetonitrile). From these results, it was worth to mention that there was a major impact on both conversion and selectivity due to increment of H₂O₂ concentration in the vanillyl alcohol oxidation reaction. Increment in the molar ratio of H₂O₂ facilitates generation of excess -OH⁻ ion which further benefited the conversion. However, the selectivity was dropped moderately with high concentration of H₂O₂. It resulted the further oxidation of produced vanillin towards corresponding acid in the presence of excess ⁻OH ion. For 1 mmol amount of H₂O₂, 42% conversion with 73% selectivity was obtained. In case of 2 mmol H₂O₂, the conversion substantially improved by 53% with 71% selectivity. Similar trend was also observed for 3 mmol of H₂O₂ which shows conversion of 62% with 72% selectivity of vanillin. However, reverse trend was observed for 4 mmol H₂O₂ (61 % conversion with 52 % selectivity towards vanillin). It could be possibly due to the fast formation of water during oxidation reaction which resulted in deactivation of the catalyst active site on the surface. Thus, 3 mmol of H₂O₂ was chosen as the optimum concentration as it served to render superior catalytic activity with moderate selectivity via vanillyl alcohol oxidation over perovskite type CuZrO₃ (Cu: 2Zr) catalysed process.

To study the probable response of temperature on conversion and selectivity for vanillyl alcohol oxidation reaction, a range of temperatures from 65 °C to 85 °C was considered (reaction conditions: 1 mmol vanillyl alcohol, 3 mmol H₂O₂, 0.0037 g/cm³ catalyst , 4 h, 20 ml acetonitrile) (Fig. 4.43d). A progressive trend on the conversion was expectedly observed in range of 65 °C to 90 °C. At 65 °C, the catalytic activity of CuZrO₃ (Cu: 2Zr) catalyst was obtained by 34 % conversion with 72 % selectivity towards vanillin. When the temperature was rose up to 75 °C, the conversion was improved by

44 % conversion with 74% selectivity towards vanillin. The best catalytic efficiency was exhibited by 62% conversion and 72 % selectivity towards vanillin at elevated temperature of 85 °C. However, a marginal decrement on conversion (58 %) with selectivity (72 %) was obtained at 90 °C. Thermodynamically, elevated temperature favored the enrichment of conversion due to the activation energy was reached optimum point for catalyst to perform the catalyzed oxidation reaction. Hence, from the observed data, we concluded that 85 °C was the suitable temperature condition for vanillyl alcohol oxidation.

In order to illustrate the catalytic activity and selectivity in different nature of solvents, various solvents with different polarity were used in CuZrO₃ (Cu: 2Zr) catalyzed oxidation reaction (reaction conditions: 1 mmol vanillyl alcohol, 3 mmol H₂O₂, 0.0037 g/cm³ catalyst, 85 °C, 4 h) (Fig. 4.44). The experiment was done in acetonitrile, dimethylformamide, tetrahydrofuran, ethanol and acetic acid under optimized reaction condition. In acetonitrile, CuZrO₃ catalyst shows superior catalytic activity by 62 % conversion with 72 % selectivity. In isopropanol, lower conversion of vanillyl alcohol 34 % with better selectivity (78 %) were obtained. When dimethylformide was used as solvent, there were further decrease in the conversion (26 %) and 76 % selectivity. In case of tetrahydrofuran, the catalytic activity (21 %) and selectivity (74 %) observed were also seems not much impressive. Unfavorable polarity and dielectric constant of the nonpolar solvents towards the reaction intermediates might cause adverse effect in the catalytic action for vanillyl alcohol oxidation (Andrade et al., 2005). Therefore, there was visibly a declined trend on the catalytic activity in order of MeCN > Isopropanol > DMF > THF. Interestingly, in acetic acid media, a surprising catalytic conversion (90 %) with poor selectivity (42 %) were noticed. It might be associated also to the in situ formation of peroxy radicals generated by reaction between acetic acid and H₂O₂ (Zhao et al., 2008).

Hence, acetonitrile was found to be the suitable solvent for vanillyl alcohol oxidation in base free condition.

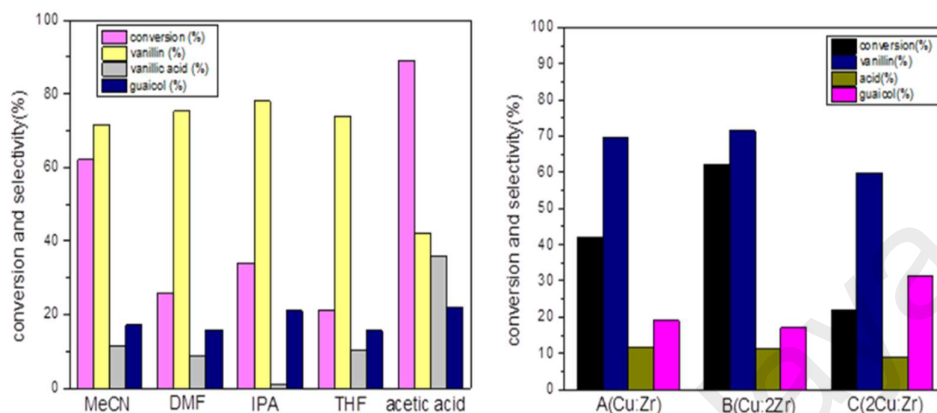


Figure 4.44: Influence of nature of solvents (left); effect of catalyst compositions (right) in oxidation of vanillyl alcohol by Cu-Zr (Cu: 2Zr) mixed oxide catalyst using H₂O₂.

The vanillyl alcohol oxidation reaction by CuZrO₃ (Cu: 2Zr) was tested at suitable reaction parameters under treatment of base NaOH (reaction conditions: 1 mmol vanillyl alcohol, 3 mmol H₂O₂, 0.0037 g/cm³ catalyst, 85 °C, 4 h, 1 mmol NaOH) (Fig. 4.45). It was clearly visible that the base played an impressive role to amplify the catalytic activity. Two solvents such as acetic acid and isopropanol were aimed owing to the insolubility of NaOH in other nonpolar solvents. Prior to carry out the reaction, an equimolar ratio (1:1) of NaOH (0.15g) was dissolved to the solvent. In acetic acid media in presence of base, the catalytic selectivity (56 %) was notably improved where the conversion (89 %) remains almost unchanged. In case of isopropanol, both conversion (92 %) and selectivity (99 %) were markedly bettered which was well agreement with previously reported by Shilpy et al and Jha et al (Jha & Rode, 2013; Shilpy et al., 2015).

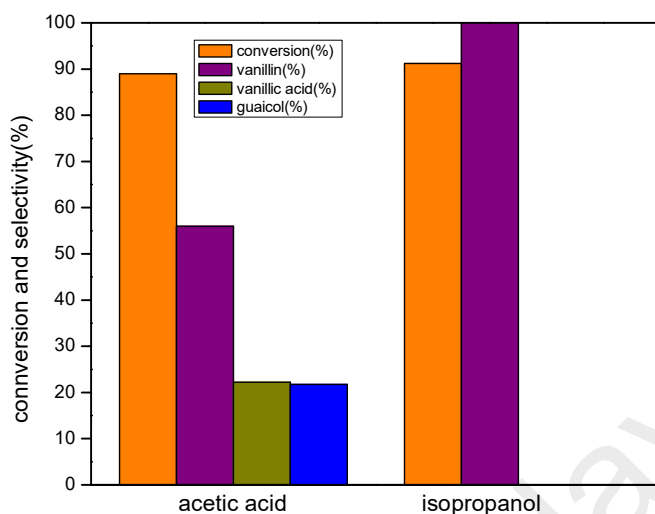


Figure 4.45: Influence of base reaction media over Cu-Zr (Cu: 2Zr) mixed oxide catalyst in oxidation of vanillyl alcohol.

The prepared catalysts (Cu: Zr), catalyst (Cu: 2Zr) and catalyst (2Cu: Zr) were tested for oxidation of vanillyl alcohol at the optimized reaction conditions (Fig. 4.44). To rationalize, commercially available pure CuO and ZrO₂ catalysts were also investigated at the same reaction conditions. The bulk CuO catalyst shown 2 % conversion with 52 % selectivity and 3 % conversion with 58 % selectivity for ZrO₂. Interestingly, the synthesized catalyst shown improved catalytic action than their counterpart single oxide catalyst. For Catalyst (Cu: Zr), conversion (42 %) with selectivity (69 %) were achieved. When catalyst (Cu: 2Zr) catalyst were used the best conversion (62 %) with selectivity (71 %) towards were obtained. The least conversion (22 %) with selectivity (66 %) were observed in case of catalyst (2Cu: Zr). It was worth to mention that the highest catalytic activity was obtained by catalyst (Cu: 2Zr) was due to the high content of ZrO₂. High loading ZrO₂ could cause large concentration of acidic site on the surface to interact with Cu²⁺ ion strongly onto the surface. Consequently formation high degree of Cu-O-Zr phase in the catalyst as it was presumed that Cu-O-Zr was the active phase for oxidation of vanillyl alcohol. And also, high dispersion of Cu on the ZrO₂ in catalyst (Cu: 2Zr)

minimize the grain size to less than 10 nm and exposed numerous grain boundaries observed in HRTEM micrograph. Moreover, it was evidenced from H₂-TPR and O₂-TPD showed large concentration of oxygen vacancies on the surface associated with defects created by the favorable stoichiometry of Cu to Zr (1:2) in the synthesis protocol of catalyst. Furthermore, the order of catalytic performance was in well agreement with that of the above mentioned BET surface area as large surface area could offer exposure of large number of active sites to partake in the reaction.

4.2.2.2 Oxidation under air by Cu-2Zr mixed oxide catalysts

The best performed catalyst (Cu: 2Zr) with high content of Zr in acetonitrile was further examined for aerobic oxidation of vanillyl alcohol in base free condition under various reaction parameters such as time, catalyst loading, temperature and pressure. The progress of the reaction was recorded after every half an hour time interval till the reaction time reached 2.5 hours and the results are displayed in Fig. 4.46a (reaction conditions: 3 mmol vanillyl alcohol, 21 bar air pressure, 0.0025 g/cm³ catalyst, 120 °C). The catalytic activity was improved expectedly at a precipitous rate with the increase of time till 2 hours of reaction time. The conversion was measured by 91 % conversion with 76 % selectivity. Thereafter, the reaction progress was not significantly forwarded. Thus, 2 hours was chosen as optimum reaction time. It was worth to note that vanillic acid and quinone was found as the side products.

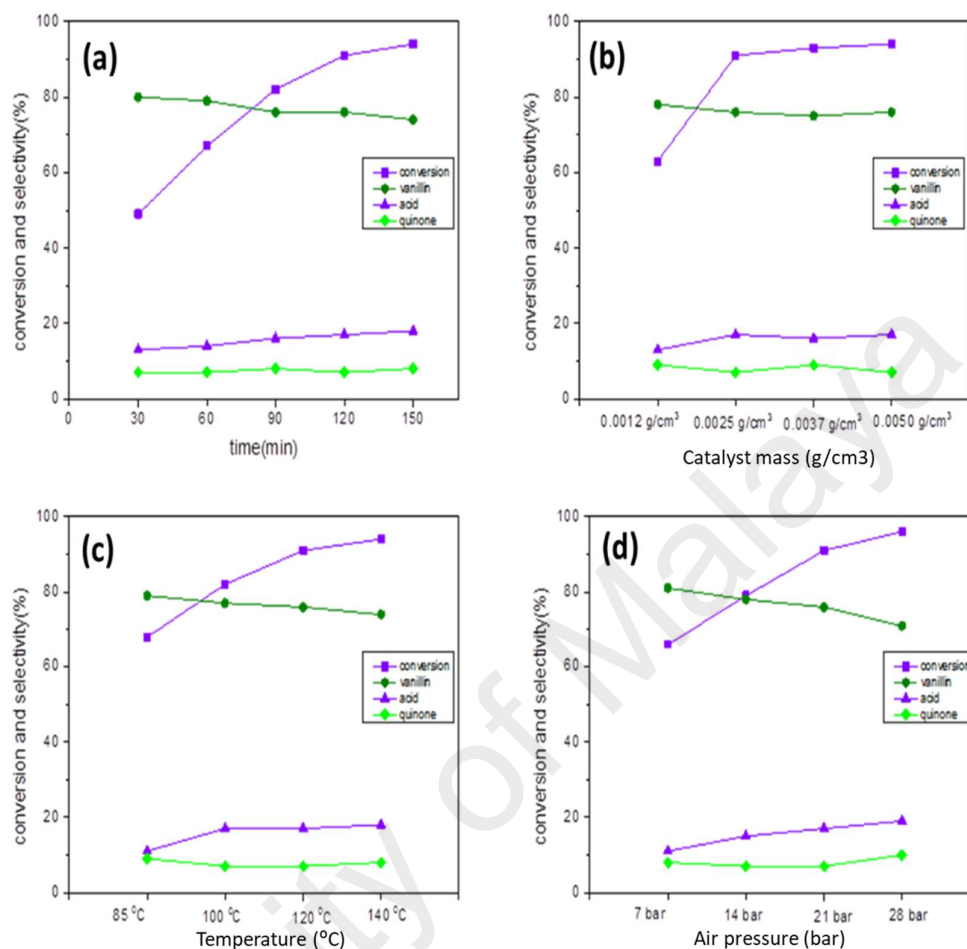


Figure 4.46: Effect of reaction parameters in oxidation of vanillyl alcohol by Cu-Zr (Cu: 2Zr) mixed oxide catalyst using air (a) progress of reaction; (b) catalyst mass; (c) temperature; (d) air pressure.

In order to examine the effect of catalyst loading, catalyst mass in a range 0.0012 g/cm³ to 0.0050 g/cm³ was considered (reaction conditions: 3 mmol vanillyl alcohol, 21 bar air pressure, 120 °C, 2 h) (Fig. 4.46b). A steep improvement in the catalytic conversion by 91 % from 63% was visible while the catalyst loading was changed by 0.0025 g/cm³ from 0.0012 g/cm³. However, further increment in the catalyst loading till 0.0050 g/cm³ was observed not to promote the catalytic conversion noticeably. This was the fact that mass

transfer effect was not significant (Klaewkla, Arend, & Hoelderich, 2011a). Noteworthy, the selectivity (76 %) was not affected by the change in the catalyst loading.

The apparent response in catalytic activity with respect to temperature was investigated in range of 85 °C to 140 °C (reaction condition: 3 mmol vanillyl alcohol, 21 bar air pressure, 0.0025 g/cm³ catalyst, 2 h) (Fig. 4.46c). The catalytic conversion was substantially better at 94 % from 68 % while the temperature was elevated from 85 °C to 140 °C. However, the selectivity was slightly dropped by 74% from 79 % with the increment of temperature. This was possible due to further oxidation of vanillin product to corresponding acid at higher temperature. It was worth to mention that char formation was observed at temperature 140 °C. Therefore, 120 °C was considered the best temperature for liquid phase aerobic oxidation of vanillyl alcohol.

The air pressure was found to be the vital determinant to obtain superior catalytic activity from 7 bar to 28 bar (reaction condition: 3 mmol vanillyl alcohol, 0.0025 g/cm³ catalyst, 120 °C, 2 h) (Fig. 4.46d). The pressure was changed from 7 bar to 14 bar with conversion was enriched by 79 % from 66 %, but a drop in the selectivity to 78 % from 81 % towards vanillin. When the pressure was increased to 21 bar air pressure, excellent catalytic activity was measured at 91 % conversion with 76 % selectivity. Further rise in the air pressure was found to be detrimental to the selectivity by 71 % from 76 %. However, conversion was improved up to 96 %. The slight drop in the selectivity was associated with the over-oxidation of vanillin to vanillic acid in presence of excess desorbed oxygen in the reaction media. Based on the experimental data, 21 bar air pressure was selected as the optimum pressure for liquid phase aerobic oxidation of vanillyl alcohol.

The stability of the catalyst was also examined by the reused catalyst at the optimum reaction condition for vanillyl alcohol oxidation using H₂O₂ (reaction condition : 1 mmol

vanillyl alcohol, 3 mmol H₂O₂, 0.0037 g/cm³ catalyst, 85 °C, 4 h) (Fig. 4.47). The catalyst was recovered by filtration after the first run of the catalyst in the reaction and washed off several times by acetonitrile for removal desorbed oxygenated products onto the surface. The spent catalyst was dried at 80 °C for 4 hours. The subsequent reactions were carried out at the optimum reaction conditions following the similar recovery procedure. The conversion was dropped by 56 % from 62 % after the first catalytic reaction. In case of third run of the catalyst, the conversion was further reduced to 52 %. In fourth run, lowest conversion (48 %) was observed.

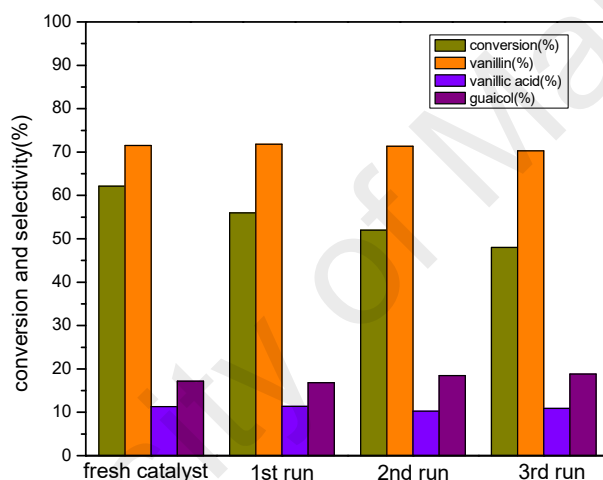


Figure 4.47: Recyclability study of Cu-Zr (Cu: 2Zr) mixed oxide catalyst.

However, the selectivity stands almost unchanged at 72 %, indicative of similar reaction pathways was dominant at every recycling experiments. As the XRD (section 4.1.2.1) and SEM (section 4.1.2.5) shown the same fingerprints and morphology for spent catalyst as the fresh catalyst, the selectivity was unaffected. But, the conversion was influenced possibly owing to transformation of uneven surface to plain surface (Fig. 4.13)

4.2.3 Catalytic evaluation of Cu-Mn mixed oxide catalyst

4.2.3.1 Oxidation under H₂O₂ by Cu-Mn mixed oxide catalysts

As described above, these findings from XRD, HRTEM and SAED confirmed formation of Cu_{1.5}Mn_{1.5}O₄ phase in all synthesized catalysts. And also, XPS revealed co-existence of two oxidation state of Cu²⁺ and Cu⁺ with Mn³⁺ species. In addition, presence of surface oxygen vacancies was confirmed by the O 1s spectra and O₂-TPD studies. It was postulated that great catalytic activity could be achieved by enrichment of surface defects oxygen which are surface reactive oxygen species to facilitate the oxidation process. Moreover, the grain boundaries as form of surface defects as additional active sites was marked in the interface of the plane. The reducing temperature of the prepared Cu_{1.5}Mn_{1.5}O₄ catalyst phase was significantly lower than corresponding isolated phases because of synergistic combination of the metals and also large concentrations of structural defective oxygen species. These structural and chemical properties of synthesized Cu_{1.5}Mn_{1.5}O₄ catalyst enhanced the catalyst robustness for the liquid phase oxidation of vanillyl alcohol.

To evaluate the catalytic activity, catalyst (Cu: Mn) was considered due to better catalytic activity to optimize the reaction variables after primary catalytic evaluation. No conversion was observed in acetonitrile with and without the presence of catalyst using H₂O₂ oxidant. However, in the presence of equimolar base NaOH in Isopropanol relative to vanillyl alcohol was added and oxidation reaction was carried out. Interestingly, a surprising catalytic activity was achieved. To determine the role of the base, reaction without the catalyst in presence of base NaOH and H₂O₂ in solvent isopropanol was also considered. No conversion of vanillyl alcohol was found. Therefore, it was worth to mention that presence of base in liquid phase oxidation of vanillyl alcohol by Cu_{1.5}Mn_{1.5}O₄ was crucial as it probably deprotonate the phenoxy ion and favors the coordination with the catalyst. It is a well-known fact that H₂O₂ coupled with NaOH

avored the lignin valorization over metal oxides (Tarabanko et al., 2004; Tomlinson 2nd & Hibbert, 1936) (Jha & Rode, 2013).

To monitor the progress of the oxidation reaction, HPLC analysis was done after every 0.5 h of reaction time interval (reaction conditions: 1 mmol vanillyl alcohol, 1 mmol NaOH (0.15g), 3 mmol H₂O₂, 20 ml Isopropanol, catalyst 0.0037 g/cm³) (Fig. 4.48a). A steeply progressive trend on the amount of conversion was visible. After two and half hour reaction time, the conversion reached to 94 % with 99 % selectivity to vanillin. With the increase of reaction time, the conversion remained almost constant (99 %). Based on the found results, 2.5 h was chosen as the optimum time for vanillyl alcohol oxidation by Cu_{1.5}Mn_{1.5}O₄ catalyst using H₂O₂ oxidant.

To determine the optimum loading of catalyst in the reaction, four different loading 0.0012 g/cm³, 0.0025 g/cm³, 0.0037 g/cm³ and 0.0050 g/cm³ were considered (reaction conditions: 1 mmol vanillyl alcohol, 1 mmol NaOH (0.15g), 3 mmol H₂O₂, 20 ml Isopropanol, 85 °C, 2.5 h) (Fig. 4.48b). A sharp increase by 94 % from 56 % was observed in the amount of conversion while catalyst loading was changed from 0.0012 g/cm³ to 0.0037 g/cm³ owing to significant mass transfer effect. However, in case of 0.0050 g/cm³ catalyst loading, the conversion was further enriched by 2 %. It was due to possibly mass transfer resistance (Klaewkla et al., 2011a). Surprisingly, the selectivity towards vanillin stood constant at 99 % for all loading of the catalysts. Thus, 0.0037 g/cm³ was the best catalyst mass for liquid phase selective oxidation of vanillyl alcohol to vanillin using H₂O₂ oxidant.

Four different molar ratios such as 1 mmol, 2 mmol, 3 mmol and 4 mmol of H₂O₂ concentration to vanillyl alcohol was studied in order to scrutinize the effect of oxidant concentration in the reaction (reaction conditions: 1 mmol vanillyl alcohol, 1 mmol NaOH (0.15g), 20 ml Isopropanol, 2 h, 85 °C, catalyst 0.0037 g/cm³) (Fig. 4.48c). The

conversion was markedly improved while the concentration of the H_2O_2 was increased. The conversion was maximum at 94 % in case of 3 mmol. Increased amount of H_2O_2 facilitate to accelerate the rate of oxidation reaction. However, 4 mmol shown slightly declined amount of conversion (92 %). This was possibly due to degradation of H_2O_2 becomes predominant over oxidation of vanillyl alcohol. Noteworthy, the selectivity was not affected for abovementioned concentratio of H_2O_2 . Based on the experimental data, 3 mmol was chosen as the best concentration for liquid phase oxidation of vanillyl alcohol by H_2O_2 .

The oxidation reaction was carried out at four different temperatures such as 65 °C, 75 °C, 85 °C and 90 °C under optimized reaction conditions to investigate the probable response (reaction conditions: 1 mmol vanillyl alcohol, 1 mmol NaOH (0.15g), 3 mmol H_2O_2 , 20 ml Isopropanol, 2h, catalyst 0.0037 g/cm^3) (Fig. 4.48d). With the increase of temperature to 85 °C from 65 °C, the catalytic conversion was improved expectedly to 94 % from 56 % conversion. However, at temperature of 90 °C, the conversion was slightly reduced to 92 %. In previous literature, it was reported that H_2O_2 degradation was higher above temperature 90 °C and thus resulted to lower conversion (Andas, Adam, Rahman, & Taufiq-Yap, 2014). Similar observation was made in our study. Thus, 85 °C was considered as the best temperature for maximum amount of conversion in liquid phase oxidation of vanillyl alcohol using H_2O_2 .

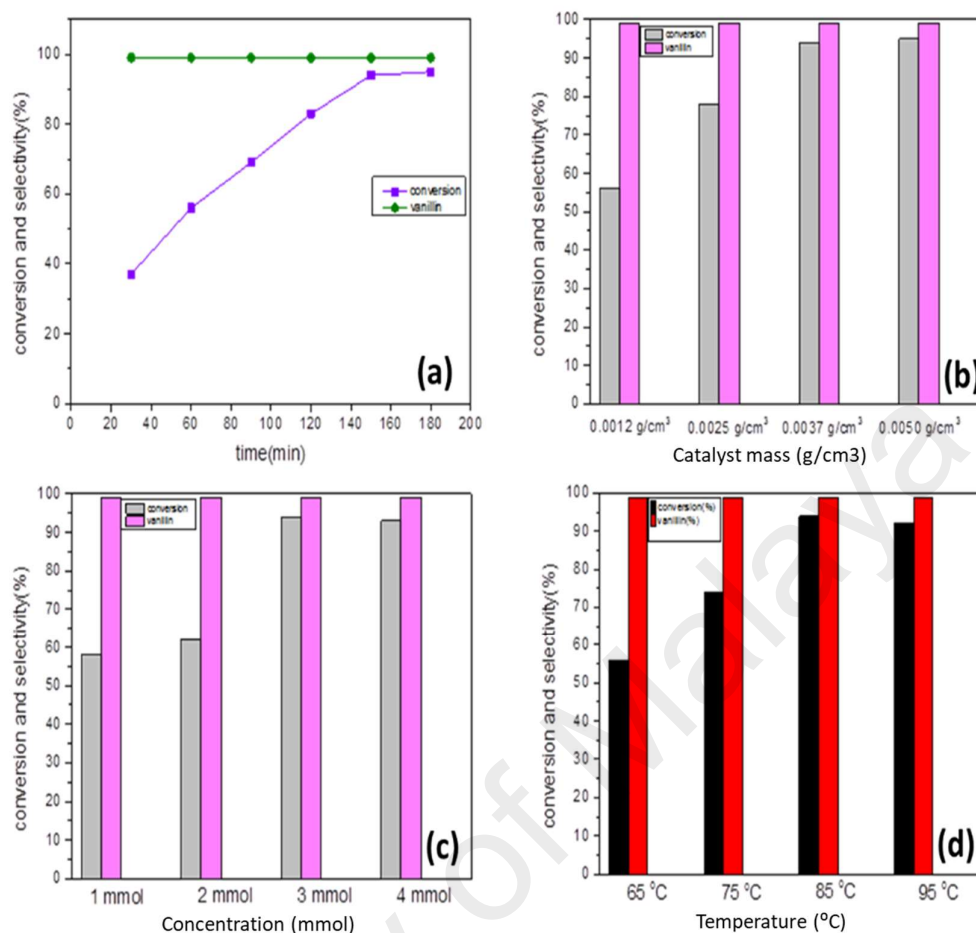


Figure 4.48: Effect of reaction parameters in oxidation of vanillyl alcohol by Cu-Mn (Cu: Mn) mixed oxide catalyst using H₂O₂ (a) progress of reaction; (b) catalyst mass; (c) concentration of H₂O₂; (d) temperature.

Two solvents acetic acid and isopropanol was considered to study the profound influence of nature of the solvent as NaOH is well soluble in both media (reaction condition: 1 mmol vanillyl alcohol, 1 mmol NaOH (0.15g), 3 mmol H₂O₂, 2h, 85 °C catalyst 0.0037 g/cm³) (Fig. 4.49). For isopropanol, the highest catalytic activity was obtained by 94 % conversion with 99 % selectivity to vanillin. In case of acetic acid, there was a marginal decrement in the catalytic conversion by 3 %. But, the selectivity was remarkably impacted to 61 %. This was probably due to the both polarity and pH of the reaction. At lower pH, formation of peracetic acid was expected which could further generate peroxy ([•]OOH) radicals (Fujita & Que, 2004). This resulted further oxidation of

vanillin to vanillic acid in acetic acid media. Therefore, isopropanol was the best solvent to obtain maximum conversion with excellent selectivity towards vanillin.

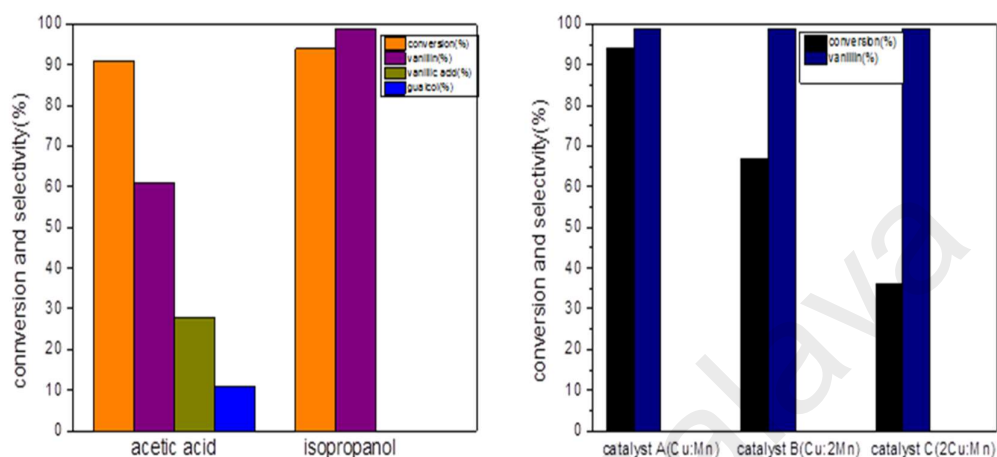


Figure 4.49: Influence of nature of solvents (left); and effect of catalyst compositions (right) in oxidation of vanillyl alcohol by Cu-Mn (Cu: Mn) mixed oxide catalyst.

The catalyst composition was also a vital parameter to survey the profound effect of the catalytic conversion (reaction condition: 1 mmol vanillyl alcohol, 1 mmol NaOH (0.15g), 3 mmol H₂O₂, 2h, 85 °C, 20 ml isopropanol, catalyst 0.0037 g/cm³) (Fig. 4.49). The catalyst contains equivalent loading of Cu and Mn was found to be most effective in oxidation of vanillyl alcohol using H₂O₂. Catalytic conversion by 94 % with 99 % selectivity in presence of base NaOH was obtained for catalyst (Cu:Mn) under optimized reaction conditions. Inferior catalytic conversion was noted for catalyst (Cu: 2Mn) and catalyst (2Cu: Mn) 67 % and 36% respectively. Notably, the selectivity was not affected by the ratio of the metals loaded. It suggested that the reaction pathways were similar in all catalysts as Cu_{1.5}Mn_{1.5}O₄ phase was formed in all catalysts. The above experimental data implies that the catalytic activity was well influenced by the chemical composition of the metal loading in the synthesis protocol. The metal loading in the bulk phase of the

catalyst could significantly assisted to alter the concentration of surface reactive oxygen species. Thus, it could be concluded that formation Cu-O-Mn linkage in catalyst (Cu:Mn) was higher as it was expected as the key active sites in the catalyst. Superiority of the catalyst (Cu:Mn) was further confirmed by the reducing properties of the catalyst in H₂-TPR profile. Hence, the control of the surface composition in Cu-Mn mixed oxide is vital to improved catalytic activity in oxidation of vanillyl alcohol. In addition, it is well recognized that the origin of excellent catalytic activity by Cu-Mn mixed oxide catalyst was attributed to presence of two Jahn Teller ions Cu²⁺ and Mn³⁺ and their solid state charge transfer redox cycle (Cocke & Vepřek, 1986; Puckhaber, Cheung, Cocke, & Clearfield, 1989).

4.2.3.2 Oxidation under air by Cu-Mn mixed oxide catalysts

The best catalyst (Cu: Mn) in terms of conversion was further considered for aerobic oxidation of vanillyl alcohol to avoid use of base NaOH. Acetonitrile was chosen as the solvent as it was the suitable solvent in case of other catalysts. Furthermore, reaction variables was optimized by using air. A blank reaction in absence of catalyst was performed in aerobic oxidation of vanillyl alcohol. No conversion was noticed. To inspect the progress of aerobic oxidation reaction in presence of catalyst was carried out (reaction condition: 3 mmol vanillyl alcohol, T= 120 °C, P= 21 bar air, 60 ml acetonitrile, 0.0025 g/cm³) (Fig. 4.50a). The substrate conversion was sharply enriched with the increase of reaction time. It reached the maxima at 97 % conversion with selectivity to vanillin in 2 h reaction time. After that, the reaction did not proceed with appreciable improvement in conversion. And also, the selectivity dropped owing to over oxidation of vanillin product to corresponding acids. Hence, 2 h of reaction time was the best reaction time to achieve optimum catalytic activity for liquid phase aerobic oxidation in base free condition.

Four different loadings such as 0.0006 g/cm^3 , 0.0012 g/cm^3 , 0.0025 g/cm^3 and 0.0037 g/cm^3 of catalyst was loaded to study the apparent effect in aerobic oxidation of vanillyl alcohol (reaction condition: 3 mmol vanillyl alcohol, $T = 120 \text{ }^\circ\text{C}$, $P = 21 \text{ bar}$ air, 60 ml acetonitrile) (Fig. 4.50b). The best catalytic activity was obtained for catalyst loading of 0.0025 g/cm^3 due to significant mass transfer attaining. The worst catalytic activity was for 0.0006 g/cm^3 by 48 %. In case of 0.0037 g/cm^3 there was no significant achievement in the conversion possibly owing to insignificant mass transfer (Klaewkla et al., 2011a). Worth mentioning, the selectivity was maintain constant for vary of catalyst loading.

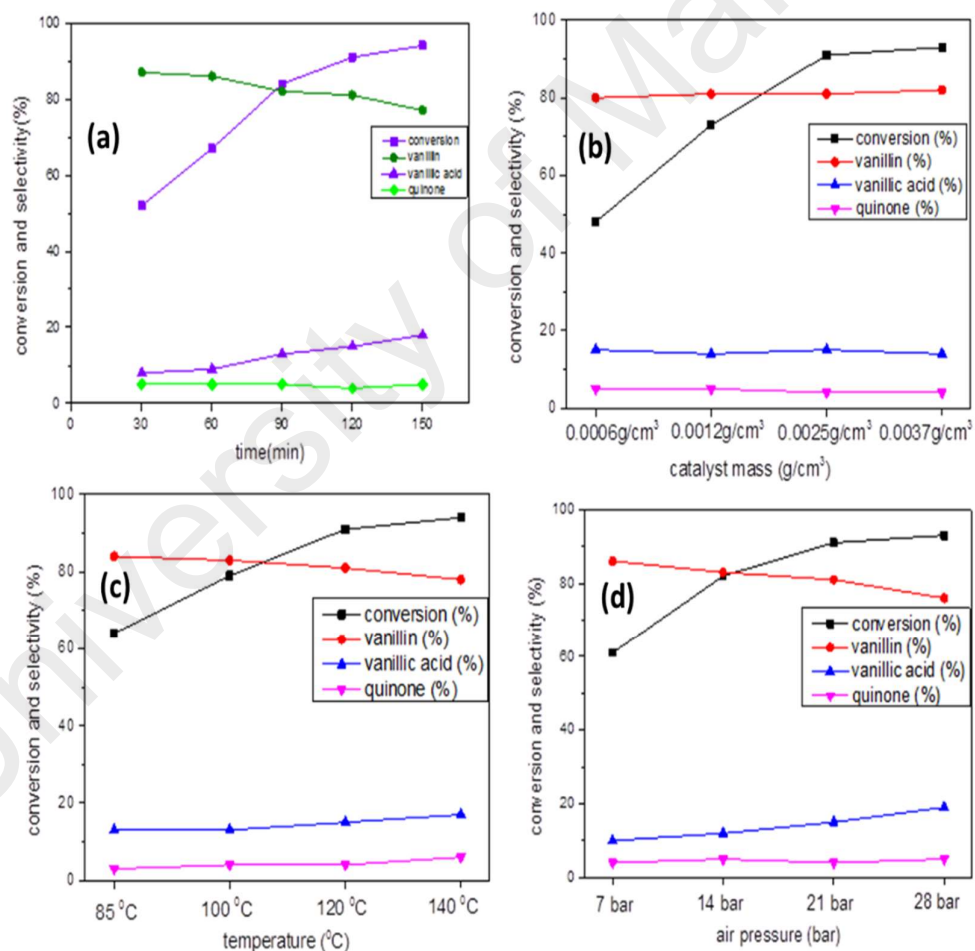


Figure 4.50: Effect of reaction parameters in oxidation of vanillyl alcohol by Cu-Mn (Cu: Mn) mixed oxide catalyst using air (a) progress of reaction; (b) catalyst mass; (c) temperature; (d) air pressure.

The temperature in range of 85 to 140 °C was found to have a vital role in the catalytic activity for liquid phase aerobic oxidation of vanillyl alcohol (reaction condition: 3 mmol vanillyl alcohol, P= 21 bar air, 60 ml acetonitrile, 0.0025 g/cm³) (Fig. 4.50c). At 85 °C the least catalytic activity was measured by 64% conversion. As temperature rose to 120 °C, excellent catalytic activity by 91 % conversion with 81 % selectivity to vanillin was obtained. Further rise in the temperature to 140 °C shown slight increment in the conversion but selectivity was reduced. It was possibly due to over oxidation of vanillin to vanillic acid at higher temperature. However, char formation was also observed at 140 °C. Thus, it was worth to note that 120 °C was the suitable temperature for liquid phase aerobic oxidation of vanillyl alcohol.

To investigate the perceptible influence of the air pressure, the reaction was carried out at four different pressures such as 7 bar, 14 bar, 21 bar and 28 bar (reaction condition: reaction condition: 3 mmol vanillyl alcohol, 120 °C, 60 ml acetonitrile, 0.0025 g/cm³) (Fig. 4.50d). The catalytic conversion was found in an ascending order with the increase of pressure in the order of 7 bar < 14 bar < 21 bar < 28 bar whereas the selectivity was in a descending order. The selectivity was reduced due to presence of more adsorbed oxygen in the reaction which caused over oxidation of the product vanillin. The optimum catalytic conversion by 91 % conversion with 81 % selectivity towards vanillin was attained for 21 bar air pressure while the worst conversion (61%) was measured at for 7 bar air pressure. Based on the observed results, one can conclude that 21 bar air pressure was the optimum condition for aerobic oxidation of vanillyl alcohol.

The catalyst was recovered after the reaction and washed thoroughly with the solvent to remove any desorbed products. Thereafter, it was dried for four hours at 60 °C. An oxidation reaction using spent catalyst was carried out in the optimized conditions as fresh catalyst (reaction conditions: 3 mmol vanillyl alcohol, T= 120 °C, P= 21 bar air, 60 ml

acetonitrile, 0.0025 g/cm³ catalyst mass, 2 h) (Fig. 4.51). Similarly, three cyclic reaction was performed and showed negligible change in the catalytic activity after the third run. The catalytic activity was slightly lower owing to the decrement in the roughness of the surface by some degree possibly. It was possibly due to metastability of the rough surface. Similar observation in reduction of roughness of the catalyst surface after catalytic reaction in vanillyl alcohol oxidation was made in previous report (Shilpy et al., 2015). And also, there was reasonable expectation of blockage on the few active sites by the residual un-desorbed products after washing. Noteworthy, the selectivity stood almost constant. It suggested that the reaction pathway was not changed as the catalyst phase remained unchanged after oxidation reaction.

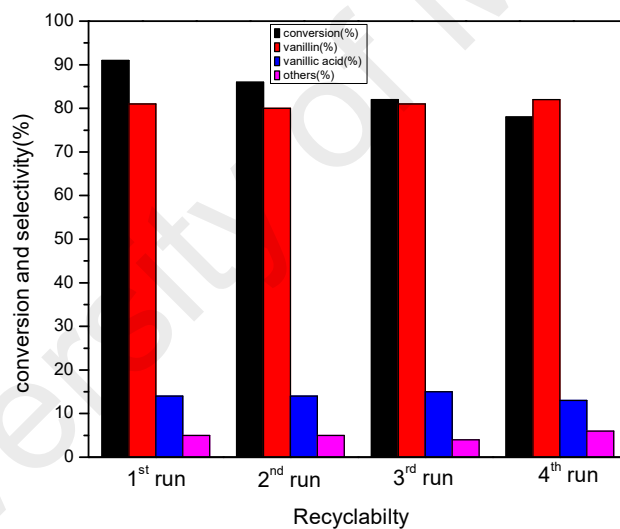


Figure 4.51: Recyclability study of Cu-Mn (Cu: Mn) mixed oxide catalyst in oxidation of vanillyl alcohol by using air as oxidant.

4.2.4 Catalytic performance of Ce-2Ti mixed oxide catalyst

4.2.4.1 Oxidation under H₂O₂ by Ce-2Ti mixed oxide catalyst

The above discussed properties of synthesized CeO₂-TiO₂ mixed oxide catalyst confirms that it possessed strong reducing ability and strong interaction between Ce and Ti. Moreover, presence of surface oxygen vacancies and grain boundaries as active sites

of the catalyst makes the catalyst stand out in liquid phase oxidation of vanillyl alcohol using different oxygen source of H_2O_2 and air. Surface oxygen vacant sites at the catalyst surface held weakly bonded various oxygen species. These weakly held oxygen species can contribute significantly to improve the catalytic performance in oxidation reaction as they partake in the reaction to oxidize at low temperature. Therefore, trifluoroacetic acid was involved in the synthesis technique to achieve great amount of surface oxygen vacancies as measured 42.24 % in O 1s XPS spectrum in the mixed oxide catalyst. And also, the reducing profile reveals that lattice oxygen was reduced at low temperature than isolated oxide phase by the effect of high interaction between metals (Ce and Ti). Therefore, the migration rate of lattice oxygen to the surface will be fast at low temperature resulting faster oxygen mobility towards better catalytic performance.

A blank reaction without the catalyst was carried out using both H_2O_2 and air. No significant change in the initial concentration of the substrate was observed indicating no conversion occurred. Hence, in order to investigate the progress of the oxidation reaction, reaction mixture was collected after every 30 mins reaction time interval and analyzed by HPLC as displayed in Fig. 4.52a (reaction conditions: 1 mmol vanillyl alcohol, 3 mmol H_2O_2 , 0.0037 g/cm³, 85 °C, 20 ml acetonitrile). The conversion was sharply improved to 64 % from initial 16 % with moderate selectivity (36%) to vanillin when the reaction time reached 3 h. Thereafter, no significant advancement in the amount of conversion was speculated. It is a well-established fact that H_2O_2 is a slow oxidant. Based on the experimental data, 3 h was selected as the optimum time to obtain maximum conversion in liquid phase oxidation of vanillyl alcohol using H_2O_2 . Worth noting that vanillic acid and guaiacol were also generated as the side products due to over-oxidation of vanillin.

The apparent effect of catalyst mass on conversion and selectivity in liquid phase oxidation of vanillyl alcohol was studied (reaction conditions: 1 mmol vanillyl alcohol, 3

mmol H₂O₂, 85 °C, 20 ml acetonitrile, 3 h). Four different catalyst mass 0.0012 g/ cm³, 0.0025 g/ cm³, 0.0037 g/ cm³ and 0.0050 g/ cm³ was loaded and reaction was carried out (Fig. 4.52b). The obtained results showed a progressive trend in case of conversion till 64 % for 0.0037g/cm³ while the catalyst amount was increased. There was no significant increment in conversion (66 %) for 0.0050 g/ cm³ due to insignificant mass transfer effect. Interestingly, the selectivity towards vanillin was maintained approximately at 36 %.

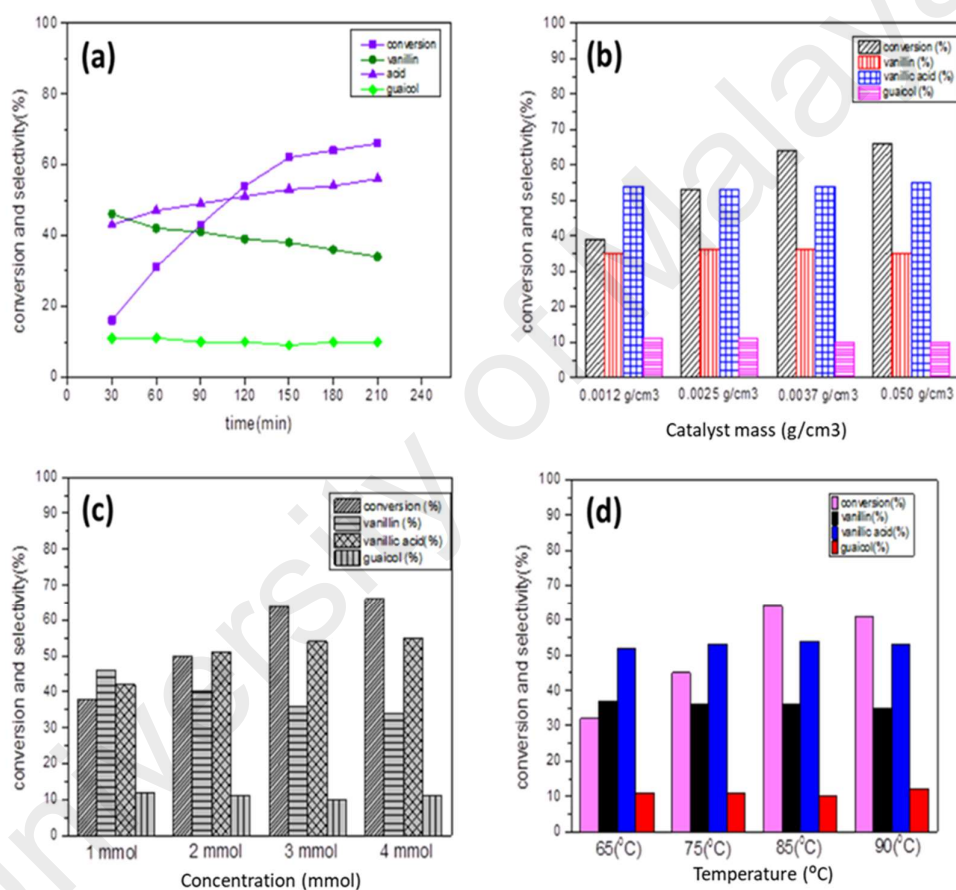


Figure 4.52: Effect of reaction parameters in oxidation of vanillyl alcohol by Ce-Ti mixed oxide catalyst using H₂O₂ (a) progress of reaction; (b) catalyst mass; (c) concentration of H₂O₂; (d) temperature.

Concentration of H₂O₂ was considered as one of the important reaction parameters to observe the impact on conversion and selectivity (reaction conditions: 1 mmol vanillyl alcohol, 0.0037 g/cm³, 85 °C, 20 ml acetonitrile, 3 h). The obtained results are displayed

in Fig. 4.52c for four different molar ratios of 1, 2 3 and 4 to the substrate. Under influence of high H_2O_2 concentration, it was inspected that the conversion was steeply enriched and reached it maxima at 66 % whereas the selectivity to vanillin was gradually dropped to 46 % from 34 %. High concentration of H_2O_2 provides sufficient active oxygen rich species to accelerate the rate of reaction and thus enriched the substrate transformation. Simultaneously, the aldehyde product formed initially was further oxidized to corresponding acid in presence of excess oxygen species and by-product water, thereby selectivity to vanillin was reduced. The observed reaction concluded that 3 mmol was the suitable concentration of H_2O_2 in terms of conversion (67 %) and selectivity (72 %) for liquid phase oxidation of vanillyl alcohol.

The oxidation reaction was performed at four different temperatures 65, 75, 85 and 90 °C respectively and results are showed in Fig. 4.52d (reaction conditions: 1 mmol vanillyl alcohol, 3 mmol H_2O_2 , 0.0037 g/cm³, 20 ml acetonitrile, 3h). The temperature was found to have a major impact on conversion but a slight improvement in selectivity. The conversion was found to improve with the rise of the temperature where conversion reached highest (64 %) at 85 °C. However, there was slight decrement in conversion (61 %) was noticed at 90 °C. This could be due to fast self-degradation of H_2O_2 in acetonitrile at high temperature and hence reducing the conversion in lies with previous report. Note that, the selectivity was slightly decreased owing to over-oxidation of formed products at high temperature.

Five solvents such as acetonitrile, isopropanol, dimethylformide, ethanol, Tetrahydrofuran of different polarity was investigated to monitor the apparent effect of solvent in conversion and selectivity (reaction conditions: 1 mmol vanillyl alcohol, 3 mmol H_2O_2 , 0.0037 g/cm³, 85 °C, 3 h) (Fig. 4.53). The conversion was affected in order of acetic acid (92 %) > acetonitrile (64 %) > isopropanol (37 %) > Dimethylformamide

(27 %) > Tetrahydrofuran (18 %). It was due to favorable polarity of the solvent to the substrate. The selectivity (77 %) was the best in case of isopropanol. In acetic acid, high catalytic conversion (92 %) with poor selectivity towards vanillin (32 %) was observed and could be explained by the low pH value of the reaction media. According to the Wu's report, Au supported on reduced graphene oxide catalyst showed high catalytic activity for veratryl alcohol oxidation using H₂O₂ at low pH reaction media which bolster the observed experimental data in present study.(Wu, Guo, & Zhang, 2015) Furthermore, peracetic acid formation by reaction between acetic acid and H₂O₂ could be one of the probable reason which can act as oxygen rich, strong oxidant. Considering both conversion and selectivity, acetonitrile was the suitable solvent for vanillyl alcohol conversion.

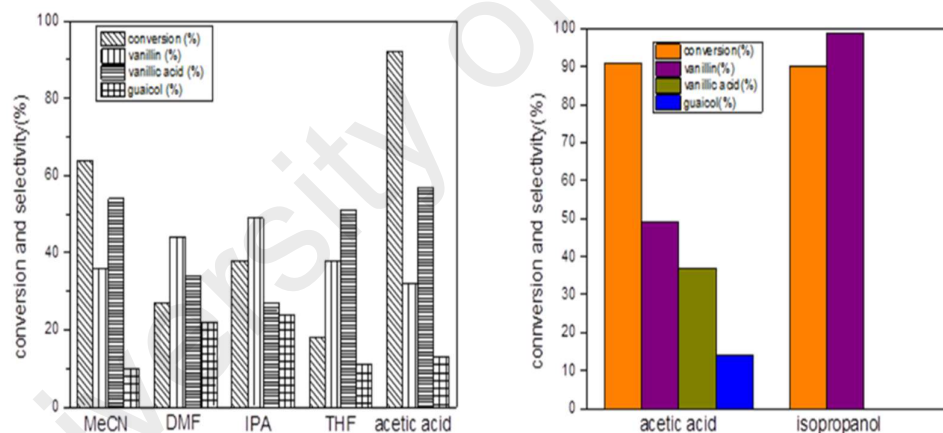


Figure 4.53: Influence of nature of solvents (left) and effect of base media (right) in oxidation of vanillyl alcohol by Ce-2Ti mixed oxide catalyst using H₂O₂.

Moreover, the reaction was carried out in the presence of base NaOH as shown in Fig. 4.53 (reaction conditions: 1 mmol vanillyl alcohol, 3 mmol H₂O₂, 1 mmol NaOH 0.0037 g/cm³, 85 °C, 3 h). Isopropanol and acetic acid were taken as solvents because of solubility of NaOH. For isopropanol, in base media with equimolar ratio of NaOH to the substrate, surprising catalytic activity was found by conversion (90 %) with 99 % selectivity towards vanillin. In case of acetic acid, the selectivity (49 %) was enriched to a certain extent with no noticeable impact on the conversion (91%).

4.2.4.2 Oxidation under air by Ce-2Ti mixed oxide catalyst

For aerobic oxidation of vanillyl alcohol, optimum reaction time was also investigated and displayed in Fig. 4.54a (reaction conditions: 3 mmol vanillyl alcohol, catalyst mass 0.0025 g/cm³, 120 °C, 21 bar air pressure, 60 ml acetonitrile). Reaction analysis was done periodically in every 30 mins interval. The reaction was continued with increment in the substrate conversion to 97 % with 71 % selectivity towards vanillin till reaction time reached 2 h. After 2.5 h reaction time, it was speculated that no more noticeable change in the substrate concentration (97 %). In fact, minor reaction pathways leading to formation of vanillic acid and quinone was also noticed. One could conclude that 2 h was the optimum time for maximum catalytic conversion.

The best catalyst mass was determined by changing the catalyst loading in aerobic oxidation of vanillyl alcohol (reaction conditions: 3 mmol vanillyl alcohol, 120 °C, 21 bar air pressure, 60 ml acetonitrile, 2 h). Fig. 4.54b shown that a steep rise in the amount of conversion was achieved while the catalyst mass was increased. The best catalytic performance was measure for catalyst loading of 0.0025 g/cm³. Further increment in the catalyst loading had no impact on the catalyst activity due to insignificant mass transfer effect. Worth mention, the selectivity stood almost constant with the change in the catalyst mass.

In order to study the obvious effect of temperature on catalyst reactivity a range of 85 °C to 140 °C (reaction conditions: 3 mmol vanillyl alcohol, catalyst mass 0.0025 g/cm³, 21 bar air pressure, 60 ml acetonitrile, 2 h). It was evident from the obtained experimental results displayed in Fig. 4.54c that the reaction was thermodynamically favored to promote the conversion with the rise in temperature. However, char formation was visible for temperature 140 °C with no obvious improvement in the conversion (98 %). Therefore, 120 °C was selected as the suitable reaction temperature in view of conversion (97 %), selectivity (71 %) as well.

The pressure of air was found to have a prominent effect in the catalytic reaction of liquid phase aerobic oxidation of vanillyl alcohol (reaction conditions: 3 mmol vanillyl alcohol, catalyst mass 0.0025 g/cm³, 120 °C, 60 ml acetonitrile, 2h). Four different air pressure such as 7 bar, 14 bar, 21 bar, 28 bar was considered to speculate the impact of it (Fig. 4.54d). An inclined trend for conversion whereas a declined trend was noticed for the increment of air pressure. The conversion was increased from 64 % to 97 % with selectivity drop from 79 % to 67 %. The reason for drop in the selectivity was over oxidation of initial products in excess desorbed oxygen in the solvent at high air pressure

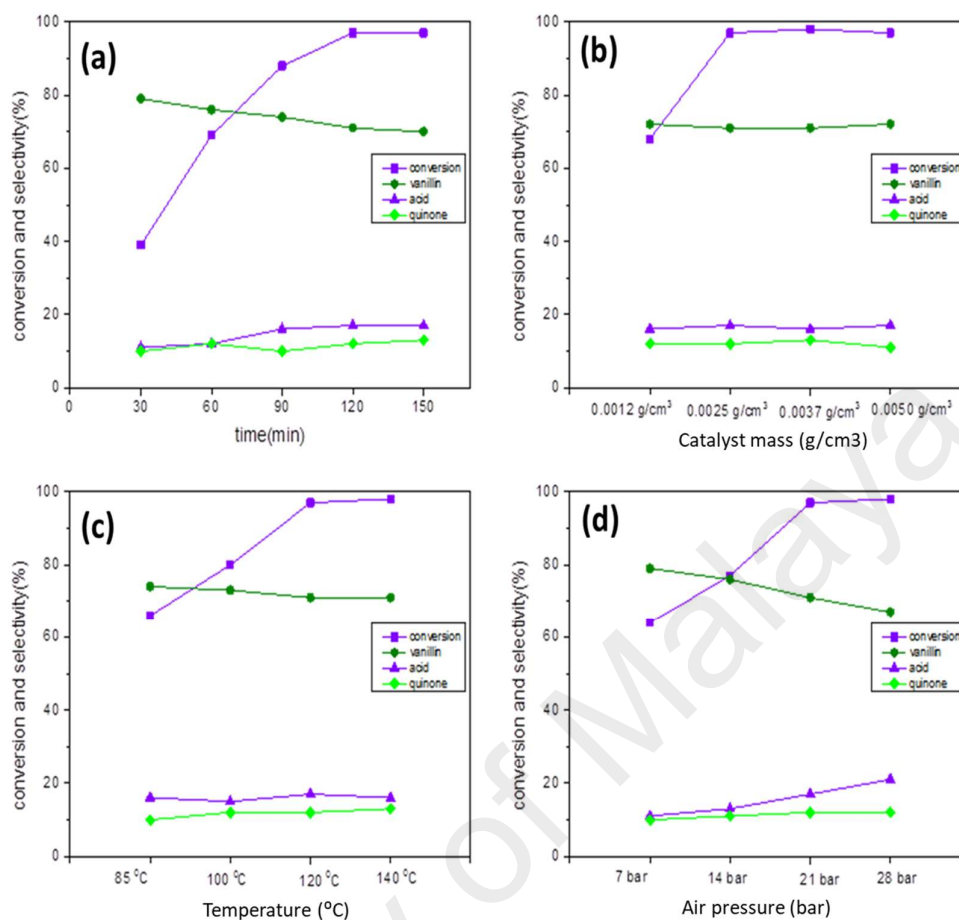


Figure 4.54: Effect of reaction parameters in oxidation of vanillyl alcohol by Ce-Ti mixed oxide catalyst using air (a) progress of reaction; (b) catalyst mass; (c) temperature; (d) air pressure.

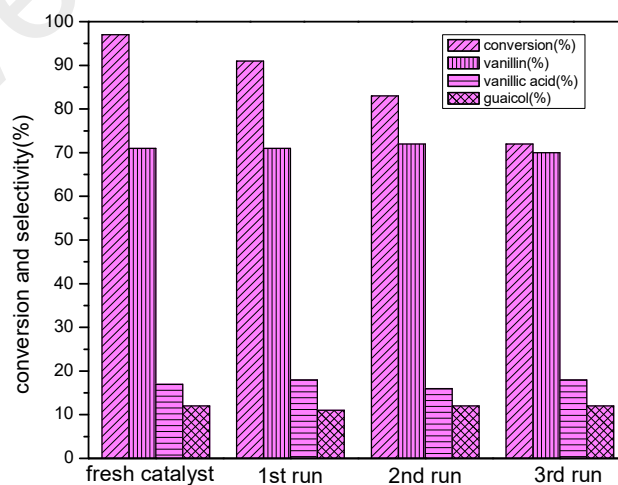


Figure 4.55: Stability study of Ce-2Ti mixed oxide catalysts in oxidation of vanillyl alcohol.

The stability of the catalyst was also examined for three subsequent reactions using the similar reaction parameters as fresh catalyst (reaction conditions: 3 mmol vanillyl alcohol, catalyst mass 0.0025 g/cm^3 , $120 \text{ }^\circ\text{C}$, 21 bar air pressure, 60 ml acetonitrile, 2 h) (Fig. 4.55). Prior to catalytic reaction, catalyst was filtrated off and washed thoroughly with acetonitrile. Hereafter, the catalyst was dried off for four hours at $80 \text{ }^\circ\text{C}$. The similar procedure was followed during all carried out reactions by spent catalyst. The catalyst shown promising stability by the indication of no significant loss of catalytic conversion (91 %) at second run. For the third run, the catalytic activity was measured at conversion (84 %). At the fourth reaction, a marginal decrement of catalytic conversion (71 %) was measured. It was postulated that the reduction of catalyst performance was associated with the roughness of the surface. As after catalytic reaction, the degree of metastable edges of catalyst surface would be minimized. In addition, another assumption could be made that the residual un-desorbed products after wash might cause blockage on the active sites and therefore drop at the conversion. And also, byproduct H_2O in alcohol oxidation lead to catalyst deactivation in some degree. However, almost constant selectivity (71 %) in all above cases suggest that the governing reaction pathway was not changed as similar catalyst phase was maintained in recycled catalyst as fresh catalyst.

4.2.5 Catalytic activity measurement of Fe-2Ti mixed oxide catalyst

4.2.5.1 Oxidation under H_2O_2 by Fe-2Ti mixed oxide catalyst

Catalytic activity of Fe-2Ti mixed oxide catalyst was done under influence of two oxidants H_2O_2 and air. Under mediation of H_2O_2 , five different reaction parameters such as time, catalyst mass, concentration of H_2O_2 , temperature, nature of solvent were investigated. Firstly, the reaction progress was analyzed by taking 0.5 cm^3 reaction mixture in every 30 mins interval of reaction time for oxidation by H_2O_2 (Reaction condition: 1 mmol vanillyl alcohol, 0.0025 g/cm^3 catalyst, $85 \text{ }^\circ\text{C}$, 20 ml acetonitrile, 3 mmol H_2O_2). The reaction progress was observed to have a steep increment in the amount

of conversion from 17 % to 58 % till 2 hours of reaction time (Fig. 4.56a). After that, there was no considerable improvement in the amount of conversion (59%). The selectivity slightly dropped at 62 % reaction time 2 hours from the initial amount (66 %). Hence, based on the experimental data, 2 hours was chosen as the optimum time to achieve maximum conversion (58 %) with good selectivity (62 %).

Catalyst mass from range of 0.0006 g/cm^3 to 0.0037 g/cm^3 were considered to investigate the apparent effect of catalyst mass on the catalytic activity (Reaction condition: 1 mmol vanillyl alcohol, $85 \text{ }^\circ\text{C}$, 20 ml acetonitrile, 3 mmol H_2O_2 , 2 h) (Fig. 4.56b). The catalytic conversion was enriched substantially from 33 % to 58 % while the catalyst amount was increased from 0.0006 g/cm^3 to 0.0025 g/m^3 . Further increment in the catalyst mass did not have affect in the catalytic conversion (60 %). It is worth noting that the selectivity (58 %) remained constant for every amount of catalyst mass.

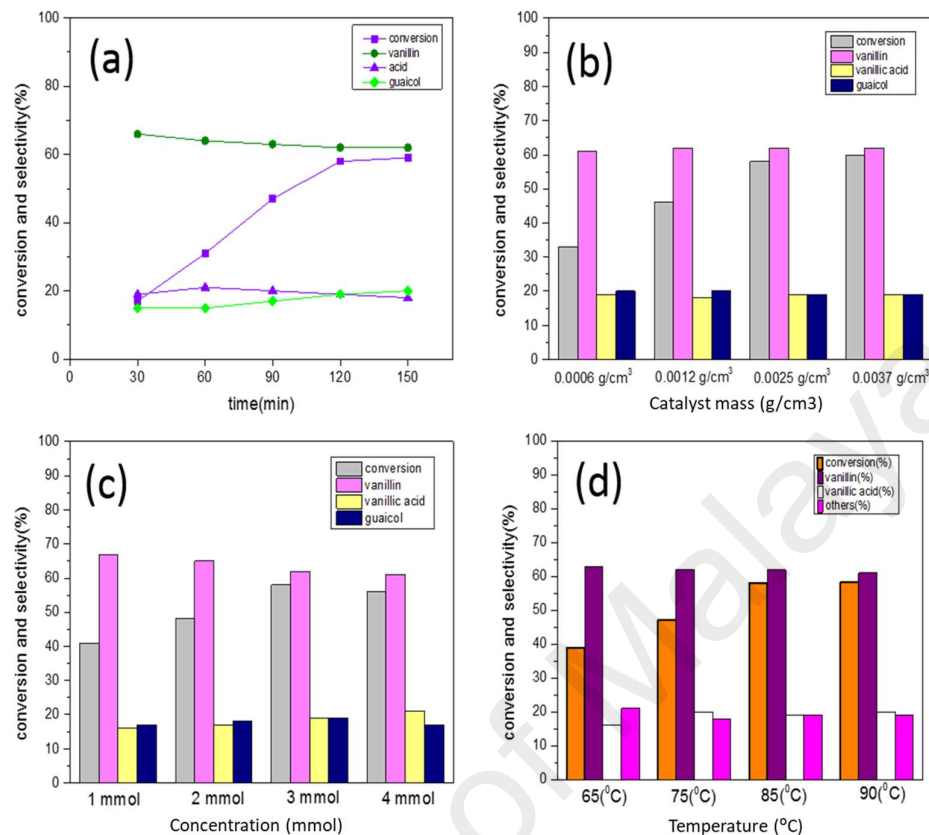


Figure 4.56: Effect of reaction parameters in oxidation of vanillyl alcohol by Fe-Ti mixed oxide catalyst using H₂O₂ (a) progress of reaction; (b) catalyst mass; (c) concentration of H₂O₂; (d) temperature.

Moreover, the effect of H₂O₂ concentration was investigated to find the optimum concentration (Reaction condition: 1 mmol vanillyl alcohol, 85 °C, 20 ml acetonitrile, 2 h) (Fig. 4.56c). Four different concentration from 1 mmol to 4 mmol of H₂O₂ was considered as concentration for oxidation of vanillyl alcohol. 3 mmol concentration of H₂O₂ shown the best catalytic activity whereas other concentrations shows gradual increase in the catalytic conversion from 1 mmol to 3 mmol. However, in case of selectivity to vanillin, the enrichment in the concentration shown negative trend which was possibly due to excess oxidation of vanillin to vanillic acid.

Temperature was found to have a prominent influence in the amount of catalytic conversion within 65 °C to 90 °C (Reaction condition: 1 mmol vanillyl alcohol, 0.0025

g/cm³ catalyst, 2 h, 20 ml acetonitrile, 3 mmol H₂O₂) (Fig. 4.56d). The conversion was increased sharply from 39 % to 58 % when the temperature was rose from 65 °C to 85 °C. However, at 90° C, there was a loss in the catalytic activity (56 %) due to fast decomposition of H₂O₂.

A wide range of solvents was considered in order to observe the obvious effect of nature of solvent in the catalytic activity by Fe-Ti mixed oxide catalyst under mediation of H₂O₂ (Reaction condition: 1 mmol vanillyl alcohol, 0.0025 g/cm³ catalyst , 2 h, 85 °C, 3 mmol H₂O₂) (Fig. 4.57). The catalytic activity was measured in the order of CH₃COOH> MeCN > Isopropanol > DMF > THF. Although, acetic acid shown promising catalytic conversion but it displayed poor selectivity (44 %) to vanillin. Hence, considering both the conversion and selectivity, acetonitrile shown the best catalytic activity (58 % conversion with 62 % selectivity) by Fe-Ti mixed oxide catalyst due to its favorable polarity.

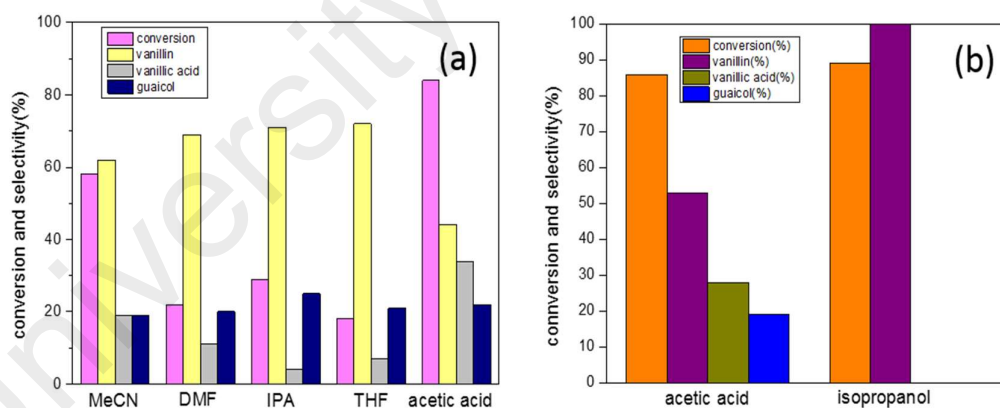


Figure 4.57: Liquid phase oxidation of vanillyl alcohol using H₂O₂ oxidant (a) effect of nature of solvent; (b) influence of base NaOH.

To examine the effect of base NaOH, two solvent acetic acid and isopropanol were considered as NaOH is only soluble in these two solvents (Reaction condition: 1 mmol vanillyl alcohol, 0.0025 g/cm³ catalyst , 85 °C, 20 ml acetonitrile, 3 mmol H₂O₂) (Fig.

4.57). In case of acetic acid, the catalytic conversion (86 %) was not changed appreciably but in isopropanol (88 % conversion). However, the selectivity was observed to be enriched substantially in both solvents. In acetic acid, the selectivity to vanillin was measured 52 % whereas surprising selectivity (99 %) was found in isopropanol.

4.2.5.2 Oxidation under air by Fe-2Ti mixed oxide catalyst

Aerobic oxidation of vanillyl alcohol was also performed by Fe-Ti mixed oxide catalyst in suitable solvent acetonitrile. Four various reaction parameters such as time, catalyst mass, air pressure and temperature were investigated in liquid phase aerobic oxidation of vanillyl alcohol by Fe-Ti mixed oxide catalysts. To determine the optimum time for aerobic oxidation of vanillyl alcohol, the reaction progress was speculated in every 30 mins time interval of reaction time. (Reaction condition: 3 mmol vanillyl alcohol, 0.0025 g/cm³ catalyst, 120 °C, 60 ml acetonitrile, 21 bar air pressure) (Fig. 4.58a). The catalytic conversion reached at its maxima (97 % conversion) in 2 hours reaction time. The conversion was not further increased if the reaction was continued till 2.5 hours. The selectivity was measured at 73 % to vanillin.

Four different catalyst mass was loaded in aerobic oxidation of vanillyl alcohol to examine the apparent effect on catalytic activity (Reaction condition: 3 mmol vanillyl alcohol, 120 °C, 60 ml acetonitrile, 21 bar air pressure, 2 h) (Fig. 4.58b). There was a sharp increment in the catalytic conversion from 56 % to 97 % while the loading of the catalyst was changed from 0.0006 g/cm³ to 0.0025 g/cm³. Further increment in the catalyst mass till 0.0037 g/cm³ in the reaction was not observed to have considerable effect in the conversion (98 %). Worth to mention, the selectivity (73 %) stood similar in all cases.

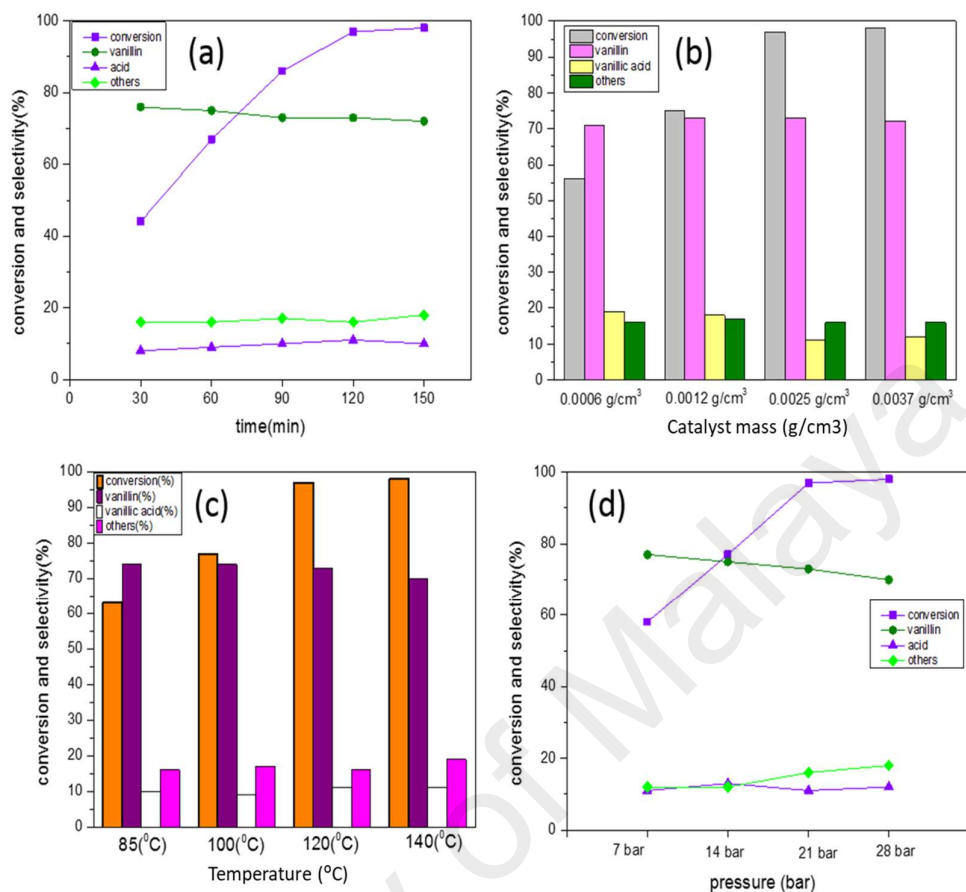


Figure 4.58: Effect of reaction parameters in oxidation of vanillyl alcohol by Fe-Ti mixed oxide catalyst using air (a) progress of reaction; (b) catalyst mass; (c) temperature; (d) air pressure.

Four aerobic oxidation reactions were performed in a temperature range of 85° C to 140 °C (Reaction condition: 3 mmol vanillyl alcohol, 0.0025 g/cm³ catalyst, 60 ml acetonitrile, 21 bar air pressure, 2 h) (Fig. 4.58c). It was observed that the catalytic performance was enhanced with the rise in the temperature. The catalytic conversion was increased sharply from 63 % to 97 % while the temperature of the reaction was rose from 85 °C to 120 °C. At the temperature of 140 °C, char formation was observed without further increment of the catalytic conversion. Hence, 120 °C was chosen as the optimum temperature in liquid phase aerobic oxidation of vanillyl alcohol. To note, the selectivity was slightly dropped from the initial amount with the rise of temperature.

Four different air pressure in range of 7 bar to 28 bar was examined in liquid phase aerobic oxidation of vanillyl alcohol (Reaction condition: 3 mmol vanillyl alcohol, 0.0025 g/cm³ catalyst, 120 °C, 60 ml acetonitrile, 2 h) (Fig. 4.58d). The air pressure was found to have a prominent effect on both conversion and selectivity. The conversion was sharply increased from 58 % to 98 % with the increment in air pressure till 28 bar whereas the selectivity decreased from 77 % to 71 %.

The reusability study of the synthesized Fe-2Ti mixed oxide catalyst was also examined under aerobic oxidation at the optimum conditions (Reaction condition: 3 mmol vanillyl alcohol, 0.0025 g/cm³ catalyst, 120 °C, 60 ml acetonitrile, 21 bar air pressure, 2 h) (Fig. 4.59). The spent catalyst was recovered from the reactor and washed thoroughly with acetonitrile and dried under vacuum at 80 °C for 6 hours. The spent catalyst was investigated for aerobic oxidation of vanillyl alcohol at the similar optimum conditions as fresh catalyst. The catalytic conversion was slightly reduced to 85 % in the fourth run. This is due to the possible blockage on the active sites by the undesorbed products and slight reduce of the surface roughness. However, the selectivity to vanillin was almost similar in all the run for spent catalyst which indicated that the reaction pathways governs by the Fe-2Ti mixed oxide catalyst was not changed for the spent catalyst.

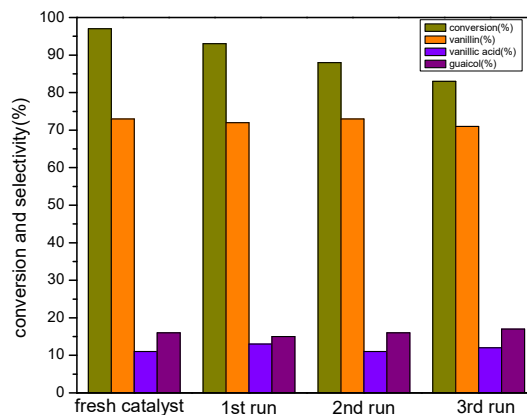


Figure 4.59: Reusability study of Fe-2Ti mixed oxide catalysts in aerobic oxidation of vanillyl alcohol.

4.3 Comparison of overall catalytic activity of synthesized mixed oxides catalysts

The comparison study of all synthesized catalyst with different cationic charge and radii revealed that Cu-2Ti mixed oxide catalyst shown the overall performance in both aerobic oxidation and treatment of H_2O_2 in liquid phase oxidation of vanillyl alcohol. The catalytic performance of different synthesized mixed oxides catalysts is displayed in Table 4.10. The results for two different oxidants (H_2O_2 and air) conclude that that the catalytic activity was strongly enriched under air condition with 1.5 magnitude increment for conversion. Though the catalytic activity of synthesized catalysts shown very promising performance under treatment of base NaOH with H_2O_2 , usage of base in such oxidation reaction caused unwanted environmentally waste, also separation process of the product is costly. As aerobic oxidation was experimented in absence of any base coupled with promoted catalytic activity, one can conclude that aerobic oxidation over synthesized catalysts is convincing in terms of economy, green and industrial scale. The comparison in the catalytic performance was probably affected with the physiochemical characteristics of the catalysts which was reflected on the various spectroscopic analysis.

Table 4.10: Overall comparison of performance by synthesized mixed oxide catalysts.

Catalyst	H ₂ O ₂	H ₂ O ₂ +NaOH	Air
Cu-2Ti	66% conversion	86% conversion	94% conversion
	71% selectivity	99 % selectivity	86 % selectivity
Cu-2Zr	62% conversion	89% conversion	91% conversion
	70% selectivity	99 selectivity	76 % selectivity
Cu-Mn	Not active	94% conversion	91% conversion
		99% selectivity	81% selectivity
Ce-2Ti	67% conversion	90% conversion	97% conversion
	72% selectivity	99% selectivity	71% selectivity
Fe-2Ti	58 % conversion	88 % conversion	97 % conversion
	62 % selectivity	99 % selectivity	73 % selectivity

*Selectivity towards vanillin

The reduction potential of the catalyst suggested that Cu-2Ti mixed oxide catalyst had the lowest reducing temperature, substantial amount of surface defects and better surface area which contributed to enrich the catalytic conversion in both H₂O₂ and aerobic oxidation. Though, Ce-2Ti, Cu-Mn and Fe-2Ti mixed oxide catalysts shown better catalytic conversion (97 %) than Cu-2Ti (91 %) in case of base free aerobic oxidation, Cu-2Ti mixed oxide catalyst shown the best yield to targeted vanillin product (86 %). Moreover, the selectivity can be possibly related with the presence of acid sites on the catalyst which was determined by NH₃-TPD. The NH₃-TPD profile of the catalysts indicated that Cu-2Ti and Cu-Mn mixed oxide catalysts had relatively high number of weak acid sites such as Lewis acid sites on the surface which probably enriched the selectivity of the catalysts (Fig. 4.60). In addition, both Cu-2Zr and Fe-2Ti mixed oxide catalysts had relatively lower number of weak acid sites reflected on the NH₃-TPD test and hence they show almost similar selectivity which is much lesser than Cu-2Ti mixed oxide catalysts in aerobic oxidation of vanillyl alcohol. Furthermore, the Ce-2Ti mixed oxide catalyst shown the lowest peak intensity in NH₃ –TPD test and therefore the catalyst shown the lowest selectivity among all the synthesized catalysts.

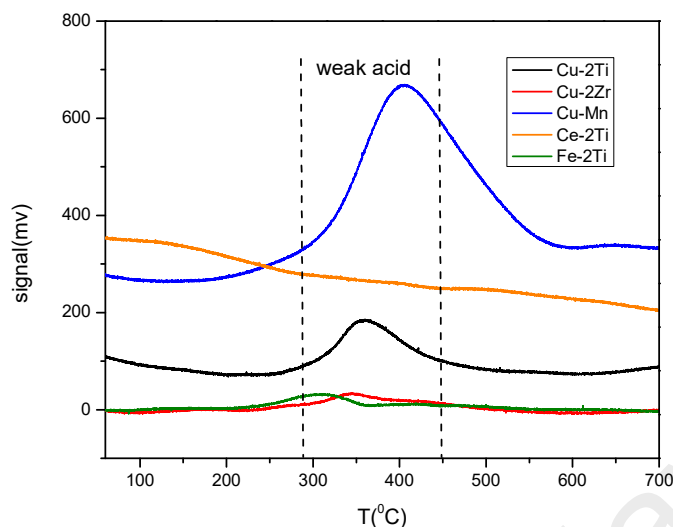


Figure 4.60: NH₃-TPD analysis of synthesized catalysts.

4.4 Reaction mechanism of vanillyl alcohol oxidation over synthesized mixed oxide catalysts

4.4.1 Possible reaction mechanism of vanillyl alcohol transformation under H₂O₂

The reaction pathway of liquid phase oxidation reaction of vanillyl alcohol is vital to understand the transformation of vanillyl alcohol to vanillin over mixed oxide catalysts. H₂O₂ is one of the potential oxidant for an oxidation reaction as water is the only by-product from H₂O₂ degradation. H₂O₂ degradation over transitional metal surface such as Ti, Zr, V, Mo etc. generally involves high valent peroxometal complexes. In the reaction mechanism, we discuss the transformation of vanillyl alcohol to vanillin by H₂O₂ over Cu-Ti mixed oxide catalyst as an example. In this experiment, the initial step governs by the dissociative adsorption of H₂O₂ on the Cu-Ti/Zr surface. It has been reported previously TiO₂/ZrO₂ itself is not active for H₂O₂ decomposition (Salem, Elhag, & Khalil, 2000). However, if transitional metal is incorporated in the matrix of TiO₂/ZrO₂, it successfully cleave the H₂O₂ to form per-oxo intermediate. Furthermore, the per-oxo intermediate will propagate into ·OH₂ radicals via one step electron oxidation and followed by formation of OH⁻ ions (Fig. 4.61) (Okamoto, Ohto, & Imanaka, 1993;

Uehara, Urade, Ueda, Sakagami, & Abe, 1998). In the postulated reaction mechanism (Fig. 4.62), Vanillyl alcohol will be adsorbed on Ti metal site of Ti per-oxo intermediate (I) (Fig. 4.62) via hydrogen linkage to produce vanilloxy intermediate state (I) (Fig. 4.62). The process followed by one benzylic hydrogen attracted towards the electron rich nucleophile OH⁻ and removed as water molecule. Simultaneously, the hydrogen of the alcoholic group will be donated on the catalyst Cu-Ti surface to produce selective product benzaldehyde. Moreover, the product benzaldehyde could be oxidized further in presence of excess OH⁻ to form corresponding acid

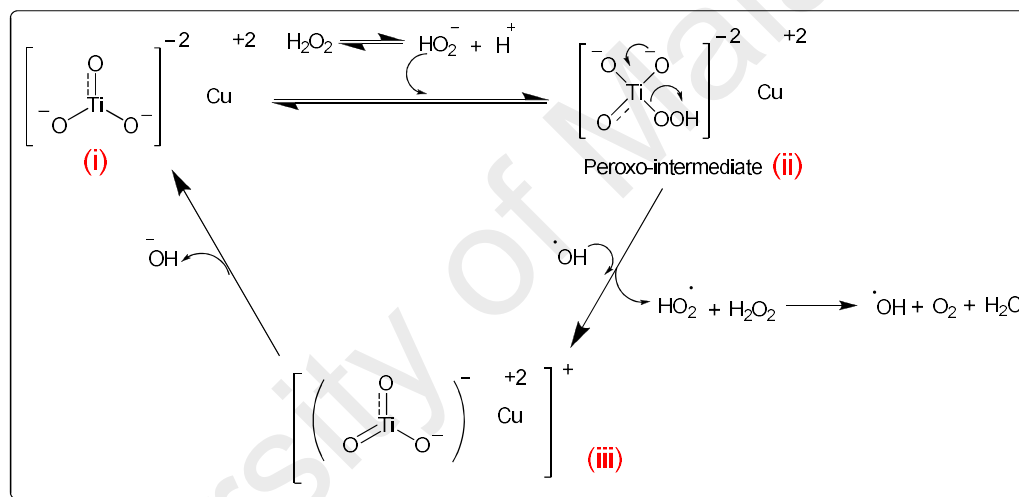


Figure 4.61: Production of peroxo intermediates by Cu-2M (M=Ti & Zr) mixed oxide catalyst with H₂O₂.

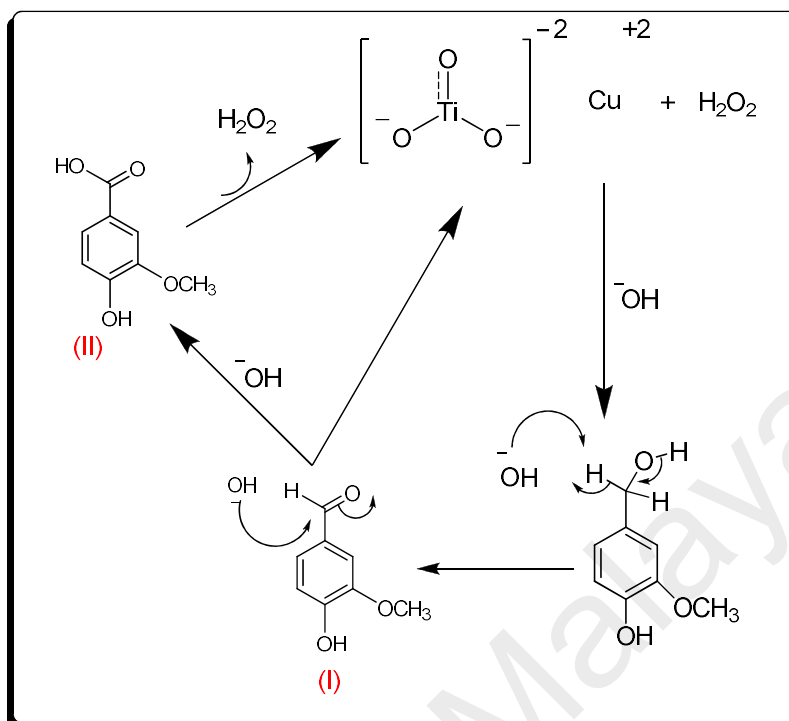


Figure 4.62: Catalytic transformation of vanillyl alcohol to vanillin over synthesized Cu/Ti mixed oxide catalysts.

4.4.2 Postulated reaction mechanism of vanillyl alcohol conversion using air as oxidant

The reaction pathways of liquid phase aerobic oxidation was also investigated in this study for catalytic transformation of vanillyl alcohol by using catalyst Cu-2Ti mixed oxide catalyst as the example of mixed oxide catalysts (Fig. 4.63). The oxidant O_2 molecule contains two unpaired electrons with parallel spins in the ground state. Therefore, the direct reaction of single organic molecules with the triplet state of oxygen molecule is a spin forbidden process with slow reaction rate. Catalysis by a paramagnetic transitional metal can overcome this and accelerate the rate of reaction (Sheldon & Van Santen, 1995). As Ti is a paramagnetic substance and Cu is a diamagnetic materials because of the Jahn Teller effect (Manna, Basu, Mitra, Mukherjee, & Das, 2009) Ti has the strong tendency to react with O_2 and form metal superoxo complex. The metal

superoxo complex further turns into metal peroxo complex which readily transforms into metal hydroperoxo complex by accepting one electron from vanillyl alcohol. Thus, the role of Ti is to activate oxygen molecules without presence of base NaOH. The reaction intermediate phenolate ions can react with $\text{Cu}^{2+}/\text{Fe}^{3+}/\text{Ce}^{4+}$ ions in the reaction media in the respective catalytic system to generate phenoxy ions (Barton, Logie, Schoonees, & Zeelie, 2005). The phenoxy intermediate further forms quinomethide by means of readily reactions which reacts with Cu superoxo species to form Cu peroxy complex. After that, the Cu peroxy complex decompose into corresponding aldehyde by abstracting proton from the reaction medium and Cu hydroxyl complex.

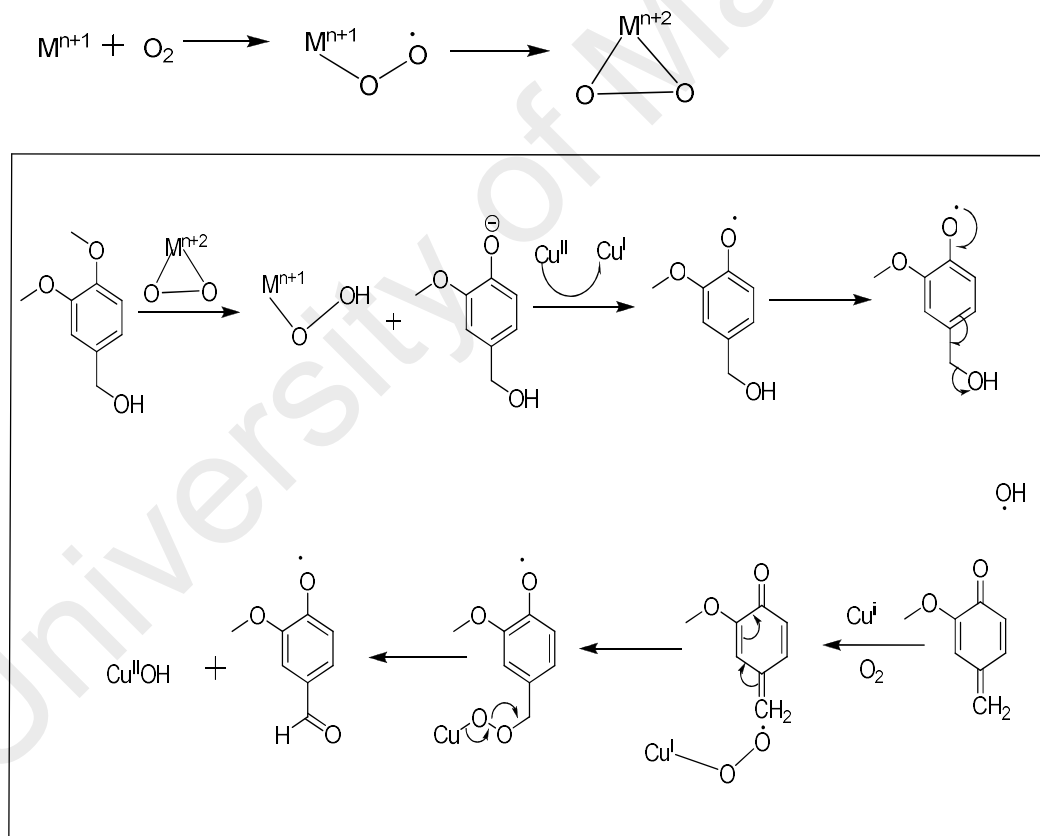


Figure 4.63: Possible reaction mechanism of aerobic oxidation of vanillyl alcohol over Cu-M (where M= Ti, Zr and Mn) mixed oxide catalyst.

CHAPTER 5: CONCLUSION AND RECOMMENDATION

5.1 Conclusion

The solvent evaporation method was highly effective to synthesize mixed oxide catalysts with high crystallinity, stable, and mesoporous materials (Cu-Ti, Cu-Zr, Cu-Mn, Ce-2Ti and Fe-2Ti) successfully supported by various spectroscopic analytical tools such as XRD, H₂-TPR, O₂-TPD, XRD, Raman, BET and XPS etc. The physico chemical and structural properties evidently revealed that the synthesized mixed oxide catalysts shown excellent catalytic activity in liquid phase oxidation of vanillyl alcohol due to strong reducing ability and presence of surface oxygen vacancies to a great extent. In addition, alteration of electronic arrangements to favor the redox cycle was caused owing to high degree of homogeneity of the metals evidenced in chemical mapping . This study revealed that effect of different cations and their charges to significantly modify the chemical properties of the catalysts which is further supported by the catalytic activity. The synthesized mixed oxide catalysts could be sequenced as followed Ce: 2Ti (66 %) > Cu-2Ti (67 %) > Cu: 2Zr (62 %) > Fe-Ti (58 %) > Cu: Mn (inactive) in view of catalytic conversion using H₂O₂ oxidant in base free condition at suitable reaction variables: 1 mmol Vanillyl alcohol, 3 mmol H₂O₂, 0.0025 g/cm³ catalysts mass, 20 ml acetonitrile. The measured catalytic performance in case of liquid phase aerobic oxidation revealed the superiority as followed in terms of catalytic conversion Ce-2Ti (97 %) = Fe-2Ti (97 %) > Cu-2Ti (94 %) > Cu-Zr (91 %) at optimized reaction conditions: 3 mmol vanillyl alcohol, 21 bar air pressure, 120 °C). In addition, the metals loading in synthesized materials was evidently found to impact the catalytic conversion significantly but not the reaction pathway supported by observed similar amount of selectivity. Increase of parameters concentration such as time, temperature, catalysts mass enriched the catalytic conversion till the optimum point in case of all the synthesized catalysts. Furthermore, all the mixed oxide catalysts shown significant enrichment of both conversion and selectivity

when air was used as the oxidant which suggested of green process with effective catalytic performance. The surprising catalytic activity was measured using H₂O₂ coupled with base NaOH which led to almost 99 % selectivity to vanillin along with substantial enrichment in the amount of conversion. Besides, the mixed oxide catalysts were observed to be stable at subsequent four oxidation reactions with minimum loss of catalytic activity. And also, unchanged amount of selectivity to vanillin during the stability test evidently suggested of well preservation of the catalysts phase in the oxidation reactions.

In summary, the work concluded that among synthesized mixed oxide catalyst via solvent evaporation method, Cu-2Ti was the best performed catalysts in terms of both catalytic conversion and selectivity under investigated different reaction variables (66 % conversion with 71 % selectivity to vanillin under H₂O₂ and 94 % conversion with 86 % selectivity to vanillin under air) in liquid phase oxidation of vanillyl alcohol. These mixed oxide catalyst prepared via solvent evaporation technique are potential candidate as a catalyst to be used for lignin valorization. These mixed oxide catalysts open up a new possibility of lignin valorization in industrial scale to reduce dependency on fossil fuels.

5.2 Recommendations

A further investigation can be further studied in the catalyst synthesis protocol considering various parameters such as temperature, pressure, techniques of solvent evaporation and nature of solvents. The effect of such parameters for catalyst synthesis protocol will possibly contribute to control the structural and surface properties of the catalysts which will eventually promote the catalytic performance. Besides, different non-ionic surfactants as structure directing or crystal size control agents also can be examined to resist the agglomeration of the particles during the thermal treatment in order to obtain fine nanoparticles of expected shape along with better catalytic performance and stability.

As solvent evaporation techniques was effective and successful to synthesize mixed oxide catalysts with homogeneous metal distribution, other mixed oxide catalysts with different metals except above mentioned metals could be prepared for various application purpose. Such catalysts also can be further studies for various oxidation reaction of different substrate including raw lignin. A tuned synthesis protocol via solvent evaporation for mixed oxide catalysts can be a potential replacement of other homogeneous catalysts such as chromium salts or manganese salts used in oxidation reactions generally in industrial scale to minimize the cost and environmentally friendly process.

University of Malaya

REFERENCES

- Abad, A., Corma, A., & García, H. (2008). Catalyst parameters determining activity and selectivity of supported gold nanoparticles for the aerobic oxidation of alcohols: The molecular reaction mechanism. *Chemistry-A European Journal*, 14(1), 212-222.
- Acharya, B., Sule, I., & Dutta, A. (2012). A review on advances of torrefaction technologies for biomass processing. *Biomass Conversion and Biorefinery*, 2(4), 349-369.
- Adschiri, T., Hakuta, Y., & Arai, K. (2000). Hydrothermal synthesis of metal oxide fine particles at supercritical conditions. *Industrial & Engineering Chemistry Research*, 39(12), 4901-4907.
- Aguilera, D. A., Perez, A., Molina, R., & Moreno, S. (2011). Cu-Mn and Co-Mn catalysts synthesized from hydrotalcites and their use in the oxidation of VOCs. *Applied Catalysis B: Environmental*, 104(1), 144-150.
- Alifanti, M., Baps, B., Blangenois, N., Naud, J., Grange, P., & Delmon, B. (2003). Characterization of CeO₂-ZrO₂ mixed oxides. Comparison of the citrate and sol-gel preparation methods. *Chemistry of materials*, 15(2), 395-403.
- Andas, J., Adam, F., Rahman, I. A., & Taufiq-Yap, Y. H. (2014). Optimization and mechanistic study of the liquid-phase oxidation of naphthalene over biomass-derived iron catalyst. *Chemical Engineering Journal*, 252, 382-392.
- Andrade, Z., Carlos, K., & Alves, L. M. (2005). Environmentally benign solvents in organic synthesis: Current topics. *Current Organic Chemistry*, 9(2), 195-218.

Angelov, S., Zhecheva, E., Petrov, K., & Menandjiev, D. (1982). The properties of a spinel copper cobaltite prepared at low temperatures and normal pressure. *Materials Research Bulletin*, 17(2), 235-240.

Aresta, M., Dibenedetto, A., & Dumeignil, F. (2012). *Biorefinery: from biomass to chemicals and fuels*: Walter de Gruyter.

Argyropoulos, D. S. (2001). *Oxidative delignification chemistry*: American Chemical Society.

Argyropoulos, D. S., Jurasek, L., Křištofová, L., Xia, Z., Sun, Y., & Paluš, E. (2002). Abundance and reactivity of dibenzodioxocins in softwood lignin. *Journal of agricultural and food chemistry*, 50(4), 658-666.

Armor, J. N. (2011). A history of industrial catalysis. *Catalysis Today*, 163(1), 3-9.

Ayres, D. C., & Loike, J. D. (1990). *Lignans: chemical, biological and clinical properties*: Cambridge university press.

Badamali, S. K., Luque, R., Clark, J. H., & Breeden, S. W. (2009). Microwave assisted oxidation of a lignin model phenolic monomer using Co (salen)/SBA-15. *Catalysis Communications*, 10(6), 1010-1013.

Barton, B., Logie, C. G., Schoonees, B. M., & Zeelie, B. (2005). Practical process for the air oxidation of cresols: Part A. Mechanistic investigations. *Organic process research & development*, 9(1), 62-69.

Beeman, L. A. (1953). *The bleaching of pulp*: Technical Association of the Pulp and Paper Industry.

Beeman, L. A., & Reichert, J. S. (1951). *Peroxides in pulp bleaching processes*: EI du Pont de Nemours & Company.

Behling, R., Valange, S., & Chatel, G. (2016). Heterogeneous catalytic oxidation for lignin valorization into valuable chemicals: what results? What limitations? What trends? *Green Chemistry*, 18(7), 1839-1854.

Berzelius, J. J., & Wöhler, F. (1936). *Einige Ideen über eine bei der Bildung organischer Verbindungen in der lebenden Natur wirksame aber bisher noch nicht bemerkte Kraft*.

Bessone, F., Colombato, L., Passamonti, M., Ferrer, J., Godoy, A., Bagnulo, H., . . . Guma, C. (2001). Nimesulide: clinical and histological evidences of severe hepatotoxicity. *Journal of Hepatology*, 34, 46.

Bouxin, F. P., McVeigh, A., Tran, F., Westwood, N. J., Jarvis, M. C., & Jackson, S. D. (2015). Catalytic depolymerisation of isolated lignins to fine chemicals using a Pt/alumina catalyst: part 1—impact of the lignin structure. *Green Chemistry*, 17(2), 1235-1242.

Bozell, J. J., Hames, B. R., & Dimmel, D. R. (1995). Cobalt-Schiff base complex catalyzed oxidation of para-substituted phenolics. Preparation of benzoquinones. *The Journal of Organic Chemistry*, 60(8), 2398-2404.

Bozell, J. J., Hoberg, J. O., & Dimmel, D. R. (1998). Catalytic oxidation of para-substituted phenols with nitrogen dioxide and oxygen. *Tetrahedron letters*, 39(16), 2261-2264.

- Bozell, J. J., Hoberg, J. O., & Dimmel, D. R. (2000). Heteropolyacid catalyzed oxidation of lignin and lignin models to benzoquinones. *Journal of wood chemistry and technology*, 20(1), 19-41.
- Braun, J., Holtman, K., & Kadla, J. (2005). Lignin-based carbon fibers: Oxidative thermostabilization of kraft lignin. *Carbon*, 43(2), 385-394.
- Brebu, M., & Vasile, C. (2010). Thermal degradation of lignin—a review. *Cellulose Chemistry & Technology*, 44(9), 353.
- Brogdon, B. N., Mancosky, D. G., & Lucia, L. A. (2005). New insights into lignin modification during chlorine dioxide bleaching sequences (I): Chlorine dioxide delignification. *Journal of wood chemistry and technology*, 24(3), 201-219.
- Brown, D., & Abbot, J. (1995). Effects of metal ions and stabilisers on peroxide decomposition during bleaching. *Journal of wood chemistry and technology*, 15(1), 85-111.
- Burrington, J., Kartisek, C., & Grasselli, R. (1984). Surface intermediates in selective propylene oxidation and ammoxidation over heterogeneous molybdate and antimonate catalysts. *Journal of Catalysis*, 87(2), 363-380.
- Canevali, C., Orlandi, M., Pardi, L., Rindone, B., Scotti, R., Sipila, J., & Morazzoni, F. (2002). Oxidative degradation of monomeric and dimeric phenylpropanoids: reactivity and mechanistic investigation. *Journal of the Chemical Society, Dalton Transactions*(15), 3007-3014.
- Carlucci, C., Scremin, B. F., Sibillano, T., Giannini, C., Filippo, E., Perulli, P., . . . Ciccarella, G. (2014). Microwave-assisted synthesis of boron-modified TiO₂ nanocrystals. *Inorganics*, 2(2), 264-277.

- Carnö, J., Ferrandon, M., Björnbom, E., & Järås, S. (1997). Mixed manganese oxide/platinum catalysts for total oxidation of model gas from wood boilers. *Applied Catalysis A: General*, 155(2), 265-281.
- Centi, G., & Perathoner, S. (2003). Catalysis and sustainable (green) chemistry. *Catalysis Today*, 77(4), 287-297.
- Cetin, N. S., & Özmen, N. (2002). Use of organosolv lignin in phenol-formaldehyde resins for particleboard production: II. Particleboard production and properties. *International Journal of Adhesion and Adhesives*, 22(6), 481-486.
- Chatel, G., & Rogers, R. D. (2013). Review: Oxidation of lignin using ionic liquids · An innovative strategy to produce renewable chemicals. *ACS Sustainable Chemistry & Engineering*, 2(3), 322-339.
- Chen, D., Chen, C., Baiyee, Z. M., Shao, Z., & Ciucci, F. (2015). Nonstoichiometric oxides as low-cost and highly-efficient oxygen reduction/evolution catalysts for low-temperature electrochemical devices. *Chemical Reviews*, 115(18), 9869-9921.
- Chen, L.-F., Guo, P.-J., Qiao, M.-H., Yan, S.-R., Li, H.-X., Shen, W., . . . Fan, K.-N. (2008). Cu/SiO₂ catalysts prepared by the ammonia-evaporation method: texture, structure, and catalytic performance in hydrogenation of dimethyl oxalate to ethylene glycol. *Journal of Catalysis*, 257(1), 172-180.
- Cherubini, F., & Strømman, A. H. (2011). Chemicals from lignocellulosic biomass: opportunities, perspectives, and potential of biorefinery systems. *Biofuels, Bioproducts and Biorefining*, 5(5), 548-561.

- Choi, J.-G., Brenner, J. R., Colling, C. W., Demczyk, B. G., Dunning, J. L., & Thompson, L. T. (1992). Synthesis and characterization of molybdenum nitride hydrodenitrogenation catalysts. *Catalysis Today*, 15(2), 201-222.
- Choo, W., & Lee, J. Y. (1982). Thermal analysis of trapped hydrogen in pure iron. *Metallurgical Transactions A*, 13(1), 135-140.
- Christiansen, S. H. (1986). Stabilization of peroxide systems in the presence of alkaline earth metal ions: Google Patents.
- Chu, D., Younis, A., & Li, S. (2012). Direct growth of TiO₂ nanotubes on transparent substrates and their resistive switching characteristics. *Journal of Physics D: Applied Physics*, 45(35), 355306.
- Clerici, M. G., & Kholdeeva, O. A. (2013). *Liquid phase oxidation via heterogeneous catalysis: organic synthesis and industrial applications*: John Wiley & Sons.
- Cocke, D., & Vepřek, S. (1986). First direct evidence of a solid state charge transfer redox system $\text{Cu}^{+2} + \text{Mn}^{3+} \rightleftharpoons \text{Cu}^{1+} + \text{Mn}^{4+}$ in copper manganese oxide. *Solid state communications*, 57(9), 745-748.
- Collinson, S., & Thielemans, W. (2010). The catalytic oxidation of biomass to new materials focusing on starch, cellulose and lignin. *Coordination chemistry reviews*, 254(15), 1854-1870.
- Crestini, C., Caponi, M. C., Argyropoulos, D. S., & Saladino, R. (2006). Immobilized methyltrioxo rhenium (MTO)/H₂O₂ systems for the oxidation of lignin and lignin model compounds. *Bioorganic & medicinal chemistry*, 14(15), 5292-5302.

Crestini, C., Crucianelli, M., Orlandi, M., & Saladino, R. (2010). Oxidative strategies in lignin chemistry: A new environmental friendly approach for the functionalisation of lignin and lignocellulosic fibers. *Catalysis Today*, 156(1), 8-22.

Crestini, C., Pro, P., Neri, V., & Saladino, R. (2005). Methyltrioxorhenium: a new catalyst for the activation of hydrogen peroxide to the oxidation of lignin and lignin model compounds. *Bioorganic & medicinal chemistry*, 13(7), 2569-2578.

Crocker, M. (2010). *Thermochemical conversion of biomass to liquid fuels and chemicals*: Royal Society of Chemistry.

Cui, F., & Dolphin, D. (1995). Metallophthalocyanines as possible lignin peroxidase models. *Bioorganic & medicinal chemistry*, 3(5), 471-477.

Dalla Betta, R. A. (1997). Catalytic combustion gas turbine systems: the preferred technology for low emissions electric power production and co-generation. *Catalysis Today*, 35(1-2), 129-135.

Dauscher, A., Hilaire, L., Le Normand, F., Müller, W., Maire, G., & Vasquez, A. (1990). Characterization by XPS and XAS of supported Pt/TiO₂ □ CeO₂ catalysts. *Surface and Interface Analysis*, 16(1 - 12), 341-346.

Dawange, M., Galkin, M. V., & Samec, J. S. (2015). Selective Aerobic Benzylic Alcohol Oxidation of Lignin Model Compounds: Route to Aryl Ketones. *ChemCatChem*, 7(3), 401-404.

De Faria, D., Venâncio Silva, S., & De Oliveira, M. (1997). Raman microspectroscopy of some iron oxides and oxyhydroxides. *Journal of Raman spectroscopy*, 28(11), 873-878.

- De, K. A., Chaudhuri, B., & Bhattacharjee, S. (1999). A kinetic study of the oxidation of phenol, o - chlorophenol and catechol by hydrogen peroxide between 298 K and 333 K: the effect of pH, temperature and ratio of oxidant to substrate. *Journal of Chemical Technology and Biotechnology*, 74(2), 162-168.
- De Menezes, A. J., Pasquini, D., Curvelo, A., & Gandini, A. (2007). Novel thermoplastic materials based on the outer-shell oxypropylation of corn starch granules. *Biomacromolecules*, 8(7), 2047-2050.
- Dence, C. (1996). Chemistry of chemical pulp bleaching. *Pulp Bleaching—Principles and Practice*, 125-160.
- Dence, C., & Reeve, D. (1996). *Pulp Bleaching—Principles and Practice*; TAPPI: Atlanta, GA, 1996. *There is no corresponding record for this reference.*
- Dence, C., & Sarkanen, K. (1960). A proposed mechanism for the acidic chlorination of softwood lignin. *Tappi*, 43(1), 87-96.
- Deng, H., Lin, L., & Liu, S. (2010). Catalysis of Cu-doped Co-based perovskite-type oxide in wet oxidation of lignin to produce aromatic aldehydes. *Energy & fuels*, 24(9), 4797-4802.
- Deng, H., Lin, L., Sun, Y., Pang, C., Zhuang, J., Ouyang, P., . . . Liu, S. (2008a). Activity and stability of perovskite-type oxide LaCoO₃ catalyst in lignin catalytic wet oxidation to aromatic aldehydes process. *Energy & fuels*, 23(1), 19-24.
- Deng, H., Lin, L., Sun, Y., Pang, C., Zhuang, J., Ouyang, P., . . . Liu, S. (2008b). Perovskite-type oxide LaMnO₃: An efficient and recyclable heterogeneous catalyst for the wet aerobic oxidation of lignin to aromatic aldehydes. *Catalysis letters*, 126(1-2), 106-111.

- Deng, W., Zhang, H., Wu, X., Li, R., Zhang, Q., & Wang, Y. (2015). Oxidative conversion of lignin and lignin model compounds catalyzed by CeO₂-supported Pd nanoparticles. *Green Chemistry*, 17(11), 5009-5018.
- Devaraju, M., Liu, X., Yusuke, K., Yin, S., & Sato, T. (2009). Solvothermal synthesis and characterization of ceria–zirconia mixed oxides for catalytic applications. *Nanotechnology*, 20(40), 405606.
- Dimmel, D. R., Bozell, J. J., Von Oepen, D. G., & Savidakis, M. C. (2002). Pulping Catalysts from Lignin—The Diels-Alder Step *Chemical Modification, Properties, and Usage of Lignin* (pp. 199-219): Springer.
- Drago, R., Corden, B., & Barnes, C. (1986). Novel cobalt (II)-catalyzed oxidative cleavage of a carbon-carbon double bond. *Journal of the American Chemical Society*, 108(9), 2453-2454.
- Eachus, S., & Dence, C. (1975). Hydrogenation of lignin model compounds in the presence of a homogeneous catalyst. *Holzforschung-International Journal of the Biology, Chemistry, Physics and Technology of Wood*, 29(2), 41-48.
- Egami, H., & Katsuki, T. (2007). Fe (salan)-catalyzed asymmetric oxidation of sulfides with hydrogen peroxide in water. *Journal of the American Chemical Society*, 129(29), 8940-8941.
- Einaga, H., Kiya, A., Yoshioka, S., & Teraoka, Y. (2014). Catalytic properties of copper–manganese mixed oxides prepared by coprecipitation using tetramethylammonium hydroxide. *Catalysis Science & Technology*, 4(10), 3713-3722.
- Ek, M., Gellerstedt, G., & Henriksson, G. (2009). *Wood Chemistry and Biotechnology* (Vol. 1): Walter de Gruyter.

Fan, J., Wu, X., Wu, X., Liang, Q., Ran, R., & Weng, D. (2008). Thermal ageing of Pt on low-surface-area CeO₂-ZrO₂-La₂O₃ mixed oxides: effect on the OSC performance. *Applied Catalysis B: Environmental*, 81(1), 38-48.

Fellows, C. M., Brown, T. C., & Doherty, W. O. (2011). Lignocellulosics as a renewable feedstock for chemical industry: Chemicals from lignin. *Green Chemistry for Environmental Remediation*, 561-610.

Feng, W., Xu, J., & Liao, S.-j. (2002). One-step heterogeneously catalytic oxidation of o-cresol by oxygen to salicylaldehyde. *Chemical Communications*(6), 626-627. doi: 10.1039/B200385F

Feng, W., Yang, G., Zhang, W., Wu, W., & Xu, J. (2004). Oxidation of p - Cresol to p - Hydroxybenzaldehyde with Molecular Oxygen in the Presence of CuMn - Oxide Heterogeneous Catalyst. *Advanced Synthesis & Catalysis*, 346(6), 633-638.

Ferrandon, M., Carnö, J., Järås, S., & Björnbom, E. (1999). Total oxidation catalysts based on manganese or copper oxides and platinum or palladium I: Characterisation. *Applied Catalysis A: General*, 180(1), 141-151.

Fleming, I. (1976). Frontier orbitals and organic reactions. *J. Wiley & Sons*.

Forzatti, P., & Lietti, L. (1999). Catalyst deactivation. *Catalysis Today*, 52(2), 165-181.

Fujita, M., & Que, L. (2004). In situ Formation of Peracetic Acid in Iron - Catalyzed Epoxidations by Hydrogen Peroxide in the Presence of Acetic Acid. *Advanced Synthesis & Catalysis*, 346(2 - 3), 190-194.

- Gao, X., Jiang, Y., Fu, Y., Zhong, Y., Luo, Z., & Cen, K. (2010). Preparation and characterization of CeO₂/TiO₂ catalysts for selective catalytic reduction of NO with NH₃. *Catalysis Communications*, 11(5), 465-469.
- Gawande, M. B., Pandey, R. K., & Jayaram, R. V. (2012). Role of mixed metal oxides in catalysis science—versatile applications in organic synthesis. *Catalysis Science & Technology*, 2(6), 1113-1125.
- Gellerstedt, G., & Pettersson, I. (1982). Chemical Aspects of Hydrogen Peroxide Bleaching. Part II the Bleaching of Kraft Pulps. *Journal of wood chemistry and technology*, 2(3), 231-250.
- Gierer, J. (1985). Chemistry of delignification. *Wood Science and technology*, 19(4), 289-312.
- Gierer, J., & Imsgard, F. (1977). The reactions of lignins with oxygen and hydrogen peroxide in alkaline media. *Svensk papperstidning*, 80(16), 510-518.
- Granata, A., & Argyropoulos, D. S. (1995). 2-Chloro-4, 4, 5, 5-tetramethyl-1, 3, 2-dioxaphospholane, a reagent for the accurate determination of the uncondensed and condensed phenolic moieties in lignins. *Journal of agricultural and food chemistry*, 43(6), 1538-1544.
- Grasselli, R. K. (2001). Genesis of site isolation and phase cooperation in selective oxidation catalysis. *Topics in Catalysis*, 15(2-4), 93-101.
- Gratzl, J. (1987). Abbaureaktionen von kohlenhydraten und lignin durch chlorfreie bleichmittel-mechanismen sowie möglichkeiten der stabilisierung. *Das Papier*, 41(3), 120-130.

Gu, X., Kanghua, C., Ming, H., Shi, Y., & Li, Z. (2012). La-modified SBA-15/H₂O₂ systems for the microwave assisted oxidation of organosolv beech wood lignin. *Maderas. Ciencia y tecnologia*, 14(1), 31-41.

Gul, I., Abbasi, A., Amin, F., Anis-ur-Rehman, M., & Maqsood, A. (2007). Structural, magnetic and electrical properties of Co_{1-x}Zn_xFe₂O₄ synthesized by co-precipitation method. *Journal of magnetism and magnetic materials*, 311(2), 494-499.

Hadjiivanov, K. I., & Klissurski, D. G. (1996). Surface chemistry of titania (anatase) and titania-supported catalysts. *Chemical Society Reviews*, 25(1), 61-69.

Hagemann, H., Bill, H., Walker, E., & François, M. (1990). Raman spectra of single crystal CuO. *Solid state communications*, 73(6), 447-451.

Halilu, A., Ali, T. H., Atta, A. Y., Sudarsanam, P., Bhargava, S. K., & Abd Hamid, S. B. (2016). Highly Selective Hydrogenation of Biomass-Derived Furfural into Furfuryl Alcohol using a Novel Magnetic Nanoparticles Catalyst. *Energy & fuels*.

Hall, G. S. (1984). Chemist's wood. *Nature*, 310, 521.

Hanson, S. K., Baker, R. T., Gordon, J. C., Scott, B. L., & Thorn, D. L. (2010). Aerobic oxidation of lignin models using a base metal vanadium catalyst. *Inorganic chemistry*, 49(12), 5611-5618.

Hatakeyama, H., Kosugi, R., & Hatakeyama, T. (2008). Thermal properties of lignin-and molasses-based polyurethane foams. *Journal of Thermal Analysis and Calorimetry*, 92(2), 419-424.

He, M., Sun, Y., & Han, B. (2013). Green carbon science: scientific basis for integrating carbon resource processing, utilization, and recycling. *Angewandte Chemie International Edition*, 52(37), 9620-9633.

Hennings, D. (1980). Phase equilibria and thermodynamics of the double oxide phase Cu₃TiO₄. *Journal of Solid State Chemistry*, 31(2), 275-279.

Hernandez, M., Fernández - Bertrán, J., Farias, M., & Diaz, J. (2007). Reaction of imidazole in gas phase at very low pressure with Cu foil and Cu oxides studied by X - ray photoelectron spectroscopy. *Surface and Interface Analysis*, 39(5), 434-437.

Hessien, M., Rashad, M., & El-Barawy, K. (2008). Controlling the composition and magnetic properties of strontium hexaferrite synthesized by co-precipitation method. *Journal of magnetism and magnetic materials*, 320(3), 336-343.

Holladay, J. E., White, J. F., Bozell, J. J., & Johnson, D. (2007). Top Value-Added Chemicals from Biomass-Volume II—Results of Screening for Potential Candidates from Biorefinery Lignin: Pacific Northwest National Laboratory (PNNL), Richland, WA (US).

Hosokawa, S., Jeon, H. J., Iwamoto, S., & Inoue, M. (2009). Synthesis of Rare Earth Iron - Mixed Oxide Nanoparticles by Solvothermal Methods. *Journal of the American Ceramic Society*, 92(12), 2847-2853.

Jayakumar, O., Salunke, H., Kadam, R., Mohapatra, M., Yaswant, G., & Kulshreshtha, S. (2006). Magnetism in Mn-doped ZnO nanoparticles prepared by a co-precipitation method. *Nanotechnology*, 17(5), 1278.

- Jha, A., Patil, K. R., & Rode, C. V. (2013). Mixed Co–Mn Oxide - Catalysed Selective Aerobic Oxidation of Vanillyl Alcohol to Vanillin in Base - Free Conditions. *ChemPlusChem*, 78(11), 1384-1392.
- Jha, A., & Rode, C. V. (2013). Highly selective liquid-phase aerobic oxidation of vanillyl alcohol to vanillin on cobalt oxide (Co₃O₄) nanoparticles. *New Journal of Chemistry*, 37(9), 2669-2674.
- Jiang, Z. H., Argyropoulos, D. S., & Granata, A. (1995). Correlation analysis of ³¹P NMR chemical shifts with substituent effects of phenols. *Magnetic resonance in chemistry*, 33(5), 375-382.
- Joseph, B., Guo - Hua, D., Nicolas, J., Grahame, M., Nadja, C., Bouchra, B. M., & Michel, D. (2015). A critique on the structural analysis of lignins and application of novel tandem mass spectrometric strategies to determine lignin sequencing. *Journal of Mass Spectrometry*, 50(1), 5-48. doi: doi:10.1002/jms.3541
- Kadla, J., Kubo, S., Venditti, R., Gilbert, R., Compere, A., & Griffith, W. (2002). Lignin-based carbon fibers for composite fiber applications. *Carbon*, 40(15), 2913-2920.
- Kapteijn, F., Singoredjo, L., Andreini, A., & Moulijn, J. (1994). Activity and selectivity of pure manganese oxides in the selective catalytic reduction of nitric oxide with ammonia. *Applied Catalysis B: Environmental*, 3(2-3), 173-189.
- Kholdeeva, O. A., Timofeeva, M. N., Maksimov, G. M., Maksimovskaya, R. I., Neiwert, W. A., & Hill, C. L. (2005). Aerobic oxidation of formaldehyde mediated by a Ce-containing polyoxometalate under mild conditions. *Inorganic chemistry*, 44(3), 666-672.

Kirchhoff, G. (1811). C: Observations, expériences, et notices intéressantes, faites et communiquées à l'Académie, 9. *Académie Imperiale des Sciences de St. Petersbourg, Mémoires*, 4.

Klaewkla, R., Arend, M., & Hoelderich, W. F. (2011a). *A review of mass transfer controlling the reaction rate in heterogeneous catalytic systems* (Vol. 5): INTECH Open Access Publisher.

Klaewkla, R., Arend, M., & Hoelderich, W. F. (2011b). *A review of mass transfer controlling the reaction rate in heterogeneous catalytic systems*: INTECH Open Access Publisher.

Klein-Marcuschamer, D., Oleskowicz-Popiel, P., Simmons, B. A., & Blanch, H. W. (2010). Technoeconomic analysis of biofuels: A wiki-based platform for lignocellulosic biorefineries. *biomass and bioenergy*, 34(12), 1914-1921.

Kolar, J., Lindgren, B., & Pettersson, B. (1983). Chemical reactions in chlorine dioxide stages of pulp bleaching. *Wood Science and technology*, 17(2), 117-128.

Kondrat, S. A., Davies, T. E., Zu, Z., Boldrin, P., Bartley, J. K., Carley, A. F., . . . Hutchings, G. J. (2011). The effect of heat treatment on phase formation of copper manganese oxide: Influence on catalytic activity for ambient temperature carbon monoxide oxidation. *Journal of Catalysis*, 281(2), 279-289.

Kummer, J. (1975). Oxidation of CO and C₂H₄ by base metal catalysts for honeycomb substrates. ACS series 143, Catalyst for the control of automotive pollutants. J. McECOY ed: American Chemical Society.

Lange, H., Decina, S., & Crestini, C. (2013). Oxidative upgrade of lignin—Recent routes reviewed. *European polymer journal*, 49(6), 1151-1173.

- Lenoir, D. (2006). Selective oxidation of organic compounds—sustainable catalytic reactions with oxygen and without transition metals? *Angewandte Chemie International Edition*, 45(20), 3206-3210.
- Li, M., Feng, Z., Ying, P., Xin, Q., & Li, C. (2003). Phase transformation in the surface region of zirconia and doped zirconia detected by UV Raman spectroscopy. *Physical Chemistry Chemical Physics*, 5(23), 5326-5332.
- Li, Z., Court, G., Belliveau, R., Crowell, M., Murphy, R., Gibson, A., . . . Ni, Y. (2004). USING MAGNESIUM HYDROXIDE (MG (OH)₂) AS THE ALKALI SOURCE IN PEROXIDE BLEACHING AT IRVING PAPER. Paper presented at the ANNUAL MEETING-PULP AND PAPER TECHNICAL ASSOCIATION OF CANADA.
- Lin, J., & Jimmy, C. Y. (1998). An investigation on photocatalytic activities of mixed TiO₂-rare earth oxides for the oxidation of acetone in air. *Journal of Photochemistry and photobiology A: Chemistry*, 116(1), 63-67.
- Lin, X.-M., Li, L.-P., Li, G.-S., & Su, W.-H. (2001). Transport property and Raman spectra of nanocrystalline solid solutions Ce_{0.8}Nd_{0.2}O_{2-δ} with different particle size. *Materials chemistry and physics*, 69(1), 236-240.
- Liotta, L., Ousmane, M., Di Carlo, G., Pantaleo, G., Deganello, G., Marci, G., . . . Giroir-Fendler, A. (2008). Total oxidation of propene at low temperature over Co₃O₄-CeO₂ mixed oxides: Role of surface oxygen vacancies and bulk oxygen mobility in the catalytic activity. *Applied Catalysis A: General*, 347(1), 81-88.
- Liu, F., Lu, L., Xiao, P., He, H., Qiao, L., & Zhang, Y. (2012). Effect of oxygen vacancies on photocatalytic efficiency of TiO₂ nanotubes aggregation. *Bulletin of the Korean Chemical Society*, 33(7), 2255-2259.

- Liu, R., Liang, X., Dong, C., & Hu, X. (2004). Transition-metal-free: A highly efficient catalytic aerobic alcohol oxidation process. *Journal of the American Chemical Society*, 126(13), 4112-4113.
- Lora, J. H., & Glasser, W. G. (2002). Recent industrial applications of lignin: a sustainable alternative to nonrenewable materials. *Journal of Polymers and the Environment*, 10(1-2), 39-48.
- Luo, M., Chen, J., Chen, L., Lu, J., Feng, Z., & Li, C. (2001). Structure and Redox Properties of $Ce_x Ti_{1-x} O_2$ Solid Solution. *Chemistry of materials*, 13(1), 197-202.
- Ma, R., Guo, M., & Zhang, X. (2014). Selective conversion of biorefinery lignin into dicarboxylic acids. *ChemSusChem*, 7(2), 412-415.
- Ma, R., Xu, Y., & Zhang, X. (2015). Catalytic Oxidation of Biorefinery Lignin to Value-added Chemicals to Support Sustainable Biofuel Production. *ChemSusChem*, 8(1), 24-51.
- Mai, H., Zhang, D., Shi, L., Yan, T., & Li, H. (2011). Highly active $Ce_{1-x} Cu_x O_2$ nanocomposite catalysts for the low temperature oxidation of CO. *Applied Surface Science*, 257(17), 7551-7559.
- Manna, J. S., Basu, S., Mitra, M., Mukherjee, S., & Das, G. C. (2009). Study on the biostability of chlorophyll a entrapped in silica gel nanomatrix. *Journal of Materials Science: Materials in Electronics*, 20(11), 1068-1072.
- Mate, V., Jha, A., Joshi, U., Patil, K., Shirai, M., & Rode, C. (2014). Effect of preparation parameters on characterization and activity of Co_3O_4 catalyst in liquid phase oxidation of lignin model substrates. *Applied Catalysis A: General*, 487, 130-138.

- Mate, V., Shirai, M., & Rode, C. V. (2013). Heterogeneous Co_3O_4 catalyst for selective oxidation of aqueous veratryl alcohol using molecular oxygen. *Catalysis Communications*, 33, 66-69.
- Mathew, T., Shiju, N., Sreekumar, K., Rao, B. S., & Gopinath, C. S. (2002). Cu–Co synergism in $\text{Cu}_{1-x}\text{Co}_x\text{Fe}_2\text{O}_4$ —catalysis and XPS aspects. *Journal of Catalysis*, 210(2), 405-417.
- McBride, J., Hass, K., Poindexter, B., & Weber, W. (1994). Raman and x - ray studies of $\text{Ce}_{1-x}\text{RE}_x\text{O}_{2-y}$, where RE= La, Pr, Nd, Eu, Gd, and Tb. *Journal of Applied Physics*, 76(4), 2435-2441.
- McDonough, T. J. (1989). Oxygen delignification. *Institute of Paper Chemistry* (319), 1-9.
- McFarland, E. W., & Metiu, H. (2013). Catalysis by doped oxides. *Chemical reviews*, 113(6), 4391-4427.
- McNaught, A. D., & McNaught, A. D. (1997). *Compendium of chemical terminology* (Vol. 1669): Blackwell Science Oxford.
- McNaught, A. D., & Wilkinson, A. (1997). *Compendium of chemical terminology. IUPAC recommendations*, 2nd Edition, Blackwell Science Publications, Oxford.
- Mohan, D., Pittman, C. U., & Steele, P. H. (2006). Pyrolysis of wood/biomass for bio-oil: a critical review. *Energy & fuels*, 20(3), 848-889.

- Morales, M. R., Barbero, B. P., & Cadús, L. E. (2006). Total oxidation of ethanol and propane over Mn-Cu mixed oxide catalysts. *Applied Catalysis B: Environmental*, 67(3), 229-236.
- Morgan, K., Cole, K. J., Goguet, A., Hardacre, C., Hutchings, G. J., Maguire, N., . . . Taylor, S. H. (2010). TAP studies of CO oxidation over CuMnOX and Au/CuMnOX catalysts. *Journal of Catalysis*, 276(1), 38-48.
- Moura, J. C. M. S., Bonine, C. A. V., De Oliveira Fernandes Viana, J., Dornelas, M. C., & Mazzafera, P. (2010). Abiotic and biotic stresses and changes in the lignin content and composition in plants. *Journal of integrative plant biology*, 52(4), 360-376.
- Mrabet, D., Abassi, A., Cherizol, R., & Do, T.-O. (2012). One-pot solvothermal synthesis of mixed Cu-Ce-O_x nanocatalysts and their catalytic activity for low temperature CO oxidation. *Applied Catalysis A: General*, 447, 60-66.
- Musser, M. T. (2005). Cyclohexanol and cyclohexanone. *Ullmann's Encyclopedia of Industrial Chemistry*.
- Nakajima, A., Yoshihara, A., & Ishigame, M. (1994). Defect-induced Raman spectra in doped CeO₂. *Physical Review B*, 50(18), 13297.
- Ni, Y., Shen, X., & Van Heiningen, A. (1994). Studies on the reactions of phenolic and non-phenolic lignin model compounds with chlorine dioxide. *Journal of wood chemistry and technology*, 14(2), 243-262.
- Nimz, H. (1966). Der abbau des lignins durch schonende hydrolyse. *Holzforschung-International Journal of the Biology, Chemistry, Physics and Technology of Wood*, 20(4), 105-109.

- Nonni, A. J., Falk, L. E., & Dence, C. W. (1982). Methoxy-P-Benzoquinone and Methoxyhydroquinone as Models for Chromophore Changes in the Bleaching of Softwood Mechanical Pulps. I the Detection of Methoxyhydroquinone in the Spent Liquor from the Peroxide Bleaching of Thermo-Mechanical Pulp. *Journal of wood chemistry and technology*, 2(3), 223-229.
- O'Connell, M., Norman, A., Hüttermann, C., & Morris, M. (1999). Catalytic oxidation over lanthanum-transition metal perovskite materials. *Catalysis Today*, 47(1), 123-132.
- Okamoto, Y., Ohto, Y., & Imanaka, T. (1993). REDUCTION OF NITRIC-OXIDE BY CARBON-MONOXIDE OVER ZIRCONIA-SUPPORTED METAL-OXIDE CATALYSTS. *Kagaku Kogaku Ronbunshu*, 19(5), 863-869.
- Omae, I. (2007). Three characteristic reactions of organocobalt compounds in organic synthesis. *Applied Organometallic Chemistry*, 21(5), 318-344.
- Ostwald, W. (1923). *Über katalyse*: Akademische verlagsgesellschaft mbh.
- Pan, X., Zhang, X., Gregg, D. J., & Saddler, J. N. (2004). *Enhanced enzymatic hydrolysis of steam-exploded Douglas fir wood by alkali-oxygen post-treatment*. Paper presented at the Proceedings of the Twenty-Fifth Symposium on Biotechnology for Fuels and Chemicals Held May 4-7, 2003, in Breckenridge, CO.
- Panayotov, D., & Yates, J. (2003). Electron exchange on TiO₂-SiO₂ photocatalysts during O₂ and organic molecule adsorption—the role of adsorbate electrophilicity. *Chemical physics letters*, 381(1), 154-162.
- Pandey, M. P., & Kim, C. S. (2011). Lignin depolymerization and conversion: a review of thermochemical methods. *Chemical Engineering & Technology*, 34(1), 29-41.

- Patai, S., & Rappoport, Z. (1988). *The chemistry of the quinonoid compounds* (Vol. 2): John Wiley & Sons.
- Perry, C., LIU, D. W., & INGEL, R. P. (1985). Phase characterization of partially stabilized zirconia by Raman spectroscopy. *Journal of the American Ceramic Society*, 68(8).
- Pham, M.-H., Dinh, C.-T., Vuong, G.-T., Ta, N.-D., & Do, T.-O. (2014). Visible light induced hydrogen generation using a hollow photocatalyst with two cocatalysts separated on two surface sides. *Physical Chemistry Chemical Physics*, 16(13), 5937-5941.
- Pintar, A., Batista, J., & Hočevár, S. (2005). TPR, TPO, and TPD examinations of Cu_{0.15} Ce_{0.85} O_{2-y} mixed oxides prepared by co-precipitation, by the sol-gel peroxide route, and by citric acid-assisted synthesis. *Journal of colloid and interface science*, 285(1), 218-231.
- Piskorz, J., Majerski, P., Radlein, D., & Scott, D. (1989). Conversion of lignins to hydrocarbon fuels. *Energy & fuels*, 3(6), 723-726.
- Preuss, A., & Gruehn, R. (1994). Preparation and Structure of Cerium Titanates Ce₂ TiO₅, Ce₂ TiO₇, and Ce₄ Ti₉ O₂₄. *Journal of Solid State Chemistry*, 110(2), 363-369.
- Pu, Y., Lucia, L., & Ragauskas, A. (2002). Institute of Paper Science and Technology Atlanta, Georgia.
- Puckhaber, L. S., Cheung, H., Cocke, D. L., & Clearfield, A. (1989). Reactivity of copper manganese oxides. *Solid State Ionics*, 32, 206-213.

Punniyamurthy, T., Velusamy, S., & Iqbal, J. (2005). Recent advances in transition metal catalyzed oxidation of organic substrates with molecular oxygen. *Chemical reviews*, 105(6), 2329-2364.

Radhakrishnan, R., Oyama, S. T., Chen, J. G., & Asakura, K. (2001). Electron transfer effects in ozone decomposition on supported manganese oxide. *The Journal of Physical Chemistry B*, 105(19), 4245-4253.

Rahimi, A., Azarpira, A., Kim, H., Ralph, J., & Stahl, S. S. (2013). Chemosselective metal-free aerobic alcohol oxidation in lignin. *Journal of the American Chemical Society*, 135(17), 6415-6418.

Rapson, W. H. (1963). The bleaching of pulp.

Reddy, B. M., Khan, A., Lakshmanan, P., Aouine, M., Loridant, S., & Volta, J.-C. (2005). Structural characterization of nanosized CeO₂-SiO₂, CeO₂-TiO₂, and CeO₂-ZrO₂ catalysts by XRD, Raman, and HREM techniques. *The Journal of Physical Chemistry B*, 109(8), 3355-3363.

Reddy, B. M., Khan, A., Yamada, Y., Kobayashi, T., Loridant, S., & Volta, J.-C. (2003). Structural characterization of CeO₂-MO₂ (M= Si⁴⁺, Ti⁴⁺, and Zr⁴⁺) mixed oxides by Raman spectroscopy, X-ray photoelectron spectroscopy, and other techniques. *The Journal of Physical Chemistry B*, 107(41), 11475-11484.

Reller, A., & Williams, T. (1989). Chemistry in Britain: December.

Ren, Y., Ma, Z., & Bruce, P. G. (2012). Ordered mesoporous metal oxides: synthesis and applications. *Chemical Society Reviews*, 41(14), 4909-4927.

- Rencoret, J., Gutiérrez, A., Nieto, L., Jiménez-Barbero, J., Faulds, C. B., Kim, H., . . . José, C. (2010). Lignin composition and structure in young versus adult *Eucalyptus globulus* plants. *Plant Physiology*, pp. 110.167254.
- Roberts, M. (1989). Chemisorption and reaction pathways at metal surfaces: the role of surface oxygen. *Chemical Society Reviews*, 18, 451-475.
- Robertson, A. (1975). The early history of catalysis. *Platinum Metals Rev*, 19(2), 64-69.
- Robinson, M. J., Wright, L. J., & Suckling, I. D. (2000). Fe (TSPc)-catalysed benzylic oxidation and subsequent dealkylation of a non-phenolic lignin model. *Journal of wood chemistry and technology*, 20(4), 357-373.
- Royer, S., Duprez, D., & Kaliaguine, S. (2005). Role of bulk and grain boundary oxygen mobility in the catalytic oxidation activity of $\text{LaCo}_{1-x}\text{Fe}_x\text{O}_3$. *Journal of Catalysis*, 234(2), 364-375.
- Salanti, A., Zoia, L., Orlandi, M., Zanini, F., & Elegir, G. (2010). Structural characterization and antioxidant activity evaluation of lignins from rice husk. *Journal of agricultural and food chemistry*, 58(18), 10049-10055.
- Salem, I. A., El - Maazawi, M., & Zaki, A. B. (2000). Kinetics and mechanisms of decomposition reaction of hydrogen peroxide in presence of metal complexes. *International Journal of Chemical Kinetics*, 32(11), 643-666.
- Salem, I. A., Elhag, R. I., & Khalil, K. M. (2000). Catalytic activity of a zirconium (IV) oxide surface supported with transition metal ions. *Transition metal chemistry*, 25(3), 260-264.

Sales, F. G., Maranhão, L. C., Lima Filho, N. M., & Abreu, C. A. (2007). Experimental evaluation and continuous catalytic process for fine aldehyde production from lignin. *Chemical Engineering Science*, 62(18), 5386-5391.

Samsudin, E. M., Hamid, S. B. A., Juan, J. C., Basirun, W. J., & Centi, G. (2015). Enhancement of the intrinsic photocatalytic activity of TiO₂ in the degradation of 1, 3, 5-triazine herbicides by doping with N, F. *Chemical Engineering Journal*, 280, 330-343.

Samsudin, E. M., Hamid, S. B. A., Juan, J. C., Basirun, W. J., Kandjani, A. E., & Bhargava, S. K. (2015). Controlled nitrogen insertion in titanium dioxide for optimal photocatalytic degradation of atrazine. *RSC Advances*, 5(55), 44041-44052.

Samsudin, E. M., Hamid, S. B. A., Juan, J. C., Basirun, W. J., Kandjani, A. E., & Bhargava, S. K. (2016). Effective role of trifluoroacetic acid (TFA) to enhance the photocatalytic activity of F-doped TiO₂ prepared by modified sol-gel method. *Applied Surface Science*, 365, 57-68.

Sannigrahi, P., Pu, Y., & Ragauskas, A. (2010). Cellulosic biorefineries—unleashing lignin opportunities. *Current Opinion in Environmental Sustainability*, 2(5), 383-393.

Sathasivam, S., Bhachu, D. S., Lu, Y., Chadwick, N., Althabaiti, S. A., Alyoubi, A. O., . . . Parkin, I. P. (2015). Tungsten Doped TiO₂ with Enhanced Photocatalytic and Optoelectrical Properties via Aerosol Assisted Chemical Vapor Deposition. *Scientific reports*, 5.

Sheehan, J. R. (2000). Terephthalic acid, dimethyl terephthalate, and isophthalic acid. *Ullmann's Encyclopedia of Industrial Chemistry*.

- Sheldon, R. (1993a). A history of oxygen activation: 1773–1993 *The activation of dioxygen and homogeneous catalytic oxidation* (pp. 9-30): Springer.
- Sheldon, R. (1993b). Homogeneous and heterogeneous catalytic oxidations with peroxide reagents. *Organic Peroxygen Chemistry*, 21-43.
- Sheldon, R. (2007). The E factor: fifteen years on. *Green Chemistry*, 9(12), 1273-1283.
- Sheldon, R. (2008). E factors, green chemistry and catalysis: an odyssey. *Chemical Communications*(29), 3352-3365.
- Sheldon, R. (2012). *Metal-catalyzed oxidations of organic compounds: mechanistic principles and synthetic methodology including biochemical processes*: Elsevier.
- Sheldon, R., & Van Santen, R. (1995). *Catalytic oxidation: principles and applications: a course of the Netherlands Institute for Catalysis Research (NIOK)*: World Scientific.
- Sheldon, R., Wallau, M., Arends, I. W., & Schuchardt, U. (1998). Heterogeneous catalysts for liquid-phase oxidations: Philosophers' stones or Trojan horses? *Accounts of Chemical Research*, 31(8), 485-493.
- Shi, Z., Yang, P., Tao, F., & Zhou, R. (2016). New insight into the structure of CeO₂-TiO₂ mixed oxides and their excellent catalytic performances for 1, 2-dichloroethane oxidation. *Chemical Engineering Journal*, 295, 99-108.

- Shilpy, M., Ehsan, M. A., Ali, T. H., Hamid, S. B. A., & Ali, M. E. (2015). Performance of cobalt titanate towards H₂O₂ based catalytic oxidation of lignin model compound. *RSC Advances*, 5(97), 79644-79653.
- Shyu, J., Weber, W., & Gandhi, H. (1988). Surface characterization of alumina-supported ceria. *The Journal of Physical Chemistry*, 92(17), 4964-4970.
- Singh, R. P. (1979). *The bleaching of pulp: a project of the Pulp Bleaching Committee, Pulp Manufacture Division*: Tappi press.
- Sippola, V., & Krause, A. (2005). Bis (o-phenanthroline) copper-catalysed oxidation of lignin model compounds for oxygen bleaching of pulp. *Catalysis Today*, 100(3), 237-242.
- Sixta, H., Iakovlev, M., Testova, L., Roselli, A., Hummel, M., Borrega, M., . . . Schottenberger, H. (2013). Novel concepts of dissolving pulp production. *Cellulose*, 20(4), 1547-1561.
- Somorjai, G. A., & Kliewer, C. J. (2009). Reaction selectivity in heterogeneous catalysis. *Reaction Kinetics and Catalysis Letters*, 96(2), 191-208.
- Son, S., & Toste, F. D. (2010). Non - Oxidative Vanadium - Catalyzed C-O Bond Cleavage: Application to Degradation of Lignin Model Compounds. *Angewandte Chemie International Edition*, 49(22), 3791-3794.
- Sonnen, D. M., Reiner, R. S., Atalla, R. H., & Weinstock, I. A. (1997). Degradation of pulp-mill effluent by oxygen and Na₅ [PV₂Mo₁₀O₄₀], a multipurpose delignification and wet air oxidation catalyst. *Industrial & Engineering Chemistry Research*, 36(10), 4134-4142.

- Stewart, D. (2008). Lignin as a base material for materials applications: Chemistry, application and economics. *Industrial crops and products*, 27(2), 202-207.
- Strassberger, Z., Tanase, S., & Rothenberg, G. RCS Adv. 2014, 4, 25310. *CrossRef| Web of Science® Times Cited*, 5.
- Subramaniam, B. (2010). Exploiting neoteric solvents for sustainable catalysis and reaction engineering: opportunities and challenges. *Industrial & Engineering Chemistry Research*, 49(21), 10218-10229.
- Sun, Y., & Cheng, J. (2002). Hydrolysis of lignocellulosic materials for ethanol production: a review. *Bioresource technology*, 83(1), 1-11.
- Svenson, D. R., Jameel, H., Chang, H. m., & Kadla, J. F. (2006). Inorganic reactions in chlorine dioxide bleaching of softwood kraft pulp. *Journal of wood chemistry and technology*, 26(3), 201-213.
- Szatkowski, T., Wysokowski, M., Lota, G., Peźiak, D., Bazhenov, V. V., Nowaczyk, G., Himcinski, C. (2015). Novel nanostructured hematite–spongin composite developed using an extreme biomimetic approach. *RSC Advances*, 5(96), 79031-79040.
- Tanaka, H., & Misono, M. (2001). Advances in designing perovskite catalysts. *Current Opinion in Solid State and Materials Science*, 5(5), 381-387.
- Tang, X., Li, Y., Huang, X., Xu, Y., Zhu, H., Wang, J., & Shen, W. (2006). MnO_x-CeO₂ mixed oxide catalysts for complete oxidation of formaldehyde: effect of preparation method and calcination temperature. *Applied Catalysis B: Environmental*, 62(3), 265-273.

- Tang, X., Zhang, B., Li, Y., Xu, Y., Xin, Q., & Shen, W. (2005). CuO/CeO₂ catalysts: redox features and catalytic behaviors. *Applied Catalysis A: General*, 288(1), 116-125.
- Tarabanko, V., Petukhov, D., & Selyutin, G. (2004). New mechanism for the catalytic oxidation of lignin to vanillin. *Kinetics and Catalysis*, 45(4), 569-577.
- Tarasov, A., Kustov, L., Bogolyubov, A., Kiselyov, A., & Semenov, V. (2009). New and efficient procedure for the oxidation of dioxybenzylic alcohols into aldehydes with Pt and Pd-based catalysts under flow reactor conditions. *Applied Catalysis A: General*, 366(2), 227-231.
- Tarasov, A., Kustov, L., Isaeva, V., Kalenchuk, A., Mishin, I., Kapustin, G., & Bogdan, V. (2011). Platinum-containing catalyst supported on a metal-organic framework structure in the selective oxidation of benzyl alcohol derivatives into aldehydes. *Kinetics and Catalysis*, 52(2), 273.
- Thielemans, W., Can, E., Morye, S., & Wool, R. (2002). Novel applications of lignin in composite materials. *Journal of Applied Polymer Science*, 83(2), 323-331.
- Thring, R. W., Katikaneni, S. P., & Bakhshi, N. N. (2000). The production of gasoline range hydrocarbons from Alcell® lignin using HZSM-5 catalyst. *Fuel Processing Technology*, 62(1), 17-30.
- Tian, B., Liu, X., Solovyov, L. A., Liu, Z., Yang, H., Zhang, Z., . . . Yu, C. (2004). Facile synthesis and characterization of novel mesoporous and mesorelief oxides with gyroidal structures. *Journal of the American Chemical Society*, 126(3), 865-875.
- Tian, B., Liu, X., Yang, H., Xie, S., Yu, C., Tu, B., & Zhao, D. (2003). General Synthesis of Ordered Crystallized Metal Oxide Nanoarrays Replicated by Microwave - Digested Mesoporous Silica. *Advanced Materials*, 15(16), 1370-1374.

- Tian, H., Zhang, X. L., Scott, J., Ng, C., & Amal, R. (2014). TiO₂-supported copper nanoparticles prepared via ion exchange for photocatalytic hydrogen production. *Journal of Materials Chemistry A*, 2(18), 6432-6438.
- Tomlinson 2nd, G. H., & Hibbert, H. (1936). Studies on Lignin and Related Compounds. XXV. Mechanism of Vanillin Formation from Spruce Lignin Sulfonic Acids in Relation to Lignin Structure1. *Journal of the American Chemical Society*, 58(2), 348-353.
- Trawczyński, J., Bielak, B., & Miśta, W. (2005). Oxidation of ethanol over supported manganese catalysts—effect of the carrier. *Applied Catalysis B: Environmental*, 55(4), 277-285.
- Trost, B. M. (1995). Atom economy—a challenge for organic synthesis: homogeneous catalysis leads the way. *Angewandte Chemie International Edition in English*, 34(3), 259-281.
- Tseng, I.-H., Wu, J. C., & Chou, H.-Y. (2004). Effects of sol-gel procedures on the photocatalysis of Cu/TiO₂ in CO₂ photoreduction. *Journal of Catalysis*, 221(2), 432-440.
- Uehara, M., Urade, M., Ueda, A., Sakagami, N., & Abe, Y. (1998). High Activities of Hydrogen Peroxide Decomposition Catalyzed by Dinuclear Schiff Base Mn (III)-Cu (II) Complexes Accompanying Metal Substitution in N, N-Dimethylformamide and the Crystal Structure of a Substituted Schiff Base Cu (II) Complexes. *Bulletin of the Chemical Society of Japan*, 71(5), 1081-1088.
- Van Dyk, J., & Pletschke, B. (2012). A review of lignocellulose bioconversion using enzymatic hydrolysis and synergistic cooperation between enzymes—factors affecting enzymes, conversion and synergy. *Biotechnology advances*, 30(6), 1458-1480.

- Vandenbergh, R., Legrand, E., Scheerlinck, D., & Brabers, V. (1976). Neutron diffraction study of the cation ordering in $\text{Cu}_1.5\text{Mn}_1.5\text{O}_4$ and $\text{CuMg}_0.5\text{Mn}_1.5\text{O}_4$. *Acta Crystallographica Section B: Structural Crystallography and Crystal Chemistry*, 32(10), 2796-2798.
- Vazquez, G., Rodríguez-Bona, C., Freire, S., Gonzalez-Alvarez, J., & Antorrena, G. (1999). Acetosolv pine lignin as copolymer in resins for manufacture of exterior grade plywoods. *Bioresource technology*, 70(2), 209-214.
- Vidruk, R., Landau, M. V., Herskowitz, M., Talianker, M., Frage, N., Ezersky, V., & Froumin, N. (2009). Grain boundary control in nanocrystalline MgO as a novel means for significantly enhancing surface basicity and catalytic activity. *Journal of Catalysis*, 263(1), 196-204.
- Wang, H., Gao, L., & Niihara, K. (2000). Synthesis of nanoscaled yttrium aluminum garnet powder by the co-precipitation method. *Materials Science and Engineering: A*, 288(1), 1-4.
- Wang, J., Shi, T. J., & Jiang, X. (2009). Synthesis and characterization of core-shell $\text{ZrO}_2/\text{PAAEM}/\text{PS}$ nanoparticles. *Nanoscale research letters*, 4(3), 240-246.
- Wang, L., Teng, J., Liu, P., Hirata, A., Ma, E., Zhang, Z., . . . Han, X. (2014). Grain rotation mediated by grain boundary dislocations in nanocrystalline platinum. *Nature communications*, 5.
- Wang, Y., Lü, Y., Zhan, W., Xie, Z., Kuang, Q., & Zheng, L. (2015). Synthesis of porous $\text{Cu}_2\text{O}/\text{CuO}$ cages using Cu-based metal-organic frameworks as templates and their gas-sensing properties. *Journal of Materials Chemistry A*, 3(24), 12796-12803.

- Wang, Y., Wang, Y., Liu, X., Guo, Y., Guo, Y., Lu, G., & Schüth, F. (2008). Nanocasted synthesis of mesoporous metal oxides and mixed oxides from mesoporous cubic (Ia3d) vinylsilica. *Journal of nanoscience and nanotechnology*, 8(11), 5652-5658.
- Wang, Y., Yang, C. M., Schmidt, W., Spliethoff, B., Bill, E., & Schüth, F. (2005). Weakly Ferromagnetic Ordered Mesoporous Co₃O₄ Synthesized by Nanocasting from Vinyl - Functionalized Cubic Ia3d Mesoporous Silica. *Advanced Materials*, 17(1), 53-56.
- Wang, Y., Yuan, X., Liu, X., Ren, J., Tong, W., Wang, Y., & Lu, G. (2008). Mesoporous single-crystal Cr₂O₃: Synthesis, characterization, and its activity in toluene removal. *Solid State Sciences*, 10(9), 1117-1123.
- Watanabe, S., Ma, X., & Song, C. (2009). Characterization of structural and surface properties of nanocrystalline TiO₂-CeO₂ mixed oxides by XRD, XPS, TPR, and TPD. *The Journal of Physical Chemistry C*, 113(32), 14249-14257.
- Weckhuysen, B. M., & Keller, D. E. (2003). Chemistry, spectroscopy and the role of supported vanadium oxides in heterogeneous catalysis. *Catalysis Today*, 78(1), 25-46.
- Wei, P., Bieringer, M., Cranswick, L. M., & Petric, A. (2010). In situ high-temperature X-ray and neutron diffraction of Cu-Mn oxide phases. *Journal of materials science*, 45(4), 1056-1064.
- Weinstock, I. A., Barbuzzi, E. M., Wemple, M. W., Cowan, J. J., Reiner, R. S., Sonnen, D. M., . . . Hill, C. L. (2001). Equilibrating metal-oxide cluster ensembles for oxidation reactions using oxygen in water. *Nature*, 414(6860), 191-195.

- Welker, C. M., Balasubramanian, V. K., Petti, C., Rai, K. M., DeBolt, S., & Mendu, V. (2015). Engineering plant biomass lignin content and composition for biofuels and bioproducts. *Energies*, 8(8), 7654-7676.
- Werpy, T., Petersen, G., Aden, A., Bozell, J., Holladay, J., White, J., . . . Jones, S. (2004). Top value added chemicals from biomass. Volume 1-Results of screening for potential candidates from sugars and synthesis gas: DTIC Document.
- Wertheim, G., Hüfner, S., & Guggenheim, H. (1973). Systematics of Core-Electron Exchange Splitting in 3 d-Group Transition-Metal Compounds. *Physical Review B*, 7(1), 556.
- Wu, X., Guo, S., & Zhang, J. (2015). Selective oxidation of veratryl alcohol with composites of Au nanoparticles and graphene quantum dots as catalysts. *Chemical Communications*, 51(29), 6318-6321.
- Xie, Q., Chen, L., Weng, W., & Wan, H. (2005). Preparation of MoVTe (Sb) Nb mixed oxide catalysts using a slurry method for selective oxidative dehydrogenation of ethane. *Journal of Molecular Catalysis A: Chemical*, 240(1), 191-196.
- Xu, G., Yang, J.-h., Mao, H.-h., & Yun, Z. (2011). Pulping black liquor used directly as a green and effective source for neat oil and as an emulsifier of catalytic cracking heavy oil. *Chemistry and Technology of Fuels and Oils*, 47(4), 283-291.
- Yamashita, T., & Hayes, P. (2008). Analysis of XPS spectra of Fe 2+ and Fe 3+ ions in oxide materials. *Applied Surface Science*, 254(8), 2441-2449.
- Yang, B., Chan, S., Chang, W., & Chen, Y. (1991). Surface enrichment in mixed oxides of Cu, Co, and Mn, and its effect on CO oxidation. *Journal of Catalysis*, 130(1), 52-61.

- Yang, H., & Zhao, D. (2005). Synthesis of replica mesostructures by the nanocasting strategy. *Journal of Materials Chemistry*, 15(12), 1217-1231.
- Yokoyama, T., Chang, H.-m., Reiner, R. S., Atalla, R. H., Weinstock, I. A., & Kadla, J. F. (2004). Polyoxometalate oxidation of non-phenolic lignin subunits in water: Effect of substrate structure on reaction kinetics. *Holzforschung*, 58(2), 116-121.
- Young, R. A., & Akhtar, M. (1998). *Environmentally friendly technologies for the pulp and paper industry*: John Wiley & Sons.
- Zaera, F. (2002). Outstanding mechanistic questions in heterogeneous catalysis: ACS Publications.
- Zakzeski, J., Dębczak, A., Bruijninx, P. C., & Weckhuysen, B. M. (2011). Catalytic oxidation of aromatic oxygenates by the heterogeneous catalyst Co-ZIF-9. *Applied Catalysis A: General*, 394(1), 79-85.
- Zhang, J., Deng, H., & Lin, L. (2009). Wet Aerobic Oxidation of Lignin into aromatic aldehydes catalysed by a Perovskite-type oxide: $\text{LaFe}_{1-x}\text{Cu}_x\text{O}_3$ ($x = 0, 0.1, 0.2$). *Molecules*, 14(8), 2747-2757.
- Zhang, M., Sheng, G., Fu, J., An, T., Wang, X., & Hu, X. (2005). Novel preparation of nanosized ZnO-SnO_2 with high photocatalytic activity by homogeneous coprecipitation method. *Materials letters*, 59(28), 3641-3644.
- Zhang, Q., Liu, X., Fan, W., & Wang, Y. (2011). Manganese-promoted cobalt oxide as efficient and stable non-noble metal catalyst for preferential oxidation of CO in H_2 stream. *Applied Catalysis B: Environmental*, 102(1), 207-214.

Zhang, W., Wang, J., Tanev, P. T., & Pinnavaia, T. J. (1996). Catalytic hydroxylation of benzene over transition-metal substituted hexagonal mesoporous silicas. *Chemical Communications*(8), 979-980.

Zhao, X.-b., Zhang, T., Zhou, Y.-j., & Liu, D.-h. (2008). Preparation of peracetic acid from acetic acid and hydrogen peroxide: Experimentation and modeling. *过程工程学报*, 8(1).

Zhu, W., & Ford, W. T. (1993). Oxidation of lignin model compounds in water with dioxygen and hydrogen peroxide catalysed by metallophthalocyanines. *Journal of molecular catalysis*, 78(3), 367-378.

Zoia, L., Salanti, A., Frigerio, P., & Orlandi, M. (2014). Exploring allylation and Claisen rearrangement as a novel chemical modification of lignin. *BioResources*, 9(4), 6540-6561.

Zou, Z.-Q., Meng, M., Guo, L.-H., & Zha, Y.-Q. (2009). Synthesis and characterization of $\text{CuO/Ce}_{1-x}\text{Ti}_x\text{O}_2$ catalysts used for low-temperature CO oxidation. *Journal of hazardous materials*, 163(2), 835-842.

LIST OF PUBLICATIONS AND PAPERS PRESENTED

1. Catalytic evaluation on liquid phase oxidation of vanillyl alcohol using air and H₂O₂ over mesoporous Cu-Ti composite oxide, *Applied Surface Science* 2017, 394, 205-218.
2. Nanosized spinel Cu-Mn mixed oxide catalysts prepared via solvent evaporation method for liquid phase oxidation of vanillyl alcohol using air and H₂O₂, *RSC Adv.* 2016, 6, 96314-96326.
3. CuZrO₃ nanoparticles catalysts in aerobic oxidation of vanillyl alcohol, *RSC Adv.* 2017, 7, 9914-9925.
4. Design and synthesis of silica supported nanoporous Gold –Palladium bimetallic catalyst for Alkyl Benzene oxidation, *Advanced Materials Research* 2015, 1109, 444-447.